Imperial College London

Using LC-MS and Mass Spectrometry Imaging Techniques to Identify Metabolic Adaptations of Breast Cancer Metastases to the Lung.

Yulia Panina

Imperial College London
and
The Francis Crick Institute

PhD Supervisors: Dr. Mariia Yuneva
Prof. Zoltan Takats
Prof. Ian Gilmore

A thesis submitted for the degree of
Doctor of Philosophy
Department of Surgery and Cancer at Imperial College London

May 2021

Declarations

I, Yulia Panina, confirm that the work presented in this thesis is my own. Where information has been derived from other sources, I confirm that this has been indicated in the thesis.

Copyright Declaration

The copyright of this thesis rests with the author. Unless otherwise indicated, its contents are licensed under a Creative Commons Attribution-Non Commercial 4.0 International Licence (CC BY-NC).

Under this licence, you may copy and redistribute the material in any medium or format. You may also create and distribute modified versions of the work. This is on the condition that: you credit the author and do not use it, or any derivative works, for a commercial purpose.

When reusing or sharing this work, ensure you make the licence terms clear to others by naming the licence and linking to the licence text. Where a work has been adapted, you should indicate that the work has been changed and describe those changes.

Please seek permission from the copyright holder for uses of this work that are not included in this licence or permitted under UK Copyright Law.

Abstract

One of the hallmarks of cancer is deregulated metabolism, often characterized by increased glucose and glutamine uptake for energetic and anabolic purposes. Changes in the activity of metabolic pathways can arise as a result of oncogenic mutations and tumour cell environment and contribute to signalling pathways amplifying cancer progression.

Metabolic changes contribute to well-established tumour heterogeneity, which is a major challenge for anti-cancer therapeutics. Visualising and quantifying the spatial distribution of metabolites and the activity of metabolic pathways within different tumour regions, metastatic lesions and in surrounding healthy tissue can unveil metabolic vulnerabilities for novel or combination therapies.

Mass Spectrometry Imaging (MSI) allows mass spectrometric analysis of both the composition and structural architecture of intact tissue samples. The ability of MSI instruments to detect a broad range of biomolecules allows mapping and quantification of endogenous molecules to assess metabolic heterogeneity. In this work, MSI methods were developed for specific detection, visualisation and quantification of polar and lipid metabolites *in situ*.

Acknowledgements

First and foremost, I am extremely grateful to my primary supervisor, Dr. Mariia Yuneva, for her truly unwavering support, dedication and patience throughout my PhD. Her pristine knowledge and continuous enthusiasm have encouraged me throughout my academic research. I would also like to thank all of the past and present members of the Yuneva Lab for their expertise, kindness and encouragement that allowed me to conduct my research in a positive and motivational environment. To the past and present members of the Yuneva Lab: Andy, Peter, Ersa, Amy, Shravan, Avinash, Mia, Chandan, Wei, Emma, Joanna, Daria, Ben, Richard, and Neill, thank you all for all of your immeasurable help, emotional support coffees, and an absolutely unforgettable experience; I truly hope we can continue to be friends and colleagues in the near and far future.

I would also like to extend my gratitude to two labs which welcomed me into the world of physics and helped me learn everything I know about the exciting field of Mass Spectrometry Imaging. Professor Zoltan Takats's lab at Imperial College London, with the immense help of Vincen Wu allowed me to use DESI-MSI throughout my project. Professor Ian Gilmore, as well as the members of his lab, Rasmus, Jean-Luc, Melissa, Maria and Paulina introduced me to the ins and outs of the novel OrbiSIMS instrument. Thank you for the trust, patience and extensive skills that you all brought to my PhD. I would also like to thank Adam and Spencer and Professor Josephine Bunch, who have also taught me so much and allowed me to become proficient in MSI data analysis. This project would not be possible without the support from the entire CRUK Grand Challenge Rosetta Team.

I was very lucky with my Thesis Committee advisors: Alex Gould, Zoltan Takats and James Macrae looked out for my best interest and provided an enormous amount of advice and guidance throughout my PhD years.

Thank you also to the Experimental Histopathology STP team at the Crick: Emma, Mary and Joanna, as well as the histopathologists Gordon and Ellie for all of your support and guidance. The metabolomics work in this thesis was conducted thanks to the excellent expertise of the Metabolomics STP members: James, Nathalie, Mariana and Jim. The mouse work in my project was made possible by the Biological Research Facility; thank you to Sai, Chris, Eleni and Rekha for your positivity and all the excellent work you do to guarantee the wellbeing of our animals. Thank you also to the Anastasiou Lab at the Crick for being the best metabo-family the Yuneva Lab could ever ask for.

A huge thank you to Zuzana, Flavia and Elizabeth, for helping me navigate through PhD student life. We started this journey together from day one, and this experience would have never been as wonderful as you three have made it.

I would also like to thank my parents for their endless love and all of the education they have provided me that allowed me to be writing my thesis today. My parents, my grandparents, and my brother and sister-in-law have provided an unwavering support bubble not only during this strenuous time but throughout my life, for which I will continue to express all of my love and gratitude.

A special and warmest thank you goes out to my closest friends: Asya, Oce, Helena, Electra, Alice and Gergo. They never failed to be there for me and gracefully put up with countless impromptu lectures about cancer metabolism and the struggles of academic life. A special thank you to Henrik, for his love and support during these past few years in general, and for his patience and dinner making skills during these past few months in particular.

Finally, thank you to my dog Bonnie for being the best emotional support animal a PhD student could ask for.

Sapere aude -Immanuel Kant

Table of Contents

DECLARATIONS **2**

ABSTRACT **3**

ACKNOWLEDGEMENTS **4**

LIST OF FIGURES **10**

LIST OF TABLES **14**

ABBREVIATIONS **15**

CHAPTER 1. INTRODUCTION **19**

1.1 CANCER 19

1.2 BREAST CANCER 20

1.2.1 Disease statistics *20*

1.2.2 Breast Cancer Subtypes *20*

1.3 CANCER METABOLISM 22

1.3.1 Glycolysis *23*

1.3.2 The Pentose Phosphate Pathway *26*

1.3.3 The Tricarboxylic Acid Cycle *28*

1.3.4 Non-essential amino acid metabolism *30*

1.3.5 Essential amino acid metabolism *35*

1.3.6 One carbon metabolism and glutathione synthesis *38*

1.3.7 Fatty acid metabolism *42*

1.3.8 Glycerophospholipid metabolism *43*

1.3.9 Metabolism of other lipid classes: glycerolipids, sphingolipids and cholesterol *46*

1.4 MYC AND CANCER METABOLISM 50

1.5 METABOLIC REPROGRAMING IN METASTATIC PROGRESSION 51

1.6 MASS SPECTROMETRY IMAGING 55

1.6.1 Metabolomics analysis principle *55*

1.6.2 Mass Spectrometry Imaging principle *55*

CHAPTER 2. METHODS **62**

2.1 REAGENTS AND CHEMICALS 62

2.1.1 Cell culture media *62*

2.1.2 Stable Isotope-Labelled Metabolites *64*

2.1.3 Metabolite Extraction *64*

2.1.4 Antibodies *65*

2.2 MOUSE MODELS AND *IN VIVO* EXPERIMENTAL PROCEDURES 66

2.2.1 Mouse Models *66*

2.2.2 Tumour initiation by mammary fat pad injection *66*

2.2.3 Tumour and metastasis cell isolation and propagation *66*

2.3 Molecular Biology Methods 68
2.3.1 Immunofluorescence 68
2.3.2 Haematoxylin & Eosin Staining 69
2.3.3 BCA Assay for Protein Quantification 69
2.3.4 Western Blot 70
2.3.5 DNA extraction 71
2.3.6 PCR Genotyping 71
2.4 Metabolomics Methods 72
2.4.1 Stable isotope infusions and tumour collection for metabolomics 72
2.4.2 Metabolite Extraction for LC-MS 72
2.4.3 Derivatisation for GC-MS 73
2.5 MSI Sample Preparation 74
2.6 Metabolomics and MSI technology platforms and data analysis 74
2.6.1 LC-MS 74
2.6.2 GC-MS 75
2.6.3 DESI-MSI 75
2.6.4 OrbiSIMS 78

CHAPTER 3. ASSESSING THE METABOLISM OF METASTATIC MYC-DRIVEN MAMMARY GLAND TUMOURS 79

3.1 Introduction 79
3.2 Glycolysis, TCA and PPP 83
3.3 Amino acids 86
3.4 Nucleotide biosynthesis and associated metabolites 86
3.5 One carbon metabolism and glutathione 89
3.6 Vitamins 89
3.7 Chapter Discussion 91

CHAPTER 4. COMPARING THE METABOLISM OF METASTATIC MAMMARY GLAND TUMOURS AND LUNG METASTASES DERIVED FROM THEM. 93

4.1 Introduction 93
4.2 Glycolysis and PPP 94
4.3 TCA Cycle and NEAAs 97
4.3.1 TCA Cycle 97
4.3.2 Non-essential amino acids 99
4.4 Nucleotide biosynthesis 101
4.5 EAAs, one carbon metabolism and glutathione 103
4.5.1 Essential amino acids 103
4.5.2 One carbon metabolism 105
4.6 Chapter Discussion 109

CHAPTER 5. COMPARING THE METABOLISM OF MAMMARY GLAND TUMOURS FORMED BY INJECTION OF LUNG METASTASIS CELLS INTO THE FAT PAD, AND THE LUNG METASTASES DERIVED FROM THEM. 113

5.1 ASSESSING METABOLIC PLASTICITY OF LUNG METASTASIS CELLS 113

5.1.1 Isolation and propagation of metastasis cells....113

5.1.2 Re-injection of lung metastasis cells into the mammary fat pad 115

5.2 COMPARING METABOLISM OF MYC310 MGTS AND LM MGTS 117

5.2.1 Glycolysis and PPP....117

5.2.2 TCA Cycle and Glutaminolysis....122

5.2.3 One carbon metabolism, EAAs and nucleotides....125

5.2.4 Discussion....128

5.3 COMPARING THE METABOLISM OF LM MGTS AND THEIR LUNG METASTASES 130

5.3.1 Effect of stable isotope infusions on metabolite levels....130

5.3.2 Glycolysis and PPP....132

5.3.3 TCA Cycle....134

5.3.4 Non-Essential Amino Acids 139

5.3.5 Essential amino acids....142

5.3.6 One carbon metabolism....143

5.3.7 Consideration of whole body metabolism in in vivo stable isotope labelling studies....145

5.3.8 Chapter Discussion 148

CHAPTER 6. USING DESI-MSI TO ANALYSE SPATIAL DISTRIBUTION OF POLAR METABOLITES IN PRIMARY MAMMARY GLAND TUMOURS AND THEIR LUNG METASTASES. 152

6.1 INTRODUCTION....152

6.2 EXPERIMENTAL SET-UP AND SAMPLE PREPARATION 154

6.3 TARGETED DESI-MSI ANALYSIS: LMS VS. MGTS, COMPARISON TO LC-MS RESULTS....155

6.3.1 Histological ROI Segmentation of DESI Images 160

6.3.2 Glutamine, glutamate and TCA....163

6.3.3 Nucleotides....169

6.3.4 GSH, GSSG and one carbon metabolism....171

6.4 INTRA-TUMOUR HETEROGENEITY REVEALED BY DESI-MSI....173

6.4.1 Introduction....173

6.4.2 Metabolic heterogeneity in targeted DESI-MSI analysis 173

6.4.3 Metabolic heterogeneity in untargeted DESI-MSI analysis....179

6.4.4 Network analysis of DESI-MSI imaging....182

6.5 EXPLORING INTER-TUMOUR METABOLIC HETEROGENEITY FURTHER WITH A HIGHER SPATIAL RESOLUTION MODALITY, THE ORBI-SIMS 185

6.6 METABOLIC HETEROGENEITY IN THE METASTATIC LUNG....188

6.6.1 Polar metabolic heterogeneity between metastases 188

6.6.2 Polar metabolic heterogeneity between wildtype and metastatic lung 192
6.7 Chapter Discussion 194
CHAPTER 7. USING MSI TO ANALYSE SPATIAL DISTRIBUTION OF LIPID METABOLITES IN LUNG METASTASES AND THE METASTATIC NICHE 196
7.1 Introduction 196
7.2 Distinctions in lipid metabolites between two LMs localised in the same lung lobe by DESI-MSI. 196
7.3 Analysing lipid metabolite distribution in metastatic and WT lungs by DESI-MS. 200
7.4 Comparing changes in lipid classes between Myc310 MGTs and LMs using LC-MS and DESI-MSI. 202
7.4.1 Apolar LC-MS 202
7.4.2 Apolar DESI-MSI 204
7.5 Exploring peri-metastatic lipid accumulation using the Orbi-SIMS 207
7.6 Identifying the cell population within the metastatic niche that accumulates lipids on the metastatic border. 209
7.7 Chapter Discussion 213
CHAPTER 8. DISCUSSION 215
8.1 Developing a method to study the metabolism of lung metastases. 216
8.2 Metabolic changes between MYC-driven mammary gland tumours and their metastases to the lung. 218
8.2.1 Lung metastases have increased bioenergetic demands than mammary gland tumours, as demonstrated by increased glycolysis, amino acid metabolism and nucleotide biosynthesis. 218
8.2.2 Lung metastases have an upregulated one carbon metabolism and glutathione biosynthesis. 219
8.2.3 Limitations of LC-MS for assessing metabolism of metastasis 221
8.3 Advantages and limitations of MSI for studying metabolic heterogeneity in complex tissues. 222
8.3.1 DESI-MSI reveals heterogeneous distribution of metabolites within MGTs and in the metastatic lung. 222
8.3.2 Lipid biosynthesis is upregulated by lung cells in close proximity to invasive metastatic lesions. 224
8.3.3 Future challenges for MSI analysis of complex biological tissues. 226
8.4 Conclusion 228
REFERENCES 229

List of Figures

Figure 1-1. The mammalian glycolysis pathway and other downstream metabolic pathways. 25
Figure 1-2. The mammalian pentose phosphate pathway: oxidative and non-oxidative branches. 27
Figure 1-3. The mammalian tricarboxylic acid cycle and the three main carbon sources (glucose, fatty acids, glutamine). 29
Figure 1-4. Non-essential amino acid metabolism pathways. 34
Figure 1-5. Essential amino acid metabolism pathways..... 37
Figure 1-6. One carbon metabolism pathways and glutathione biosynthesis..... 41
Figure 1-7. Pathways of *de novo* fatty acid and lipid biosynthesis. 49
Figure 1-8. Comparison of MSI modalities. 57
Figure 3-1. Comparison of metastatic burden and primary tumour characteristics between transgenic and Myc310 MGTs..... 81
Figure 3-2. LC-MS metabolomics results comparing glycolysis. 85
Figure 3-3. LC-MS metabolomics results comparing MMTV-Myc transgenic mammary gland tumours and tumours derived by intra-fat pad injection of Myc310 tumour cells. 87
Figure 3-4. LC-MS metabolomics results comparing nucleotide levels 88
Figure 3-5. LC-MS metabolomics results comparing one carbon metabolism and glutathione metabolism. 90
Figure 4-1. LC-MS metabolomics results comparing glycolysis between Myc310 MGTs and Myc310 LMs..... 95
Figure 4-2. LC-MS metabolomics results comparing PPP between Myc310 MGTs and Myc310 LMs..... 96
Figure 4-3. LC-MS metabolomics results comparing TCA between Myc310 MGTs and Myc310 LMs..... 98
Figure 4-4. LC-MS metabolomics results comparing NEAAs between Myc310 MGTs and Myc310 MGTs..... 100
Figure 4-5. LC-MS metabolomics results comparing nucleotides between Myc310 MGTs and Myc310 LMs..... 102
Figure 4-6. LC-MS metabolomics results comparing EAAs between Myc310 MGTs and Myc310 LMs..... 104

Figure 4-7. LC-MS metabolomics results comparing one carbon metabolism between Myc310 MGTs and Myc310 LMs. 107
Figure 4-8. LC-MS metabolomics results comparing one carbon metabolism between Myc310 MGTs and Myc310 LMs. 108
Figure 4-9. Regression analysis of metabolite levels with metastasis size 111
Figure 5-1. Immunofluorescent staining of Myc310 cells, and cells isolated from the lungs of mice with Myc310 MGTs. 114
Figure 5-2. Lung metastasis model to assess environmental impact and flexibility of metabolic changes between MGTs and LMs. 116
Figure 5-3. LC-MS metabolomics results comparing glycolysis metabolite levels and ^{13}C6-glucose label incorporation between Myc310 MGTs and LM MGTs. 118
Figure 5-4. LC-MS metabolomics results comparing levels and enrichment of lactate. 120
Figure 5-5. LC-MS metabolomics results comparing PPP intermediates in Myc310 MGTs and LM MGTs. 121
Figure 5-5. LC-MS metabolomics results comparing TCA cycle metabolites. 123
Figure 5-6. LC-MS metabolomics results comparing glutamine and glutamate. 124
Figure 5-7. LC-MS metabolomics results comparing one carbon metabolism intermediates, glutathione and EAAs glutamine in Myc310 MGTs and LMs. 126
Figure 5-8. LC-MS metabolomics results comparing nucleotides. 127
Figure 5-10. LC-MS metabolomics results comparing metabolite levels between heavy isotope infusion experiments. 131
Figure 5-11. LC-MS metabolomics results comparing glycolytic and PPP glucose flux in LM MGTs and metastases derived from them (LM^{2}s). 133
Figure 5-12. LC-MS metabolomics results comparing TCA flux in LM MGTs and metastases derived from them (LM^{2}s). 135
Figure 5-13. LC-MS metabolomics results comparing TCA flux in LM MGTs and metastases derived from them (LM^{2}s) following ^{13}C5-glutamine infusions. 136
Figure 5-14. LC-MS metabolomics results comparing malate and fumarate. 138
Figure 5-15. LC-MS metabolomics results comparing NEAAs 140
Figure 5-16. LC-MS metabolomics results comparing alanine 141
Figure 5-17. LC-MS metabolomics results comparing EAAs 142
Figure 5-18. LC-MS metabolomics results comparing one carbon metabolism and contributing metabolites LM MGTs and metastases derived from them (LM^{2}s). 144

Figure 5-19. LC-MS metabolomics results comparing total fractional enrichment from in serum compared to LM MGT and LM^2s. 147
Figure 6-1. Immunofluorescent staining of a metastatic lung from a mouse that had a LM MGT. 153
Figure 6-2. DESI-MSI coverage of polar metabolites. 157
Figure 6-3. Histological segmentation of DESI-MSI images 162
Figure 6-4. DESI-MSI imaging of glutamine and glutamate. 164
Figure 6-5. DESI-MSI imaging of heavy isotope labelled glutamine and glutamate. 167
Figure 6-6. DESI-MSI imaging of TCA cycle intermediates 168
Figure 6-7. DESI-MSI imaging of nucleotides. 170
Figure 6-8. DESI-MSI distribution of glutathione and dimethylgycine. 172
Figure 6-9. DESI-MSI imaging of glucose 6-phosphate and lactate. 174
Figure 6-10. DESI-MSI imaging of other polar metabolites heterogeneously distributed in MGTs, in line with LC-MS findings. 176
Figure 6-11. DESI-MSI imaging of other polar metabolites heterogeneously distributed in MGTs, in contrast to LC-MS findings. 178
Figure 6-12. Intra-tumour metabolic heterogeneity linked to histological phenotypes 182
Figure 6-13. Module analysis of DESI-MSI data to assess metabolic heterogeneity. 184
Figure 6-14. Orbi-SIMS imaging shows heterogeneous metabolite distribution between tumour cells and stromal infiltrate in a Myc310 MGT 187
Figure 6-15. Metabolic heterogeneity between two metastatic lesions in the same lung lobe shown by DESI-MSI. 191
Figure 6-17. Metabolic heterogeneity between metastatic and wildtype lungs by DESI-MSI. 193
Figure 7-1. Metabolic heterogeneity between two metastatic lesions in the same lung lobe shown by DESI-MSI. 199
Figure 7-2. Metabolic heterogeneity between metastatic and wildtype by DESI-MSI. 201
Figure 7-3. Apolar LC-MS analysis of lipid classes between LM^2s and LM MGTs – higher fold change represents enrichment in LM^2s. 203

Figure 7-5. Peri-metastatic lipid accumulation in metastatic lung identified by Orbi-SIMS imaging. 208
Figure 7-6. Analysis of FASN distribution in the metastatic lung. 210
Figure 7-7. Immunofluorescence staining to identify which cells in the metastatic lung upregulate FASN. 212

List of Tables

Table 1: MMEC Media 62
Table 2: Collagenase Buffer 62
Table 3: SDS-PAGE gel (8%) 4x solution – 40 mL 63
Table 4: Stacking gel (4%) 4x solution – 20 mL 63
Table 5: Stable Isotope Labelled Metabolites 64
Table 6: Metabolite extraction reagents 64
Table 7: Antibodies 65
Table 8: DESI Imaging Parameters 76
Table 9: KEGG Pathways used for DESI-MSI spectra annotation 77
Table 10. DESI-MSI ion annotation to polar metabolites detected by LC-MS. 158

Abbreviations

1,3BPG	1,3-bisphosphoglycerate
2/3PG	2-/3-phosphoglycerate
3PHP	3-phosphohydroxypyruvate
3PS	3-phosphoserine
6GPL	6-phosphogluconolactone
6PG	6-phosphogluconate
6PGDH	6-phosphogluconate dehydrogenase
6PGL	6-phosphogluconolactonase
ACLY	ATP citrate lyase
ACON	aconitase
aKGDH	alpha-ketoglutarate dehydrogenase
ALDO	aldolase
ALT	alanine aminotransferase
AMP	adenosine monophosphate
ADP	adenosine diphosphate
ASCT2	alanine serine cysteine transporter 2
ASL	argininosuccinate lyase
ASNS	asparagine synthetase
ASS1	argininosuccinate synthase
ATP	adenosine triphosphate
BCAA	branched chain amino acid
BCAT	branched chain amino acid aminotransferase
BCKA	branched chain keto acid
BCKD	branched chain keto acid dehydrogenase
BPG	bisphosphoglycerate
CAT	cationic amino acid transporter
CoA	coenzyme A
CS	citrate synthase
DESI-MSI	Desorption Electrospray Ionisation Mass Spectrometry Imaging
DHAP	dihydroxyacetone phosphate
DHFR	dihydrofolate reductase

DNMT	DNA methyltransferase
ECM	extra-cellular matrix
EMT	epithelial-to-mesenchymal transition
ENO1	enolase
ER	estrogen receptor
F1,6BP	fructose 1,6-bisphosphate
F6P	fructose 6-phosphate
FDG-PET	fluorodeoxyglucose-positron emission tomography
FH	fumarase
G3P	glycerol 3-phosphate
G6P	glucose 6-phosphate
G6PDH	glucose 6-phosphate dehydrogenase
GA3P	glyceraldehyde 3-phosphate
GAPDH	glyceraldehyde 3-phosphate dehydrogenase
GC-MS	gas chromatography mass spectrometry
GLDC	glycine decarboxylase
GLS	glutaminase
GLUD	glutamate dehydrogenase
GLUT1	glucose transporter 1
GMP	guanosine monophosphate
GNMT	glycine methyltransferase
GOT1/2	aspartate aminotransferase 1/2
GPI	glucose 6-phosphate isomerase
GS	glutamine synthetase
GSH	reduced glutathione
GSSG	oxidized glutathione
GTP	guanosine triphosphate
H&E	haematoxylin & Eosin staining
HER2	human epidermal growth factor receptor 2
HK	hexokinase
HKMT	histone methyltransferase
IDH	isocitrate dehydrogenase
IDO	indoleamine-2,3,-deoxygenase
KMO	kynurenine-3-monooxygenase

KYNU	kynureninase
LAT1	L-type amino acid transporter 1
LC-MS	liquid chromatography mass spectrometry
LDH	lactate dehydrogenase
LM	lung metastasis
MAT	methionine amino transferase
MDH	malate dehydrogenase
MGT	mammary gland tumour
MMTV	mouse mammary tumour virus
MPC	mitochondrial pyruvate transporter
MS	methionine synthase
MTHFR	methylenetetrahydrofolate reductase
mTOR	mechanistic target of rapamycin
NAD(P)H	nicotinamide adenine dinucleotide (phosphate)
P5C5	pyrroline 5-carboxylate synthase
PAH	phenylalanine hydroxylase
PDH	pyruvate dehydrogenase
PEP	phosphoenolpyruvate
PFK	phosphofructokinase
PGK1	phosphoglycerate kinase 1
PGM	phosphoglucomutase
PHGDH	phosphoglycerate dehydrogenase
PKM2	pyruvate kinase 2
PPP	pentose phosphate pathway
PR	progesterone receptor
PSAT	phosphohydroxythreonine aminotransferase
PYCR	pyrroline 5-carboxylate reductase
qPCR	quantitative polymerase chain reaction
REDOX	reduction and oxidation
R5P	ribose-5-phosphate
ROS	reactive oxygen species
RPE	ribulose 5-phosphate epimerase
RPI	ribulose 5-phosphate isomerase
Ru5P	ribulose 5-phosphate

SAH	S-adenosyl homocysteine
SAM	S-adenosyl methionine
SARDH	sarcosine dehydrogenase
SCS	succinyl-CoA synthetase
SDH	succinate dehydrogenase
SHMT1/2	serine hydroxymethyltransferase 1/2
SMA	smooth muscle actin
S7P	sedoheptulose-7-phosphate
TALDO	transaldolase
TAM	tumour-associated macrophage
TCA	tricarboxylic acid cycle
TKT	transketolase
TME	tumour microenvironment
TNBC	triple negative breast cancer
X5P	xylulose 5-phosphate
xCT	cystine/glutamate transporter

Chapter 1. Introduction

1.1 Cancer

Cancer is an overarching term for a diverse collection of more than 200 types of diseases that are characterised by uncontrolled cell growth. Cancer remains a leading cause of death worldwide, with 19.3 million new cases and nearly 10 million deaths in 2020 [1]. There were 367,167 new cancer cases in the UK alone in 2017, and 166,533 deaths [2]. Due to the complex and diverse mechanisms driving different types of cancer, continued efforts in cancer research are necessary for advancing our understanding of disease progression and development of novel therapeutic strategies.

Cancers are distinguished based on tissue and cell type of origin, and further classified by specific driver oncogenes. Oncogenes are genes that typically control key cellular processes such as cell growth, division, apoptosis and metabolism in healthy cells. However, when these genes acquire mutations or amplifications, they can instigate a cascade of alternative events in the cell, eventually leading to neoplastic disease. Cancer initiation and progression is a complex, multistep process and several key changes in normal cell behaviour have been defined as the hallmarks of cancer [3], [4]. These include not only increased proliferation and continuous replicative immortality, but also evasion of cell death and innate immune responses, and resistance to anti-proliferative signalling [4], [5]. Furthermore, cancer cells need to upregulate existing or new metabolic pathways to meet the increased bioenergetic demands of hyperproliferation [6]–[8], and instigate angiogenesis to maintain a sufficient supply of oxygen and nutrients to the fast-growing cells [9]–[12]. As cancer progresses, uncontrolled growth often drives further genetic deregulation, and unfortunately it is often the case that by the time the disease is detected in a patient, the fully-formed tumour is comprised of heterogeneous cell population that require multiple convoluted treatment strategies [13]–[17].

1.2 Breast cancer

1.2.1 Disease statistics

Breast cancer is the most diagnosed cancer, and the leading cancer type among women globally, with an estimated 2.3 million new cases in 2020 [1]. It is also the leading cancer type in women in the UK, with 54,724 new cases in 2017 [18]. Despite high incidence, the prognosis for breast cancer is quite positive compared to other cancer types, with a 76% chance of ten-year survival following diagnosis in the UK [19]. This is largely due to increased incidence of early detection diagnostics strategies, as well as reliable surgical treatment options. However, when breast cancer is detected at a late stage, characterised by cancer cells evading the primary site and disseminating into the vasculature, lymphatic system and eventually, other organs in the body, the survival rate decreases to 25% of a 5-year survival post-diagnosis [20]. Metastatic breast tumours have been shown to be resistant to chemotherapy treatments, due to acquisition of additional mutations or environmentally-driven adaptations in response to new stresses and survival requirements [21], [22].

1.2.2 Breast Cancer Subtypes

Breast cancer is a notoriously heterogeneous disease, which has been stratified into subtypes based on the expression status of the hormone receptors oestrogen receptor (ER) and progesterone receptor (PR), as well as the human epidermal growth factor receptor 2 (HER2) [23], [24]. Breast cancer subtypes reflect distinct gene expression profiles, morphologies and treatment strategies. The subtypes described below are in order from best to worst clinical prognosis [25]–[27].

The most common subtype is Luminal A, found in approximately 40% of all breast cancer cases [24], categorised by positive hormone receptor status (ER+ and/or PR+), and negative HER2 expression. Similar to Luminal A, the normal-like subtype is found in 2-8% of cases and is also hormone receptor positive and HER2 negative, however with worse prognosis than Luminal A tumours [28]. The Luminal B subtype (20% of cases [29]) is also hormone receptor positive (ER+ and/or PR+)

and can be either HER2 positive or negative, with a particular characteristic of higher proliferation rates as shown by high Ki67 expression [30]. The HER2-enriched subtype (10-15% of cases [24]) is hormone receptor negative (ER-, PR-) and HER2 positive. Finally, the triple negative subtype (TNBC, 15-20% of cases [24]) is negative for both hormone receptors as well as HER2 (ER-, PR-, HER2-).

Therapeutic strategies specifically targeting the aforementioned receptors have been the widely accepted based on breast cancer subtype, since downstream signalling pathways promote key oncogenic processes such as proliferation [31], [32], differentiation [33]–[35], and apoptosis evasion [36], [37] (further reviewed in [38]). Inhibitors of the oestrogen receptor, such as tamoxifen [39], [40] and fulvestrant [41], [42], are used against ER+ breast cancers (Luminal A, normal-like, Luminal B), while the monoclonal antibody against HER2, trastuzumab (Herceptin) is used against HER2-enriched breast tumours [43]. However, resistance to these therapeutics is common, especially with Herceptin, whereby 70% of patients develop resistance after one year of treatment [44]. Furthermore, targeted treatment options for TNBC are limited beyond traditional chemo- and radiotherapy [45], despite patients having the worst prognosis compared to other breast cancer subtypes [46]. Hence, there remains a clear need for alternative therapeutic strategies that will target downstream effector pathways of the diverse oncogenic signalling programs across breast cancer subtypes.

Recently, several studies employed new diagnostics tools such as DNA microarrays to further stratify breast cancer and identify links between histological subtypes and clinical outcomes [23], [47], [48]. Within the five overarching subtypes of breast cancer, tumour samples have been further classified based on specific pathway activity [49] and protein biomarkers [50], providing accurate diagnostics tools and determinants for combinational therapy strategies. Furthermore, several studies have focused specifically on metabolic distinctions between breast cancer subtypes [51]. For example, TNBC tumours have been shown to be sensitive to arginine depletion [52] and the inhibition of serine biosynthesis from glucose via the phosphoglycerate dehydrogenase (PHGDH) reaction [53]–[55]. Different subtypes of breast cancer have also been shown to rely on different sources of specific metabolites, such as increased *de novo* biosynthesis of fatty acids in luminal

subtypes and increased import of exogenous fatty acids in TNBC [56]. Given the heterogeneity across breast cancer subtypes, based on genomic, proteomic and histological classifications, it is important to also consider metabolic reprogramming when developing therapeutic strategies.

1.3 Cancer metabolism

One of the key hallmarks of cancer is deregulated metabolism [4]. As the tumour grows, cancer cells are faced with mounting stresses in their environment. Increased proliferation leads to an increase in bioenergetic demands and additional nutrient requirements to maintain cell growth, division and migration [8], [57], [58]. Furthermore, the tumour microenvironment (TME) often has limited nutrient and oxygen availability due to insufficient vascularisation [59], [60]. Cancer cells adapt by promoting angiogenesis and adapting to hypoxic conditions by upregulating anaerobic metabolic pathways [61], [62]. Metabolic flexibility – the ability to use different nutrient sources to fuel specific metabolic pathways, allows cancer cells to survive in stressful conditions when nutrient availability becomes limited [13], [63]–[66]. Tumour cells can also demonstrate metabolic plasticity by rewiring the metabolism of a specific nutrient through alternative metabolic pathway [67], [68]. Such metabolic adaptations can promote cancer progression and support increased bioenergetic demands as the tumour grows, however upregulation of cancer-specific metabolic pathways can also lead to metabolic dependencies, which can be exploited as therapeutic strategies [69]–[72]. The field of cancer metabolism focuses on identifying metabolic vulnerabilities in different tumours or tumour cell populations. While some metabolic adaptations are specific to a particular tumour type, many trends of tumour metabolic rewiring have been observed across many tumour types [73]–[76].

1.3.1 Glycolysis

Glucose is a primary nutrient for healthy and cancerous cells. Glucose is catabolised to pyruvate in the process of glycolysis, producing energy in the form of adenosine triphosphate (ATP) and the reductive cofactor nicotinamide adenine dinucleotide (NADH). Glycolytic intermediates feed in to multiple other metabolic pathways, including the pentose phosphate pathway (PPP) and nucleotide biosynthesis, the hexosamine biosynthesis pathway for protein glycosylation, the one carbon metabolism pathway via serine production, and *de novo* lipogenesis through production of glycerol-3-phosphate (G3P) (Figure 1-1). Pyruvate, the end product of glycolysis, is typically used as a substrate for the tricarboxylic acid (TCA) cycle, for further energy and biomass production. Pyruvate can also be used to produce alanine for protein synthesis and additional catabolism. Furthermore, pyruvate can be converted into lactate during anaerobic glycolysis, which takes place in some healthy tissues such as skeletal muscle when oxygen availability is limited [77], [78], or through aerobic glycolysis in highly proliferative tissues such as the gut [79]–[81].

Almost a century ago, the earliest observation of deregulated metabolism in cancer cells was Otto Warburg's discovery of cancer cells engaging in the process of aerobic glycolysis [82]. This process, coined as "the Warburg effect" by Efraim Racker in the 1970s [83], was the observation that cancer cells preferentially convert pyruvate into lactate, despite sufficient oxygenation. The Warburg effect has been widely studied in the field of cancer metabolism in the past century in order to understand why different type of cancer cells undergo this metabolic switch.

Oxidative phosphorylation is a much more efficient pathway for ATP production: 38 molecules of ATP are produced from one molecule of glucose, compared to just 2 molecules of ATP produced from glucose in aerobic glycolysis [84], [85]. However, glucose catabolism into lactate has been shown to occur 10-100 times faster than the full oxidative phosphorylation of glucose-derived pyruvate in the mitochondria [86]. Lactate has also been shown to be a direct substrate for mitochondrial oxidative phosphorylation in some cancer types [87]–[89]. Using an elegant model

of stable isotope labelling of lactate and glucose, it has been demonstrated that the flux of lactate through central carbon metabolism is higher than that of glucose in most healthy organs and in models of murine lung and pancreatic cancer [90]. Indeed, lactate taken up via the monocarboxylate transporter-1 (MCT1) was shown to be a predominant carbon source for the TCA in a model of human non-small cell lung cancer (NSCLC), and deleting this transporter reduced tumour growth [88]. On the contrary, another recent study employed metabolic flux analysis and mathematical modelling to show that the key substrate for the TCA is glucose rather than lactate in healthy tissues [91]. Cancer cells are known to upregulate the GLUT family of glucose transporters to support their increased glucose demands [92]–[94]. Preferential glucose uptake by most types of cancer cells is the basis of the fluorodeoxyglucose-positron emission tomography (FDG-PET) diagnostic tool, which uses a radioactive glucose analogue to visualise cancer occurrence and dissemination in the body [95]. Taken together, these findings suggest that cancer cells undergoing aerobic glycolysis still have the capacity to produce sufficient ATP needed for proliferation.

Apart from energy, proliferating cells require increased biomass production to sustain rapid cell division. Cancer cells that do not rely on oxidative phosphorylation for energy production more readily redirect glycolytic intermediates towards anabolic pathways such as gluconeogenesis, nucleotide biosynthesis via the PPP, as well as lipid and amino acid production [96]. Lactate synthesis from pyruvate also produces the oxidised nicotinamide adenine dinucleotide (NAD+) cofactor, which is needed to support upstream glycolytic reactions [97]. Finally, excreted lactate leads to acidification of the tumour microenvironment (TME), which has been shown to promote tumour cell migration [98]–[100] and angiogenesis pathways [101], [102]. Lower pH in the TME due to excess lactate production has also been shown to attenuate CD8+ T cell infiltration and cytotoxic response [103], [104], and stimulates tumour-associated macrophage (TAM) activation [105]. Hence, increased glycolysis and lactate production is a typical characteristic of cancer cells that provides the energy and biomass necessary for rapid proliferation, and directly promotes tumour progression and immune evasion.

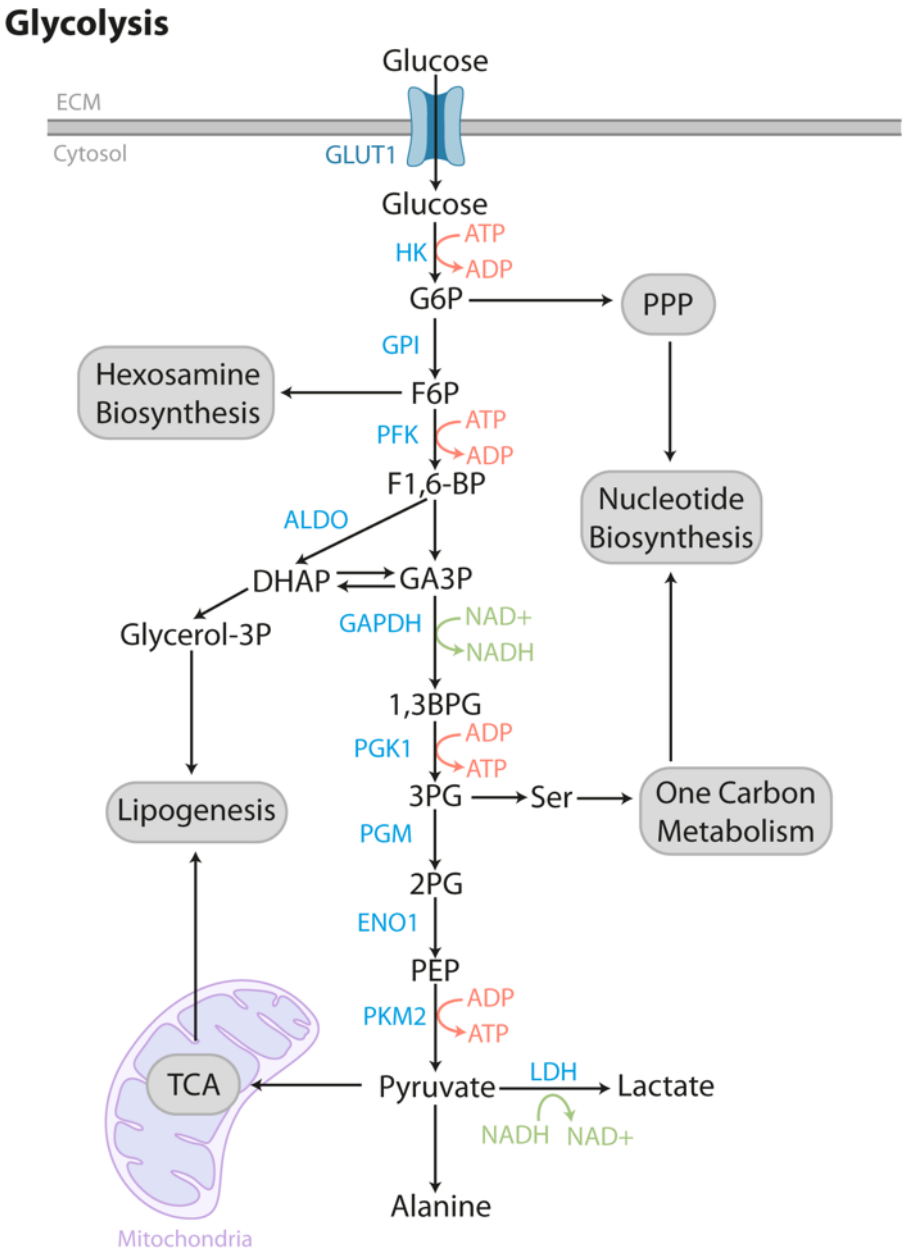


Figure 1-1. The mammalian glycolysis pathway and other downstream metabolic pathways.

Metabolites: G6P = glucose 6-phosphate, F6P = fructose 6-phosphate, F1,6BP = fructose 1,6-bisphospahte, DHAP = dihydroxyacetone phosphate, GA3P = glyceraldehyde 3-phosphate, 1,3BPG = 1,3-bisphosphoglycerate, 3PG = 3-phosphoglycerate, 2PG = 2-phosphoglycerate, PEP = phosphoenolpyruvate. Enzymes and transporters (blue): GLUT1 = glucose transporter 1, HK = hexokinase, GPI = glucose 6-phosphate isomerase, PFK = phosphofructokinase, ALDO = aldolase, GAPDH = glyceraldehyde 3-phosphate dehydrogenase, PGK1 = phosphoglycerate kinase, PGM = phosphoglucomutase, ENO1 = enolase, PKM2 = pyruvate kinase, LDH = lactate dehydrogenase. Pathways (grey): PPP = pentose phosphate pathway, TCA = tricarboxylic acid cycle.

1.3.2 The Pentose Phosphate Pathway

The PPP uses glucose-derived glucose-6-phosphate (G6P) to produce ribose-5-phosphate (R5P), a vital precursor for nucleotide biosynthesis (Figure 1-2). As described above, increased glycolytic rates and a switch to aerobic glycolysis results in a redirection of glucose carbons into the PPP in many cancer types to support rapid cell division. Importantly, the PPP also produces two molecules of the reductive cofactor nicotinamide adenine dinucleotide phosphate (NADPH), which is essential for cellular protection against oxidative stress [106]. NADPH is essential for maintaining the REDOX balance in cells by regenerating reduced glutathione (GSH) from oxidised glutathione (GSSG) [107]. Hyperproliferation and oxidative phosphorylation leads to increased levels of ROS in tumours, especially when oxygen supply is not limited in well-vascularised tumours and oxygen-rich organs such as the lungs [108]–[112]. PPP upregulation was shown to be coupled to increased ROS levels in cancer [113]–[115]. Furthermore, transcription factors promoting the epithelial to mesenchymal transition (EMT) in cancer progression directly upregulate the PPP in order to support increased oxidative stress in the process of metastasis [116], [117].

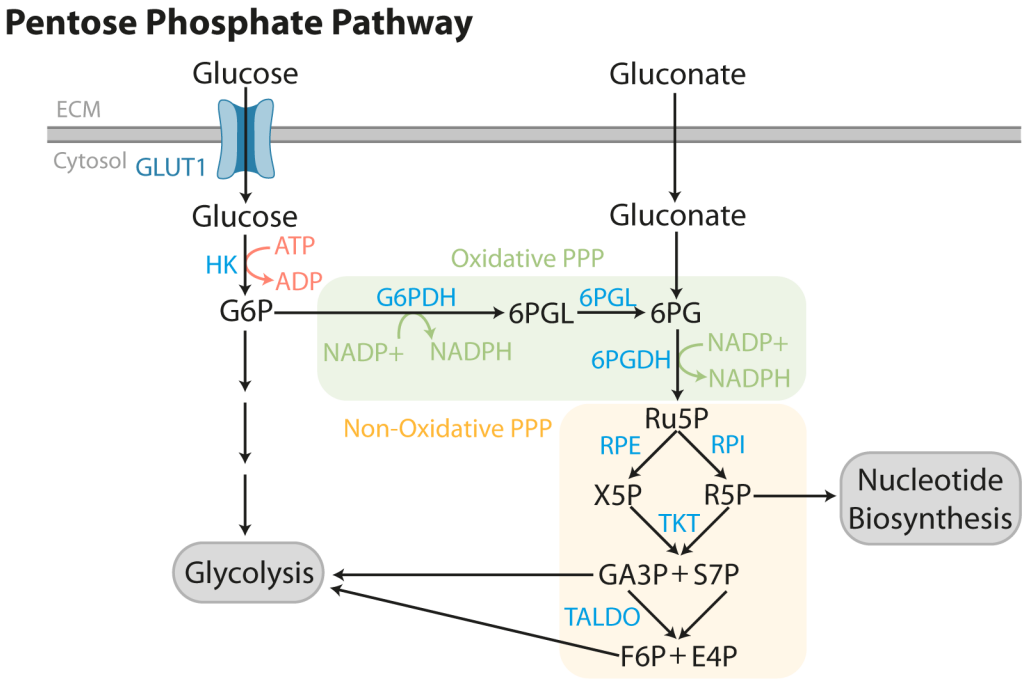


Figure 1-2. The mammalian pentose phosphate pathway: oxidative and non-oxidative branches.

Metabolites: G6P = glucose 6-phosphate, 6PGL = 6-phosphogluconolactone, 6PG = 6-phosphogluconate, Ru5P = ribulose 5-phosphate, X5P = xylulose 5-phosphate, R5P = ribose 5-phosphate, GA3P = glyceraldehyde 3-phosphate, S7P = sedoheptulose 7-phosphate. Transporter and enzymes (blue): GLUT1 = glucose transporter 1, HK = hexokinase, G6PDH = glucose 6-phosphate dehydrogenase, 6PGL = 6-phosphogluconolactonase, 6PGDH = 6-phosphogluconate dehydrogenase, RPE = ribulose 5-phosphate epimerase, RPI = ribulose 5-phosphate isomerase, TKT = transketolase, TALDO = transaldolase.

1.3.3 The Tricarboxylic Acid Cycle

In healthy tissues and given sufficient oxygen availability, pyruvate, the end product of glycolysis, is converted into acetyl-CoA and catabolised in the mitochondrial TCA through oxidative phosphorylation (Figure 1-3). The second major source of carbons for the TCA is glutamine, and the incorporation of glutamine as a major carbon source for the TCA is increased in many cancers, especially when glucose is redirected towards alternative metabolic pathways [118]–[120]. Fatty acids can also feed in to the TCA, via beta-oxidation to produce acetyl-CoA [121]–[123]. Finally, most essential and non-essential amino acids can feed in to anaplerosis reactions that contribute to TCA intermediate pools [124]–[128], and several NEAAs can in turn be synthesized as a result of cataplerotic reactions stemming from the TCA [129]–[132].

The primary function of the TCA in healthy cells is to generate substrates for oxidative phosphorylation of carbons, which leads to the production of ATP by the electron transport chain. Apart from ATP production, TCA intermediates can be used for non-essential amino acid (NEAA) biosynthesis, and acetyl-CoA can be diverted into the *de novo* fatty acid biosynthesis pathway or catabolised for acetylation [133]. Finally, the TCA generates potent reductive cofactors needed for neutralising ROS, NADH and flavin adenine dinucleotide hydroquinone form (FADH2) [134], [135]. The TCA is a metabolic focal point for energy, biomass and reductive potential, all of which are excessively required by highly proliferative cancer cells. Therefore, the enzymes and transporters involved in feeding and driving the TCA are often deregulated in cancer progression [136]–[141] and directly controlled by key oncogenes such as MYC [120], [142]–[144], KRAS [145]–[147] and HIF-1α [148]–[150].

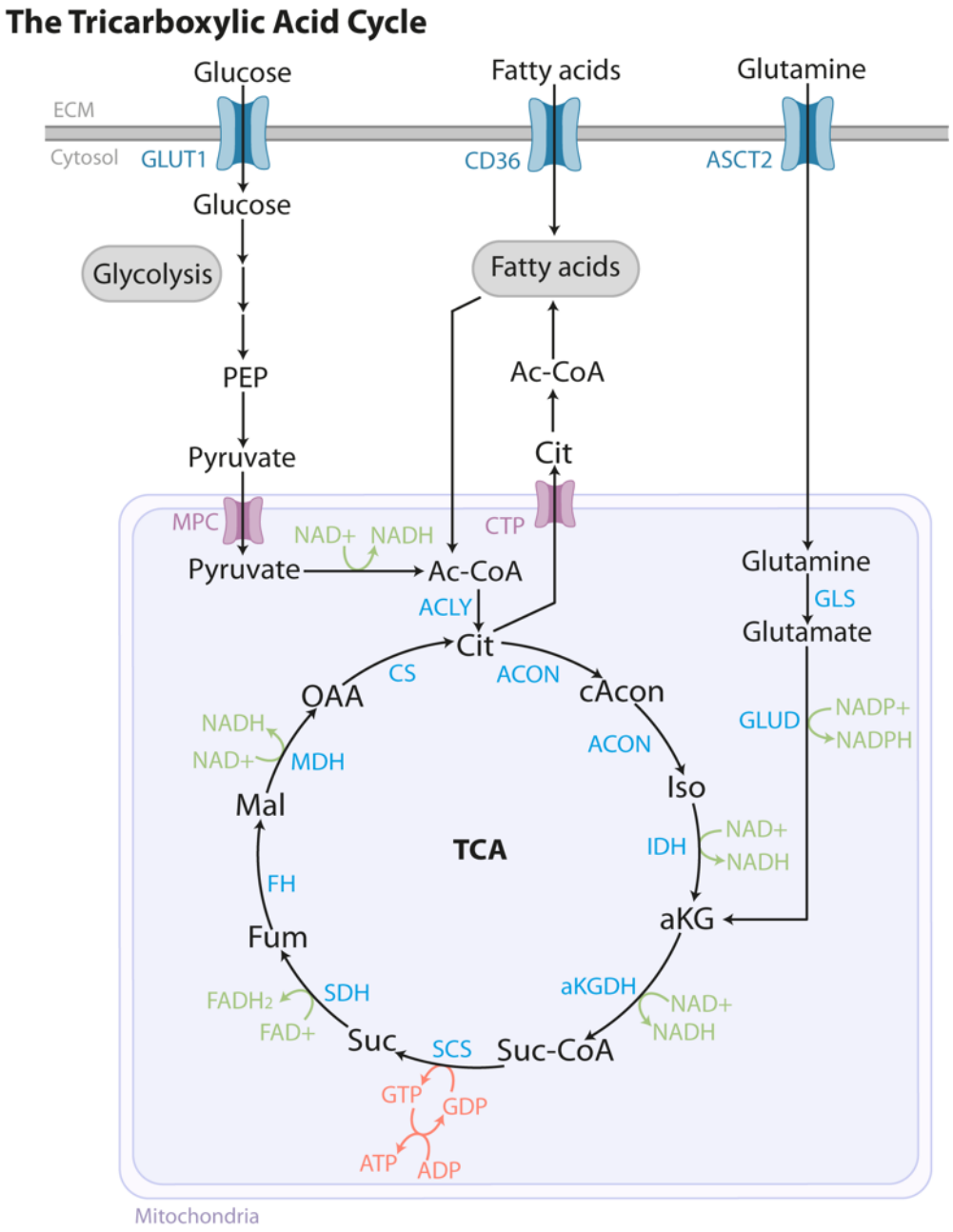


Figure 1-3. The mammalian tricarboxylic acid cycle and the three main carbon sources (glucose, fatty acids, glutamine).

Metabolites: Ac-CoA = acetyl CoA, Cit = citrate, cAcon = cis-aconitate, Iso = isocitrate, aKG = alpha-ketoglutarate, Suc-CoA = succinyl CoA, Fum = fumarate, Mal = malate, OAA = oxaloacetate. Transporters: GLUT1 = glucose transporter 1, CD36 = fatty acid transporter, ASCT2 = alanine serine cysteine transporter 2, MPC = mitochondrial pyruvate transporter (inner mitochondrial membrane), CTP = citrate transporter. Enzymes: PDH = pyruvate dehydrogenase, ACLY = ATP citrate lyase, ACON = aconitase, IDH = isocitrate dehydrogenase, aKGDH = alpha-ketoglutarate dehydrogenase, SCS = succinyl-CoA synthetase, SDH = succinate dehydrogenase, FH = fumarase, MDH = malate dehydrogenase, CS = citrate synthase, GLS = glutaminase, GLUD = glutamate dehydrogenase.

1.3.4 Non-essential amino acid metabolism

1.3.4.1 Glutamine and glutamate

Glutamine is the most abundant amino acid in blood and is readily consumed by proliferating cells. Glutamine is imported via the alanine/serine/cysteine transporter 2 (ASCT2) transporter, which is upregulated in many cancer types [151], [152], and is a promising emerging target in cancer therapy [153]. As described above, glutamine is a major carbon source for the TCA via conversion into glutamate and aKG. The nitrogen groups of glutamine are needed for synthesis of other key metabolites [13], including nucleotides [154], [155], glucosamine [156], REDOX cofactors [157] and other NEAAs [158], [159]. Glutamine conversion into glutamate via glutaminase (GLS) is a major rate-limiting step in cancer metabolism, and GLS inhibition has been proposed as a potential therapeutic target [160], [161], especially in breast cancer [72]. Glutamate conversion into TCA intermediates and other NEAAs is modulated by glutamate dehydrogenase (GDH) and aminotransferase enzymes, resulting in production of aKG, as well as alanine, aspartate and proline (Figure 1-4).

1.3.4.2 Alanine, aspartate, asparagine, arginine and proline.

Alanine has been shown to be important for proliferation [162], [163], maintenance of the TCA carbon pool [164] and metastasis [165].

Aspartate is produced from oxaloacetate and glutamate by aspartate aminotransferase (GOT) and acts as a cytosolic nitrogen donor to the urea cycle. The urea cycle is used to excrete excess ammonia produced during amino acid catabolism [166], [167]. Aspartate is combined with the mitochondria-derived nitrogen donor citrulline, to produce argininosuccinate by argininosuccinate synthetase. Argininosuccinate is then converted into fumarate and arginine, and urea is released when arginine is converted into ornithine. Ornithine is then transported back into the mitochondria, where the cycle is completed with ornithine and carbamoyl phosphate combining to form citrulline [167]–[169]. Several studies have demonstrated a downregulation of the urea cycle in cancer in order to preserve nitrogen for pyrimidine production and favour proliferation [169], [170],

and a recent study highlighted that urea cycle suppression can result in an increased mutational burden and therefore cancer progression in cancer patients due to unbalanced levels of purines and pyrimidines [166].

Aspartate also mediates the transport of electrons from the cytosol into the mitochondria via the malate-aspartate shuttle [171]. The reductive cofactor NADH is produced during glycolysis and is required to neutralise the electrons produced in the mitochondrial electron transport chain. Aspartate is transported out of the mitochondria via the aspartate-glutamate carrier (AGC) transporter, and is converted to oxaloacetate in the cytosol, which in turn is reduced to malate via malate dehydrogenase using NADH. Malate is then transported back into the mitochondria via the 2-oxoglutarate carrier (OGC) transporter, where it can be oxidized back into oxaloacetate in the TCA, yielding NADH from NAD+ and thus transferring the reductive potential back into the mitochondria[172]–[176]. Finally, aspartate can also be converted to asparagine via asparagine synthetase (ASNS), which is required for protein synthesis and metabolic pathway regulation via the mechanistic target of rapamycin (mTOR) [177]. Aspartate is more readily synthesized within cancer cells than taken up from external sources [159], [178], emphasizing its importance for cancer survival, especially under hypoxic conditions [179].

Another NEAA that is produced from glutamate is proline, which is important for collagen synthesis and degradation in the extracellular matrix (ECM) [180], which has been shown recently to be particularly important during metastatic colonisation in the lung [181]. Proline also supports cancer cell survival under hypoxic conditions [182] and was shown to be a rate-limiting metabolite in kidney cancer protein synthesis [183].

1.3.4.3 Serine, glycine and cysteine

Apart from energy and biomass production, some NEAAs contribute to cellular protection against ROS and play a role in epigenetic modifications. Serine is synthesized from the glycolytic intermediate 3-PG, and requires glutamate as a nitrogen source for the phosphoserine aminotransferase (PSAT) reaction. Serine is converted into glycine, simultaneously donating a carbon to the one carbon

metabolism pathway (Figure 1-4). The one carbon metabolism pathway and its contribution to antioxidant and methylation pathways is described in further detail below.

Both of the enzymes responsible for serine synthesis from 3PG, phosphoglycerate dehydrogenase (PHGDH) and PSAT, were shown to be deregulated in cancer [184]–[188] and several studies showed that inhibition of these enzymes reduced tumour growth [54], [189]. Since serine and glycine can be imported from the blood, recent studies have showed that combining serine biosynthesis inhibitors with a serine and glycine deficient diet significantly reduced cancer cell growth and survival due to reduced protein synthesis [186], [190]. Apart from donating its methyl group to the one carbon metabolism pathway, serine has been shown to allosterically regulate the glycolytic enzyme pyruvate kinase M2 (PKM2) [191], and is important for nucleotide [192], [193] and lipid biosynthesis [194], [195].

Serine is also required for cysteine biosynthesis in the transsulfuration pathway, in which the one carbon metabolism intermediate homocysteine is combined with serine to produce cystathionine, and subsequently cysteine (Figure 1-4). Cysteine is integral for protein folding and enzyme catalysis due to its unique thiol side chain [196], [197]. The thiol group also allows cysteine to form disulphide bonds, which are crucial not only in protein synthesis but also in the antioxidant response mediated by glutathione [198]–[200], discussed in more detail below. Most of intracellular cysteine is taken up from the extracellular space in the form of the oxidized dimer cystine, which is imported into cells through the xCT transporter. The xCT transporter requires simultaneous export of glutamate, and this ties glutamine metabolism to protein folding and antioxidant defence. Depletion of intracellular cysteine was shown to reduce cancer cell growth and elevate intracellular ROS in models of leukaemia, breast and prostate cancer [201], and therapeutic inhibition of xCT have shown promising results in reducing breast cancer growth *in vivo* [202], emphasizing the importance of cysteine metabolism for cancer survival.

1.3.4.4 Tyrosine (and phenylalanine)

Tyrosine is a key amino acid in protein biosynthesis, particularly in tyrosine kinase signalling pathways, which are regularly mutated in cancer and drive oncogenic transformations [203]–[207]. Notably, the tyrosine kinase epidermal growth factor receptor (EGFR) was shown to be mutated in 40% of adenocarcinomas in a 617 patient cohort [208]. Tyrosine is produced from the essential amino acid (EAA) phenylalanine, and deprivation of both phenylalanine and tyrosine was shown to decrease survival and migration of prostate and melanoma cells *in vitro*, due to downregulation of focal adhesion kinase and extracellular-regulated kinase (ERK) signalling [209]–[211]. The role of other EAAs in cancer is discussed below.

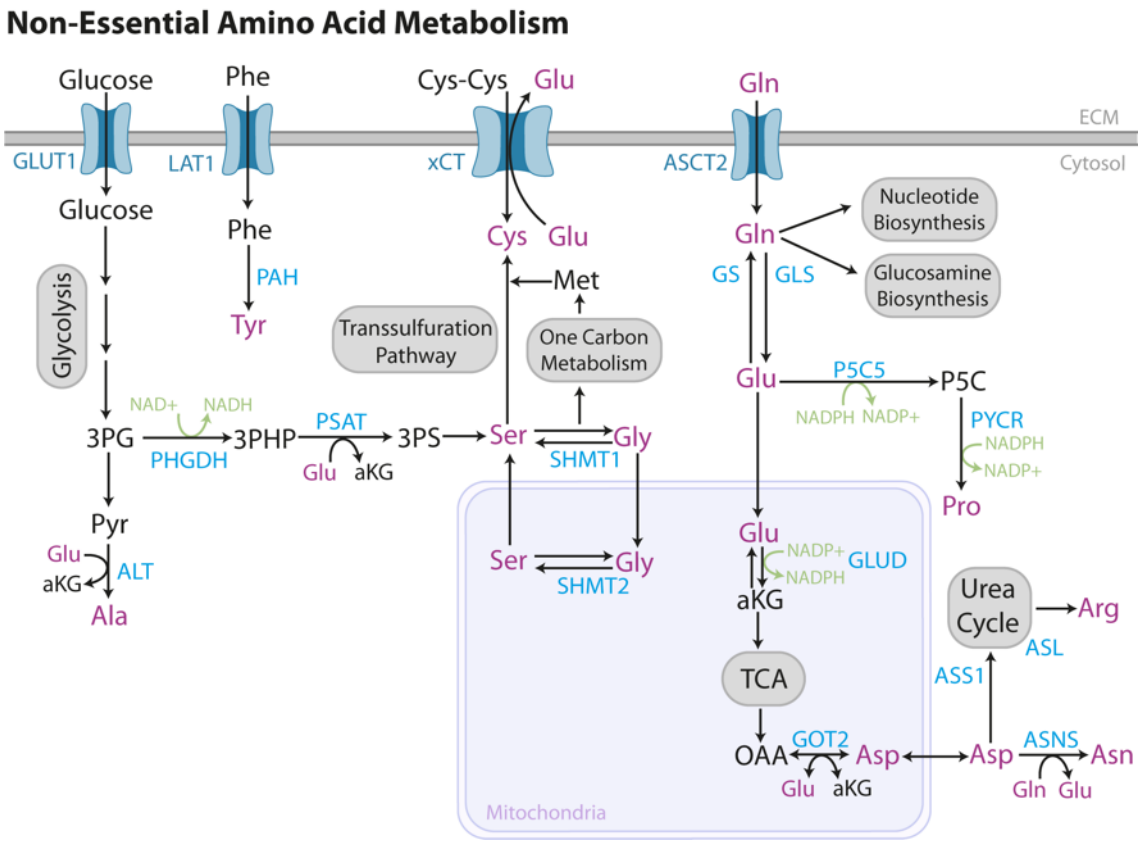


Figure 1-4. Non-essential amino acid metabolism pathways.

NEAAs shown in purple. Transporters: GLUT1 = glucose transporter 1, xCT = cystine/glutamate transporter, ASCT2 = alanine serine cysteine transporter 2, LAT1 = L-type amino acid transporter 1. Enzymes: ALT = alanine aminotransferase, PHGDH = phosphoglycerate dehydrogenase, PSAT = phosphohydroxythreonine aminotransferase, SHMT1/2 = serine hydroxymethyltransferase 1/2, GS = glutamine synthetase, GLS = glutaminase, GLUD = glutamate dehydrogenase, GOT2 = aspartate aminotransferase 2, ASNS = asparagine synthetase, ASS1 = argininosuccinate synthase, ASL = argininosuccinate lyase, P5C5 = pyrroline 5-carboxylate synthase, PYCR = pyrroline 5-carboxylate reductase 1, PAH = phenylalanine hydroxylase. Metabolites: 3PG = 3-phosphoglycerate, Pyr = pyruvate, Ala = alanine, 3PHP = 3-phosphohydroxypyruvate, 3PS = 3-phosphoserine, Ser = serine, Gly = glycine, Cys = cysteine, Cys-Cys = cystine, Gln = glutamine, Glu = glutamate, P5C = pyrroline 5-carboxylate, Pro = proline, Phe = phenylalanine, Tyr = tyrosine, aKG = alpha-ketoglutarate, OAA = oxaloacetate, Asp = aspartate, Asn = asparagine, Arg = arginine.

1.3.5 Essential amino acid metabolism

1.3.5.1 Branched-chain amino acids

Mammals cannot synthetize EAAs and require uptake of these metabolites from the diet in order to fuel intracellular metabolic pathways. Three EAAs, leucine, isoleucine and valine, are structurally classified as branched-chain amino acids (BCAAs), and are imported into cells via the L-type amino acid transporter (LAT1), encoded by the *SLC7A5* gene [212], [213]. LAT1 transports BCAAs and other amino acids (Phe, Met, His, Trp, Tyr) into cells, in exchange for glutamine, histidine or tyrosine [214]. LAT1 was shown to be upregulated at least three-fold in a variety of cancer types (brain, colon, pancreas, melanoma, lung, mammary gland, ovary, and more) [215]. Since import of amino acids through LAT1 requires simultaneous export of other amino acids, the overexpression of LAT1 frequently correlated with overexpression of the glutamine transporter ASCT2 [215], and like ASCT2, the expression of LAT1 is under transcriptional control of the MYC oncogene [127], [216] as well as HIF2α [217], [218] and Notch [219].

BCAAs contribute to several key metabolic pathways that are required for increased proliferation in cancer cells (Figure 1-5). BCAAs are converted into branched-chain keto acids (BCKAs) via the branched-chain amino acid transaminases (BCATs), and BCKAs are then converted into acetyl-CoA, which can be used to fuel the TCA and *de novo* lipid biosynthesis [128], [220]–[222]. Overexpression of BCAT is common across different cancer types [223]–[228]. Furthermore, BCAAs, especially leucine, play an integral role in nutrient sensing and metabolic pathway regulation by mTOR [229], [230]. Leucine can directly activate mTOR complex 1 (mTORC1) by binding to Sestrin2 [231], and acetyl-CoA produced from leucine promotes acetylation of Raptor [232]. Hence, BCAA metabolism is integral for cancer metabolism and presents a viable target for potential therapeutic strategies.

1.3.5.2 Tryptophan

Tryptophan is another EAA that is important for cancer metabolism as it is responsible for the kynurenine production pathway. The role of kynurenine in cancer development is emerging in several recent studies, particularly in

immunosuppressive T-cell signalling and pro-tumorigenic TAM polarization [233]–[237]. The tryptophan-kynurenine pathway also produces quinolinic acid, a metabolite that can then be used to produce the reductive cofactor NADPH, which is required for protection against ROS in tumour growth and metastasis [234], [238]–[240].

1.3.5.3 Lysine

Lysine is a key EAA that is required for histone methylation, as well as ubiquitination and acetylation [241]–[244] and therefore is involved in numerous oncogenic signalling and metabolism rewiring pathways in cancer progression [245], [246]. Lysine can also be used to produce acetyl-CoA and glutamate [247], [248], and lysine deprivation was shown to reduce tumour growth *in vivo* [249]. Interestingly, a recent study in breast cancer has shown that lysine directly promotes ER+ breast cancer dissemination [250].

1.3.5.4 Methionine, histidine and threonine

Methionine is a unique EAA in that while it cannot be synthesized *de novo* in mammalian cells, intracellular methionine pools are continuously maintained via the methionine cycle, in which a methyl group from the folate cycle is transferred onto homocysteine, producing methionine. The folate and methionine cycles together make up the one carbon metabolism pathway, the role of which is described in more detail below. Briefly, this pathway is integral for transferring methyl groups towards DNA, RNA and protein methylation, as well as purine, polyamine and glutathione biosynthesis. The EAAs histidine and threonine are also linked to the one carbon metabolism; histidine donates a methyl group to tetrahydrofolic acid (THF) to help fuel the folate cycle and produce glutamate [251]–[253], while threonine is used to synthesize glycine, which in turn can be converted to serine in the mitochondria and also donate a methyl group to the folate cycle [254]–[256]. The one carbon metabolism pathway and its role in cancer progression is discussed in further detail below.

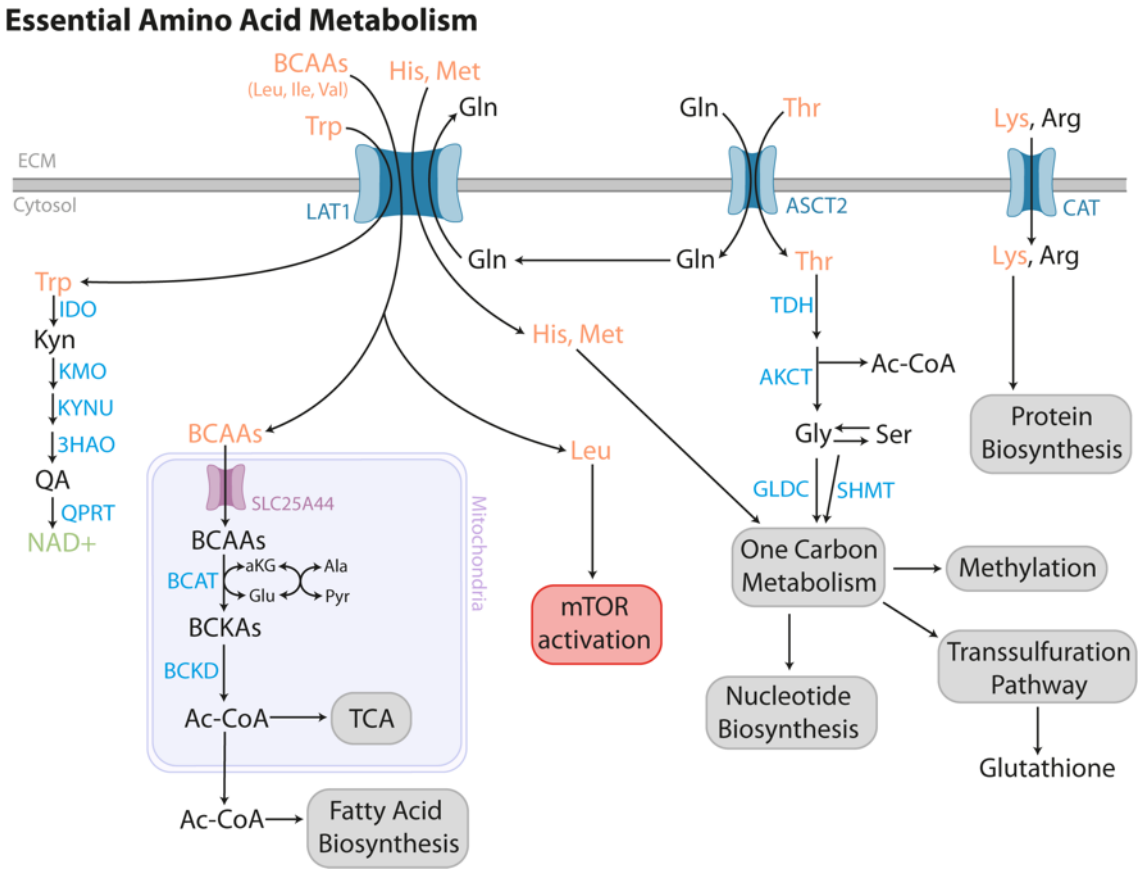


Figure 1-5. Essential amino acid metabolism pathways.

EAAs shown in orange. Folate cycle and methionine cycle are components of the one carbon metabolism pathway. Transporters: LAT1 = L-type amino acid transporter 1, ASCT2 = alanine serine cysteine transporter 2, CAT = cationic amino acid transporter. Enzymes: IDO = indoleamine-2,3-dioxygenase, KMO = kynurenine-3-monooxygenase, KYNU = kynureninase, 3HAO = 3-hydroxyanthranilate-3,4-dioxygenase, QPRT = quinolinate phosphoribosyltransferase, BCAT = branched-chain amino acid aminotransferase, BCKD = branched-chain keto acid dehydrogenase, GLDC = glycine decarboxylase, SHMT = serine hydroxymethyltransferase, AKCT = amino-ketobutyrate-CoA lyase, TDH = threonine-3-dehydrogenase, mTOR = mechanistic target of rapamycin. Metabolites: Trp = tryptophan, BCAAs = branched-chain amino acids (valine, leucine, isoleucine), Met = methionine, His = histidine, aKG = alpha-ketoglutarate, Glu = glutamate, Ala = alanine, Pyr = pyruvate, Ac-CoA = acetyl-CoA, Gly = glycine, Ser = serine, Lys = lysine, Arg = arginine.

1.3.6 One carbon metabolism and glutathione synthesis

1.3.6.1 Folate cycle

One carbon metabolism is composed of two metabolic pathways, the folate cycle and the methionine cycle. Folate is converted into THF, which is then able to accept a methyl group from serine or histidine, simultaneously producing either glycine or glutamate, respectfully. The methyl group can then be used for re-methylation of homocysteine to produce methionine, a reaction mediated by the co-factor vitamin B12 (Figure 1-6). Intermediates of the folate cycle also donate formyl and methylene functional groups for purine and pyrimidine biosynthesis. The integral role of the one carbon metabolism in cancer was first observed in the 1940s, with the observation that folate restriction in the diet of leukaemia patients reduced neoplastic cell numbers [257]. More recent studies demonstrated the role of serine and glycine in fuelling the folate cycle and thereby supporting increased nucleotide biosynthesis and antioxidant pathways in cancer progression [186], [190], [193], [258]–[262]. Furthermore, the folate pathway contributes ATP production [263] and replenishes NADPH pools and therefore contributes to antioxidant defence [264], [265].

1.3.6.2 Methionine cycle

Methionine and ATP are used for the production of S-adenosyl-methionine (SAM), which in turn donates the methionine-derived methyl group towards various methylation reactions, yielding S-adenosyl-homocysteine (SAH) [266], [267] (Figure 1-6). The glycine methyltransferase (GNMT) reaction transfers the SAM-derived methyl group onto glycine to produce sarcosine, which can then be directed back into the folate cycle [268]. The resulting SAH is converted back to homocysteine, releasing free adenosine. Homocysteine then accepts a methyl group from methyl-THF or choline-derived betaine to replenish methionine pools. Homocysteine also acts as an important substrate of the transsulfuration pathway to produce cystathionine and glutathione, described in further detail below.

Apart from its role as a methyl group donor, SAM can also undergo decarboxylation to fuel polyamine biosynthesis [269]–[271]. Importantly, decarboxylated SAM has

been shown to directly inhibit DNA methyltransferases, and therefore activation of the polyamine biosynthesis pathway can have a direct effect on epigenetic regulation [269], [272]. The polyamine biosynthesis pathway is under direct control of the MYC oncogene [273]–[275], is upregulated in several cancer types [276]–[279], and is being considered for therapeutic interventions [271], [280], [281]. Furthermore, SAM modulates mTORC1 sensing of intracellular methionine levels by activating the SAMTOR protein. When methionine and therefore SAM levels are low, SAMTOR is free to bind to the GATOR1 complex and mediates inhibition of mTORC1 and its downstream signalling pathways [282]–[284].

1.3.6.3 Transsulfuration pathway and glutathione metabolism

In the transsulfuration pathway, homocysteine is combined with serine to produce cystathionine, which in turn is used to make cysteine. Although cysteine can be taken up from the ECM in the form of cystine in healthy tissues, cystine concentration in tumour interstitial fluid was decreased compared to plasma levels in several tumour models [147], [285]. The two key enzymes of the transsulfuration pathway, cystathionine β-synthase (CBS) and cystathionine γ-lyase (CTH) were shown to be upregulated in several different human cancers, and CBS knockout prevented the growth of several cancer cell lines under cysteine-starved conditions [286].

Cysteine, glutamate and glycine are three amino acids that are required for *de novo* glutathione synthesis (Figure 1-6). The reduced form of glutathione (GSH) neutralises ROS, producing the oxidized dimer form of glutathione (GSSG) and water. The conversion of GSSG back into GSH requires NADPH, which is why this cofactor plays a key role in antioxidant defence [107], [287]. The GSH:GSSG ratio is a measure of reductive potential in cellular compartments, with lower ratio indicating oxidative stress [288], [289].

GSH levels are elevated in several types of human tumours in comparison with healthy tissues [290], [291], and elevated GSH levels have been linked to an increased incidence of metastasis [292], [293]. Furthermore, a study has demonstrated that cancer-associated fibroblasts (CAFs) upregulate glutathione

levels to modulate resistance to ROS-inducing chemotherapy treatment [294], and similar GSH-mediated resistance has also been observed in several cancer models and patient-derived xenografts (PDXs) [295]–[298].

Glutathione synthesis is under control of key signalling oncogenes, including phosphoinositide 3-kinase (PI3K) [299]–[302], and the nuclear factor E2-related factor 2 (NRF2), which is activated directly by oxidative stress [303]–[306]. Interestingly, there have been conflicting reports on the relationship between MYC activation and GSH metabolism. MYC was shown to directly stimulate GSH synthesis in response to oxidative stress in human melanoma cells . However, glutamate cysteine ligase (GCL), the enzyme responsible for *de novo* GSH synthesis, was downregulated in MYC-driven liver cancers, causing a vulnerability to oxidative stress [307].

ROS are a normal biproduct of aerobic metabolism, however their accumulation lead to widespread cellular damage and induce apoptosis [108], [109], [308], [309]. Highly proliferative cancer cells require robust antioxidant metabolism pathways in order to adapt to increased ROS generation, especially in well-oxygenated environments [310]–[312]. On the other hand, moderate levels of ROS can drive cancer progression [313], [314], emphasizing the reliance of cancer cells on tightly regulated antioxidant metabolism. Enzymes involved in glutathione production and recycling have been shown to be upregulated in several cancer types and linked directly to ROS levels [315]–[317], and downregulation of GCL, the rate limiting step in glutathione synthesis, slowed tumour growth *in vivo* [318].

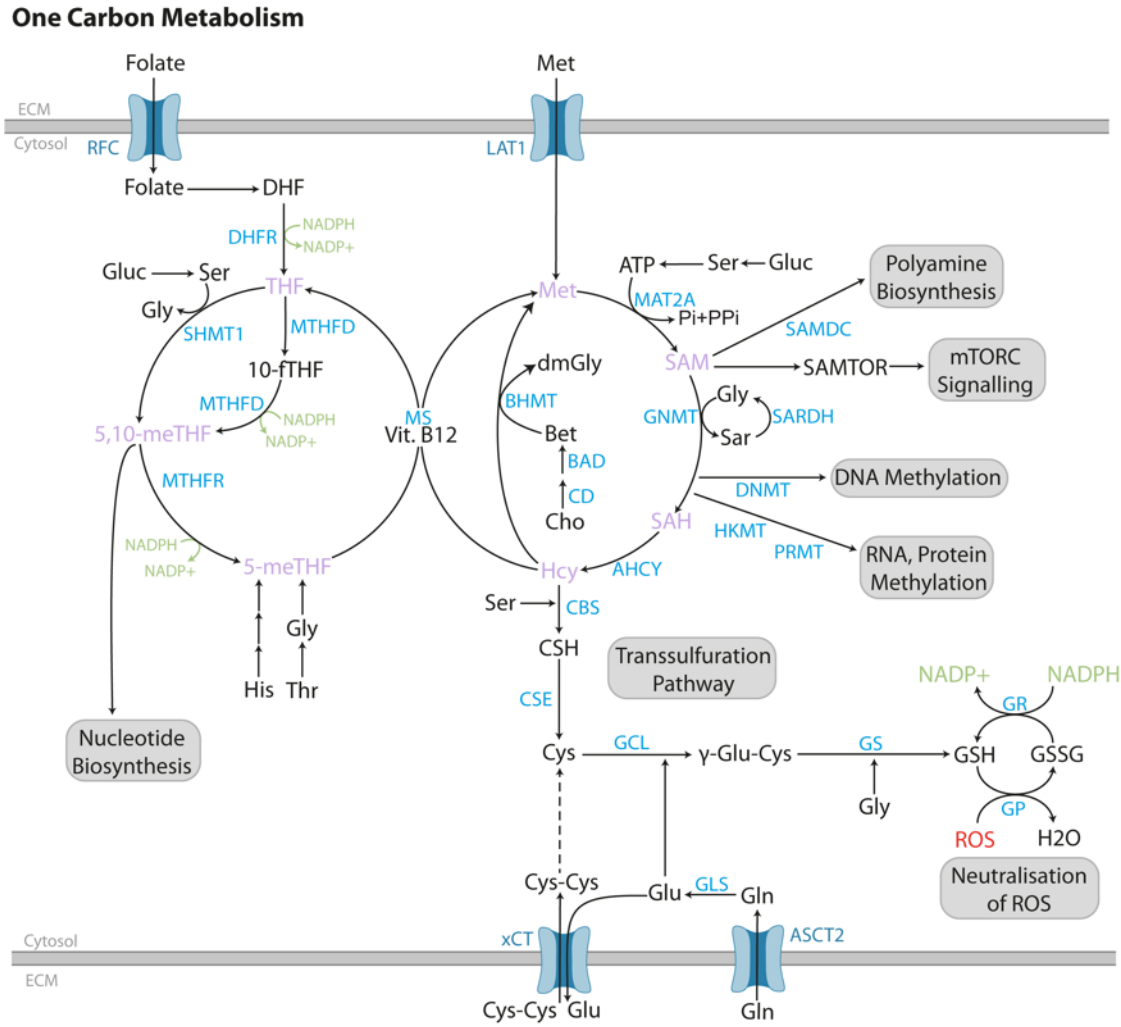


Figure 1-6. One carbon metabolism pathways and glutathione biosynthesis.

One carbon metabolism primary metabolites shown in violet. Transporters: RFC = reduced folate carrier, LAT1 = L-type amino acid transporter 1, ASCT2 = alanine serine cysteine transporter 2, xCT = cystine/glutamate transporter. Enzymes: DHFR = dihydrofolate reductase, SHMT1 = serine hydroxymethyltransferase 1, MTHFR = methylenetetrahydrofolate reductase, methylenetetrahydrofolate dehydrogenase, MS = methionine synthase, MAT2A = methionine amino transferase, SAMDC = S-adenosyl methionine decarboxylase, GNMT = glycine methyltransferase, SARDH = sarcosine dehydrogenase, DNMT = DNA methyltransferase, HKMT = histone methyltransferase, PRMT = protein arginine methyltransferase, AHCY = S-adenosyl homocysteine hydrolase, CBS = cystathionine beta-synthase, CSE = cystathionine gamma-lyase, GCL = glutamate-cysteine ligase, GS = glutathione synthase, GR = glutathione reductase, GP = glutathione peroxidase, GLS = glutaminase. Metabolites: DHF = dihydrofolate, THF = trihydrofolate, 5,10-meTHF = 5,10-methyl-THF, 10-fTHF = 10-formyl-THF, 5-meTHF = 5-methyl-THF, Gluc = glucose, Ser = serine, Gly = glycine, His = histidine, Thr = threonine, Vit. B12 = vitamin B12, Met = methionine, SAM = s-adenosyl methionine, SAH = S-adenosyl homocysteine, Hcy = homocysteine, CSH = cystathionine, Cys = cysteine, Cys-Cys = cystine, gamma-Glu-Cys = gamma-glutamyl cysteine, GSH = reduced glutathione, GSSG = oxidized glutathione, Glu = glutamate, Gln = glutamine, ROS = reactive oxygen species.

1.3.7 Fatty acid metabolism

Fatty acids (FAs) are the molecular building blocks of lipids, and are composed of a carboxyl residue and a chain of hydrocarbons of different lengths and saturation levels. FAs can be imported into the cell by fatty acid transporters such as CD36 [319], or synthesized *de novo* from acetyl-CoA (Figure 1-7). Palmitate is the first FA produced in the *de novo* FA biosynthesis pathway, and can then undergo a series of elongation and desaturation reactions to produce other FAs and various lipids, the metabolism and physiological roles of which are discussed in detail below [320].

Apart from lipogenesis, FAs play an important role in ATP and NADH generation via the beta-oxidation pathway, in which CoA-bound FAs are transported into the mitochondria and converted back into acetyl-CoA, which can then be used to fuel oxidative phosphorylation [122]. NADH is produced by both FA beta-oxidation and in the TCA, therefore FA metabolism contributes to protection against ROS [321], [322].

Another functional role of the FA arachidonic acid is the metabolic precursor for eicosanoid biosynthesis. Eicosanoids are a class of lipids produced from the FA arachidonic acid, which play integral roles in immune signalling pathways and include prostaglandins, leukotrienes and thromboxane [323]. Cyclooxygenase (COX) enzymes that mediate prostaglandin biosynthesis are upregulated in many cancer types [324]–[327] and play an important role in immunosuppression and angiogenesis [328], [329].

The importance of FA metabolism in cancer has been widely demonstrated, highlighting that many cancer types are able to produce FAs *de novo* [330], [331]. Recent studies have shown that driver oncogenes such as MYC [332]–[335], RAS [336], [337], and PI3K/AKT [338]–[340] directly upregulate the rate limiting enzyme fatty acid synthase (FASN) [341], [342], and increased FAs are needed to support high levels of proliferation through ATP production and lipogenesis [343], [123]. FASN overexpression is associated with poor patient prognosis [342], [344], [345],

and a recent study showed that FASN is required for breast cancer cell migration [346].

Other enzymes involved in FA biosynthesis also play a key role for cancer progression. Acyl-CoA synthetase short-chain family member 2 (ACSS2), the enzyme responsible for acetyl-CoA synthesis from acetate, is correlated with poor prognosis and promotes migration of cancer cells [347], [348]. Furthermore, ACSS2 is a key regulator of histone acetylation when translocated to the nucleus [349]. ATP-citrate lyase (ACLY), the enzyme that mediates the conversion of citrate to acetyl-CoA, is activated by PI3K/AKT signalling [350], is required for proliferation of several tumour types [351], [352], and promotes colon cancer cell metastasis by stabilising beta-catenin [353]. Acetyl-CoA production from either acetate or glucose is required for both FA biosynthesis and fuelling the TCA, and enzymes producing it have been reported as promising anti-cancer therapy targets [354], [355].

Exogenous fatty acids taken up via the CD36 transporter and have been shown to support the increased bioenergetic demands and progression of many tumour types [356]–[360], as well as promote survival of non-tumour cells in the tumour microenvironment: CAFs [361], regulatory T-cells [362], and TAMs [363]. Recent studies have shown that tumour cells can mediate a resistance to therapeutic treatment targeting *de novo* FA biosynthesis by upregulating exogenous FA import [362], [364]. CD36 overexpression is associated with poor prognosis in patients [365], and CD36 inhibition impaired metastasis of breast cancer and melanoma PDX tumours [358]. Exogenous FAs are stored in lipid droplets [366], and used for lipogenesis or undergo beta-oxidation to fuel ATP synthesis and protection against ROS [367], [368].

1.3.8 Glycerophospholipid metabolism

1.3.8.1 Phosphatidic acid

The first lipid class produced from free FAs and G3P are phosphatidic acids (PAs) (Figure 1-7). The intermediate lipid class lyso-PA (LPA) can alternatively be taken up externally via the LPA receptors, which have been shown to be overexpressed in cancer [369]–[371]. LPAs can directly bind to G-protein-coupled receptors

(GPCRs) and activate proliferation and migration , through HER2 [372], RAS [373] and AKT signalling [374]. PA lipids can also act as signalling molecules, binding directly to mTOR and regulating nutrient sensing and metabolism [375], [376]. PAs play a central role in phospholipid membrane composition and flexibility and mediate interactions between transporter proteins and the cellular membrane [377], [378]. As discussed in further detail below, PAs are also required for synthesis of diacylglycerols (DAGs) and therefore play a pivotal role in lipid storage.

1.3.8.2 Phosphatidylglycerol and cardiolipins

Phosphatidylglycerol (PG) lipids are synthesized from DAGs and CTP and are present in the phospholipid membrane as well as the synthesis of other lipid classes. Cancer cells require additional membrane phospholipids to sustain the demands of increased proliferation, and a recent study has demonstrated that increased PG synthesis in breast cancer is mediated by MYC and coupled to increased FA synthesis [379]. PGs also play a key role in the synthesis of cardiolipins (CLs). CLs are a key constituent of the inner mitochondrial membrane and are upregulated in several cancer types to mediate increased oxidative phosphorylation and other mitochondrial biogenesis [380]–[383].

1.3.8.3 Phosphatidylinositol

Like PGs, phosphatidylinositol (PI) lipids are synthesized from DAGs and CTP, and are important in phospholipid membrane structure, migration and signalling [384]–[386]. PIs undergo phosphorylation by PI kinases to produce various phosphoinositide-phosphates (PIPs) (Figure 1-7). PIP lipids are integral in cell signalling pathways, most notably the PI3K/AKT pathway that promotes cell growth, survival and metabolism and is often deregulated in various types of cancer [339], [387]–[390][320], [368]–[371]. Alterations to the phospholipid membrane composition of aggressive tumours has been demonstrated in breast cancer, revealing differential profiles of PIs, as well as PE and PC lipids (described below) in comparison to healthy cells [391], [392]. These changes have been attributed to changes in cell signalling pathways, as well as plasticity and invasive capacity.

1.3.8.4 Phosphatidylserine

Phosphatidylserine (PS) lipids are localised on the cytoplasmic side of the phospholipid cell membrane due to their innate negative charge, and are produced from DAGs and serine. During apoptosis, PS lipids are expressed on the outer layer of the cell membrane, acting as a signal for degradation caspase-mediated or macrophage degradation [393]. Externalization of PS lipids on the cell membrane has also been demonstrated in non-apoptotic cell death [394], and in response to elevated oxidative stress in cancer cells [395], [396]. Interestingly, this characteristic of many aggressive cancer cell types has led to the development of drug delivery systems targeting externalised PS lipids [397], [398].

1.3.8.5 Phosphatidylethanolamine

Phosphatidylethanolamine (PE) lipids are another common lipid class in the phospholipid membrane of cells, synthesized from ethanolamine, which is taken up from the diet, recycled during apoptosis or derived from other lipid classes [399]. PE lipids are typically located attached to the inner layer of the cell membrane and play a key role in cell structure due to the chemical shape of the ethanolamine head group [400]. PEs are also important in modulating ferroptosis [401], an alternative cell death programme mediated by iron-dependent lipid peroxide accumulation and emerging as a novel therapeutic target [402], [403].

1.3.8.6 Phosphatidylcholine

Phosphatidylcholine (PC) lipids are synthesized from extracellular choline and are the most abundant phospholipid class, comprising an estimated 50% of cellular phospholipids [404], [405]. PC lipids have been shown to be upregulated in several cancer types [406]–[408] and furthermore, PC upregulation was revealed as a biomarker in breast cancer patients and elevated PC levels are associated with poor prognosis [409]. PC lipids can be synthesized from PE lipids in a methylation reaction mediated by phosphatidylethanolamine N-methyltransferase (PEMT), using the one carbon intermediate SAM as a methyl donor [410], [411], [412]. It has been shown that this reaction is important for glutathione synthesis through the transsulfuration pathway and alters histone methylation profiles [410].

1.3.9 Metabolism of other lipid classes: glycerolipids, sphingolipids and cholesterol

1.3.9.1 Glycerolipid metabolism

Glycerolipids the main energy storage lipid in the human body, and are composed of a glycerol head group with one (mono-acyl glycerol, MAG), two (di-acyl glycerol, DAG) or three (tri-acyl glycerol, TAG) fatty acid side chains [413]pose. Adipose tissue is composed primarily of stored TAGs, and excess lipids in the form of TAGs are stored in many cell types within lipid droplets to prevent lipotoxicity. DAGs ire synthesized from phosphatidic acid (PA) via PA phosphatase (PAP), and TAGs are subsequently produced via diglyceride acyltransferase (DGAT) . Like many enzymes involved in lipogenesis, TAG-producing enzymes are localised to the endoplasmic reticulum [414]. Stored glycerolipids are broken down during lipolysis to glycerol and free FAs, both of which can contribute to ATP synthesis and further metabolic pathways (Figure 1-7).

TAG accumulation in the blood is a predictor of cancer risk [415], and higher TAG levels were reported in several types of cancer in comparison with healthy tissue [416]–[419]. Adipocytes have been shown to directly transfer FAs and TAGs to breast cancer cells, promoting FA oxidation [420]. Furthermore, ATGL, the first enzyme in TAG lipolysis has been linked to poor prognosis, and has recently been shown to regulate mTOR activation in highly proliferative cancer cells [421], [422]. In line with extra-tumour TAGs supporting tumour metabolism, cancer-associated cachexia has been reported to be driven by TAG depletion from adipocytes and blood [423].

1.3.9.2 Sphingolipid metabolism

Sphingolipids are produced from serine and palmitoyl-CoA by a series of reactions that lead to the synthesis of ceramide, which can then be converted into sphingosine, sphingomyelin, sulphatide and glycosphingolipids [424], [425]. All sphingolipids share the characteristic sphingoid bases, which allow them to act as signalling molecules and interact with the cell membrane [426].

Ceramide induces apoptotic signalling by releasing cytochrome C from mitochondria [427], [428]. In cancer, elevated ceramide in the membrane lead to apoptotic cell death [429]–[431], and therapies which induce ceramide biosynthesis have shown to promote sensitivity to chemotherapy agents and potentiating cell death in different cancer models [432]–[436]. Although ceramide itself potentiates cell death, its downstream metabolites sphingosine and sphingosine 1-phosphate are important for cell proliferation, survival and metastasis [437]–[440]. Sphingomyelin, another class of ceramide derivatives, promotes chemotherapy resistance and tumour proliferation, and has also been shown to inhibit autophagy [441]–[443]. Importantly, sphingolipids together with cholesterol are integral components of plasma membrane lipid rafts, which potentiate protein binding, cell adhesion and signalling cascades and have been demonstrated to mediate numerous pro-tumorigenic functions [444].

1.3.9.3 Cholesterol metabolism

Cholesterol is a steroid lipid that can be synthesized in cells from acetyl-CoA via the mevalonate pathway [445] or imported in the form of low-density lipoprotein (LDL) [446]. Cholesterol is localised to the cell membrane and regulates membrane rigidity [447], [448]. The amount of cholesterol in the membrane varies with cell type and is inversely correlated with motility [449]. In line with this, cholesterol biosynthesis was downregulated in a metastatic breast cancer cell line [450] and increased cholesterol inhibited macrophage migration [451].

On the other hand, downregulation of cholesterol lead to reduced activity of CD44, a primary cell adhesion protein that is important for metastatic dissemination [452]. This is due to reduced formation of lipid rafts, which are cholesterol- and sphingolipid-rich residues on the plasma membrane that mediate adhesion and binding of proteins, including CD44 [453]. Another study showed the importance of cholesterol biosynthesis for survival of cancer stem cells, and revealed a correlation between activation of cholesterol biosynthesis and poor prognosis [454]. Furthermore, cholesterol-lowering statin drugs, which inhibit the HMG-CoA reductase enzyme in the mevalonate pathway, have been successfully used in the clinic in breast cancer patients to reduce tumour growth [455]. Cholesterol can

activate several oncogenic pathways, including the PI3K/AKT pathway [456], [457], and the Hedgehog signalling pathway [458]. Thus, regulation of cholesterol metabolism is important for cancer survival and progression, and may potentiate different effects depending on oncogenic signalling and tumour type.

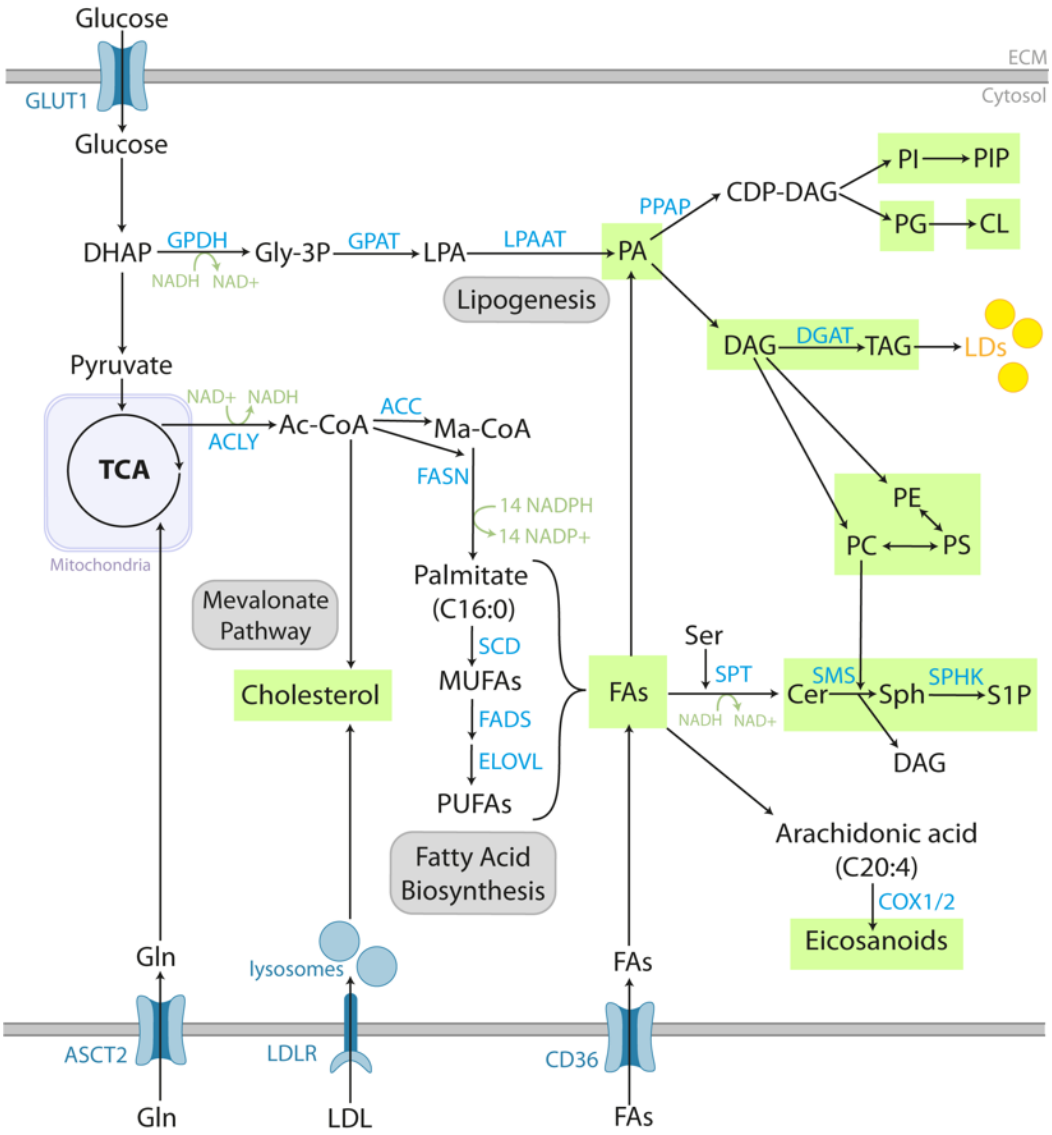


Figure 1-7. Pathways of *de novo* fatty acid and lipid biosynthesis.

Transporters: LDLR = low-density lipoprotein receptor, CD36 = fatty acid transporter. Enzymes: GPDH = glycerol-3-phosphate dehydrogenase, GPAT = glycerol-3-phosphate acyltransferase, LPAAT = lysophosphatidic acid acyltransferase, PPAP = phosphatidic acid phosphatase, DGAT = diacylglycerol acetyltransferase, EPT1 = ethanolamine phosphotransferase 1, ACLY = ATP citrate lyase, ACC = acetyl-CoA carboxylase, FASN = fatty acid synthase, SCD = stearoyl-CoA desaturase, FADS = fatty acid desaturase, ELOVL = elongation of very long chain fatty acids protein, SPT = serine palmitoyl transferase, SMS = sphingomyelin synthase, SPHK = sphingosine kinase, COX1/2 = cyclooxygenase. Metabolites: DHAP = dihydroxyacetone phosphate, Gly-3P = glycerol-3-phosphate, LPA = lysophosphatidic acid, PA = phosphatidic acid, CDP-DAG = cytidine diphosphate diacylglycerol, PI = phosphatidylinositol, PIP = phosphatidylinositol phosphate, PG = phosphatidylglycerol, CL = cardiolipins, DAG = diacylglycerol, TAG = triacylglycerol, LDs = lipid droplets, PE = phosphatidylethanolamine, PC = phosphatidylcholine, PS = phosphatidylserine, FA = fatty acid, Ac-CoA = acetyl-CoA, Ma-CoA = malonyl-CoA, MUFA = monounsaturated fatty acid, PUFA = polyunsaturated fatty acid, Ser = serine, Cer = ceramide, Sph = sphingosine, S1P = sphingosine-1-phosphate, LDL = low density lipoprotein.

1.4 MYC and cancer metabolism

MYC is a “master regulator” transcription factor which controls up to 15% of the human genome [459]. Downstream targets of MYC are involved in the processes vital for cell survival, including proliferation, apoptosis, migration and metabolism [460], [459]. MYC was found to be overexpressed or deregulated in 70% of human cancers [461], and in 30-50% of high-grade breast cancers [462]. Since MYC has the power to influence such a broad range of key cellular functions, the expression of MYC is meticulously regulated at a transcriptional, translational and post-translational level [463]–[467]. Furthermore, in order to act as a transcription factor, MYC is required to form a dimer with its binding partner protein, MYC-associated factor X (MAX) [468]. The dimerization of MYC and MAX is further regulated by MAX dimerization protein (MAD), which binds to MAX and subsequently can downregulate the transcriptional power of MYC [469], [470].

MYC has been shown to influence multiple metabolic pathways in cancer [471]. MYC regulates aerobic glycolysis by directly driving transcription of most glycolytic genes. MYC also regulates the transcription of many genes involved in mitochondrial biogenesis pathways [472], [473], and promotes glucose incorporation into the pentose phosphate pathway (PPP) for nucleotide biosynthesis and maintenance of oxidative stress in the tumour microenvironment [474], [475]. Furthermore, MYC directly regulates expression of glucose [476] and amino acid transporters [127], [216], [477], facilitating increased metabolic flux of these nutrients in tumour cells. MYC has also been shown to upregulate glutaminolysis [120], [478], [479] as well as *de novo* glutamine synthesis [143], and furthermore induces catabolism of branched chain amino acids (BCAAs) [223]. Recently, a study in breast cancer demonstrated the control of lipogenesis by MYC through the induction of the transcription factor sterol-regulated element-binding protein (SREBP1), which leads to *de novo* fatty acid biosynthesis and elongation [379]. MYC additionally upregulates serine synthesis from glucose [480], as well as the serine-glycine interconverting enzymes, SHMT1 and SHMT2 [481], thereby fuelling the one carbon metabolism pathway (further discussed below). The role of MYC has also been demonstrated in nutrient sensing via mammalian target of rapamycin (mTOR) to promote nutrient uptake and regulate cell growth [482].

Importantly, the diverse role of MYC on metabolic flexibility in cancer has been demonstrated in a MYC-driven model of hepatocellular carcinoma. MYC was able to upregulate the glycolytic enzyme hexokinase 2 (HK2), both isoforms of the glutaminolytic enzyme glutaminase (GLS1 and GLS2), as well as the serine synthesis enzyme PSAT and the *de novo* fatty acid biosynthesis enzyme FASN in response to genetic, pharmacological and dietary interventions [13].

Despite diverse metabolic reprogramming capabilities, metabolism regulation by MYC has been shown to differ between different tumour types [75]. In the context of breast cancer, high MYC expression and activity is associated with triple negative breast cancer [483], and MYC expression correlated with higher glutamine catabolism and fatty acid production [152], [334], [484].

1.5 Metabolic reprograming in metastatic progression

Metastatic disease is the primary cause of mortality across all cancer types [485]. The process of metastasis requires tumour cells to adapt to various nutrient and oxygen gradients as they leave the primary tumour site and migrate throughout the body [486]–[488].

The metastatic cascade is often instigated by tumour cells undergoing an epithelial-to-mesenchymal (EMT) progression, during which cells show mesenchymal phenotypes like extracellular matrix (ECM) degradation and migration [489].

Changes in metabolism have been shown to drive EMT initiation. Motility and invasiveness of cancer cells was shown to be increased as a result of upregulation of glycolytic enzymes hexokinase 2 in pancreatic cancer [490], and pyruvate kinase muscle isozyme M2 (PKM2) in lung cancer [491]. Additionally, phosphoglucose isomerase (PGI) was demonstrated to act as a signalling molecule that caused NFkB upregulation and EMT initiation [492]. Changes in TCA enzyme expression and metabolite levels have also shown to instigate EMT [493], [494]. A recent study has demonstrated that availability of the amino acid asparagine in the tumour microenvironment can directly promote EMT in breast cancer, and limiting it

reduces tumour aggressiveness [495]. Furthermore, a recent study has demonstrated that suppression of genes associated with mitochondrial metabolism were correlated with increased metastatic risk and poor patient prognosis in several cancer types, potentially due to a glycolytic switch favouring the Warburg Effect [496].

Furthermore, transcription factors that initiate EMT can initiate metabolic changes that prepare the cells for survival in different environments; the transcription factor SNAI1 directly downregulates fructose-1,6-bisphosphatase (FBP1) in order to promote PPP metabolism in gastric cancer , meanwhile ZEB1 activation lead to the upregulation of a glucose transporter, GLUT3 in non-small cell lung cancer (NSCLC), leading to increased glycolysis [497].

Once tumour cells successfully leave the primary tumour site, they encounter an increased oxygen availability and levels of reactive oxygen species (ROS) in the blood vasculature [498]. Circulating tumour cells (CTCs) from breast cancer were shown to increase oxidative phosphorylation when in the blood stream, utilising the additional oxygen availability for energy production [499]–[502]. Several metabolic studies on CTCs reported increased antioxidant biosynthesis compared to cells in the primary tumour [116], [503]. Furthermore, inhibiting the folate cycle reduced instances of metastases in a melanoma model, suggesting that this pathway is needed to cope with increased ROS in the blood [504]. In line with these findings, another study demonstrated that treating CTCs with an antioxidant compound, N-acetylcysteine, promoted melanoma aggressiveness [505].

ROS levels are also elevated in the lungs, one of the most common organ colonised by metastatic cells [506]. Consequently, metastatic cells in the lung have been shown to increase antioxidant metabolic pathways, irrespective of the site of tumour origin [181], [504], [507]. A recent study has also demonstrated that due to increased pyruvate availability in the lung, breast cancer metastatic cells in the lung upregulate pyruvate anaplerosis [66]. Another study showed the role of fatty acid oxidation for the survival of metastatic breast cancer cells in the lung.

These findings showed how metabolic plasticity allows metastatic cells to adapt to differential nutrient availability in the organ they colonise. Similarly, metastases to the liver show an upregulated propensity for fructose metabolism, which may be a potential alternative nutrient source more readily available in the liver [508].

Metabolic crosstalk between tumour and non-tumour cells in the metastatic niche is a growing interest in the context of metabolism, since metastatic cells have been shown to exploit their surroundings to maximise their own survival. A recent study demonstrated how breast cancer metastasis to the brain rewire their metabolism to import and catabolise the neurotransmitter gamma-amino butyric acid (GABA), which is readily secreted by neuron cells [509]. Metastases to the brain also require an upregulation of *de novo* serine biosynthesis due to limited serine and glycine levels in the brain microenvironment, and a recent study reported upregulation of the serine synthesis enzyme PHGDH in brain metastases of several cancer types [510]. Another adaptation in the serine biosynthesis pathway was reported in breast cancer metastasis to the bone. Metastatic cells upregulate serine biosynthesis and export, increasing healthy bone breakdown by osteoclasts to create space for the metastases to grow [511].

Metabolic changes often take place in the non-tumour component of the primary tumour and metastatic niche. Cancer-associated fibroblasts upregulate glycolysis and lactate production when co-cultured with metastatic gastric cancer cells [512]. CAFs also upregulate FASN-mediated fatty acid and phospholipid biosynthesis in co-culture with metastatic colorectal cancer (CRC) cells, which were shown to take up lipid species produced by CAFs [513]. Furthermore, in this study, FASN knockdown in CAFs inhibited the migratory capacity of CRC cells *in vitro* and *in vivo*. Another immune cell population that mediates tumour survival and migration are tumour-associated macrophages (TAMs) [514]. TAMs are the resident macrophages within a tumour, and have several proposed roles in tumour growth [515] and metastasis [516]–[518]. TAMs upregulate glycolytic enzymes and the glucose transporter GLUT1 in response to co-culture or conditioned media from aggressive pancreatic tumour cells, and support metastatic progression by inducing angiogenesis, tumour cell extravasation and releasing lactate that can be taken up by tumour cells to meet increased bioenergetic demands [519]. TAMs also

upregulate the FA transporter CD36 and increases lipogenesis upon activation by cancer cells, in order to mediate immunosuppressive functions and polarization [520]–[523].

The heterogeneous population of cells within a tumour or the metastatic niche adds complexity to the intricate cancer metabolic signalling. In the next section I will introduce a series of mass spectrometry imaging techniques that allow the observation of metabolite distributions *in situ*.

1.6 Mass Spectrometry Imaging

1.6.1 Metabolomics analysis principle

Mass spectrometry (MS) refers to the analysis technique in which the mass-to-charge (*m/z*) ratio of chemical ions is measured. Commonly in the field of biological -omics analysis, MS is paired with a chromatography-based separation technique, such as liquid- (LC-MS) or gas-phase (GC-MS) separation. Ions are first separated based on the time it takes for them to pass through a chromatographic column (the retention time), and this is based on the ion's stereochemistry, size, orientation and interaction with the stationary column phase. Ions are then directed to a mass analyser, such as a Time-of-Flight (ToF) or more recently, the state-of-the art Orbitrap mass analyser [524]–[528]. The m/z ratio of each detected ion can then be plotted against its intensity to produce a full mass spectrum. In metabolomic analysis, m/z values typically range between 0 and 300 m/z for polar metabolite species, and up to 1200 m/z for larger apolar metabolites. Chromatographic separation provides an additional degree of confidence when assigning a chemical formula identity to m/z values, and metabolite standards are typically used in LC- and GC-MS experiments to determine the exact retention time [529]–[531].

1.6.2 Mass Spectrometry Imaging principle

Mass Spectrometry Imaging (MSI) is an analytical tool that was developed over 50 years ago for studying surface integrity in the semiconductor industry [532], but has been increasingly enhanced for biological sample analysis in the past 30 years [533]. There are several distinct technological platforms for MSI, each of which has their own advantages and challenges. The overarching principle of MSI is that an ionisation source is focused on the surface of a sample, and this causes dislodging and ionisation of chemical species, which are then transferred to a mass analyser. The key advantage of MSI over traditional metabolomics techniques is that the sample remains intact, and the ionisation source is sequentially rastered across the entire sample, commonly a tissue section. The result is a spatially resolved image, with a full mass spectrum collected at each pixel. Spatial resolution varies between MSI modalities, but can range from as low as 2 µm to 100 µm in pixel diameter, allowing for segmentation of chemically distinct features [534]–[536].

There are three prominent MSI modalities that have been used for biological sample analysis [536]–[538] . The primary differences between MSI instruments are the ionisation sources, sample preparation requirements, and various mass analysers, including ToF and Orbitrap.

The oldest technique, secondary ion mass spectrometry (SIMS) traditionally uses a primary ion beam to ionise metabolites on the surface of the sample and these “secondary” ions are then collected for MS analysis. SIMS is a relatively destructive technique due to the harsh, collision-based ionisation of the primary ion beam, which often results in additional fragmentation of endogenous metabolites when analysing biological samples [539]–[541]. Recently, the OrbiSIMS, a hybrid SIMS instrument with a milder gas cluster ion beam and an Orbitrap mass analyser has been developed to facilitate biological sample analysis [534], [542].

Another MSI modality, matrix-assisted laser desorption ionisation (MALDI)-MSI was developed specifically for biological sample analysis with the aim to preserve metabolite integrity [543]–[546]. MALDI sample preparation requires coating the sample in different chemical matrices, which help promote metabolite ionisation and can be tailored to promote ionisation of different metabolite classes in different polarities [547]–[550]. The ionisation source in MALDI is a laser that is also quite destructive to the tissue, however the variety of matrices that can facilitate the detection of a wide range of biological molecules, from small polar metabolites to large proteins, is a definite advantage of this technique.

The most recently developed of the three MSI techniques is desorption electrospray ionisation (DESI)-MSI. This technique was developed for ambient sample analysis, avoiding the need for an inner vacuum chamber that the other two modalities require [551], [552]. The ionisation source in DESI-MSI is a relatively “soft” charged electrospray, which causes minimal disruption to biological tissue samples [553], [554]. Charged droplets of the typically methanol-based solvent are deposited on the sample surface, causing simultaneous desorption and ionisation of metabolites, which are then transferred to a mass analyser [555], [556].

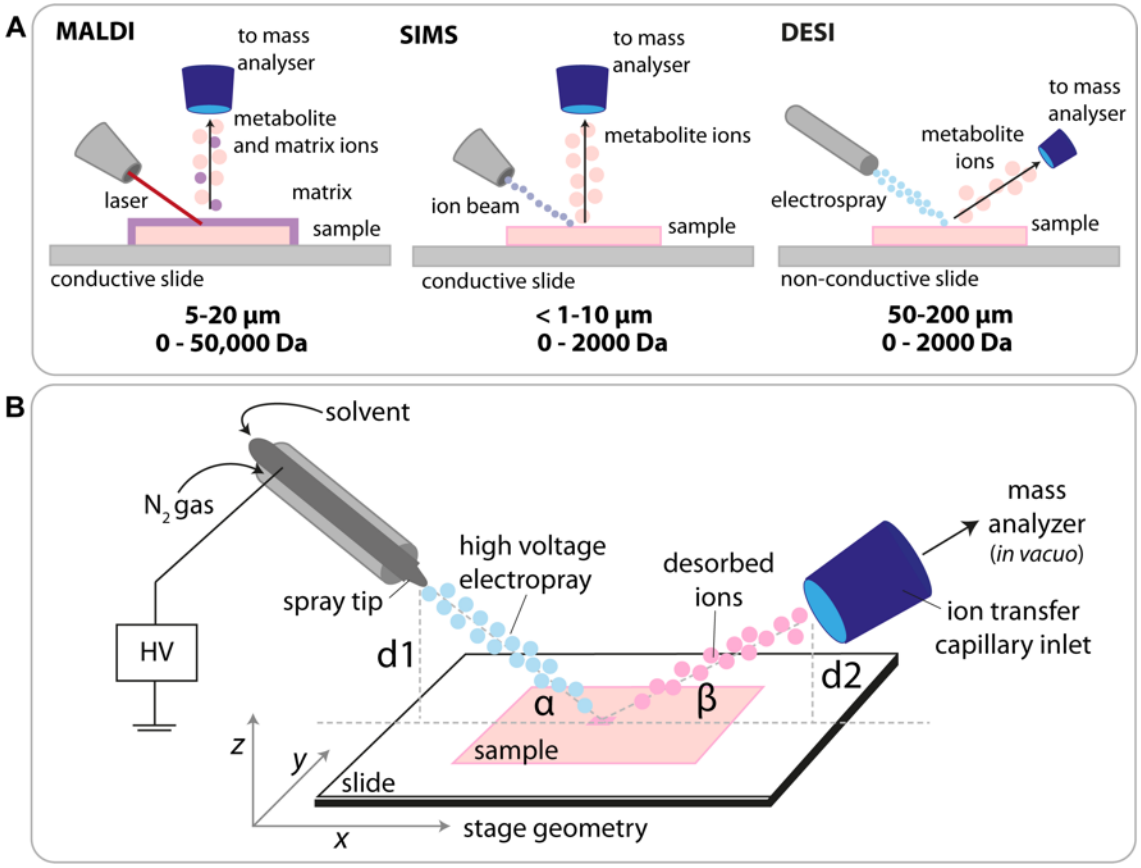


Figure 1-8. Comparison of MSI modalities.

(A) Schematic comparing MALDI, SIMS and DESI ionisation sources. Lateral resolution (µm) and ion mass range (Da) of each technique listed below. MALDI (matrix assisted laser desorption ionisation): standard instruments equipped with UV nitrogen lasers (337 nm wavelength) as ionisation source, matrix application is required prior to analysis to promote ionisation of specific chemical species in the sample. SIMS (secondary ion mass spectrometry): primary ion beams vary, for biological sample analysis typically an argon gas cluster ion beam (GCIB) is used due to less destructive impact with the sample surface. DESI (desorption electrospray ionisation): charged solvent spray, typically 95% methanol, used for simultaneous desorption and ionisation of analytes from the sample surface. Mass analysers vary depending on instrument, traditionally time-of-flight (TOF) mass analysers preferred, but recently state-of-the-art Orbitrap mass analysers have greatly advanced the mass resolving power of MSI instruments (MRP up to 240,000 at 200 m/z, compared with ~10-20,000 on a TOF analyser). (B) Detailed schematic of the principle of DESI-MSI. The ionised solvent is focused onto the sample surface, where analytes are dissolved and released towards the ion transfer inlet. The efficacy of ionisation and desorption depend on parameters including the flow rate and charge of the solvent, and the geometry of the instrument components. The distance of the sprayer tip to the sample (d1) and the distance of the ion transfer inlet to the sample (d2) are modified to obtain the ultimate incident (α) and collection (β) angles. The stage is positioned in the x, y, z co-ordinates and moves the sample under the electrospray during image acquisition. The set-up shown here is entirely under ambient conditions, however the ion transfer capillary acts as the vacuum interface and the mass analyser is located under high vacuum.

MSI in cancer research

In the last decade, considerable work in the field of MSI has been focused on adapting methods and technology platforms for biological applications, and the field is expanding particularly quickly towards cancer biology. MSI can be a highly useful

tool to study the complex histological, genetic and metabolic heterogeneity that is observed between and within tumours, as well as in comparison to healthy tissue. Previously established limitations including tissue damage during sample preparation and ion suppression effects caused by the abundance of molecules present in biological samples are currently being addressed. Several tissue embedding protocols have been established in order to facilitate tissue preservation during cryosectioning and speed up throughput, including gelatin [557] and a newly-developed mixture of HPMC/PVP [558]. Furthermore, nitrocellulose coating of samples has been shown to prevent metabolite delocalization during imaging [559]. On-tissue derivatization has also proven useful to promote ionisation of specific classes of metabolites, including fatty acids [560], neurotransmitters [561], and glycans [562]. Importantly, methods are currently being developed for imaging formalin-fixed tissue samples to make MSI compatible with standard histological guidelines for tissue collection and storage, and this has been particularly successful in peptide imaging [562]–[565]. Methods have been developed for studying protein composition of the ECM following a decellularization protocol [566], and MALDI has been used after laser ablation and lipid digestion [567].

While the work presented in this thesis focuses on the use of MSI to study metabolism, it should be noted that proteomics was the first biological application of MSI, particularly MALDI [568]. MALDI-TOF instruments have been reported to detect proteins in the range of 2 to 70 kDa [569], [570]. In breast cancer studies, proteomic MALDI was used to visualize ER and PR receptor status [563], another study reported a proteomic signature of HER2 receptor status in human tumour samples [571]. Peptide MSI was used as a robust diagnostics tool not only in breast, but also in lung [572], gastric [573], prostate [574], ovarian [575], thyroid [576] and oral carcinoma samples [577].

MSI is also extensively used to image the distribution of lipids in biological samples. MALDI-MSI was used to stratify breast tumour samples by oncogenic subtype [578], [579], and lung cancer samples by histological grade [580]. Lipidomic profiling has also been achieved using SIMS-MSI, however due to the destructive nature of the ionisation technique, many SIMS studies have been conducted in

single cells. One such study distinguished breast cancer stem cells from non-stem cells by fatty acid content [581], while another study demonstrated trends in fatty acid chain length and saturations in breast cancer cell lines of different subtypes [582]. On-tissue TOF-SIMS imaging revealed distinctions in lipid composition of tumours correlating with grade [583], and furthermore, lipid profiles of basal cell carcinoma samples were shown to be distinctly altered following chemotherapy treatment [584]. Intra-tumour heterogeneity was demonstrated with TOF-SIMS lipid imaging in breast [585] and glioblastoma [586] tumours, with the lateral resolution of SIMS allowing segmentation between tumour, stroma and necrotic regions.

DESI-MSI has also been widely used for lipidomic studies, and often favoured over other MSI modalities due to the minimal sample preparation requirements and the ambient imaging conditions that maintain metabolite localization. DESI-MSI was used to distinguish tumour-specific lipid profiles in comparison to the surrounding tissue patient samples from oesophageal cancer lymph node metastases [587], as well as breast [409], [588], brain [589] and bladder cancer samples [590]. A recent study used DESI-MSI to visualize phospholipid localization in breast tumours, demonstrating how the lipid landscape changed following MYC activation [379]. Interestingly, several of these studies converged on the lipid PI(18:0/20:4) as a marker of malignant tissue, whereas several PS and PE lipids had opposite localization profiles [579], [587]. DESI-MSI lipidomics studies contributed to the development of an innovative clinical tool known as the iKnife. This technology allows surgeons to distinguish cancerous from healthy tissue in real time, coupling together standard cauterization surgery procedures and rapid evaporative ionisation mass spectrometry (REIMS) [591]. In a unique study, the oncometabolite 2-hydroxyglutarate (2HG) was used during an intra-operative study in glioblastoma patients, where surgical margins were established based on 2HG detection by DESI-MSI on excised tissue smears directly in the operating theatre. While MSI has been proven to be a valuable diagnostics tool, currently there is a rising interest in developing methodologies to image endogenous small polar metabolites, and infer functional meaning behind heterogeneous metabolite distribution in tumour samples.

The work compiled in this thesis has been done as part of the Cancer Research UK (CRUK) Grand Challenge Rosetta Team, which aims to spatially map metabolite distributions within a variety of tumour models and clinical samples. A recent publication from Kevin Brindle's lab of the Rosetta Team has demonstrated the ability of DESI-MSI to visualize distribution of stable-isotope labelled glucose, pyruvate and lactate. This study demonstrated how DESI-MSI can be combined with hyperpolarized MRI to study the metabolic flux in different regions of the tumour, in the context of its surrounding organ [592]. Several studies have also shown localization of amino acids and glucose in diverse biological tissues and tumours [593]–[595]. Nevertheless, using MSI for cancer metabolism studies remains an exceptionally novel and exciting field. The work presented in this thesis aims to advance the current understanding of methods and capabilities of MSI to study metabolic heterogeneity between primary mammary tumours and their metastases to the lung.

1.7 Thesis Aims

- Develop the methodology and assess the capabilities of mass spectrometry imaging as a tool for analysing spatially-resolved tumour metabolism.

- Evaluate the metabolic heterogeneity in mouse mammary gland tumours induced by the Myc oncogene.

- Compare the metabolic profile of primary mammary gland tumours with lung metastasis derived from them.

- Determine potentially-targetable metabolic vulnerabilities of metastatic tumour cells.

Chapter 2. Methods

2.1 Reagents and Chemicals

2.1.1 Cell culture media

Tumour and lung metastasis cells were cultured on cell-adherent plates using the following media, originally developed to support growth of mammary epithelial cells (MMEC Media). Tumour cell lines were isolated in Collagenase Buffer.

Table 1: MMEC Media

Component	Supplier	Catalogue Number	Final Conc.
DMEM/F12	Life Technologies	21331-046	-
FBS	Gibco	10270	10%
HEPES	Gibco	15630-056	10 mM
Glutamine	Gibco	25030-024	2 mM
Insulin	Sigma	I1882	5 µg/mL
Hydrocortisone	Sigma	H0888	1 µg/mL
EGF	Life Technologies	PMG8043	10 ng/mL
Pen/Strep	Gibco	15140-122	100 µg/mL

Table 2: Collagenase Buffer

Component	Supplier	Catalogue Number	Final Conc.
DMEM/F12	Life Technologies	21331-046	-
BSA	Gibco	10270	1%
HEPES	Gibco	15630-056	10 mM
Glutamine	Gibco	25030-024	2 mM
Insulin	Sigma	I1882	5 µg/mL
Hydrocortisone	Sigma	H0888	1 µg/mL
Collagenase (Type L)	Sigma	C8176	1 mg/mL
Pen/Strep	Gibco	15140-122	100 µg/mL

Table 3: SDS-PAGE gel (8%) 4x solution – 40 mL

Component	Supplier	Volume
Water (milliQ)	-	22 mL
40% Bis-Acrylamide	Bio-Rad	8 mL
1.5 M Tris, 0.4% SDS (pH 8.8)	-	10 mL
10% APS	Sigma	400 µL
TEMED	Sigma	20 µL

Table 4: Stacking gel (4%) 4x solution – 20 mL

Component	Supplier	Volume
Water (milliQ)	-	12.9 mL
40% Bis-Acrylamide	Bio-Rad	2.1 mL
1.5 M Tris, 0.4% SDS (pH 8.8)	-	5 mL
10% APS	Sigma	200 µL
TEMED	Sigma	20 µL

2.1.2 Stable Isotope-Labelled Metabolites

The following isotope labelled metabolites were used for *in vivo* infusions of tumour-bearing and wildtype mice. Stable isotope metabolites were dissolved in sterile saline solution and either used immediately or stored at -20 °C.

Table 5: Stable Isotope Labelled Metabolites

Compound	Supplier	Catalogue Number	Concentration
$^{13}C_6$-Glucose	Cambridge Isotope Laboratories	110187-42-3	200 mg/mL
$^{13}C_5$-Glutamine	Cambridge Isotope Laboratories	184161-19-1	40 mg/mL

2.1.3 Metabolite Extraction

Reagents used for polar and apolar metabolite extractions for LC-MS and GC-MS.

Table 6: Metabolite extraction reagents

Reagent	Supplier	Cat. Number
Acetonitrile	Sigma	271004
Chloroform	Sigma	372978
HPLC-grade methanol	Sigma	494291
HPLC-grade water	Sigma	270733

2.1.4 Antibodies

The following antibodies were used for immunofluorescence and immunohistochemistry staining.

Table 7: Antibodies

Marker	Target	Supplier	Cat. Number	IF Dilution	WB Dilution
alpha-SMA	Activated fibroblasts (CAFs), basal cells	Sigma	A5228	1:300	-
FASN	FA synthesis	Cell Signalling	3180	1:100	-
CD163	Macrophages (M2, TAMs)	Abcam	ab182422	1:500	-
Ly6G	Neutrophils	Biolegend	127601	1:100	-
CD45-PerCP	Pan-immune marker	Biolegend	103129	1:400	-
CD68	Macrophages (M1)	Biolegend	137001	1:100	-
E-Cadherin	Epithelial cells	BD Pharmingen	610182	1:100	1:1000
TTF-1	Pneumocytes	Abcam	ab227652	1:100	-
Vimentin	Stroma, mesenchymal cells	Abcam	ab92547	1:300	1:1000
c-Myc	cMyc (Y59 clone)	Abcam	ab32072	1:100	1:1000
CK8/18	Luminal epithelial cells	Abcam	ab53280	1:100	-
CD3	Activated T cells (Th and Tc)	Biolegend	100208	1:50	-
B220	B cells	BD Pharmingen	550286	1:200	-
phospho-Erk	RAS signalling (P-p44/p42 MAPK)	Cell Signalling	9101	-	1:1000
Erk	RAS signalling (p44/p42 MAPK)	Cell Signalling	9102	-	1:1000
phospho-Akt	PI3K signalling	Cell Signalling	9271	-	1:1000
Akt	PI3K signalling	Cell Signalling	9272	-	1:1000
p53	p53	Santa Cruz Bio	sc-6243	-	1:1000
beta-actin	beta-actin	Sigma	A3854	-	1:5000

2.2 Mouse models and *in vivo* experimental procedures

2.2.1 Mouse Models

All mouse procedures followed United Kingdom Home Office regulations and were approved by the Animal Welfare and Ethical Review panel of the Francis Crick Institute.

The following mouse models were used in this project:

- Wildtype FVB/NJ females (Francis Crick Institute in-house colonies)
- MMTV-MYC (Tg(MMTV-MYC)141-3Led), originally acquired from the Jackson Laboratory (MGI ID: 2447500).

2.2.2 Tumour initiation by mammary fat pad injection

Mammary gland tumour cells of the Myc310 cell line were used in this project, and originally established in-house by Dr. Emma Still by multiple *in vitro* passages of cells isolated from a transgenic MMTV-MYC tumour.

Myc310 MGT or isolated lung metastasis cells were grown in MMEC media overnight prior to injection into mice. Cells were detached from the plate using Trypsin (Gibco) then passed through a 23 gauge syringe to dissociate into individual cells. Cells were then counted and washed twice with PBS to remove any remaining media. Then, 50,000 cells per mouse were resuspended in 50 uL Matrigel (Corning, 356230) on ice. Cells were then injected into the fourth inguinal mammary fat pad of 6-8-week-old virgin FVB/NJ mice, ensuring a subcutaneous injection directed just below the nipple. Tumours were detected after approximately 2 weeks, and in the case of metastatic models, mice were closely monitored for signs of metastatic burden (laboured breathing, weightloss).

2.2.3 Tumour and metastasis cell isolation and propagation

Mammary gland tumours were collected when the tumour diameter reached 1 cm by palpation. Tumours were cut up into small chunks using sterile blades. The tumour pieces were then transferred into a falcon tube containing 20 mL

Collagenase Buffer, sealed, and placed in a benchtop shaker for 1 hour at 37°C at 200 rpm. The tissue suspension was then filtered through a 70 μm filter using a syringe if necessary to break up bigger tumour pieces, if any remained. Next, the filtered tissue suspension was spun down at 530 x*g* for 5 minutes, and the supernatant was discarded. The pellet was then resuspended in TAC buffer (170 mM Tris, 150 mM ammonium chloride, pH 7.4), and placed in a 37°C water bath in order to lyse any red blood cells. The cell suspension was then spun down again and resuspended in MMEC Media for cell propagation, or frozen in Freezing Buffer (10% DMSO in FBS) for long term storage.

For metastasis cell isolation, whole lungs were collected and the same exact dissociation method was applied. Once individual cells were isolated, they were grown in MMEC media for up to two weeks, at which time any metastatic cells present were visible.

2.3 Molecular Biology Methods

2.3.1 Immunofluorescence

All immunofluorescent staining was performed on fresh frozen tissue samples in order to optimise post-MSI immunological staining. Tissues were fixed with 4% PFA for ten minutes at room temperature, then washed once with PBS-T (PBS + 0.1% Tween-20). Slides were then blocked in blocking buffer (1% BSA, 5% normal goat serum in PBS-T) for 30 minutes at room temperature. Blocking buffer serum was matched with secondary animal host animal, goat or donkey. Primary antibodies were diluted in blocking buffer, and added to the tissues. Primary incubation was typically performed for 2 hours at room temperature, or overnight at 4°C. Slides were then washed with PBS-T (5x) and then secondary antibodies were added, diluted also in blocking buffer. Secondary antibody incubation was done in the dark for 1 hour at room temperature. Slides were washed in PBS (5x) and then stained with a 1:10,000 DAPI solution for 10 minutes. Finally, slides were washed once in PBS, and a coverslip was placed using ProLong Gold Antifade Mounting Media (Thermofisher).

Immunofluorescence staining in cells was performed on ~50% confluent cells grown on 10mm coverslips (VWR) in a standard 24-well cell culture plate. Media was removed and the cells were washed once with pre-warmed (37°C) PBS. Cells were then fixed with pre-warmed 4% paraformaldehyde (PFA) for 10 minutes, then washed once with PBS. Cells were then permeabilised using 0.5% Triton-X100 (Sigma) for 10 minutes. The following staining steps for blocking, washes, primary and secondary antibody staining were performed as described above for tissue IF. Once staining was completed, the coverslips were mounted cells-down onto standard SuperFrost Plus slides (Thermofisher) using ProLong Gold Antifade Mounting Media (Thermofisher).

Immunofluorescence images were acquired using either confocal microscopy (Leica TCS SP8) or a fluorescent slidescanner (Olympus VS200) for whole slide imaging.

2.3.2 Haematoxylin & Eosin Staining

H&E staining was performed at the Experimental Histopathology (EHP) Scientific Technology Platform at The Francis Crick Institute, using a Tissue-Tek Prisma Plus Automated Slide Stainer & Coverslipper (Sakura Finetek). The slides were incubated in the following reagents at the given time intervals:

- Fixation: 10% neutral buffered formalin (NBF) 10 min.
- Water 30 sec.
- Haematoxylin 90 sec.
- Water 30 sec.
- Acid alcohol 10 sec.
- Water 30 sec.
- Eosin 2 min.
- 70% ethanol 30 sec.
- 95% ethanol 30 sec.
- 100% ethanol 30 sec.
- 100% ethanol (new) 30 sec.
- Xylene 30 sec.
- Xylene (new) 30 sec.

Slides were then coverslipped using dibutylphthalate polystyrene xylene (DPX) mounting media (Sigma), and imaged using a brightfield Axioscan 7 Microscope Slide Scanner (Zeiss).

2.3.3 BCA Assay for Protein Quantification

BCA assay was used for quantification of protein concentration for metabolomics normalisation and Western Blot analysis. Dried pellets from polar metabolite extractions, or pulverised frozen tumour powder (~3g) were dissolved in Tris-SDS Lysis Buffer (62.5 mM Tris, 2% SDS, pH 6.8). Samples were vortexed, sonicated for 16 minutes, then placed in a 95°C heat block for 10 minutes to ensure complete lysis. Samples were then spun down at 13,000 rpm for 20 minutes and the supernatant was used for protein quantification. The Pierce BCA Protein Assay Kit

(96-well plate) was used (Thermofisher) according to manufacturer instructions. Briefly, a 50:1 solution of Reagent A and Reagent B was made, and 70 µL of the resulting solution was combined with 4 µL of sample, in triplicate. Samples were incubated for 30 minutes at 37°C. Absorbance was measured in an Infinite M1000 PRO Multimode Microplate Reader (Tecan Group).

2.3.4 Western Blot

SDS-PAGE (8%) running gel and 4% stacking gels were used (see Tables 1.3 and 1.4). Following protein quantification (section 1.3.2), each sample was diluted in 4x Laemli Buffer for a final concentration of µg/µL. For Western Blot analysis, 20 µg of protein was loaded into each well of the gel. The gels were run in Protein Running Buffer (2.5 mM Trizma Base, 19.2 mM glycine, 0.10% SDS; made in-house), at 110V for approximately 80 minutes, or until sufficient protein separation was observed. A Precision Plus Protein Dual Color Standard mix (Bio-Rad) was run in one of the wells for identifying molecular weight of proteins.

Proteins were then transferred onto a nitrocellulose membrane (Bio-Rad) using an electrophoresis transfer chamber with Transfer Buffer (20% methanol, 2.5 mM Tris, 19.2 mM glycine, 0.2% SDS, pH 8.3; made in-house) at 120 V for 2 hours at 4°C. Ponceau staining was performed to visualise any anomalies in the gel or during transfer. The membrane was then blocked in 5% milk for 1 hour at room temperature. Primary antibodies were added to a solution of 1% BSA in PBS-T, and membranes were incubated overnight at 4°C. Membranes were then washed quickly in PBS-T (5 minutes, 3 times) and stained for 1 hour at room temperature, using an HRP-conjugated secondary antibody diluted in 1% BSA in PBS-T (goat anti-rabbit IgG-HRP, 1:3000 dilution (Santa Cruz sc-2301)). Membranes were then washed in PBS (3 minutes, 3 times) and incubated using the Amersham ECL detection kit (GE Healthcare) to visualise chemiluminescence, before imaging using an Amersham Imager 680 (GE Healthcare).

2.3.5 DNA extraction

Genomic DNA was purified for PCR genotyping using the Monarch® Genomic DNA Purification Kit (NEB) following manufacturer's instructions. gDNA was eluted using LC-MS grade water instead of the provided elution buffer, then quantified using the NanoDrop™2000 1-Position Spectrophotometer (Thermo Scientific).

2.3.6 PCR Genotyping

PCR genotyping was performed by first combining the PCR reagents as follows, per sample (total sample volume 21 µL):

- 2x MyTaq™ Red Mix (Meridian Bioscience) 10 µL
- Primer Mix (100 µM) 0.25 µL (x2)
- Purified gDNA 1 µL
- ddH_2O 9.5 µL

PCR program used on a C100 Thermocycler (Bio-rad):

- 94°C 3min
- 94°C, 15 sec
- 65°C, 15 sec
- 72°C, 20 sec
- Repeat steps 2-4 for 34 cycles
- 72°C, 5 min

Primer sequences:

1. MMTV promoter (825bp)

M022 5'-CCCAAGGCTTAAGTAAGTTTTTGG-3'

M023 3'-GGGCATAAGCACAGATAAAACACT-5'

2. MMTV-Myc (human Myc) (~500bp)

h-Myc 5'-GGTGATAGTCCCTTCACATC-3'

h-Myc 3'-GTGCCACCTGACGTCTAAGA-5'

2.4 Metabolomics Methods

2.4.1 Stable isotope infusions and tumour collection for metabolomics

When mammary gland tumours reached 1 cm in diameter, mice were weighed and placed under anaesthesia and infused with stable isotope labelled $^{13}C_6$-glucose (200 mg/kg) or $^{13}C_5$-glutamine (40 mg/kg) for three hours. Serum was collected using cardiac puncture prior to Schedule One Killing (S1K) [596] and tumour collection. Tumours and lungs were dissected and plunge frozen in liquid nitrogen.

2.4.2 Metabolite Extraction for LC-MS

Half of each MGT was used for LC-MS metabolite extraction and half was preserved for MSI analysis. For metabolite extraction, tumours were pulverized using a pestle and mortar submerged in liquid nitrogen. Lung metastases were cryo-dissected from frozen whole lungs in the same conditions using pre-frozen, sterile scalpel and forceps. Tumour powder and whole metastases were then lyophilised and weighed prior to metabolite extraction.

Polar metabolite extraction was performed based on methods previously described [597]. Per sample, 300 µL of polar metabolite extraction buffer (50% methanol, 30% acetonitrile, 20% HPLC-grade water) was added to approximately 3 mg of dried tissue powder or whole dried metastasis. A LC-MS internal standard, ^{13}C-^{15}N-Valine was added to each sample at a final concentration of 5 µM. Each sample was then vortexed, sonicated three times, and spun down in a 4°C centrifuge at 13,000 rpm for 20 minutes. The supernatant was then moved to a new Eppendorf tube, and the pellet was once again re-extracted using 150 µL of polar extraction buffer, this time without internal standard. The samples were vortexed, sonicated and spun down once more and the supernatants were pooled for a final extract volume of 450 µL. For LC-MS analysis, 80 µL of polar extract was used, and pooled batch quality controls (PBQC) were prepared.

For apolar metabolite extraction, the dried pellet left over from polar metabolite extraction was then resuspended in 150 µL polar extraction buffer

(choloroform:methanol solution, 2:1). The samples were vortexed, sonicated and spun down as above. The supernatant was then used for apolar LC-MS analysis. The apolar extract was dried, then resuspended in 50 µL of butanol/10 mM ammonium formate in methanol (1:1).

2.4.3 Derivatisation for GC-MS

If extracts were to be analysed by GC-MS, 3 nanomoles of the internal standard scyllo-inositol were added per sample during polar metabolite extraction. Polar metabolite extracts were subject to derivatization prior to GC-MS analysis. Each sample was dried entirely in an RVC 2-33CD vacuum concentrator (Christ), and washed twice with methanol, followed by complete drying again. Then, 20 µL of methoxamine hydrochloride (Sigma, 20 mg/ml in pyridine) was added and samples were incubated overnight at room temperature. The next day, 20 µL of the derivatisation agent N,O-bis(trimethylsilyl)-trifluoroacetamide (BSTFA) containing 1% trimethylchlorosilane (TMCS) (ThermoFisher) was added per sample.

2.5 MSI Sample Preparation

MSI sample preparation method optimisation was performed to optimise sectioning techniques and settings, and to maximize metabolite preservation and slide cleanliness. The following methods were determined to be optimal for the purpose of this project.

Fresh frozen tumour and lung samples were cryosectioned onto Superfrost slides for DESI-MSI analysis, and onto indium tin oxide (ITO)-coated slides (Bruker) for OrbiSIMS analysis. Sections were made using a Leica CM3050s cryostat and section thickness was set to 10 µM. Adjacent sections were stained with H&E to confirm presence of metastases in lung sections. Each frozen tissue sample was embedded onto a cryostat chuck using pre-cooled HPLC-water, taking care not to allow any tissue thawing. The cryostat temperature was kept at -22°C for lung sectioning, and -16°C for tumour sectioning.

Prepared slides were then dried using a nitrogen sprayer, and immediately vacuum-packed in individual slide containers, and stored at -80°C until analysis to prevent any thermal degradation of metabolites.

2.6 Metabolomics and MSI technology platforms and data analysis

2.6.1 LC-MS

LC-MS analysis was performed with the help of Dr. Nathalie Legrave at the Francis Crick Institute's Metabolomics facility. LC-MS analysis was performed on the Q Exactive Plus Mass Spectrometer (Thermofisher) for polar metabolite analysis. The chromatographic separation was performed on a SeQuant® Zic®pHILIC (Merck Millipore) column (5 µm particle size, polymeric, 150 x 4.6 mm). Apolar LC-MS analysis was performed on the Q Exactive Mass Spectrometer (Thermofisher). The chromatographic separation was performed on a C18 Zorbax Eclipse plus (Agilent) column (1.8 µm particle size, Rapid Resolution HD, 100 x 2.1 mm). The mass resolving power was set to 70,000 for both analyses, and both negative and positive ion polarities were used for maximal metabolite coverage. LC-MS data

were analysed using the Xcalibur software (Thermofisher) for selecting peaks of interest and an in-house LC-MS data analysis script developed by Dr. Avinash Ghanate, which allowed natural isotope abundance correction (https://avi-crick.shinyapps.io/MSIso/). For each metabolite, the area under the curve was normalised to the area under the curve of the internal standard (13C-15N-valine) and by dried sample weight measured prior to metabolite extraction.

2.6.2 GC-MS

GC-MS analysis was performed with the help of Dr. Nathalie Legrave, Dr. Jim Elils at the Francis Crick Institute's Metabolomics facility. Samples were analysed using the Agilent 7890A-5975C GC-MS instrument, using a 0.25 mm DB-5MS + DG column (Agilent), at 270°C injection temperature using helium carrier gas and electron ionisation mode. The exact GC-MS acquisition parameters were previously reported [13]. GC-MS data were analysed using the MassHunter software (Agilent), correcting for natural isotope abundance. For each metabolite, the area under the curve was normalised to the area under the curve of the internal standards (scyllo-inositol and L-norleucine) and by dried sample weight measured prior to metabolite extraction.

2.6.3 DESI-MSI

DESI-MSI was performed with the help and guidance of Vincen Wu at the lab of Professor Zoltan Takats at Imperial College London. Tissue sections were thawed at room temperature before breaking the vacuum seal to prevent moisture accumulation on the sample surface. DESI-MSI was performed using the Xevo™ G2-XS QToF mass spectrometer (Waters). The optimised parameter of the DESI sprayer and inlet geometry are summarised in the table below in Table 1.5 (see Figure 1-8b for detailed DESI schematic). Following DESI-MSI, samples were re-vacuum packed to preserve tissue morphology, and stored at -80°C. For post DESI-MSI H&E staining, samples were rehydrated in decreasing ethanol concentrations prior to fixation and staining. DESI-MSI data analysis was performed using the HDImaging software (Waters), the MATLAB-based MSI data analysis software developed at the National Physical Laboratory, SpectralAnalysis

[598], and an in-house DESI-MSI data visualisation script developed by Dr. Avinash Ghanate (https://clvd1-ws-u-p-58.thecrick.org/MIMA/e6194c9e457c1/). DESI-MSI ion annotation was performed using the CEUMass Mediator WCGNA analysis was performed by Dr. Avinash Ghanate, as reported and developed by Dr. Paolo Inglese [599], [600].

Table 8: DESI Imaging Parameters

Parameter	Setting
Spray voltage	4.5 kV
Nitrogen gas pressure	5 bar
Solvent composition	95% methanol in HPLC-grade water
Solvent flow rate	1.5 µL/min.
Sprayer to inlet capillary distance	3 mm
Sprayer to surface distance (d1)	0.5 mm
Sprayer impact angle (α)	75°
Collection angle (β)	10°
Mass range	50 - 1000 *m/z*
Scan rate	1 scan/sec
Acquisition speed	100 um/sec
Mass resolving power	10,000 at 200 *m/z*
Pixel diameter	100 um

Table 9: KEGG Pathways used for DESI-MSI spectra annotation

KEGG Pathways	Code
Alanine, aspartate and glutamate metabolism	00250
Amino sugar and nucleotide sugar metabolism	00520
Arginine and proline metabolism	00330
Ascorbate and aldarate metabolism	00053
beta-Alanine metabolism	00410
Biosynthesis of amino acids	01230
Citrate cycle (TCA cycle)	00020
Cysteine and methionine metabolism	00270
Glutathione metabolism	00480
Glycine, serine and threonine metabolism	00260
Glycolysis / Gluconeogenesis	00010
Histidine metabolism	00340
Inositol phosphate metabolism	00562
Lysine degradation	00310
One carbon pool by folate	00670
Oxidative phosphorylation	00190
Pantothenate and CoA biosynthesis	00770
Pentose and glucuronate interconversions	00040
Pentose phosphate pathway	00030
Phenylalanine metabolism	00360
Primary bile acid biosynthesis	00120
Purine metabolism	00230
Pyrimidine metabolism	00240
Pyruvate metabolism	00620
Taurine and hypotaurine metabolism	00430
Tryptophan metabolism	00380
Tyrosine metabolism	00350
Valine, leucine and isoleucine degradation	00280

2.6.4 OrbiSIMS

OrbiSIMS method development for biological sample analysis was conducted by me with the help and guidance of Dr. Melissa Passarelli, Dr. Rasmus Havelund and Dr. Jean-Luc Vorng in Professor Ian Gilmore's lab at the National Physical Laboratory.

The exact sample preparation and image acquisition procedures followed for biological tissue samples by OrbiSIMS has been described in detail in a publication that I contributed to [601]. The OrbiSIMS instrument was operated and data was subsequently analysed using the SurfaceLab (IONTOF) and Q Exactive (Thermofisher) software. The argon gas cluster ion beam (GCIB) of the OrbiSIMS was set to a cluster size of Ar3000, with 20 keV energy. The Orbitrap mass analyser was calibrated using a silver block prior to each acquisition, for positive and negative ion mode consecutively. Vacuum-packed biological samples on ITO-coated slides were allowed to thaw and dry at room temperature before opening the vacuum seal. Slides were then mounted onto the OrbiSIMS stage and transferred into the OrbiSIMS instrument's vacuum chamber for imaging.

Chapter 3. Assessing the metabolism of metastatic MYC-driven mammary gland tumours.

3.1 Introduction

As reviewed in detail in the Introduction chapter of this thesis, specific metabolic reprogramming has been shown to be associated with a driver MYC oncogene in several tumour types (upregulated glycolysis [476], [602], glutaminolysis [120]-[478], lipid metabolism [334]-[603]. Many MYC-driven metabolic changes have been demonstrated in specific tumour types and may be dependent on the organ of tumour origin. In breast cancer, MYC expression has been shown to be highly heterogeneous, which adds to the complexity of metabolic transformations supporting tumour growth and progression [604]–[608].

Metabolic heterogeneity is particularly pertinent in the context of metastasis. Different clonal sub-types of tumour cells may exhibit different metabolic profiles defining their capacity to metastasise [609]–[611]. Non-tumour components of the tumour microenvironment (TME) [612], [613] and the metastatic niche [22], [614] also contribute to metabolic reprogramming of the tumour cells, and this has been shown to support metastatic dissemination and progression. Furthermore, it has been shown that transcription factors driving epithelial-to-mesenchymal transition (EMT), a process widely characterised as integral to metastatic dissemination, can stimulate metabolic changes [117], [497]. On the other hand, metabolic changes in the tumour have been shown to drive EMT [490], [615], [616]. MYC overexpression in human breast tumours has been linked to poor prognosis and increased malignancy [617], however, the relationship between MYC-dependent metabolism and metastatic tumour progression has not been evaluated so far.

The transgenic MMTV-MYC mouse line is widely used to study the role of MYC in breast tumourigenesis [618], [619]. In this model, MYC is ectopically overexpressed at the MMTV promoter. These mice develop tumours at the age of 20-30 weeks, and tumours are typically collected for metabolomic studies at a diameter of ~10 mm (500 mm^3 volume). I used the MMTV-MYC model to compare the metabolic

changes between MYC-driven MGTs and their lung metastases. Lung metastasis incidence in the MMTV-MYC mouse tumours was relatively low, and any visible metastases were very small (<100 μm diameter) at the time of collection (Figure 3-1a), in accordance with previous reports of low metastatic potential in this model [620], [621]. However, we observed that one of the tumour cell lines generated from a MMTV-MYC tumour by a previous PhD student, Dr. Emma Still, yielded lung metastasis when it was injected into the fat pad of wildtype FVB/NJ female mice. This cell line, referred to as Myc310, originated from a mouse that surprisingly had three separate MGTs at the same time (typically only one MGT is observed per mouse), and was previously propagated *in vitro* over multiple passages for approximately a year. Unfortunately, the lungs from the original Myc310 mouse were not collected therefore the metastatic burden is unknown, although it is likely that the original tumour had a metastatic propensity. Nonetheless, the incidence and size of lung metastases from mice injected with Myc310 cells was on average significantly larger compared to MMTV-MYC MGTs (Figure 3-1b), therefore this was selected as a model to study the metabolism of MYC-driven metastatic tumours and their lung metastases.

Since MYC-driven tumours are notoriously heterogeneous, I first evaluated the metabolism of tumours formed by the injection of the metastatic Myc310 cells and a range of transgenic MMTV-MYC MGTs of comparable size. The aim of these experiments was to determine whether a particular metabolic transformation was associated with the higher metastatic burden of Myc310 MGTs. Notably, when looking at the timeline between tumour detection (typically at around 5 mm in diameter) and tumour collection (1.0-1.2 cm in diameter), Myc310 tumours were comparable in proliferation rate to transgenic tumours (Figure 3-1c). Interestingly, Myc310 MGTs on average showed lower levels of MYC than transgenic MGTs (Figure 3-1d). Since ectopic MYC is expressed from the luminal MMTV promoter in this model, the de-differentiation of primary tumour cells that often occurs during EMT [622], [623] may lead to promoter downregulation and therefore lower MYC expression in Myc310 tumours. This is concurrent with higher expression of the mesenchymal marker vimentin in Myc310 tumours, and higher expression of the epithelial marker E-cadherin in transgenic tumours (Figure 3-1d).

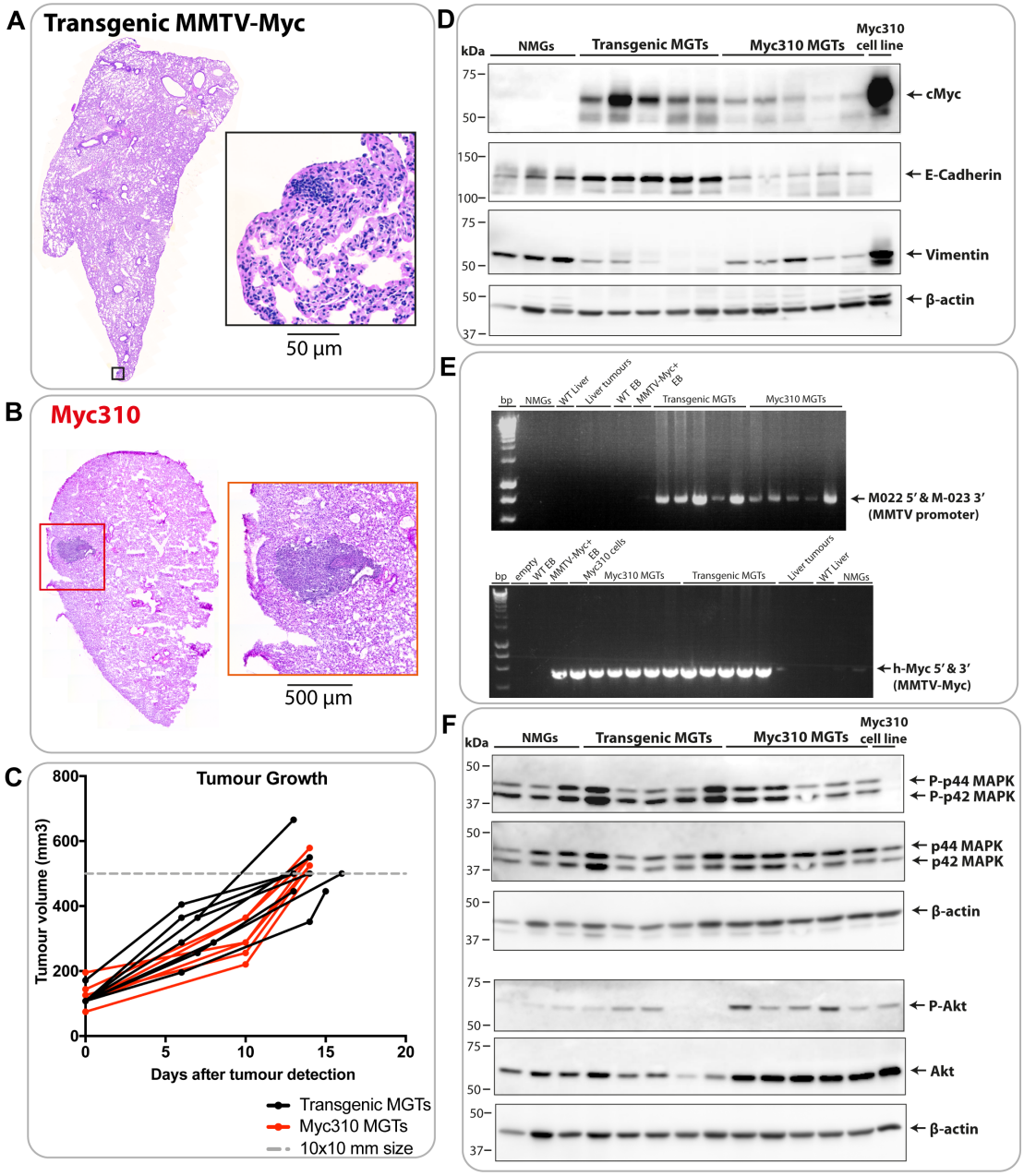


Figure 3-1. Comparison of metastatic burden and primary tumour characteristics between transgenic and Myc310 MGTs.

(A) Lung from mouse with a transgenic MMTV-Myc tumour, showing micro-metastasis in the lung. (B) Lung from mouse with a Myc310 tumour, showing larger metastasis. (C) Growth of primary transgenic and Myc310 MGTs from day of detection (~5-6 mm diameter) to collection (~10-12 mm diameter). (D) WB comparing protein levels of the MYC oncogene, epithelial marker E-Cadherin and mesenchymal marker vimentin in normal mammary glands (NMGs), transgenic MGTs and Myc310 MGTs. (E) PCR genotyping with two sets of primers against the MMTV promoter and the MMTV-Myc transgene confirming that Myc310 MGTs originated from a transgenic MMTV-MYC tumour. EB = ear biopsy. (F) Western blots comparing levels of proteins in several oncogenic signalling pathways: P-Erk/Erk (P-p44/p42 MAPK) as a readout for RAS activation, and P-Akt/Akt as a readout for PI3K activation.

In order to demonstrate that the Myc310 cell line was derived originally from a transgenic MMTV-MYC tumour, PCR genotyping followed by agarose gel electrophoresis was performed, using two sets of primers that were previously reported to confirm the expression of the MMTV-MYC transgene (Figure 3-1e). The first set of primers was designed against the MMTV long terminal repeat (LTR) sequence and the p21 gene that follows the MMTV-LTR on the 3' end [624]. The second set of primers was reported to specifically recognise the MMTV-MYC transgene [625]. Tissues negative for MMTV-MYC were used as negative controls, including NMGs, liver and ear biopsy (EB) from WT mice, a liver tumour that was not driven by MYC. Transgenic MMTV-MYC tumours and an EB from a MMTV-MYC positive mouse was used as positive controls.

The MMTV-MYC model has been reported to harbour multiple secondary oncogenic mutations [75], [604], [626]. To better characterise how the Myc310 cell line and Myc310 MGTs compare to the transgenic MGTs, western blot analysis was performed to survey the activity of three major oncogenic signalling pathways (Figure 3-1f). The levels of Erk (p44/p42 MAPK) and phosphorylated Erk were lower in the Myc310 MGTs, and there was no phospho-Erk expression in the Myc310 cell line. This suggests that there is a higher activation of the RAS oncogenic signalling pathway in transgenic tumours [627], [628]. On the other hand, Myc310 MGTs and Myc310 cells had higher levels of Akt and phosphorylated Akt than transgenic MGTs, suggesting a higher activation of the PI3K signalling pathway [629]–[631]. Taken together, the Myc310 cell line shows several oncogenic distinctions from transgenic MGTs, and tumours derived from this cell line show differential oncogenic signalling *in vivo* compared to the cell line *in vitro*. Activation of secondary oncogene signalling pathways on top of the expression of MYC was therefore likely a clonal selection *in vitro* as the MYC310 cell line was being established. Further investigation is needed to determine if these differences in oncogenic signalling are responsible for the more aggressive phenotype of these cells, as well as their ability to metastasize and survive in the vasculature and distal organs such as the lung.

Having better characterised the Myc310 model, transgenic MMTV-Myc MGTs were compared to Myc310 MGTs first using LC-MS. The polar metabolite extraction, as

well as LC-MS instrumental and data analysis methods used are described in details in the Methods chapter of this thesis. Notably there was a wide distribution of metabolite levels in the transgenic MGTs, aptly reflecting the high degree of heterogeneity in MYC-driven MGTs. The Myc310 cells were propagated *in vitro* for multiple passages, possibly undergoing a clonal selection that resulted in more a homogeneous metabolic profile in tumours generated from these cells.

3.2 Glycolysis, TCA and PPP

First, the levels of central carbon metabolites were compared between transgenic MMTV-MYC and Myc310 MGTs. Metabolites that were significantly higher in the more metastatic Myc310 MGTs are summarised in Figure 3-2. The levels of glycolytic intermediates dihydroxyacetone phosphate (DHAP), 2- and 3-phosphoglycerate (2/3PG) and phosphoenolpyruvate (PEP) were significantly higher in Myc310 MGTs than in transgenic MGTs, suggesting higher glycolytic flux in Myc310 MGTs Figure 3-2a). Pyruvate could not be detected using the LC-MS that was used throughout this study. The exact reason for this was not investigated as it was outside of the scope of this project, however this may be due to the column that was used, or as a result of the pH of the mobile phase, as other studies have frequently demonstrated pyruvate detection by LC-MS [66], [191], [634], [635].

Given the limitations in pyruvate detection by our established LC-MS methods, the polar extracts from the same samples were further analysed using GC-MS, which revealed higher pyruvate levels in Myc310 MGTs just below the significance threshold (Figure 3-2a). This was in line with the LC-MS-based hypothesis that Myc310 MGTs have higher glucose catabolism than transgenic MGTs. Lactate levels were comparable between the two tumour groups, which may indicate a preference for glucose catabolism into the TCA cycle in Myc310 MGTs. Consistently, although most TCA cycle intermediates were present at comparable levels between the two groups, citrate and cis-aconitate levels were significantly higher in Myc310 MGTs than in transgenic MGTs. Using stable isotope tracing is

necessary to determine the degree of carbon contribution from glucose and glutamine to the TCA cycle in these two tumour models.

Furthermore, higher levels of 6-phosphogluconate (6PG), ribose-5-phosphate (R5P) and sedoheptulose-7-phosphate (S7P) in Myc310 MGTs compared to transgenic MGTs suggested increased PPP activity in Myc310 tumours (Figure 3-2c). Indeed, the PPP has been shown to be upregulated in more aggressive tumours [636], [637]. In particular, the increased production of NADPH in the PPP results in a higher reductive potential, which can support metastasising tumour cells and promote their survival and growth in environments with increased levels of ROS [116], [638].

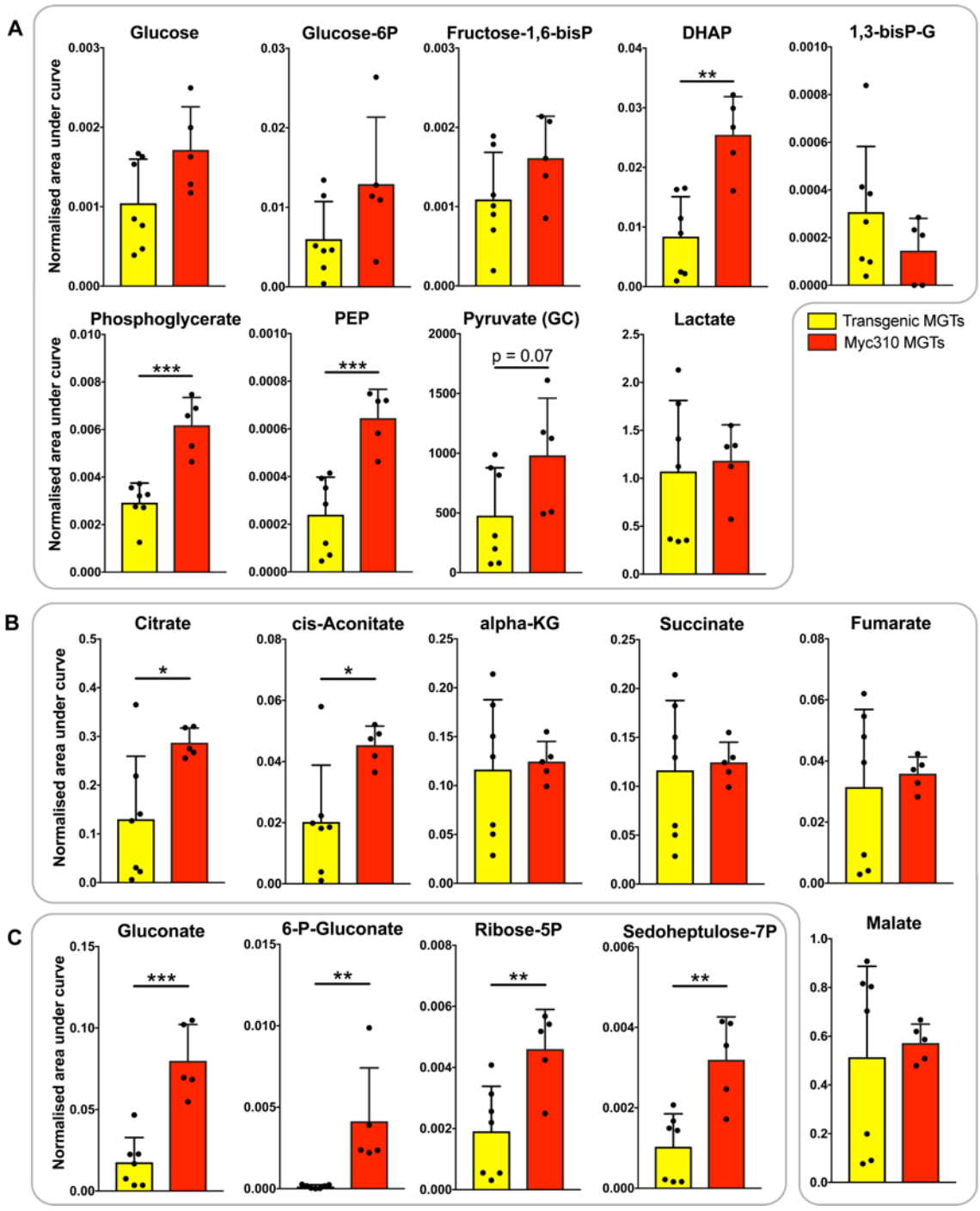


Figure 3-2. LC-MS metabolomics results comparing glycolysis.
(A), TCA (B) and PPP (C) pathways in MMTV-Myc transgenic mammary gland tumours and tumours derived by intra-fat pad injection of Myc310 tumour cells. Unpaired t-test statistics used to generate significance levels (* $p < 0.05$, ** $p < 0.01$, *** $p < 0.001$).

3.3 Amino acids

Levels of essential and non-essential amino acids showed no significant changes between the two tumour groups, with the exception of significantly elevated levels of glycine in Myc310 MGTs (Figure 3-3 a-c).

3.4 Nucleotide biosynthesis and associated metabolites

The levels of mono- and di-phosphorylated purines and pyrimidines were comparable between Myc310 and transgenic MGTs. However, nucleotide triphosphates (ATP, GTP, UTP) were all significantly increased in the Myc310 MGTs, as well as the levels of free uracil (Figure 3-4a). The ATP/AMP ratio was noticeably but not significantly higher in the Myc310 MGTs, possibly indicating a higher energetic capacity in these tumours. The GTP/GMP and UTP/UMP ratios were significantly elevated in Myc310 MGTs (Figure 3-4b).

Consistently, Myc310 MGTs had higher levels of creatine-phosphate Figure 3-5c), indicating an increased storage of phosphate groups to support bioenergetic demands. Finally, Myc310 MGTs also had significantly increased levels in glucosamine-6-phosphate suggesting increased nucleotide sugar biosynthesis from glutamine (Figure 3-4c).

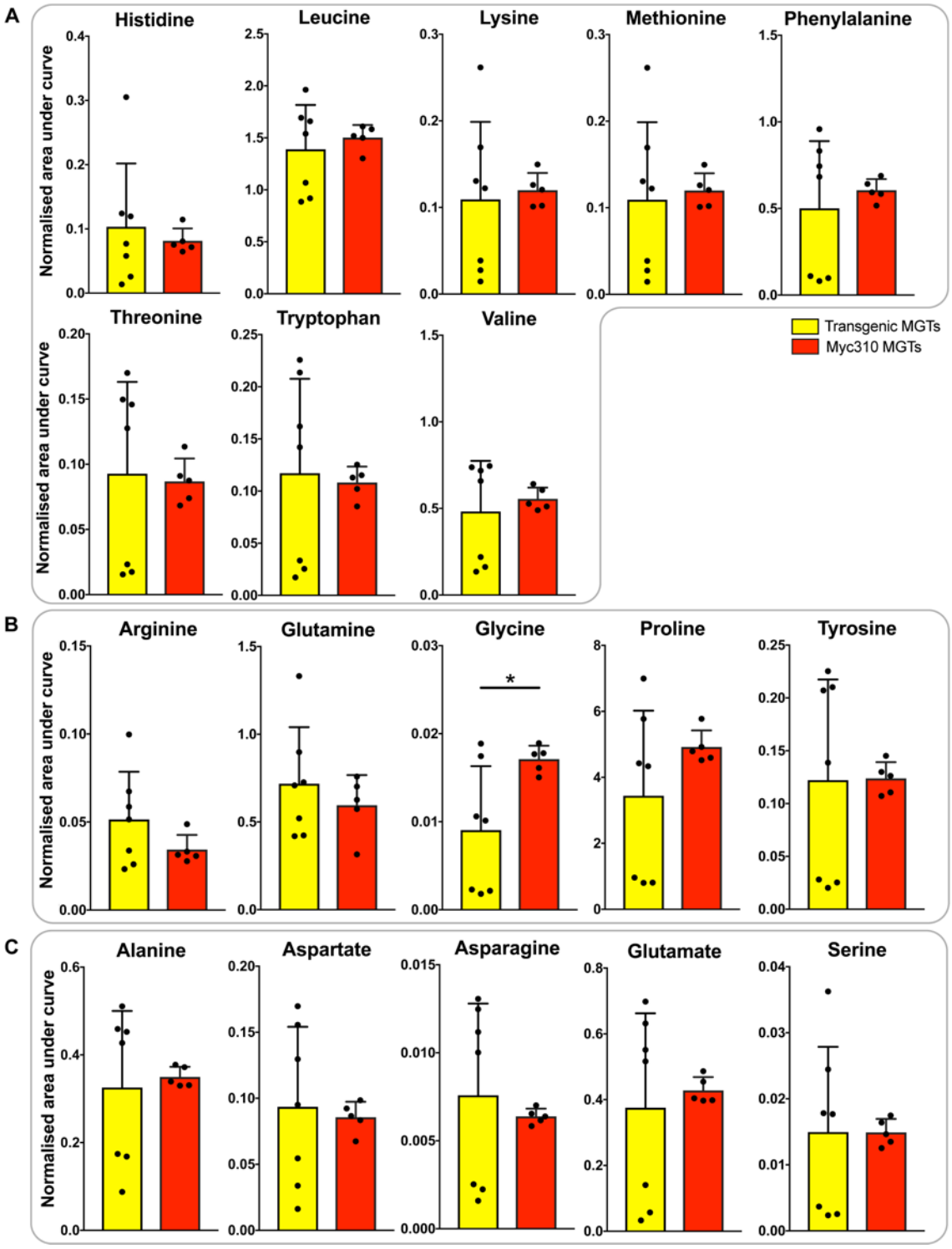


Figure 3-3. LC-MS metabolomics results comparing MMTV-Myc transgenic mammary gland tumours and tumours derived by intra-fat pad injection of Myc310 tumour cells. Levels essential amino acids (A), conditionally non-essential amino acids (B), non-essential amino acids (C) compared, with only glycine showing significantly higher levels in Myc310 MGTs. Unpaired t-test statistics used to generate significance levels (* $p < 0.05$, ** $p < 0.01$, *** $p < 0.001$).

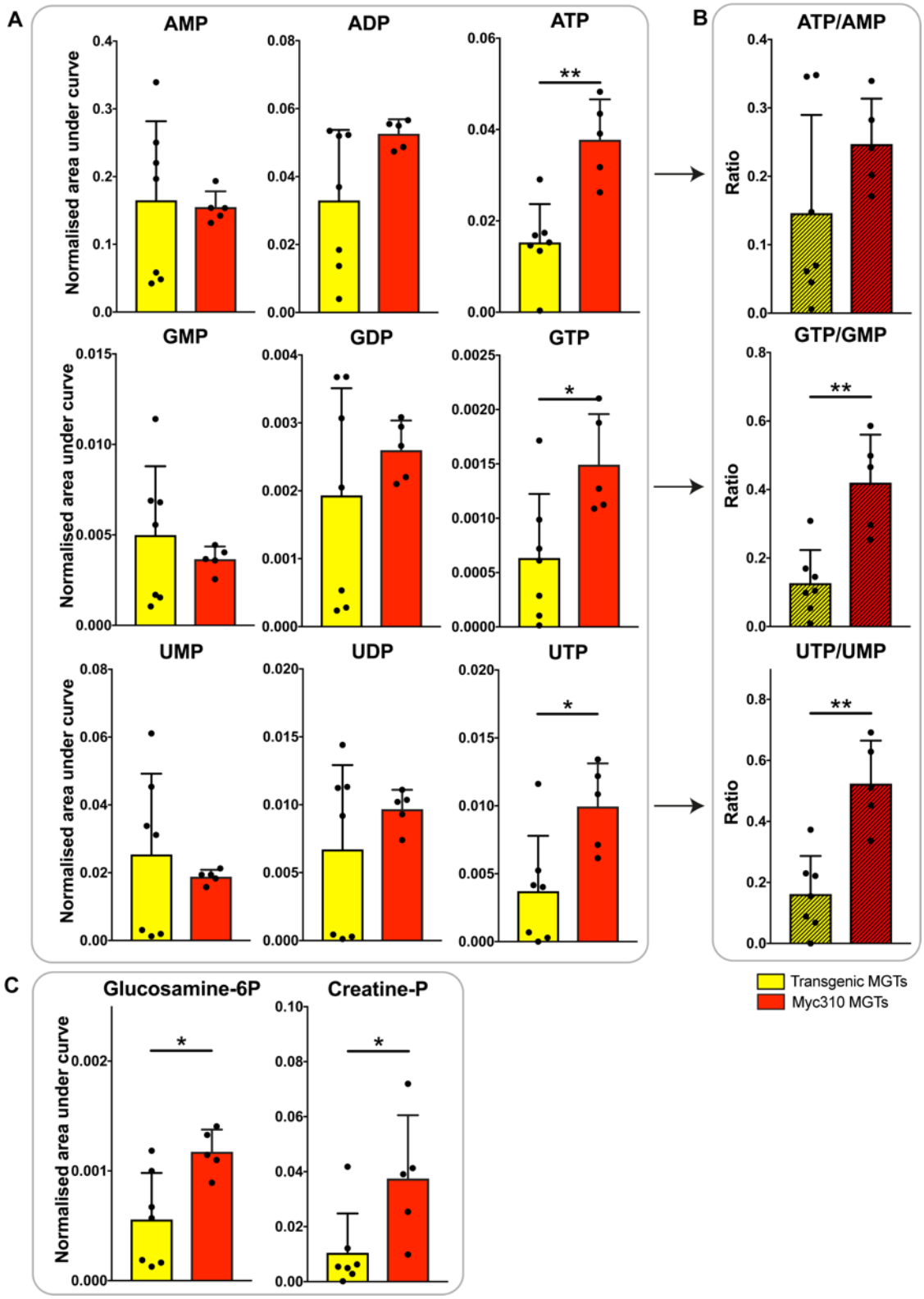


Figure 3-4. LC-MS metabolomics results comparing nucleotide levels
(A), ratios of tri-phosphated to mono-phosphated nucleotides, and (C) glucosamine-6-phosphate and creatine-phosphate levels in transgenic and Myc310 tumours. Unpaired t-test statistics used to generate significance levels (* $p < 0.05$, ** $p < 0.01$, *** $p < 0.001$).

3.5 One carbon metabolism and glutathione

One carbon metabolism intermediates were present in comparable levels between the two tumour groups, with the exception of betaine, which was significantly higher in Myc310 MGTs (Figure 3-5a). Notably the SAM/SAH ratio, which is an indicator of methylation capacity in the cells, was elevated in Myc310 MGTs ($p = 0.028$) (Figure 3-5b). Furthermore, while levels of reduced glutathione were also comparable, levels of oxidized glutathione were significantly raised in Myc310 MGTs. This translated into a lower GSH/GSSG ratio in Myc310 tumours (although below significance threshold), which may be an indicator of higher oxidative stress in comparison to transgenic tumours.

3.6 Vitamins

The levels of vitamin C (ascorbic acid) and vitamin B5 (pantothenic acid) were notably different between the two tumour types. However, both of these differences did not reach statistical significance due to high variability in the transgenic MGT group (Figure 3-5c). The higher levels of ascorbic acid in Myc310 MGTs in comparison with MMTV-Myc tumours are consistent with its role in protein biosynthesis and, importantly, in REDOX homeostasis, protecting cells from oxidative stress. The latter is in line with increased levels of PPP intermediates and decreased GSH/GSSG ratio suggesting that Myc310 cells have increased activity of antioxidant pathways protecting from increased ROS production.
Pantothenic acid was the only polar metabolite that was detected at higher levels in the transgenic MGTs compared to Myc310 MGTs (Figure 3-5c). Given higher proliferation rates, it can be assumed that the bioenergetic and biomass demands of Myc310 MGTs were overall higher to support tumour growth. Pantothenic acid is a vitamin that is used for synthesis of Coenzyme A, which in turn is a key cofactor in the oxidation reactions involved in the TCA and fatty acid biosynthesis. Lower pantothenic acid levels in Myc310 MGTs can be a result of its higher usage in these pathways.

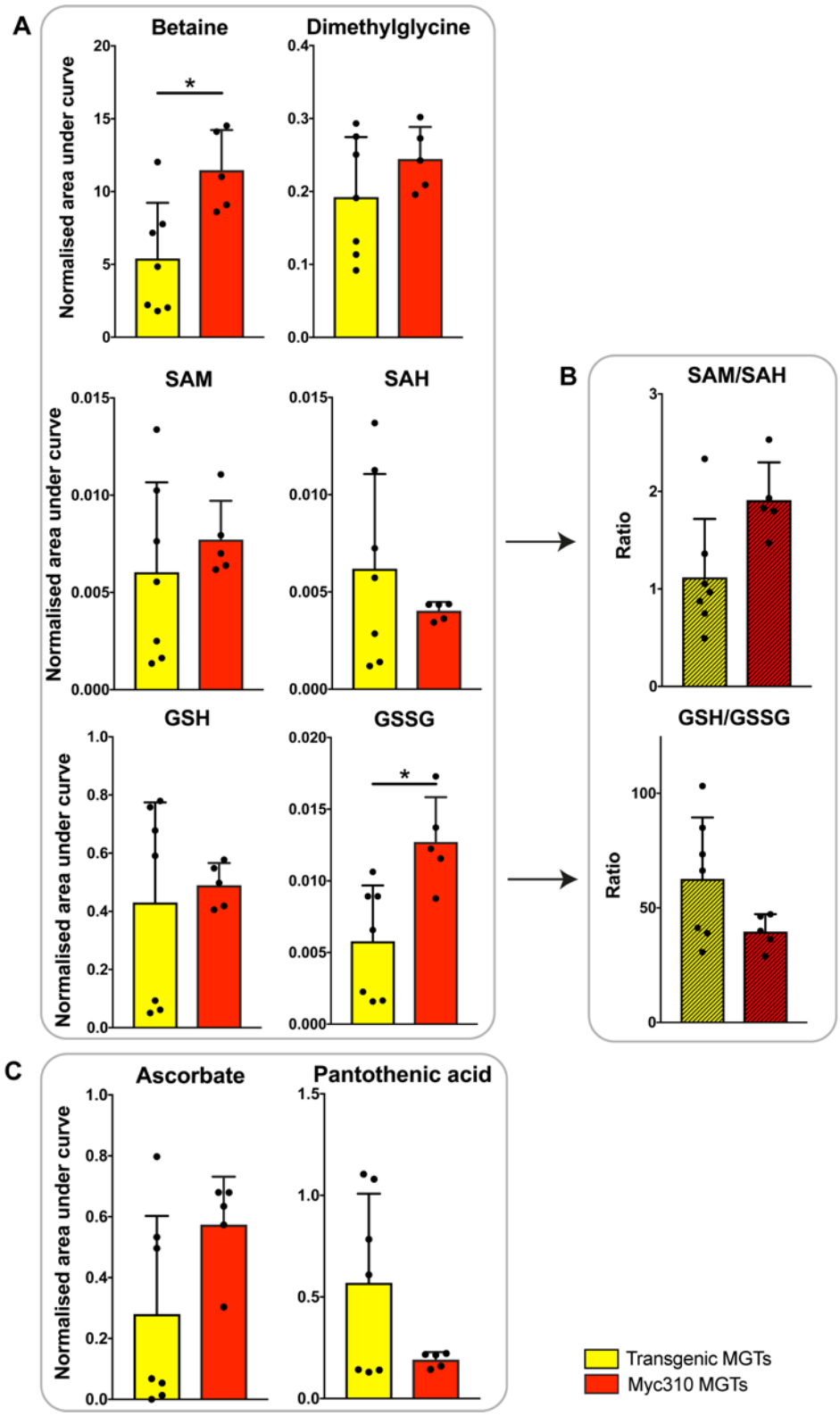


Figure 3-5. LC-MS metabolomics results comparing one carbon metabolism and glutathione metabolism.
One carbon metabolism and glutathiones (A), SAM/SAH and GSH/GSSG ratios (B) and vitamins (C) in MMTV-Myc transgenic and Myc 310 tumours. Unpaired t-test statistics used to generate significance levels (* $p < 0.05$, ** $p < 0.01$, *** $p < 0.001$).

3.7 Chapter Discussion

In this chapter I have described the similarities and differences in metabolite levels between transgenic and Myc310 MGTs. Several metabolic changes, namely increased glycolysis [96], [639] and nucleotide biosynthesis [85], [154], [640] have been attributed to increased bioenergetic demands of highly proliferative tumours. Also, increased ATP/AMP ratio indicates an active proliferative state [641]. While I have shown that the tumour growth rate between initial detection and resection were comparable, the actual proliferation rate and viability of Myc310 MGT cells may be upregulated than that of transgenic MGTs and needs to be further investigated by examining proliferation marker expression such as Ki-67. Tumour size measurements do not take into account the proportion of apoptotic or necrotic cell death within the tumour compared to viable cells.

Myc310 MGTs had higher total levels of the antioxidant metabolites glutathione [642], [643] and ascorbic acid [644]–[646], as well as a lower GSH/GSSG ratio [504], [647], suggesting increased oxidative stress. Furthermore increased PPP has been shown to be associated with metastatic progression and NADPH production in oxidative stress [116], [638], [648], [649]. The ability of tumour cells to cope with elevated levels of ROS has been reported as a feature of increased proliferation [650], [651], but also as a key metabolic adaptation associated with tumour aggressiveness and metastasis [313], [652], [653]. Therefore, these adaptations may be playing a direct role in allowing Myc310 MGT cells to survive in high oxygen environments, such as inside the vasculature [654] and lung tissue [655], resulting in metastatic tumour formation [499], [503], [656]. Upregulation of *de novo* nucleotide biosynthesis, as seen in Myc310 MGTs, has recently been shown to directly drive metastasis through activation of cGMP-dependent protein kinase downstream of MAPK [657]. Furthermore, the increase in SAM and the SAM/SAH ratio suggests a higher methylation capacity [658] in the Myc310 MGTs. This observation is of particular interest since epigenetic modifications directly link metabolism to changes in gene expression that can support cancer progression [659], [660] and metastasis [661].

Western blot analysis revealed lower protein levels of MYC in Myc310 MGTs compared to transgenic MGTs, and differential levels of MYC are likely to directly impact metabolism in these tumours. Lower MYC levels were contradictory to the comparable proliferation rates of Myc310 tumours, since MYC is a known driver of proliferation [662]. On the other hand, high levels of MYC have also been reported to be associated with apoptosis [663], [664], potentially explaining slower development of the transgenic tumours. In this model, MYC is overexpressed at the MMTV promoter, which is expressed in mammary luminal epithelial cells [665]. A common feature of more aggressive tumours is a de-differentiation program, during which tumour cells revert to a more stem-like state [666], [667] that may facilitate EMT and metastasis [622], [668]. Since the Myc310 cell line was generated as a result of numerous continuous *in vitro* passages, it is highly likely that a clonal selection event had occurred, selecting for a particularly aggressive clone or clones. To confirm MMTV levels in the two tumour types qPCR analysis of MMTV expression should be performed.

The metabolic differences between transgenic and Myc310 MGTs, including upregulated PPP, nucleotide biosynthesis, and antioxidant response pathways, can be attributed to both increased proliferation and more aggressive phenotype of the latter tumours. These changes potentially can be exploited in targeted therapies to prevent MYC-driven tumours from metastasising. However, further work is needed to confirm the dependency of Myc310 MGTs on these pathways and to determine their exact impact on metastatic burden. In order to accurately deduce information about metabolic flux and activated pathways, stable isotope tracing needs to be performed. Furthermore, enzyme and transporter expression need to be assessed in order to confirm metabolomic findings. For example, while amino acid levels were comparable between transgenic and Myc310 MGTs, the Myc310 MGTs were more proliferative and are therefore likely to have a higher amino acid turnover. In this case, comparative levels may signify upregulated amino acid transporters or increased biosynthesis of particular amino acids in these tumours. Due to time constraints and a primary focus on studying metabolic changes between MGTs and lung metastases, these changes were not assessed further in the scope of this project, however this exploratory analysis introduced several avenues of interest for future projects in the lab.

Chapter 4. Comparing the metabolism of metastatic mammary gland tumours and lung metastases derived from them.

4.1 Introduction

Having established several metabolic adaptations in metastatic Myc310 MGTs compared to average MMTV-MYC transgenic MGTs, I evaluated the metabolic differences between Myc310 MGTs and their lung metastases (Myc310 LMs). The aim of this experiment was to determine metabolic adaptations which may be required for metastasis survival and growth in the lungs.

Although Myc310 MGTs were associated with higher incidence of metastasis and metastatic burden than transgenic MGTs, the metastases were still on average very small and therefore still difficult to dissect accurately from the infiltrated lungs. In the cases when the size allowed I dissected metastatic lesions from flash-frozen lungs to preserve metabolism in its native state as much as possible. The dissected metastatic lesions and their parental tumours were analysed by LC-MS. In Chapters 6 and 7 I will present how LC-MS analysis was followed by DESI-MSI to visualise the distribution of metabolites not only within MGTs but also in the metastatic lung distinguishing between tumour cells and components of their microenvironment.

The sample set analysed in this experiment included four mice; only one LM was identified in two of them, one mouse had two, and one mouse had six individual LMs, excluding 5 other LMs that were too small to accurately detect all common polar metabolites in (less than 0.4 mg dry weight). Grouped analysis between Myc310 LMs (n = 10) and Myc310 MGTs (n = 4) was first conducted using an un-paired t-test to generate p-values. However, this analysis had several limitations, including variations in LM size and therefore dissection accuracy, as well as the possibility of inherently heterogeneous metabolic profiles of MGTs. Because of this, fold change analysis of metabolite levels of each Myc310 LM compared to the Myc310 MGT that it originated from was performed. These fold changes were then

averaged between Myc310 LM and Myc310 MGT groups, and this is referred to as the “grouped” analysis in this section. Paired t-tests could not be conducted in this case since there were four MGTs, and different numbers of LMs resulting from each, therefore including the same MGT multiple times in cases where there are more than one LM would lead to inaccuracies of the mean and standard deviation in the MGT group. It was important to demonstrate metabolite levels in individual metastases rather than simply comparing the two groups in order to highlight the possibility of heterogeneous metabolic profiles in different metastases and the surrounding niche. Taking advantage of mass spectrometry imaging (described in Chapter 6 and 7), I was able to demonstrate how different metastatic lesions within even the same lung lobe can be metabolically different. An important consideration is the cellularity of individual metastatic lesions. LC-MS results were normalised to sample dry weight prior to metabolite extraction, however this did not account for the amount and identity of cells making up the metastatic lesion. This poses a limitation to the analysis presented here, however protein pellets from each sample were preserved for future RNAseq analysis, from which the contribution of different cell types to the total population of LMs and MGTs can be derived.

4.2 Glycolysis and PPP

Grouped LC-MS analysis between all Myc310 LMs and Myc310 MGTs revealed significantly higher levels of F1,6BP, 1,3BPG and 3PG (Figure 4-1a,b). Paired analysis comparing each Myc310 LM to the Myc310 MGT that it originated from similarly showed significantly elevated levels F1,6BP and 1,3BPG, with 3PG falling below significance threshold (Figure 4-1c). Conversely, G6P levels were lower in LMs in all groups by both grouped and paired analysis (Figure 4-1c).

Among PPP intermediates, both grouped and individual comparison between Myc310 LMs and Myc310 MGTs showed a significant decrease in 6PG levels in LMs in both grouped and paired analyses (Figure 4-2a-c). The rest of the PPP metabolites detected had comparable levels between the two groups, with only a few instances of differential levels in individual Myc310 LMs compared to paired

Myc310 MGTs. All together these results suggest an increased glycolysis and decreased PPP in Myc310 LMs in comparison with Myc310 MGTs.

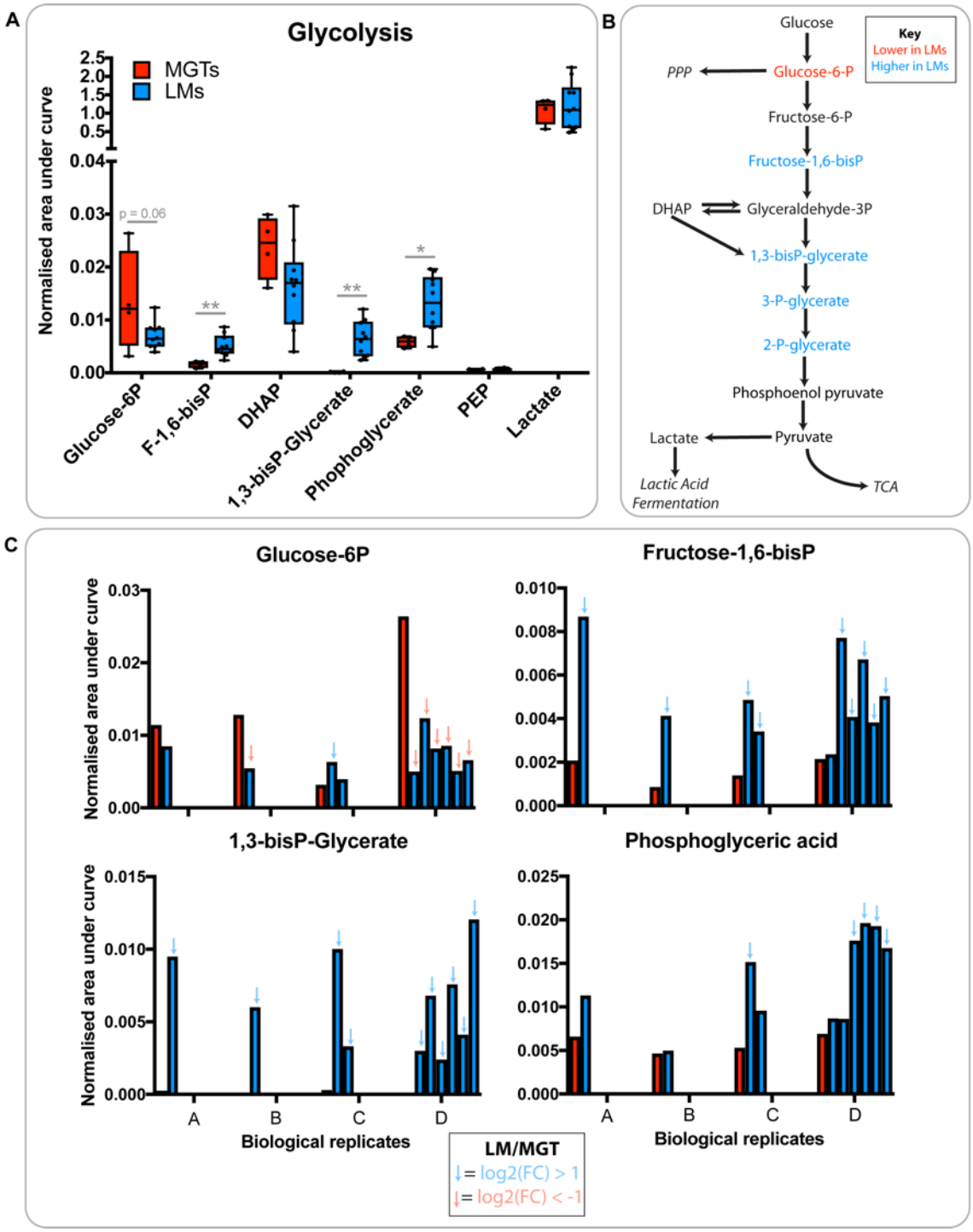


Figure 4-1. LC-MS metabolomics results comparing glycolysis between Myc310 MGTs and Myc310 LMs.
(A) Grouped comparison (* $p < 0.05$, ** $p < 0.01$, *** $p < 0.001$). (B) Pathway diagram, indicating changes based on grouped comparison. (C) Metabolite levels in individual samples, arrows indicating pair-wise significance between each LM and the MGT that it originated from (log2FC > 1).

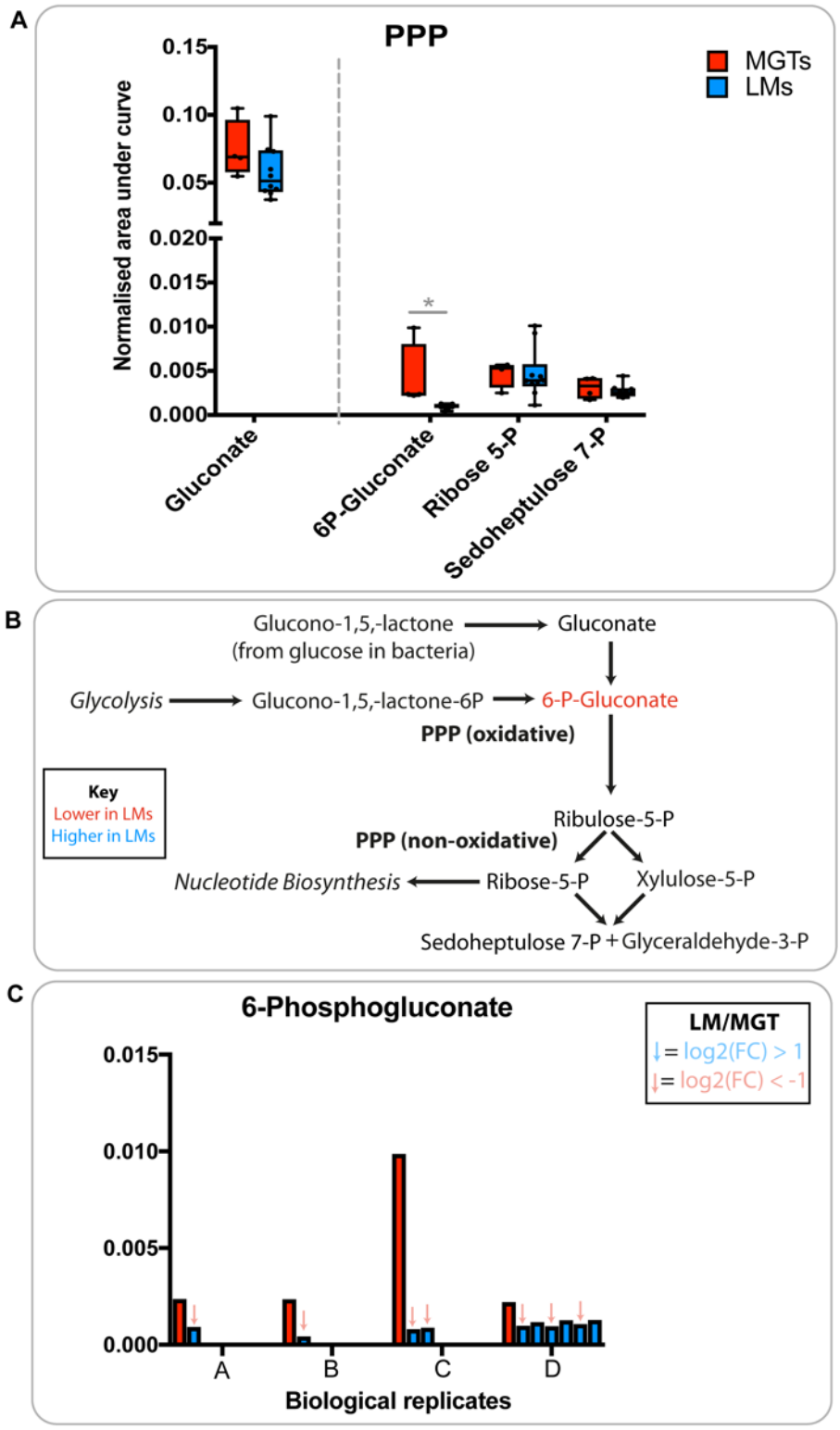


Figure 4-2. LC-MS metabolomics results comparing PPP between Myc310 MGTs and Myc310 LMs.
(A) Grouped comparison (* $p < 0.05$, ** $p < 0.01$, *** $p < 0.001$). (B) Pathway diagram, indicating changes based on grouped comparison. (C) Metabolite levels in individual samples, arrows indicating pair-wise significance between each LM and the MGT that it originated from ($log_2FC > 1$).

4.3 TCA Cycle and NEAAs

4.3.1 TCA Cycle

Despite increased levels of glycolytic intermediates in Myc310 LMs in comparison with Myc310 MGTs, their levels of lactate were comparable (Figure 4-1). Although the levels of both fumarate and malate were significantly higher in Myc310 LMs in comparison with Myc310 MGTs, albeit not reaching statistical significance in paired comparison (Figure 4-3c). Consistent with increased levels of fumarate and malate, Myc310 LMs had significantly higher levels of glutamate and aspartate in comparison with Myc310 MGTs (Figure 4-4a). Aspartate was also significant in paired analysis, while glutamate was below the significance threshold (Figure 4-4b). Surprisingly the levels of citrate and cis-aconitate were significantly decreased in Myc310 LMs in comparison with Myc310 MGTs (Figure 4-3a,b).

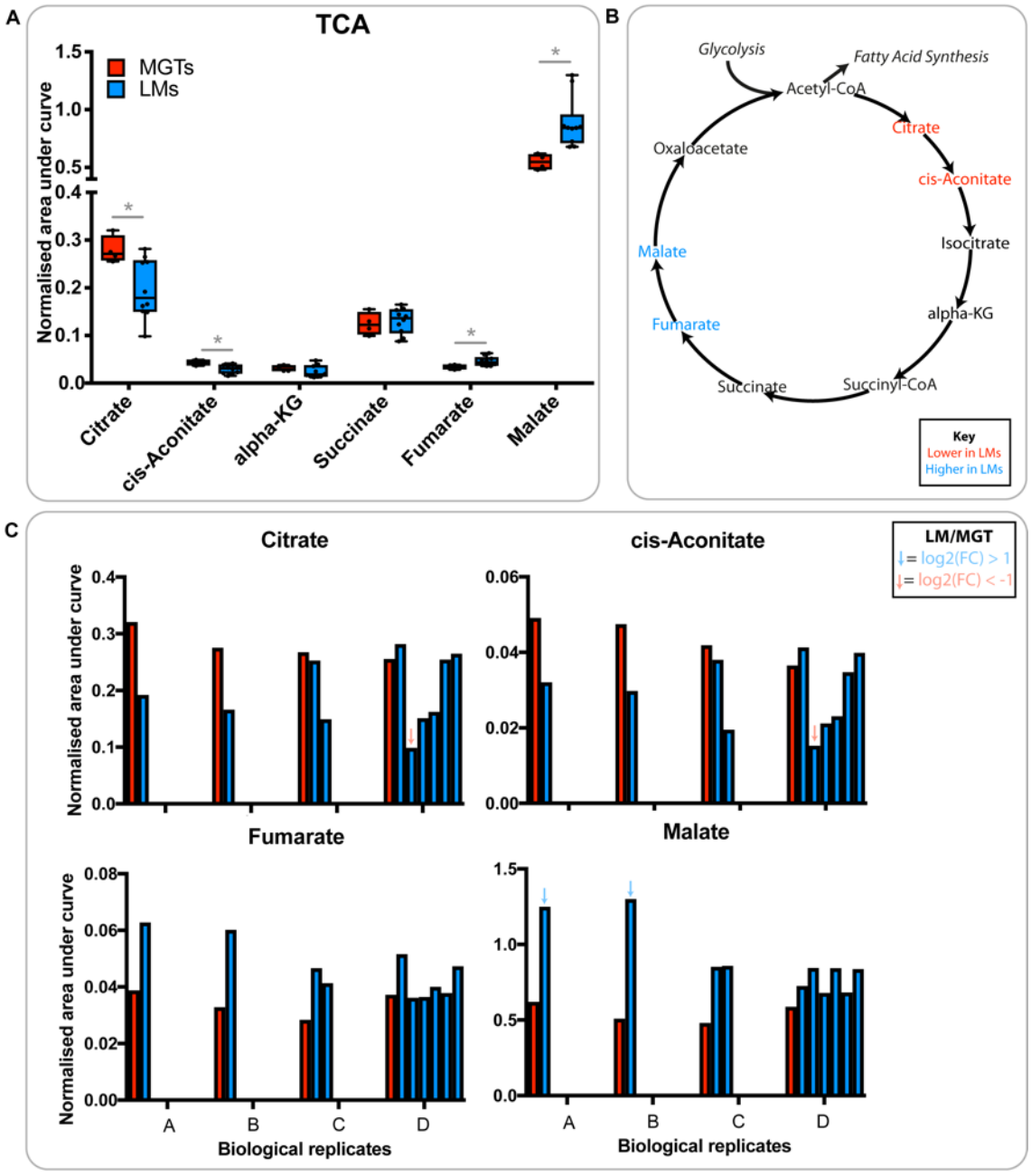


Figure 4-3. LC-MS metabolomics results comparing TCA between Myc310 MGTs and Myc310 LMs.
(A) Grouped comparison (* $p < 0.05$, ** $p < 0.01$, *** $p < 0.001$). (B) Pathway diagram, indicating changes based on grouped comparison. (C) Metabolite levels in individual samples, arrows indicating pair-wise significance between each LM and the MGT that it originated from ($log_2FC > 1$).

4.3.2 Non-essential amino acids

Glucose and glutamine are two major substrates for the activity of the TCA cycle. The levels of glutamine were significantly increased in LMs in grouped and paired comparisons (Figure 4-4a,b), which can be the result of either increased uptake and catabolism or biosynthesis. These results are consistent with recent findings that glutamine metabolism is correlated with invasiveness of breast cancer cells [72], [669]–[671], and can be required to support invasiveness of breast cancer cells through glutamate release and activation of the metabotropic glutamate receptor, which in turn drives ECM degradation the MT1 matrix metalloproteinase [669]. The contribution of glucose and glutamine to the activity of the TCA cycle in LMs will be further discussed in the next chapter where it was evaluated using stable isotope tracing.

Proline levels were decreased in LMs in grouped comparison, but this change was only significant in one LM in paired comparison (Figure 4-4a,c). This finding is consistent with recent studies demonstrating that in a model of metastatic breast cancer, more aggressive cells have lower intracellular proline levels than less aggressive cells due to upregulated proline catabolism, which contributes to ATP synthesis and ECM remodelling [165], [181].

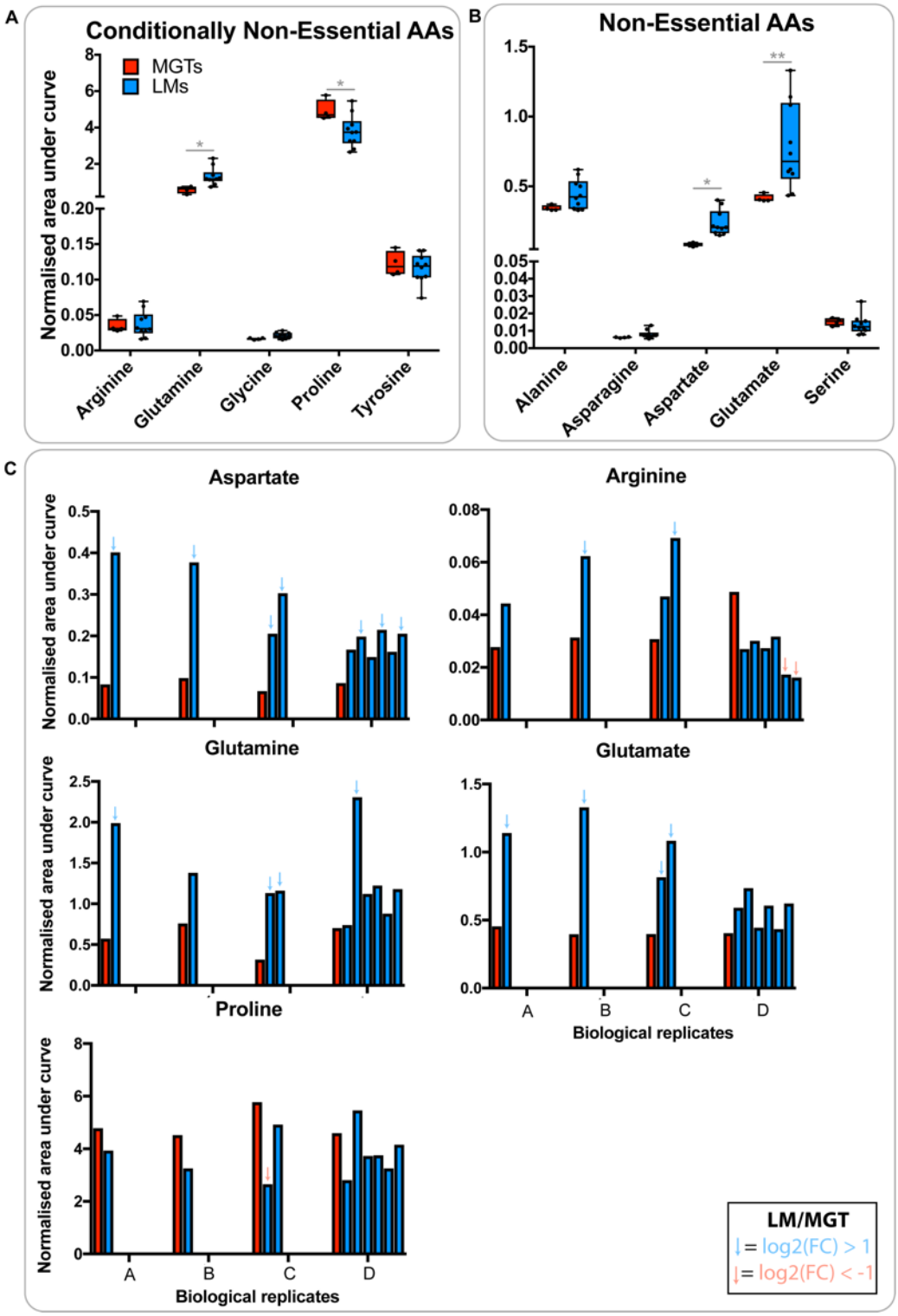


Figure 4-4. LC-MS metabolomics results comparing NEAAs between Myc310 MGTs and Myc310 MGTs.
Levels of conditionally NEAAs (A) and NEAAs (B) (* $p < 0.05$, ** $p < 0.01$, *** $p < 0.001$). (C) Metabolite levels in individual samples, arrows indicating pair-wise significance between each LM and the MGT that it originated from ($log_2FC > 1$).

4.4 Nucleotide biosynthesis

The levels of all analysed nucleotide mono-, di- and triphosphates remained comparable between Myc310 LMs and Myc310 MGTs in grouped analysis. There was a significant increase in uric acid, the biproduct of purine biosynthesis, and a significant decrease in thymine and thymidine in LMs in comparison with MGTs (Figure 4-5a). However, the paired analysis revealed a wide spread of levels of nucleotide metabolites between different Myc310 LMs and in some cases between different Myc310 MGTs (Figure 4-5b). For example, two out of ten LMs showed significantly higher ATP levels, and five LMs showed increased GTP levels compared to their respective MGTs. The significance of thymine and thymidine being significantly decreased in the Myc310 LMs group is dictated by higher levels of these metabolites in some of the Myc310 MGTs, while the overall level across Myc310 LMs remains relatively comparable. GTP and uric acid was near-significantly up in paired analysis, however in the case of uric acid this again is due to only a small subset of metastases exhibiting significantly higher levels. These results suggest that the energetic demands of specific LMs may be responsible for differential levels of nucleotides, and this must be considered when using metabolite levels to form overarching hypotheses about the metabolic changes in metastases. Also, the ratio of tri-phosphorylated to di-phosphorylated nucleotides as a readout for the energetic state of the tissue. The ATP/ADP and GTP/GDP ratios suggest that there is no significant difference between MGTs and LMs in grouped analysis and only a few cases of significantly higher ratios in individual metastases (Figure 4-5b).

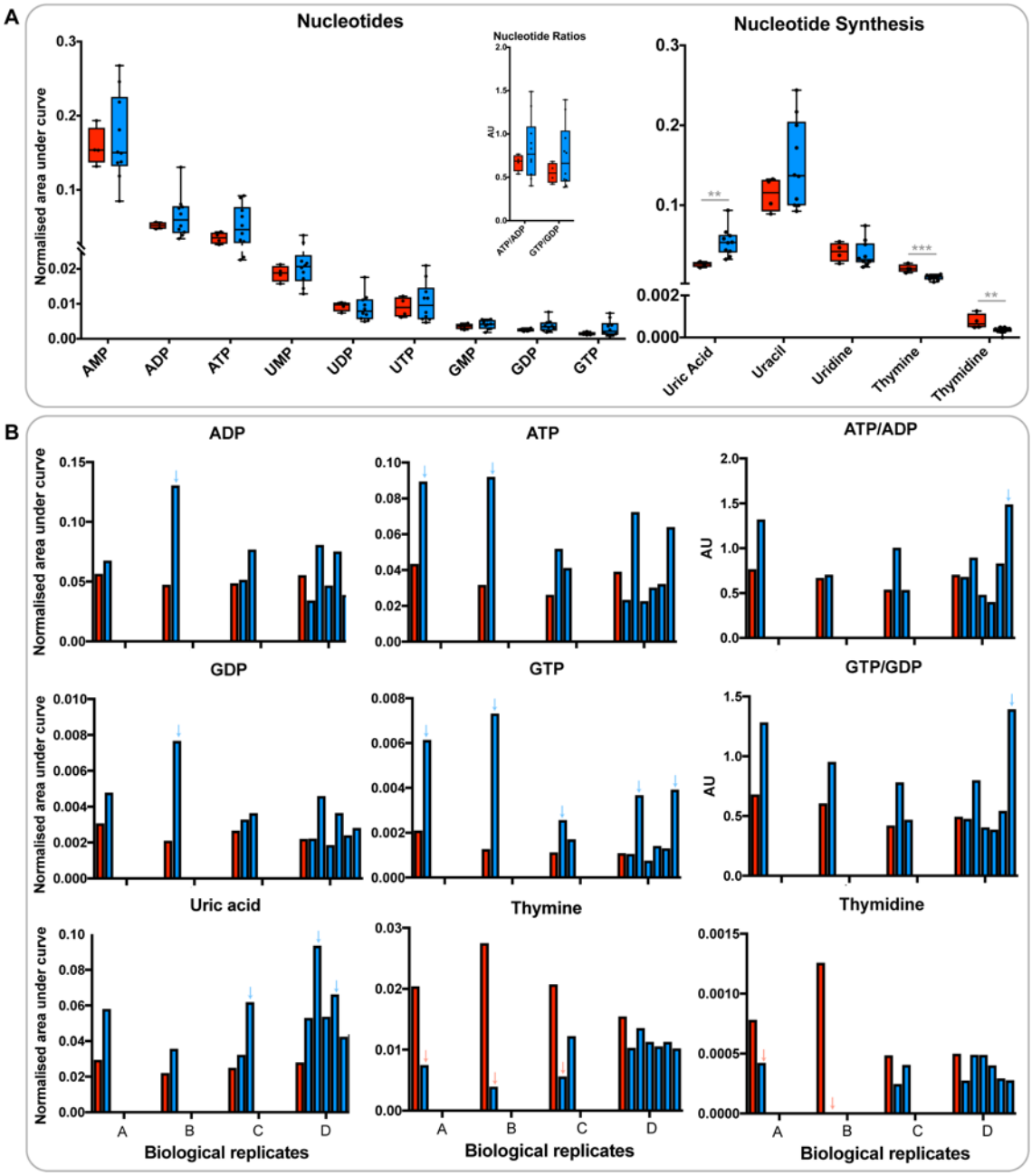


Figure 4-5. LC-MS metabolomics results comparing nucleotides between Myc310 MGTs and Myc310 LMs.
(A) Grouped comparison (* $p < 0.05$, ** $p < 0.01$, *** $p < 0.001$). (B) Metabolite levels in individual samples, arrows indicating pair-wise significance between each LM and the MGT that it originated from ($log_2FC > 2$).

4.5 EAAs, one carbon metabolism and glutathione

4.5.1 Essential amino acids

There was a trend towards increased levels of leucine, histidine and valine in Myc310 LMs in comparison with MGTs in grouped analysis albeit it did not reach statistical significance (Figure 4-6a). The levels of threonine were statistically significantly higher in Myc310 LMs than in MGTs (Figure 4-6a). Consistently, paired analysis of each LM to its MGT showed significant variability in histidine and leucine levels between metastases, with histidine levels higher in four out of ten LMs and leucine levels higher in three out of ten LMs (Figure 4-6b).

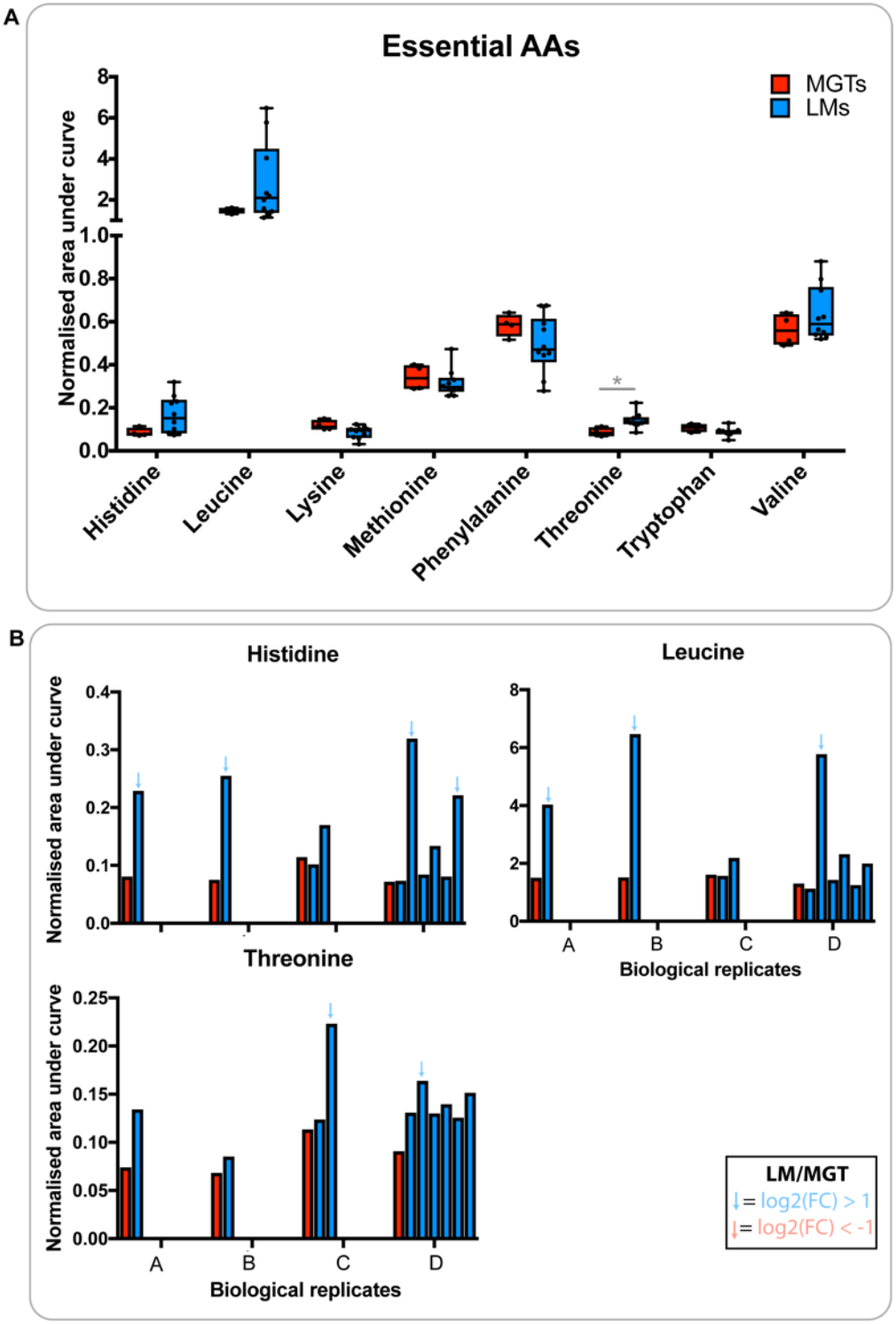


Figure 4-6. LC-MS metabolomics results comparing EAAs between Myc310 MGTs and Myc310 LMs.
(A) Grouped comparison (* $p < 0.05$, ** $p < 0.01$, *** $p < 0.001$). (B) Metabolite levels in individual samples, arrows indicating pair-wise significance between each LM and the MGT that it originated from (log2FC > 1).

4.5.2 One carbon metabolism

One carbon metabolism plays an important role in cellular growth and survival by providing carbon units for DNA, RNA and protein methylation, as well as contributing to synthesis of polyamines, phospholipids and several amino acids. Importantly it also contributes to glutathione synthesis, which is required to neutralise reactive oxygen species, and this process is supported by the reductive cofactor NADPH.

Grouped analysis showed significantly higher levels of S-adenosyl homocysteine (SAH) as well as significantly higher levels of oxidized glutathione (GSSG) and NADP in Myc310 LMs in comparison with Myc310 MGTs (Figure 4-7a). Paired comparison further revealed that due to the heterogeneity in LM metabolism, some LMs have significantly higher levels of other intermediates, including S-adenosyl methionine (SAM), with six out of ten metastases have paired higher levels compared to the parental MGTs (Figure 4-7b). On the contrary, in pairwise comparison, SAH is not deemed as significantly upregulated in LMs (Figure 4-7a,b).

The SAM/SAH ratio is used to measure the methylation capacity of the cell ([658], [672]), which can contribute to the control of different stages of cancer progression including proliferation ([673]) and metastasis ([661], [674]). The SAM/SAH ratio in grouped analysis showed no significant difference between MGTs and LMs (Figure 4-7a), however pairwise analysis revealed that four of the ten LMs had a significantly higher SAM/SAH ratio than the parental MGTs (Figure 4-7b). This suggests that some LMs have an upregulated methylation capacity, and elevated levels of these metabolites may be necessary for a survival of a specific metastasis subset or development stage.

Pairwise comparison showed a significant decrease in GSH/GSSG ratio, a readout for oxidative stress, in four out of ten LMs (Figure 4-8b) even though grouped comparison reveals no significant difference (Figure 4-7a). Therefore, some LMs can be faced with higher levels of ROS than others, potentially depending on their size or other environmental factors such as vascularisation and intra-pulmonary

invasion. Finding vulnerabilities in a subset of LMs can reveal the relationship between specific metabolic activities and specific environmental factors and can also help to identify targeted therapies towards resistant lesions.

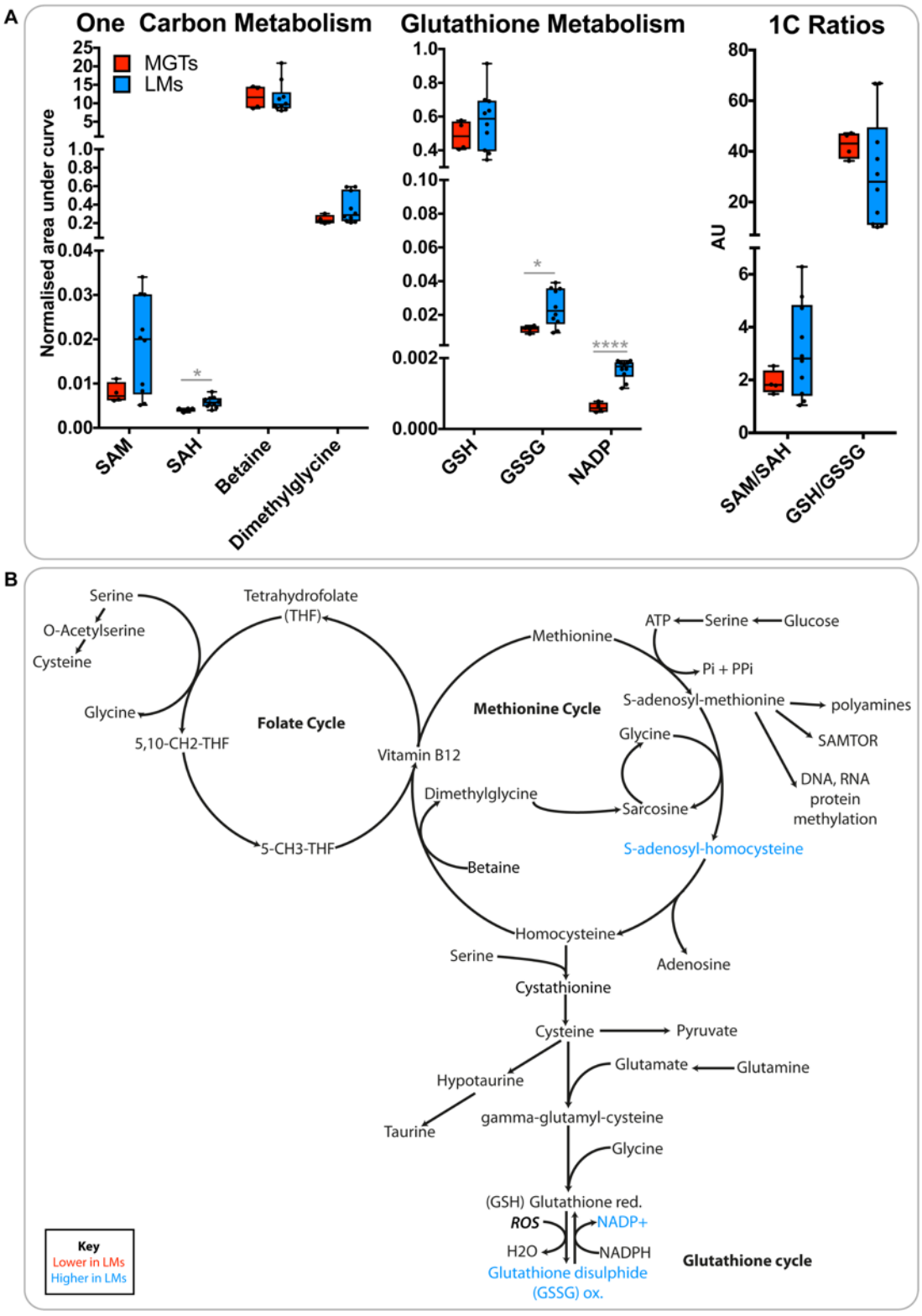


Figure 4-7. LC-MS metabolomics results comparing one carbon metabolism between Myc310 MGTs and Myc310 LMs.
(A) Grouped comparison of metabolite levels and ratios of SAM/SAH and GSH/GSSG (* $p < 0.05$, ** $p < 0.01$, *** $p < 0.001$). (B) Pathway diagram, indicating changes based on grouped comparison.

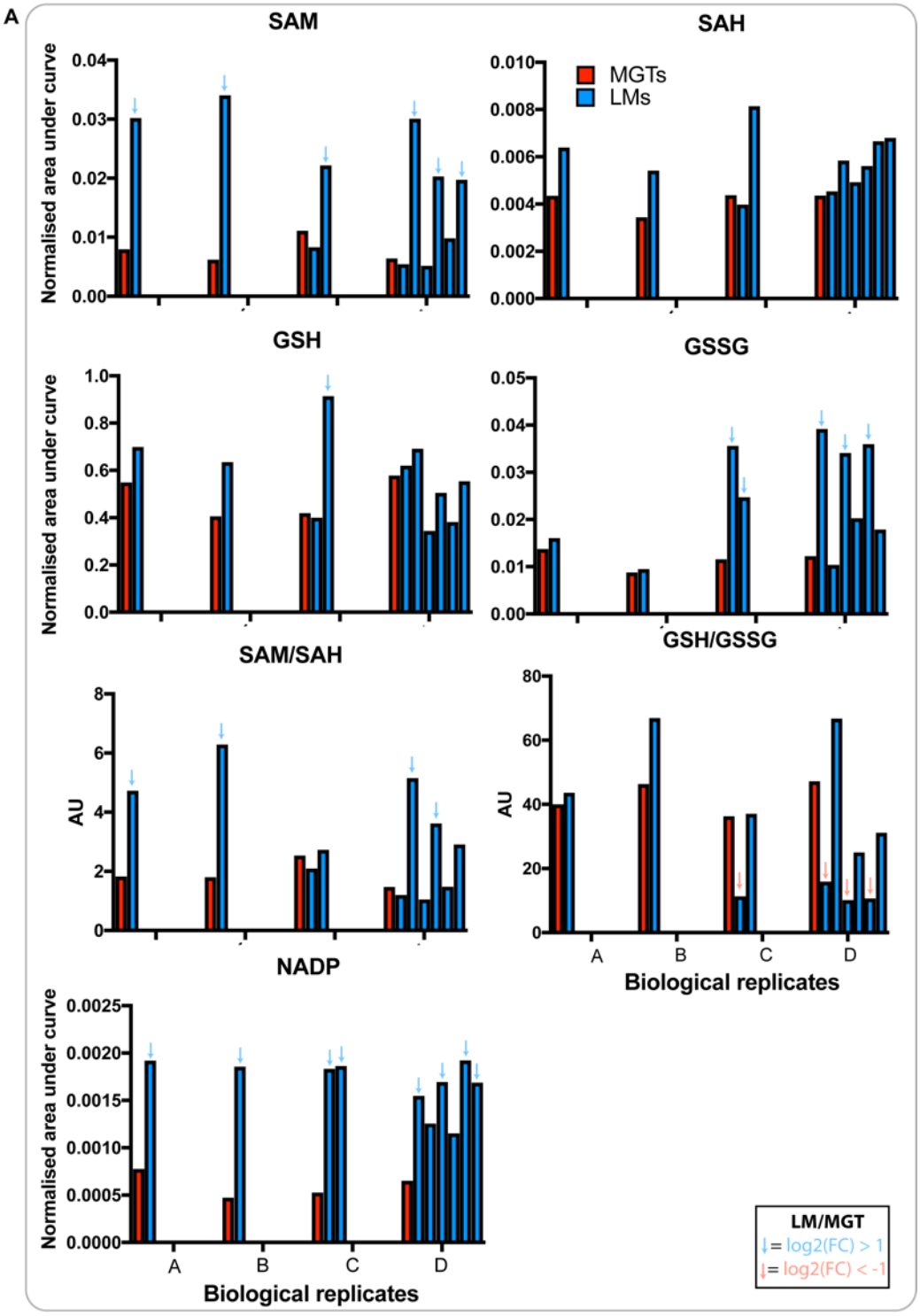


Figure 4-8. LC-MS metabolomics results comparing one carbon metabolism between Myc310 MGTs and Myc310 LMs.
(A) Metabolite levels and ratios of GSH/GSSG and SAM/SAH in individual samples, arrows indicating pair-wise significance between each LM and the MGT that it originated from ($log_2FC > 1$).

4.6 Chapter Discussion

In this chapter I have described the metabolic differences between Myc310 LMs compared to the MGTs that they originated from. Myc310 LMs had higher levels of glycolytic intermediates, which is in line with several studies showing glycolytic enzymes upregulated in more aggressive tumours [675], [676]. Glycolytic enzymes also directly promote EMT and metastasis survival [490], [677], [678] and transcription factors responsible for driving the metastatic cascade were shown to upregulate glycolysis [679]–[681]. Furthermore, the expression of the glucose transporter GLUT1 is correlated with expression of matrix metalloproteinases in metastatic pancreatic cancer [682]. Glucose flux analysis requires stable isotope labelling, which will be discussed further in the next chapters. However, from total metabolite levels it was observed that Myc310 LMs had lower levels of PPP intermediates than Myc310 MGTs. PPP produces NADPH, which is required to support antioxidant pathways. As cells in the primary tumour undergo EMT, they often upregulate antioxidant pathways in preparation for the harsh oxygenated conditions in the blood stream and well-perfused distal organs like the lung [683]. In fact, EMT transcription factors have been shown to promote PPP in metastatic gastric tumours [117]. Since EMT signalling can evoke various metabolic transformation, the EMT status and transcription factor expression of Myc310 MGTs and Myc310 LM lesions needs to be investigated further.

Despite higher levels of glycolytic intermediates than in Myc310 MGTs, Myc 310 LMs had lower levels of citrate and cis-aconitate, suggesting a reduced influx into the TCA or increased *de novo* fatty acid biosynthesis from acetyl-CoA. Since glutamine, glutamate, fumarate, malate and aspartate are all present at higher levels in Myc310 LMs, this hints at the metastases increasing glutamine catabolism towards the TCA and aspartate production. As discussed above, increased glutamine catabolism is correlated with aggressiveness [669], [670], however stable-isotope labelling is required to conclusively understand glutamine flux. Importantly, both the primary tumour and the metastatic lesion are made up of a variety of cells, which may exhibit differential metabolism and this diversity needs to be considered when drawing conclusion from bulk tissue metabolomics analysis. In

chapters 6 and 7 I will discuss how mass spectrometry imaging can help elucidate the distribution of different metabolites within these complex tissues.

One of the key characteristics of LMs was higher levels of oxidized glutathione (GSSG). There were also higher levels of NADP, the oxidised product formed from NADPH when GSSG is converted back to reduced glutathione (GSH). Since GSH levels were comparable between MGTs and LMs, these findings indicate a potential increased utilisation of NADPH for glutathione recycling by glutathione reductase in LMs, rather than increased *de novo* glutathione biosynthesis ([684], [685]). However, spontaneous NADPH oxidation during metabolite extraction must be considered in future work ([686]). Importantly, levels of GSSG were heterogeneous between different LMs. When metabolite levels were plotted against resected LM dry weight, there was a significant linear relationship ($R^2 = 0.912$) between dry weight and increased GSSG, but not GSH levels (Figure 4-9a). These result point to increased ROS in bigger LMs, which may occur as a result of increased proliferation ([687]), or originate from non-tumour cells in the metastatic niche ([688], [689]). The potential impact of infiltrating immune cells and lung cells on the metabolism of LMs will be further discussed in future chapters.

GSH production via the transsulfuration pathway requires the one carbon metabolism intermediate homocysteine. While this metabolite was not detected using our LC-MS method, other intermediates of this pathway, including SAM and SAH were upregulated in Myc310 LMs. Upregulated one carbon metabolism in metastases is further supported by increased levels of the EAAs leucine, threonine and histidine. Threonine and histidine contribute carbons to the folate pathway. Leucine is a potent regulator of mTOR, which in turn upregulates *de novo* serine biosynthesis, which contributes to one carbon metabolism [186], [690], and also expression of the xCT transporter, which regulates cysteine import for glutathione synthesis [691].

The elevated levels of SAM and SAH in Myc310 LMs compared to Myc310 MGTs indicate an increased methylation capacity in Myc310 LM cells ([658], [692], [693]). SAM acts as a methyl group donor for DNA methylation, which has been linked to metastatic progression and aggressiveness in several cancer types ([694], [695]),

including breast cancer ([661], [696]). Notably, increased SAM synthesis from serine was shown to drive DNA hypermethylation in pancreatic cancer ([697]), however serine levels were comparable in the Myc310 model. On the other hand, SAM as also shown to impede tumour invasion and metastasis in another model of breast cancer ([698]), highlighting that DNA methylation is involved in both pro- and anti-metastatic signalling in different tumours. Interestingly, SAM was not increased in all LMs, supporting the emerging trend of inter-LM metabolic heterogeneity. As with GSSG, SAM levels were found to be correlated with LM size, however the relationship was the opposite, with lower SAM levels in larger LMs (Figure 4-9b). This finding requires further analysis of the methylation targets and expression of methyltransferase enzymes in these tumours. Correlating the levels of different metabolites with the size of metastasis, however, must be considered with caution because of the limited accuracy of dissection from frozen lung samples.

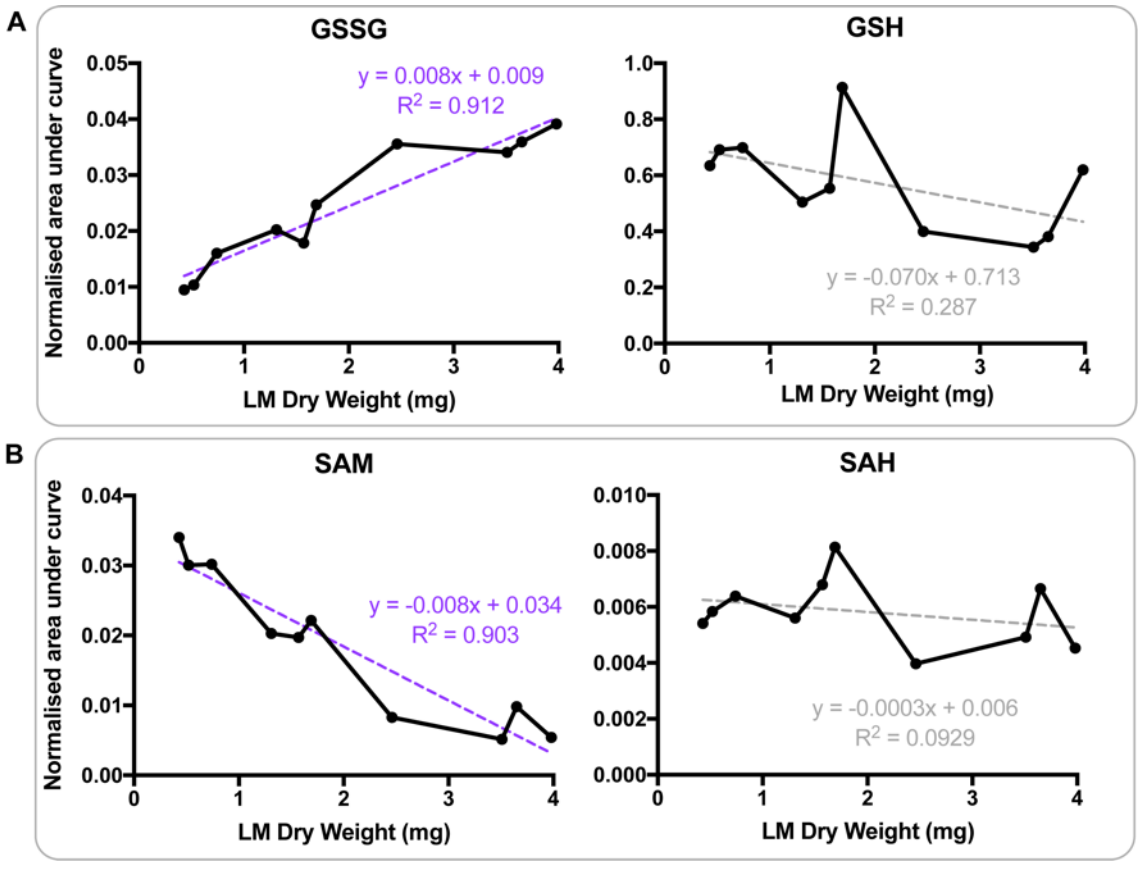


Figure 4-9. Regression analysis of metabolite levels with metastasis size.
Levels of GSSG and GSH (A), and SAM and SAH (B) as a function of dissected metastasis dry weight (mg). Positive correlation with metastasis size was observed in GSSG levels, and negative correlation with metastasis size was observed in SAM levels.

Although the results of the analysis performed in this chapter have already identified metabolic pathways differentially presented in Myc310 LMs and MGTs, I subsequently used stable isotope labelling to confirm the differential activity of these pathways. I have also addressed the question of whether the metabolic traits of LMs are acquired in response to different tissue environment or if they are an internal characteristic of primary tumour cells that enables them to survive and grow in the distant organ.

Chapter 5. Comparing the metabolism of mammary gland tumours formed by injection of lung metastasis cells into the fat pad, and the lung metastases derived from them.

In the previous chapter I have described LC-MS experiments showing metabolic heterogeneity of MGTs derived from Myc310 tumour cells and their lung metastases. My results demonstrated several notable changes in LM metabolism in comparison with MGTs. Next, I evaluated if the observed changes in metabolism of LMs were environmentally-driven or a result of an inherently different metabolism of mammary gland tumour cells that were able to form metastasis in the lung. To address this question metastasis cells were isolated from the lungs of Myc310 MGT-bearing mice. Once LM cells were expanded in vitro, they were re-injected into the fat pads of wild type female mice.

5.1 Assessing metabolic plasticity of lung metastasis cells

5.1.1 Isolation and propagation of metastasis cells

Tumours derived from Myc310 cells were collected when the diameter of the MGT reached 10 mm. Following the same procedure as typically used to isolate tumour cells from MGTs (see Methods), all five lobes were collected from several mice with Myc310 MGTs, dissociated and passaged in MMEC media to establish lung metastasis (LM) cell lines. Cells isolated from lungs were left to grow for 2 weeks, changing media after one week. After 2 weeks in culture, individual LM cell colonies could be observed, and after one passage the proliferation rate of the cells in culture was comparable to the original Myc310 cells.

The identity of LM cells was confirmed by positive immunofluorescence staining of the driver oncogene Myc and the luminal epithelial marker cytokeratin 8 (CK8) (Figure 5-1a, b). Presence of fibroblasts in the cultures was monitored by staining for vimentin, as well as the cancer associated fibroblast (CAF) marker alpha-

smooth muscle actin (alpha-SMA) [699]. Cells positive for alpha-SMA were seen in cultures that were passaged once, however they were entirely absent in cultures after two passages (Figure 5-1c). Importantly, all LM cells were vimentin-positive, as were cells in the original Myc310 cell line. This suggests a mesenchymal phenotype in LM and Myc310 cells that is often associated with increased metastatic potential [700]–[702].

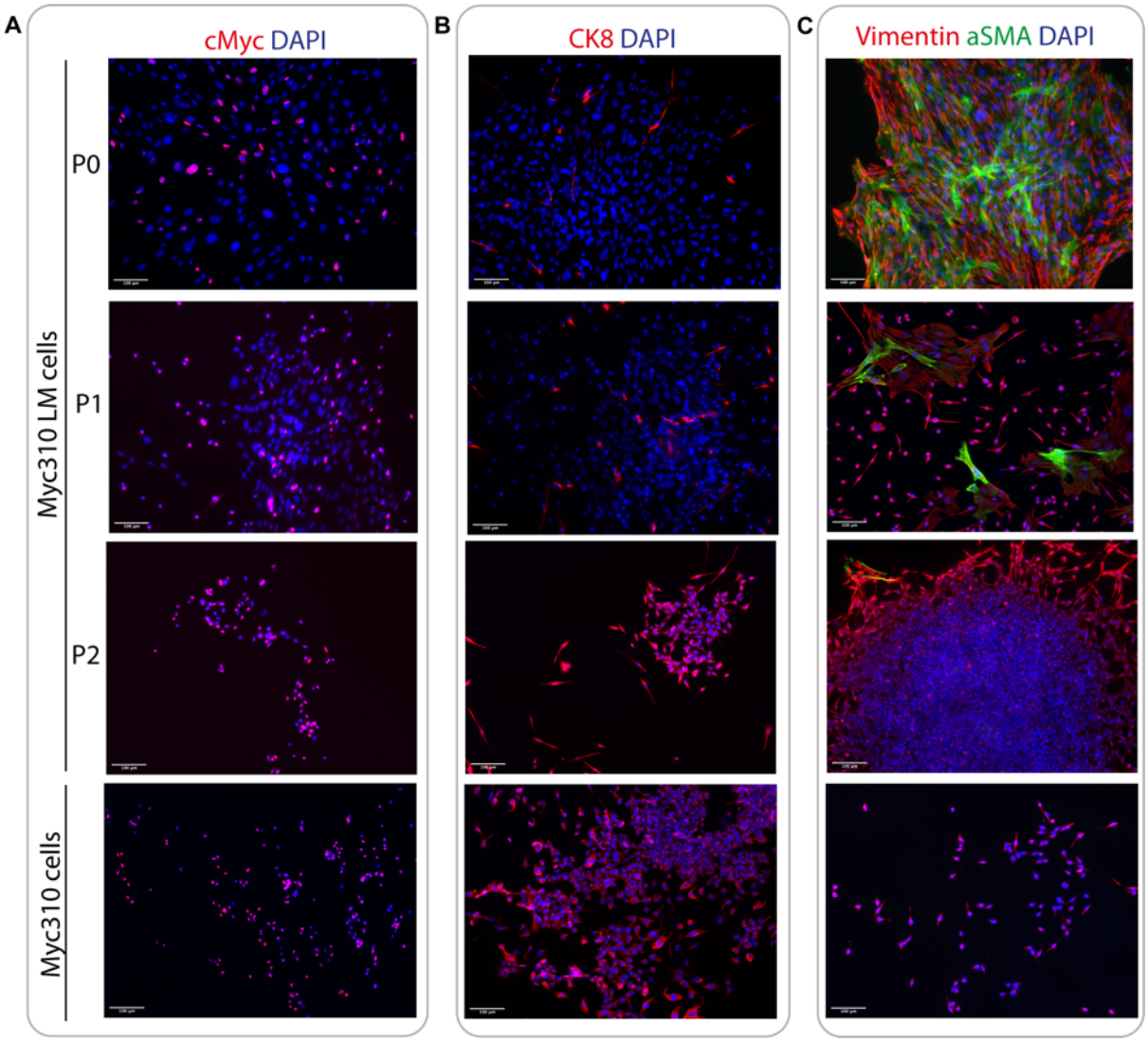


Figure 5-1. Immunofluorescent staining of Myc310 cells, and cells isolated from the lungs of mice with Myc310 MGTs.
Passage number of Myc310 LM cells denoted by P0-P2. After two passages the MYC (A) and CK8 (B) positive cells expand and phenotypically resemble Myc310 cells. Vimentin-positive fibroblasts and aSMA-positive CAFs present in early cultures are depleted after two passages, and cancer cells continuously express vimentin (C). Myc310 LM cells (P2) injected into the fat pad of wildtype mice successfully formed tumours, confirming their neoplastic identity.

5.1.2 Re-injection of lung metastasis cells into the mammary fat pad

Once the identity of Myc310 LM cell lines was established, four of these cell lines were injected individually into the fat pads of recipient wildtype mice (Figure 5-2a). Myc310 LM cells were injected at the same cell number (50,000 cells) as the parental Myc310 cells in previous experiments. Tumours were collected when they reached 10 mm in diameter, which was approximately 3 weeks after the injection of cells into the fat pad (Figure F-2b). Myc310 LM cells injected into the fat pad developed tumours that yielded significantly bigger and more frequent metastatic lesions (LM^2) than Myc310 cell derived tumours (Figure 5-2c).

These results demonstrated that the cells originated from lung metastases had higher metastatic potential in comparison with the parental cells, which can either be caused by clonal selection of more metastatic and/or fit cells from a primary tumour [703]–[706], genetic or epigenetic reprogramming via EMT-driving transcription factors [707]–[709], metabolic remodelling , or a combination of these factors. Each of these selective events results in the better capacity of tumour cells to migrate out of the primary tumour, survive in the lung micro-environment, or both. Interestingly, a recent study demonstrated that breast cancer sub-clones are predisposed to dissemination to specific distal organs, and are reprogrammed to secrete vascular mimicry proteins to potentiate migration and metastasis [609].

The larger size of metastasis derived from Myc310 LM and their higher frequency allowed for more reliable analysis not only by mass spectrometry imaging, but also by LC-MS and stable isotope tracing of glucose and glutamine catabolism. The metabolomics results of these studies will be discussed in further detail below.

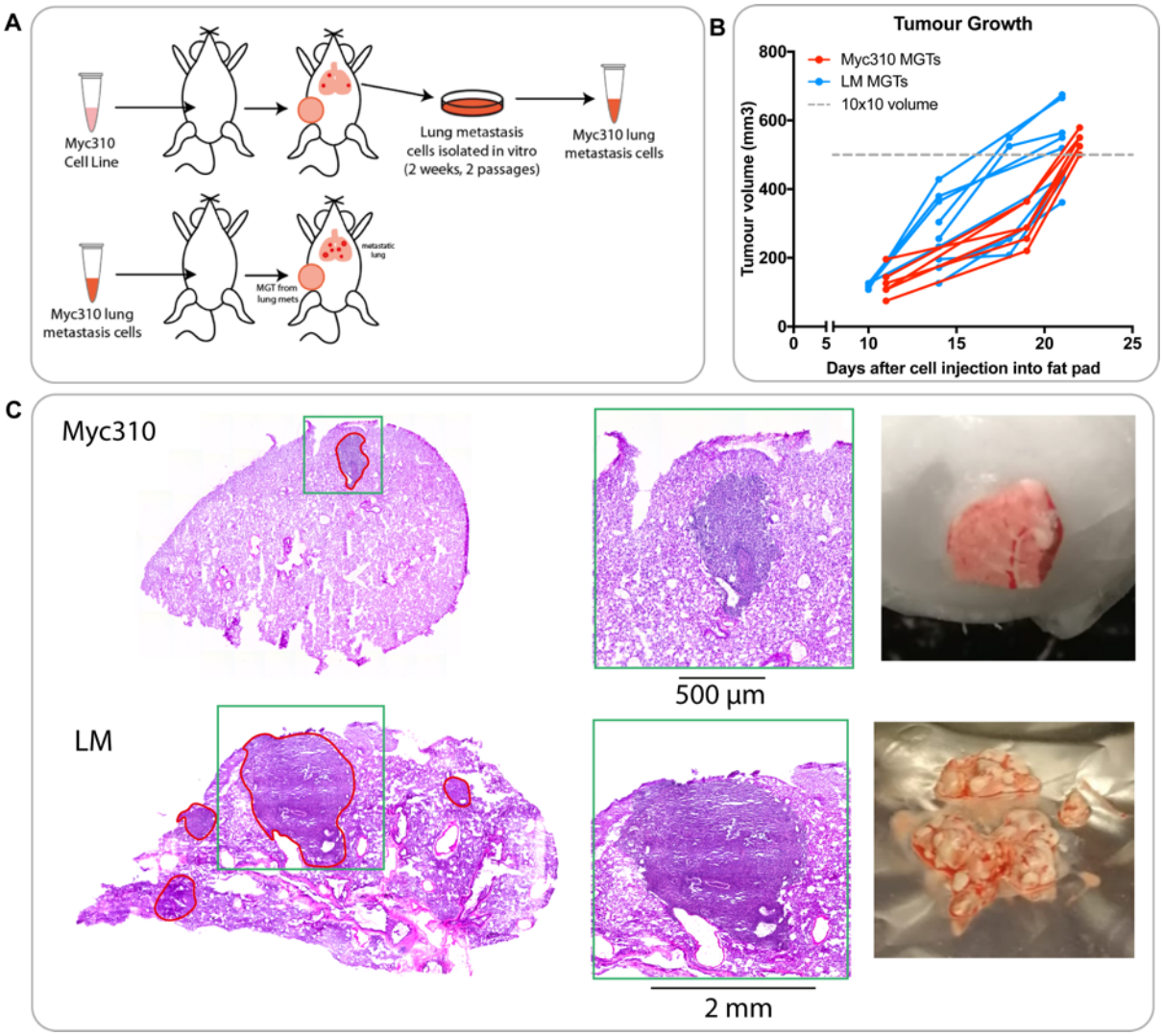


Figure 5-2. Lung metastasis model to assess environmental impact and flexibility of metabolic changes between MGTs and LMs.
(A) Schematic of the Myc310 LM model, where cells isolated from Myc310 MGT-bearing mice are expanded *in vitro* and re-injected into the fat pad of WT female mice to generate MGTs with increased metastatic potential. (B) Growth curve of Myc310 MGTs and LM MGTs. (C) Increased metastasis incidence and size of LM MGTs compared to Myc310 MGTs.

5.2 Comparing metabolism of Myc310 MGTs and LM MGTs

To assess if the metabolic changes of the LMs were driven by the lung environment or were an inherent property of these cells regardless of location in the body, I compared polar metabolite levels of LM MGTs to Myc310 MGTs. Stable isotope labelling of glucose and glutamine was also performed in order to assess the metabolic flux. Overall, the two tumour types showed similar levels and enrichment patterns in most metabolites analysed, however there were a few notable differences.

5.2.1 Glycolysis and PPP

$^{13}C_6$-glucose infusion resulted in a significantly higher glucose M+6 fractional enrichment in LM MGTs in comparison with Myc310 MGTs (Figure 5-3a). Total levels and enrichment of glycolytic intermediates were comparable between the two tumour types (Figure 5-3b), except for a significant increase in PEP M+2 enrichment from glucose in LM MGTs (Figure 5-3c); this may suggest higher PEP carboxykinase (PEPCK) activity, which synthesizes PEP from oxaloacetate, following one cycle of the TCA. PEPCK activity was show to support increased glucose catabolism, mTOR activity and anabolic production of lipids and nucleic acids in cancer cells [714]. Mitochondrial isoform of PEPCK (PCK2) plays a role in tumour initiation and is upregulated in metastasis compared to primary tumours in a study of NSCLC [715], supporting cancer cell growth through ATP production and maintaining the REDOX balance [716]. Importantly, PCK2 activity in the liver may be contributing to the presence of PEP M+2 in tumours, through excretion and re-uptake of glucose-derived pyruvate or lactate [717]. Furthermore,

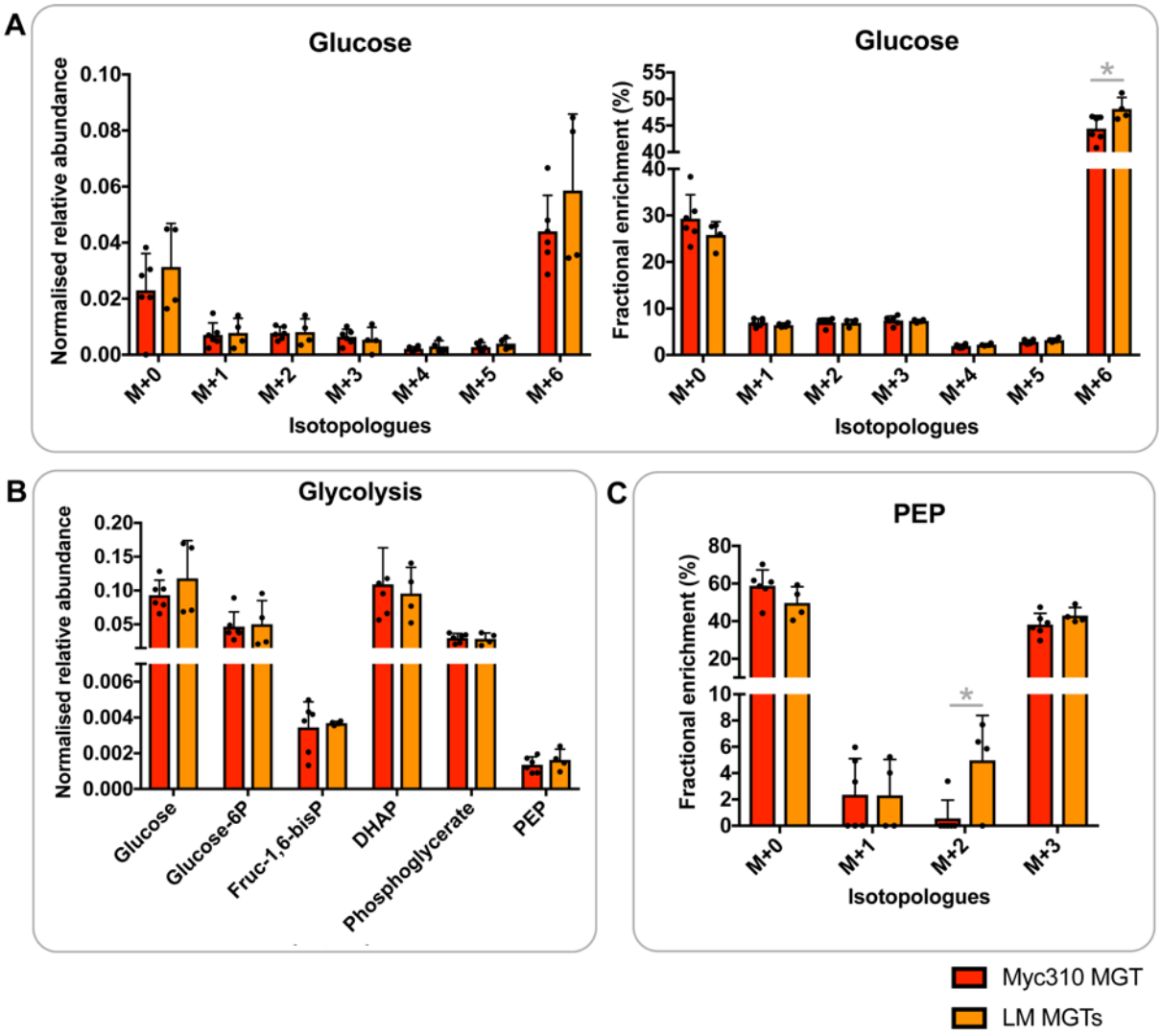


Figure 5-3. LC-MS metabolomics results comparing glycolysis metabolite levels and $^{13}C_6$-glucose label incorporation between Myc310 MGTs and LM MGTs.
(A) Normalised relative abundance and fractional enrichment of glucose isotopologues. (B) Total levels of glycolytic intermediates. (C) Phosphoenolpyruvate (PEP) fractional enrichment from $^{13}C_6$-glucose, showing significant increase in PEP M+2 in LM MGTs. Significance calculated using an unpaired parametric t-test (* $p < 0.05$, ** $p < 0.01$, *** $p < 0.001$).

While glucose derived enrichment in lactate did not differ between two tumour types (Figure 5-4a), the total and glucose-derived lactate levels were significantly decreased in LM MGTs in comparison with Myc310 MGTs (Figure 5-4a). Furthermore, $^{13}C_5$-glutamine infusion resulted in lower levels and ^{13}C enrichment of glutamine-derived lactate in LM MGTs in comparison with Myc310 MGTs (Figure 5-4b). Lactate is produced from glutamine through malic enzyme (ME) activity, which synthesizes pyruvate from malate, and pyruvate is then converted to lactate via lactate dehydrogenase (LDH). These results suggest lower lactate production from both glucose and glutamine lactate in LM MGTs in comparison with Myc310 MGTs.

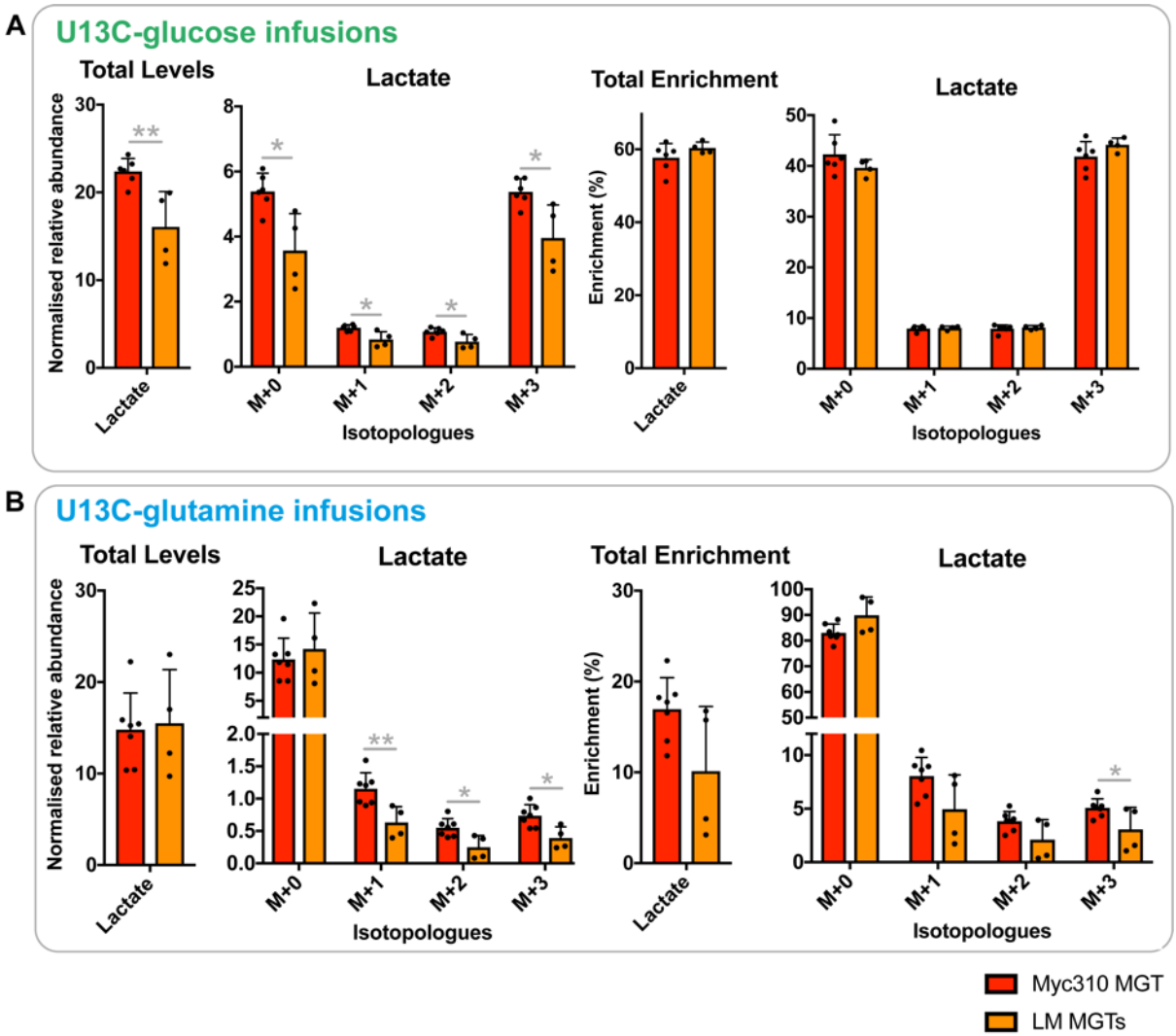


Figure 5-4. LC-MS metabolomics results comparing levels and enrichment of lactate. Total and isotopologue levels of lactate from $^{13}C_6$-glucose (A) and $^{13}C_5$-glutamine (B) infusions of Myc310 MGTs and LM MGTs. Significance calculated using an unpaired parametric t-test (* $p < 0.05$, ** $p < 0.01$, *** $p < 0.001$).

Neither total and glucose-derived levels of PPP intermediates, nor their glucose-derived enrichment, differed between two tumour types (Figure 5-5a), except a minor increase in sedoheptulose 7-phosphate (S7P) M+5 enrichment from glucose in LM MGTs (Figure 5-5b).

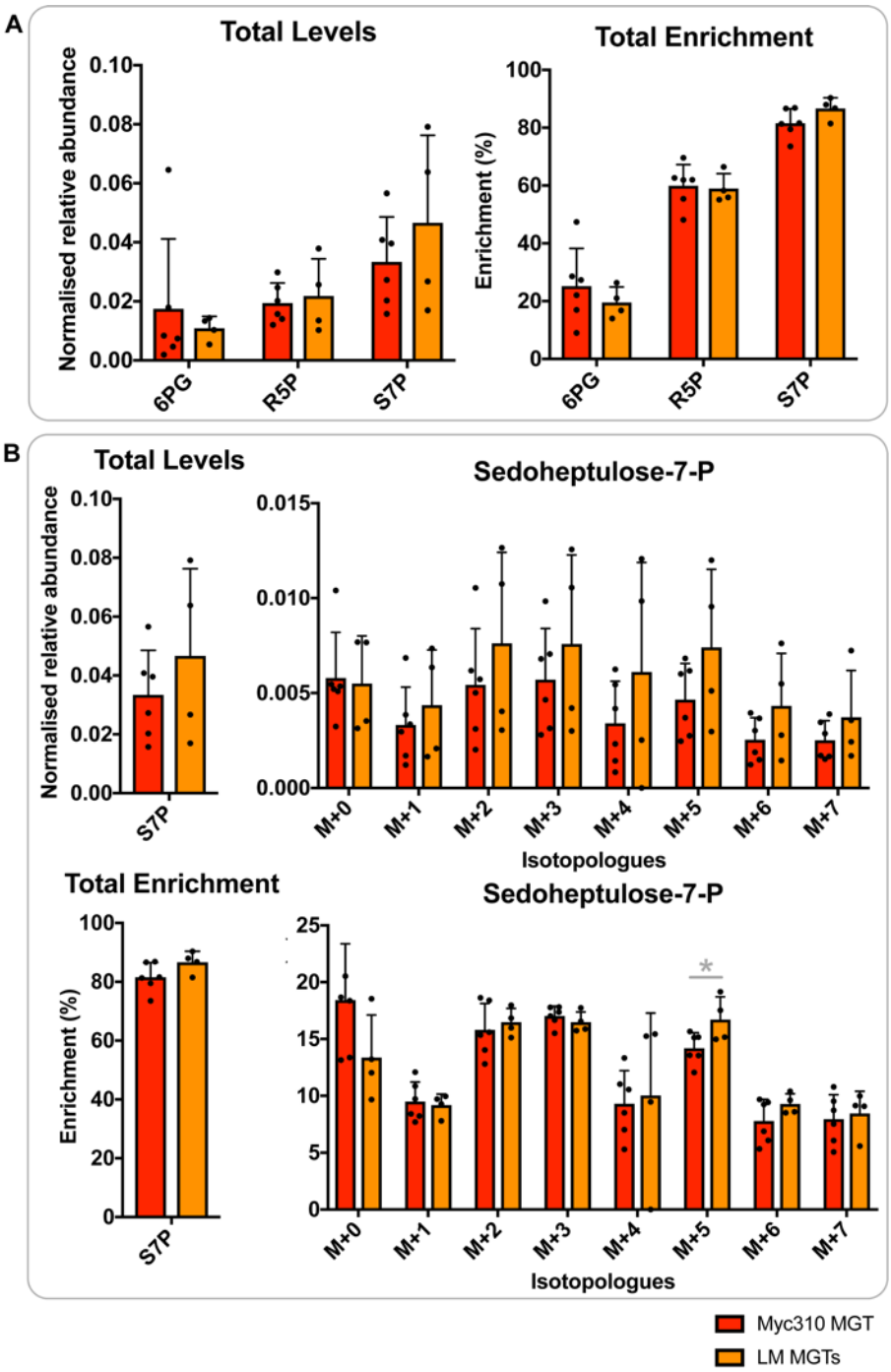


Figure 5-5. LC-MS metabolomics results comparing PPP intermediates in Myc310 MGTs and LM MGTs.
(A) Total levels and fractional enrichment from $^{13}C_6$-glucose. (B) Total and isotopologue levels and fractional enrichment of sedoheptulose-7-phosphate, showing a significant increase in M+5 fractional enrichment in LM MGTs. Significance calculated using an unpaired parametric t-test (* $p < 0.05$, ** $p < 0.01$, *** $p < 0.001$).

5.2.2 TCA Cycle and Glutaminolysis

Although LMs had higher levels of malate, fumarate, aspartate and glutamate than Myc310 MGTs (Figure 4-3 and 4-4), the total levels and enrichment of TCA cycle intermediates were comparable between two types of tumours infused with $^{13}C_6$-glucose (Figure 5-5a, Figure 5-6a). While the levels of glutamate also did not differ, LM MGTs had higher glucose-derived enrichment of glutamate as the result of increased enrichment of M+4 and M+5 isotopologues. Since glutamate M+2 was not changed although it should be the predominant isotope of glutamate originating from glucose, more biological replicates may be required to confirm these findings.

LM MGTs tumours infused with $^{13}C_5$-glutamine had decreased levels and glutamine-derived enrichment of glutamate and decreased enrichment of TCA cycle intermediates, including malate and fumarate, in comparison with Myc310 MGTs (Figure 5-5b, Figure 5-6b). These findings indicate a potentially reduced glutamine catabolism in LM MGTs compared to Myc310 MGTs and are in contrast to previously published results demonstrating that increased glutaminolysis correlates with more aggressive tumours ([718]–[720]).

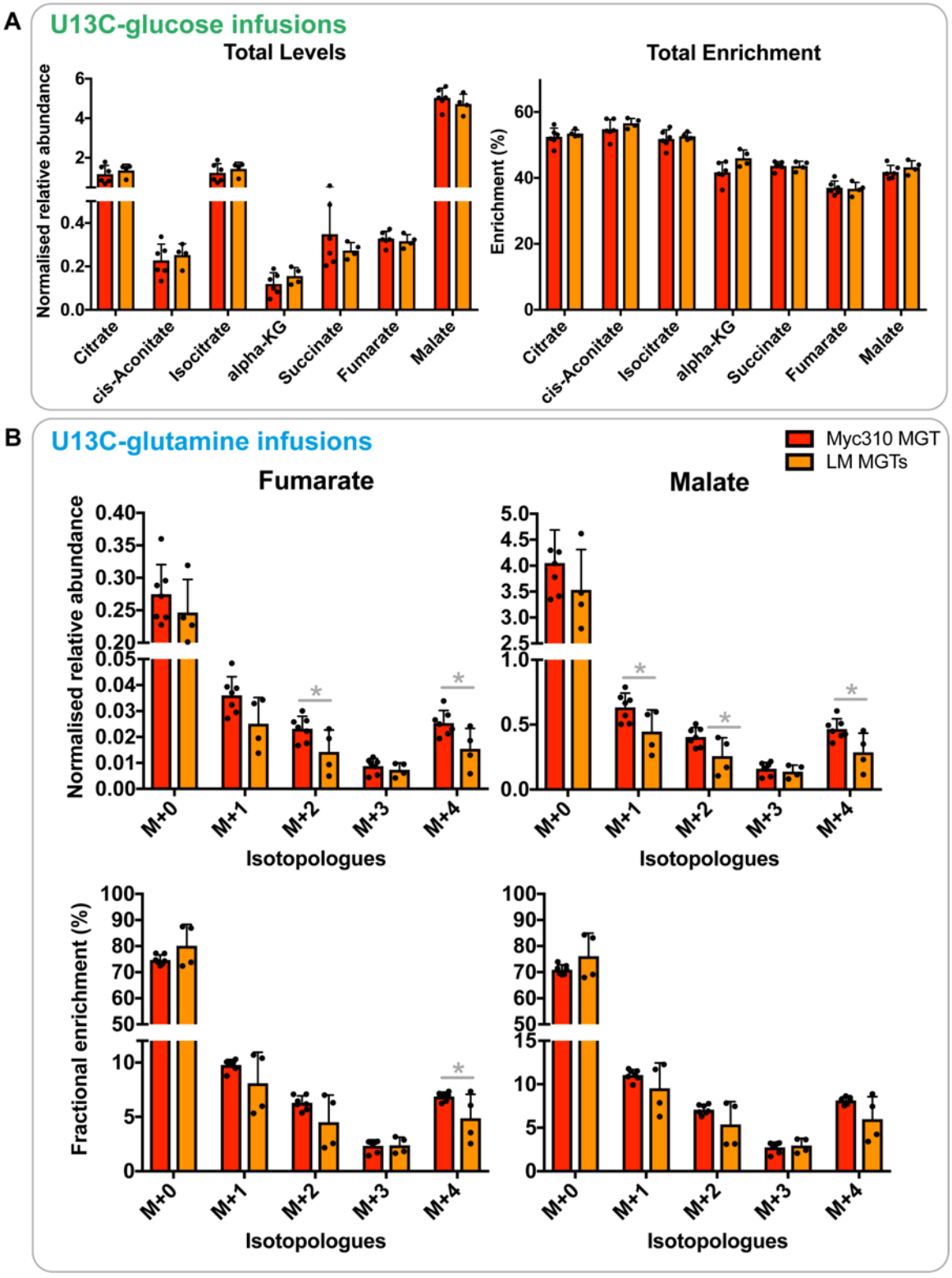


Figure 5-5. LC-MS metabolomics results comparing TCA cycle metabolites.
Total and isotopologue levels and fractional enrichment from $^{13}C_6$-glucose (A) and $^{13}C_5$-glutamine (B) infusions of Myc310 MGTs and LM MGTs. Decreased glutamine-derived label incorporation into glutamate was observed in LM MGTs. Significance calculated using an unpaired parametric t-test (* $p < 0.05$, ** $p < 0.01$, *** $p < 0.001$).

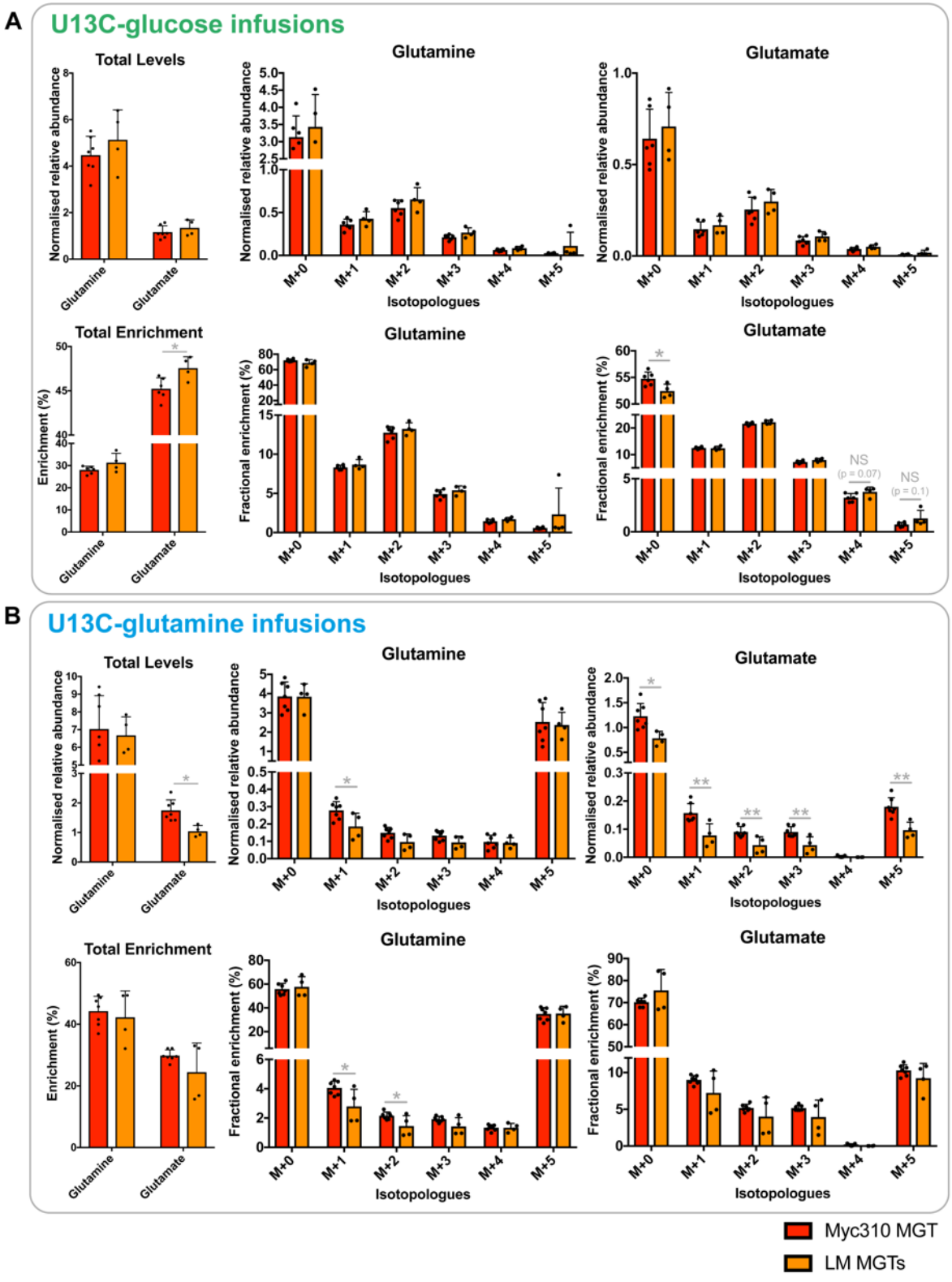


Figure 5-6. LC-MS metabolomics results comparing glutamine and glutamate.
Total and isotopologue levels of glutamine and glutamate and fractional enrichment from $^{13}C_6$-glucose (A) and $^{13}C_5$-glutamine (B) infusions of Myc310 MGTs and LM MGTs. Decreased glutamine-derived label incorporation into glutamate was observed in LM MGTs. Significance calculated using an unpaired parametric t-test (* $p < 0.05$, ** $p < 0.01$, *** $p < 0.001$).

5.2.3 One carbon metabolism, EAAs and nucleotides

Although there was a significant increase in the levels of one carbon metabolites in LMs in comparison with Myc310 MGTs (Figure 4-7), the levels of these metabolites were mostly comparable between the two tumour types (Figure 5-7a), except for a significant increase in choline levels and a decrease in betaine levels in LM MGTs (Figure 5-7b). Betaine is produced from choline in the mitochondria and is used as an additional methyl group donor for the methionine cycle. The methyl group is added to homocysteine, producing methionine and dimethylglycine (Figure 1-6). These findings suggest that LM MGTs may have a lower requirement for this alternative methyl donor than Myc310 MGTs.

In the previous chapter I showed that Myc310 LMs had higher level of the EAAs histidine, threonine and leucine compared to Myc310 MGTs. The levels of these metabolites were comparable between LM MGTs and Myc310 MGTs (Figure 5-7c), suggesting that their elevation in LMs is reversible and may be required for specifically metastatic growth and survival.

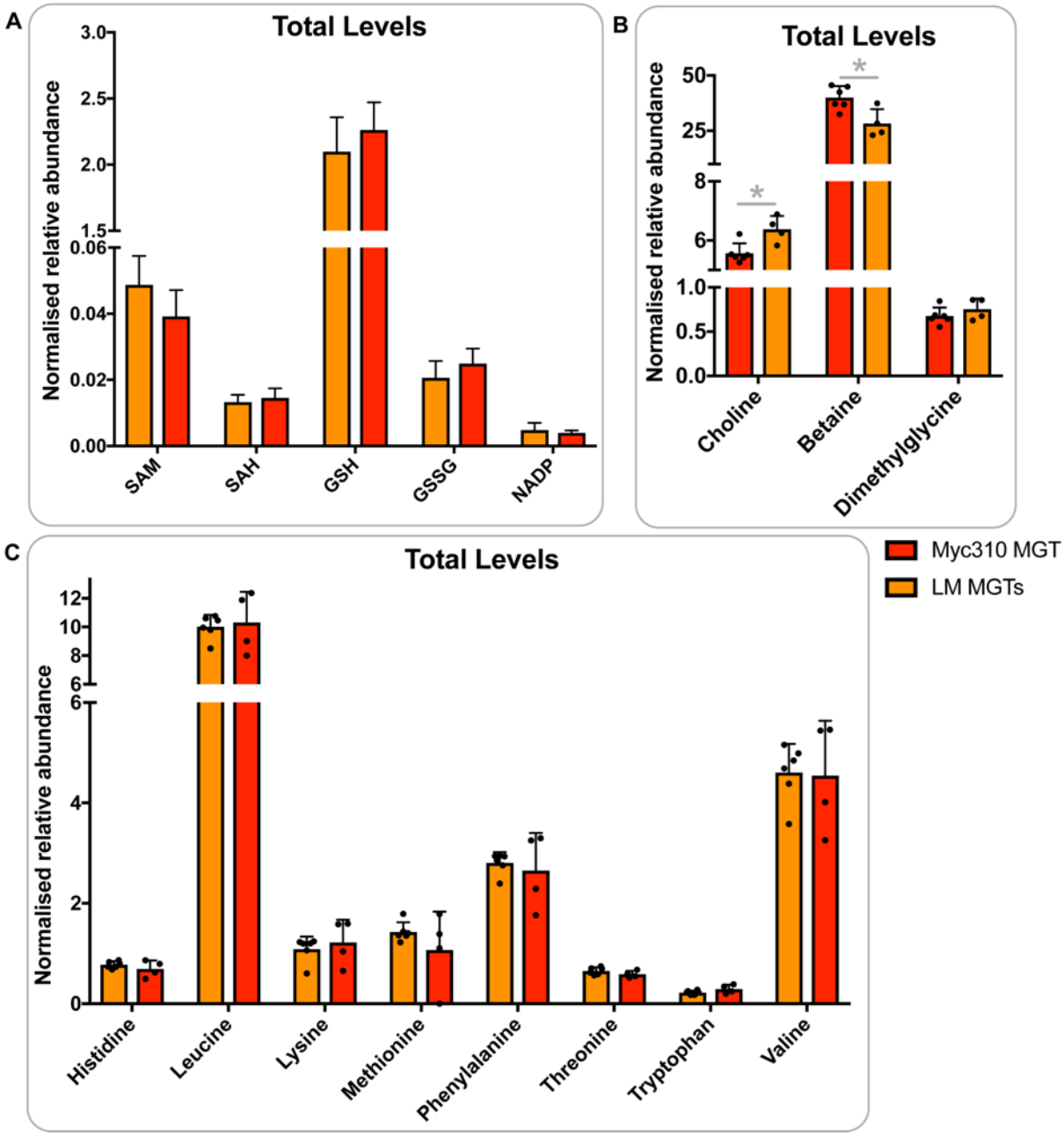


Figure 5-7. LC-MS metabolomics results comparing one carbon metabolism intermediates, glutathione and EAAs glutamine in Myc310 MGTs and LMs.
(A) Total levels of metabolites previously shown to be upregulated in Myc310 LMs are comparable between LM MGTs and Myc310 MGTs. (B) Choline levels are increased and betaine levels are decreased in LM MGTs, suggesting an increased choline carbon incorporation into the methionine cycle. (C) Levels of EAAs are comparable between LM MGTs and Myc310 MGTs, despite histidine, leucine and threonine levels being significantly upregulated in Myc310 LMs suggesting a transient, lung-specific metabolic reprogramming. Significance calculated using an unpaired parametric t-test (* $p < 0.05$, ** $p < 0.01$, *** $p < 0.001$).

Nucleotide levels between Myc310 MGTs and LM MGTs were also comparable, and this correlates with similar growth rates of the two tumour types (Figure 5-8). The increased metastatic potential of LM MGTs, therefore, is not likely a factor of the bioenergetic state in the primary tumour.

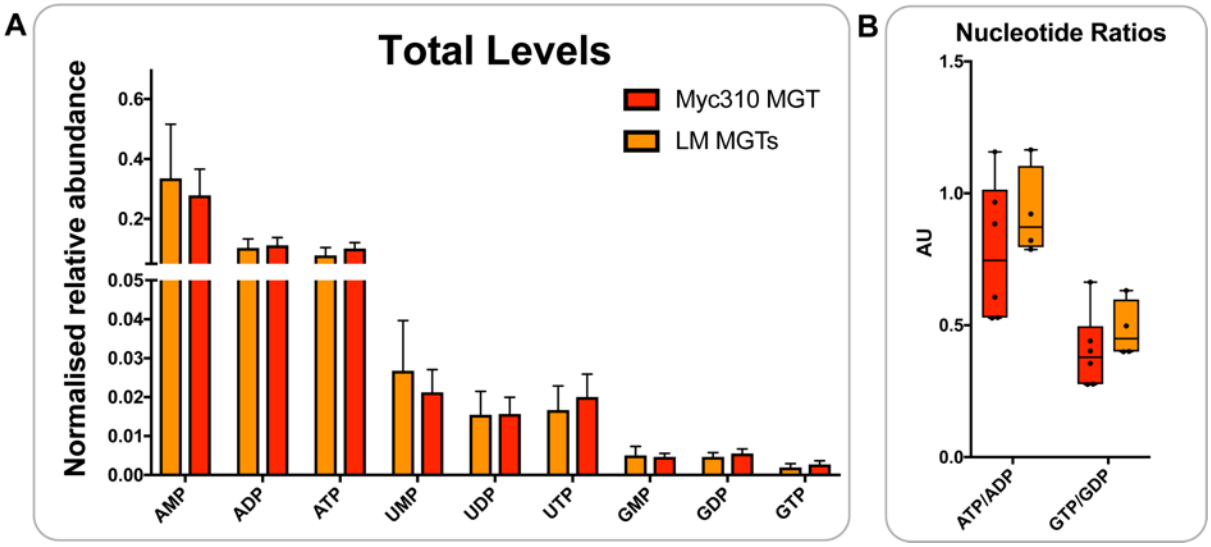


Figure 5-8. LC-MS metabolomics results comparing nucleotides.
Nucleotide levels (A) and ratios (B) in LM MGTs and Myc310 MGTs. Significance calculated using an unpaired parametric t-test (* $p < 0.05$, ** $p < 0.01$, *** $p < 0.001$).

5.2.4 Discussion

Altogether my results demonstrate a flexible metabolism of LM cells. While LMs had increased levels of glycolytic intermediates, glutamate and most of TCA intermediates, significantly higher levels of one carbon metabolism intermediates and glutathione, the mammary gland tumours derived from LM cells did not present most of these differences when compared to Myc310 tumours.

Notably, LM MGTs had higher glucose uptake, increased PEPCK activity and lower lactate production from both glucose and glutamine than Myc310 MGTs suggesting higher flexibility of LM MGTs. Increased PEPCK activity may provide a metabolic advantage for metastasis generation through potentiating not only gluconeogenesis for ATP production, but also regulate central carbon metabolism and TCA flux through mTORC1 signalling [714], [721]. Furthermore, a recent study demonstrated that PEPCK silencing resulted in increased ROS formation due to increased oxidative metabolism [716], and the importance of antioxidant responses and REDOX balance in metastasis has been widely demonstrated in several cancer models [683], [722], [503]. On the other hand, increased LDH activity has been shown to help drive EMT and its expression in the primary tumour correlates with poor prognosis [723], [724]. Furthermore, the LDH reaction requires the reductive co-factor NADH, and has been reported to increase ROS levels [725], therefore metastatic tumours that are more dependent on antioxidant responses may downregulate LDH activity to minimise ROS. The correlation with LDH activity and HIF-1a expression suggests that primary MGTs may be more hypoxic than lung metastases [726]–[728], however this needs to be confirmed in future studies.

In the previous chapter I showed that LMs were more glycolytic than Myc310 MGTs from which they originate. The findings shown here suggest that when LM cells are injected into the fat pad, many of these metabolic transformations revert back to a more MGT-like state, however some adaptations, such as increased glucose utilisation, are retained. PPP was not increased in metastases, however the increased S7P labelling from glucose may be indicative of PPP playing a role in the increased metastatic potential of LM MGTs compared to Myc310 MGTs [729]–

[731]. This is consistent with Myc310 MGTs having significantly higher levels of PPP intermediates compared to less-metastatic transgenic MMTV-Myc tumours.

Altogether, these results suggest that the metabolic differences observed between Myc310 cells and their metastasis could rather be induced by the environment of the lung, for example due to varying oxygen or nutrient availability and required for the tumour cells to survive at the secondary cite [732], [733]. It should also be taken into account that the LM cells were expanded in culture for two weeks prior to injection into the fat pad, therefore media conditions may also have influenced some of these metabolic changes. Finally, the differences between LMs and MGTs might be attributed to the presence of lung-specific cells that infiltrated metastases or the surrounding metastatic niche and had specific metabolic profiles [734]. These cells were removed during in vitro expansion of the metastatic cells; this may be particularly true for lipid species that are produce by specific immune or lung cells. Lipid changes will be further explored in Chapter 7 using apolar LC-MS and DESI-MSI.

5.3 Comparing the metabolism of LM MGTs and their lung metastases

I have demonstrated that when Myc310 LM cells were injected into the mammary fat pad, they formed tumours which were highly metastatic. The metabolism of LM MGTs closely resembled that of Myc310 MGTs, suggesting that metabolic changes previously seen between LMs and MGTs were driven by the environment in which these cells reside. To confirm the metabolic rewiring observed in LMs in comparison with MGTs I compared the metabolism of LM MGTs and their metastases (LM^2s) using LC-MS. The increased maximum size and incidence of LM^2s allowed to evaluate the activity of metabolic pathways using stable isotope labelling and more accurate dissection and therefore more reliable LC-MS results.

5.3.1 Effect of stable isotope infusions on metabolite levels

Animals bearing LM MGTs were infused with either $^{13}C_6$-glucose or $^{13}C_5$-glutamine. Importantly, $^{13}C_6$-glucose infusions resulted in higher levels of glucose in LM^2s, however this was not seen in $^{13}C_5$-glutamine infusions (Figure 5-10a). Total levels of other metabolites were comparable between $^{13}C_6$-glucose or $^{13}C_5$-glutamine infusions, with the exception of higher alanine levels in the $^{13}C_6$-glucose-infused set (Figure 5-10 a-c). There was a slight increase in glutamine levels in the $^{13}C_5$-glutamine-infused set. These findings show that long term (3 hour) isotope labelling may stimulate higher uptake and subsequent catabolism of the infused metabolite, and could have an effect on total levels of downstream metabolites. Transporter availability and downstream enzyme kinetics are likely bottlenecks, but in future experiments it would be beneficial to compare isotope-labelled metabolite infusions with non-labelled metabolite infusions to fully understand the effect on global metabolism. The three hour timepoint for infusions was chosen guided by previous reports of isoflurane anaesthesia toxicity following long term exposure, while still maximising the amount of isotope label incorporation into downstream pathways [735]–[738].

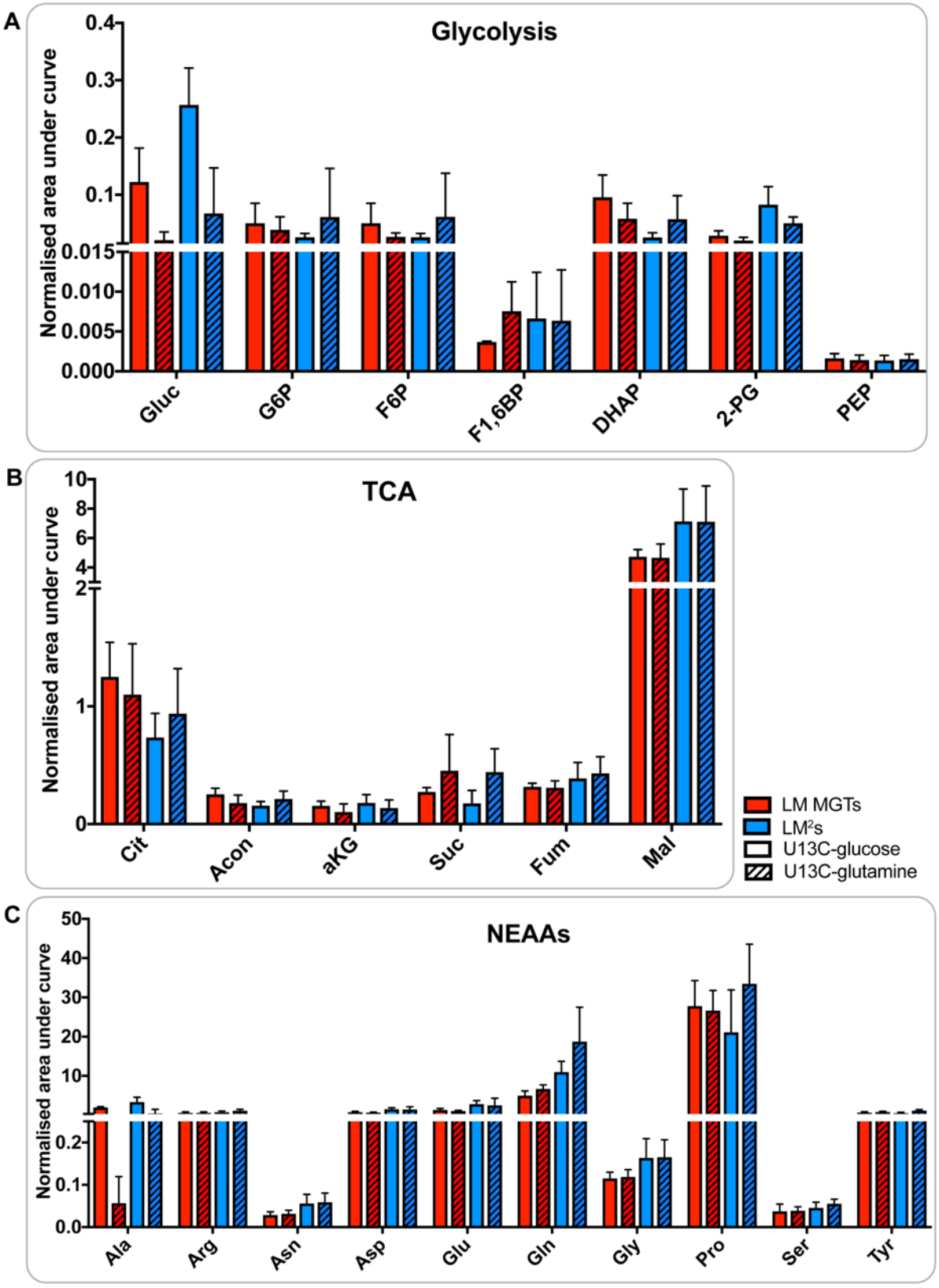


Figure 5-10. LC-MS metabolomics results comparing metabolite levels between heavy isotope infusion experiments.
(A) Glycolysis, (B) TCA, and (C) NEAAs levels in LM MGTs and metastases derived from them (LM2s), in mice infused with $^{13}C_6$-glucose or $^{13}C_5$-glutamine.

5.3.2 Glycolysis and PPP

Changes in glycolysis between LM^2s and LM MGTs were consistent with the results described in the previous chapter (Chapter 4, Figure 4-1). Total levels of G6P and DHAP were decreased while levels of F1,6BP and 2-PG were increased in LM^2s in comparison with LM MGTs (Figure 5-11a). Employing $^{13}C_6$-glucose tracing allowed me to demonstrate that there was an overall higher glycolytic flux in LM^2s with significantly higher fractional enrichment in F1,6BP and 2-PG, and just below significance level in G6P and glucose (Figure 5-11b). Glucose-derived total fractional enrichment of PEP M+3 was higher in LM^2s in comparison with LM MGTs, and lower in M+1 and M+2 isotopologues (Figure 5-11c), demonstrating increased synthesis of PEP directly through glycolysis in LM2s and decreased contribution of PEPCK (Figure 5-11d).

Consistently with previous findings, PPP intermediates were present at lower levels in LM2s in comparison with their parental tumours (Figure 5-11e), with reduced fractional enrichment from $^{13}C_6$-glucose in R5P (just below significance, $p = 0.07$), and S7P (Figure 5-11f). This confirms that PPP activity fuelled by glucose is downregulated in LMs in comparison with mammary gland tumours. Interestingly, enrichment in 6PG was significantly higher in LM^2s, despite significantly lower levels. This may be a result of overall higher labelled glucose intake by LM^2s. Also, 6PG synthesis generates NADPH and thus increases the reductive potential in LM^2s (Figure 5-11g). ROS levels are increased in the lung microenvironment due to increased oxygen availability: 100 mmHg oxygen pressure in lung alveoli compared to 1-45 mmHg in other peripheral organs [739], [740]. Hence, the oxidative arm of PPP can still be functional in order to support REDOX balance in metastasis cells [731], [741].

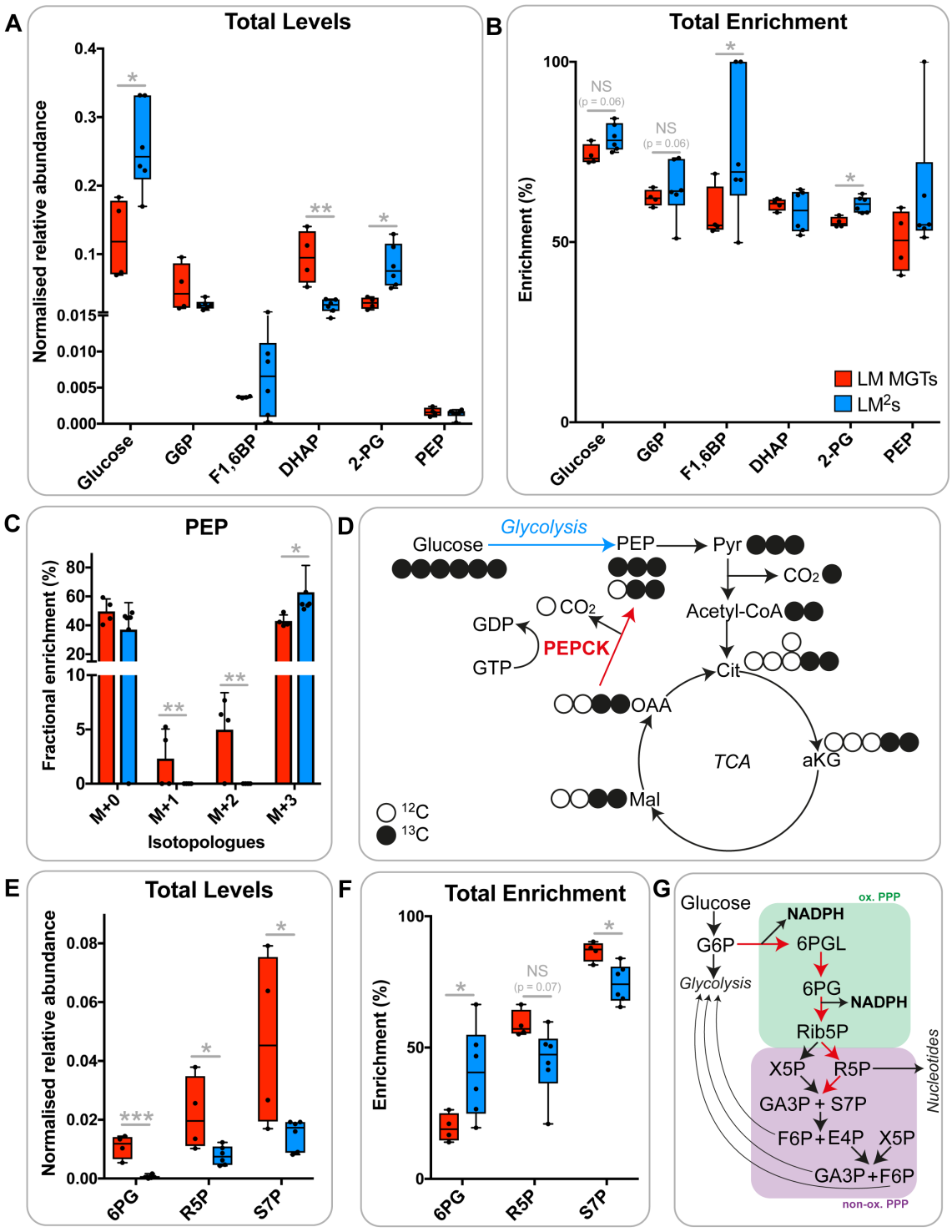


Figure 5-11. LC-MS metabolomics results comparing glycolytic and PPP glucose flux in LM MGTs and metastases derived from them (LM^{2}s).
(A) Total levels and (B) fractional enrichment from $^{13}C_6$-glucose of glycolytic intermediates. (C) Differences in phosphoenolpyruvate (PEP) fractional enrichment from glucose suggestive of PEPCK activity (D). (E) Total levels and (F) fractional enrichment from $^{13}C_6$-glucose of PPP intermediates. (G) Schematic of decreased PPP flux in LM^{2}s. Significance calculated using an unpaired parametric t-test (* $p < 0.05$, ** $p < 0.01$, *** $p < 0.001$).

5.3.3 TCA Cycle

Consistent with the results obtained from the Myc310 MGTs and LMs comparison (Figure 4-3), the total levels, the levels of $^{13}C_6$-glucose-derived isotopologues and fractional enrichment of citrate, isocitrate and cis-aconitate were reduced in LM^2s in comparison with LM MGTs (Figure 5-12 a-c). The total levels of these intermediates, however, were not different in LM^2s and LM MGTs from $^{13}C_6$-glutamine-infused animals (Figure 5-12 d,e), suggesting that LM MGTs have a higher capacity to catabolise glucose into citrate than LM^2s.

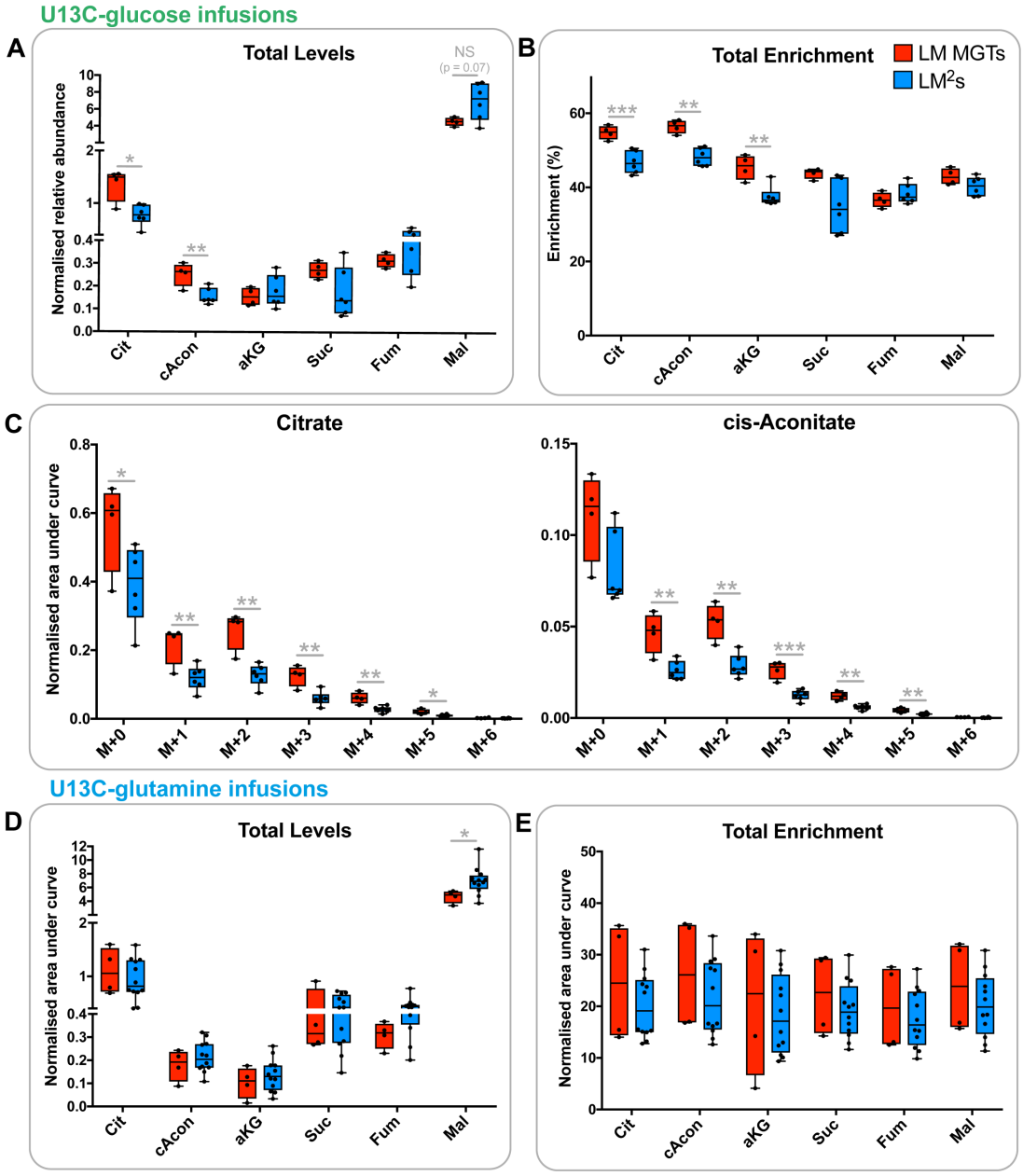


Figure 5-12. LC-MS metabolomics results comparing TCA flux in LM MGTs and metastases derived from them (LM^{2}s).
(A) Total levels and (B) fractional enrichment from $^{13}C_6$-glucose. (C) Isotopologue levels of citrate and cis-aconitate showing lower $^{13}C_6$-glucose carbon incorporation in (LM^{2}s). (D) Total levels and (E) enrichment from $^{13}C_5$-glutamine, showing no changes except for a significant increase in malate levels. Significance calculated using an unpaired parametric t-test (* $p < 0.05$, ** $p < 0.01$, *** $p < 0.001$).

Despite comparable total levels of citrate between LM MGTs and LM^{2}s in the $^{13}C_5$-glutamine-infused set, individual levels of citrate isotopologues (M+3, M+5 and M+6) were significantly decreased in LM2s in comparison with LM MGTs (Figure 5-13a). Furthermore, glutamine-derived fractional enrichment of M+5 citrate, cis-aconitate and isocitrate was decreased, identifying that reductive carboxylation of alpha-ketoglutarate is downregulated in LM^{2}s in comparison with LM MGTs (Figure 5-13 b-d).

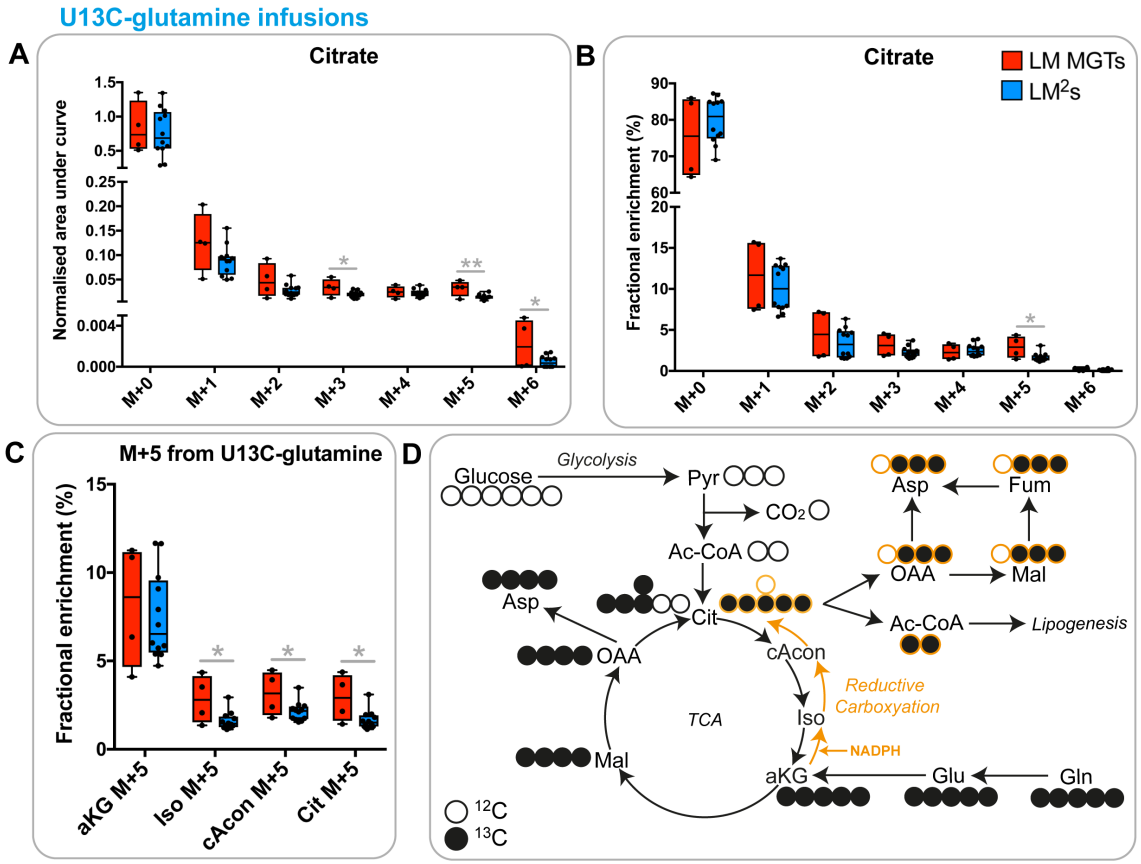


Figure 5-13. LC-MS metabolomics results comparing TCA flux in LM MGTs and metastases derived from them (LM^{2}s) following $^{13}C_5$-glutamine infusions.
(A) Total levels and (B) fractional enrichment of citrate from $^{13}C_5$-glutamine. (C) Fractional enrichment from $^{13}C_5$-glutamine of the M+5 isotopologue of alpha-ketoglutarate (aKG), isocitrate (Iso), cis-aconitate (cAcon) and citrate (Cit), showing decreased reductive carboxylation of glutamate in LM^{2}s (D). Significance calculated using an unpaired parametric t-test (* $p < 0.05$, ** $p < 0.01$, *** $p < 0.001$).

Consistent with the Myc310 MGTs and LMs comparison, the total level of malate was higher in LM^{2}s in comparison with LM MGTs from animals infused with either

$^{13}C_6$-glucose ($p = 0.07$) (Figure 5-12a, 5-14a) or $^{13}C_5$-glutamine (Figure 5-12d). Fumarate levels were slightly increased as well, albeit below the significance threshold (Figure 5-12a). Although the levels of $^{13}C_6$-glucose-derived malate isotopologue levels were higher in LM^2s in comparison with LM MGTs, glucose-derived enrichment was lower in the M+2 (Figure 5-14b). This suggests that although glucose catabolism through the TCA cycle is increased in LM^2s, its contribution to TCA cycle pools is proportionally lower than in LM MGTs. Interestingly, $^{13}C_5$-glutamine-derived malate and fumarate enrichment was not higher in LM^2s than in LM MGTs (Figure 5-14c-f) suggesting that another carbon source is contributing to the TCA cycle in LM^2s. Glutamine-derived fractional enrichment of malate and fumarate M+3 was significantly decreased in LM^2s in comparison with LM MGTs (Figure 5-14d,f), in line with increased reductive carboxylation of alpha-KG (Figure 5-13d).

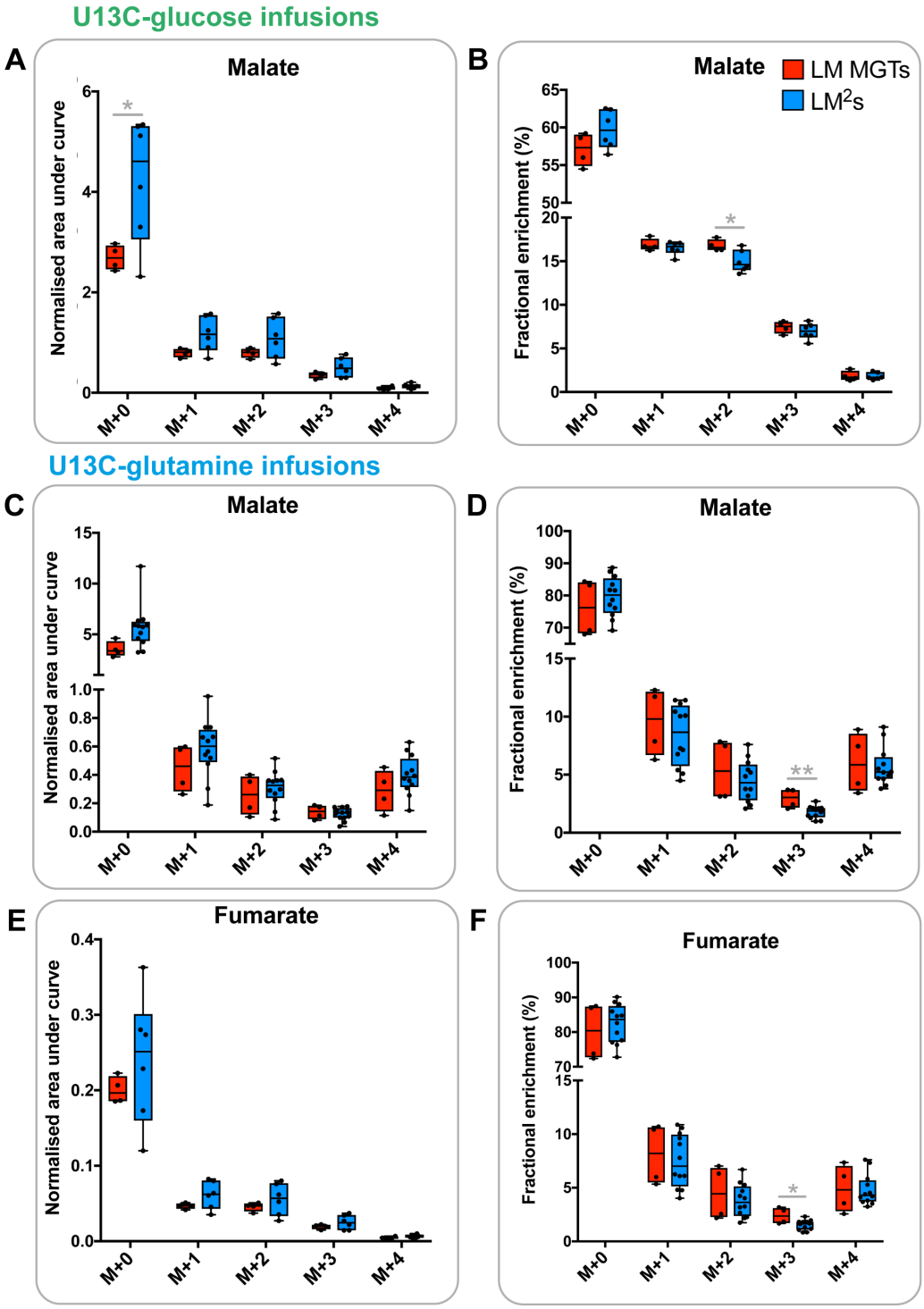


Figure 5-14. LC-MS metabolomics results comparing malate and fumarate. **L**evels and fractional enrichment in LM MGTs and metastases derived from them (LM^2s) following $^{13}C_6$-glucose (A) and $^{13}C_5$-glutamine (B) infusions. Decrease in glucose-derived M+2 malate enrichment and glutamine-derived M+3 malate enrichment in LM^2s. Significance calculated using an unpaired parametric t-test (* $p < 0.05$, ** $p < 0.01$, *** $p < 0.001$).

5.3.4 Non-Essential Amino Acids

Consistent with the results from the comparison between Myc310 MGTs and LMs (Chapter 4), LM^2s also had significantly higher levels of glutamine and glutamate compared to their parental tumours (Figure 5-15a). Increased levels of isotopologues derived from $^{13}C_6$-glucose and $^{13}C_5$-glutamine demonstrated that both nutrients were contributing to increased levels of glutamine in LM^2s (Figure 5-15b), even though glutamine contribution to TCA cycle was not increased (Figure 5-12e).

In line with previous findings, LM^2s had higher aspartate and asparagine levels than LM MGTs (Figure 5-15c). Despite higher levels, fractional enrichment of aspartate derived either from glucose or glutamine was lower in LM^2s than in LM MGTs (Figure 5-15d), suggesting an external source of aspartate in LM^2s. Aspartate can then feed into the TCA cycle as an alternative carbon source via the aspartate amino transferase reaction (Figure 5-15f). Furthermore, there was no labelling in asparagine from glucose or glutamine (Figure 5-15e), indicating that asparagine is taken up from the environment by LM^2s more than by LM MGTs, rather than produced from aspartate [177], [495], [742].

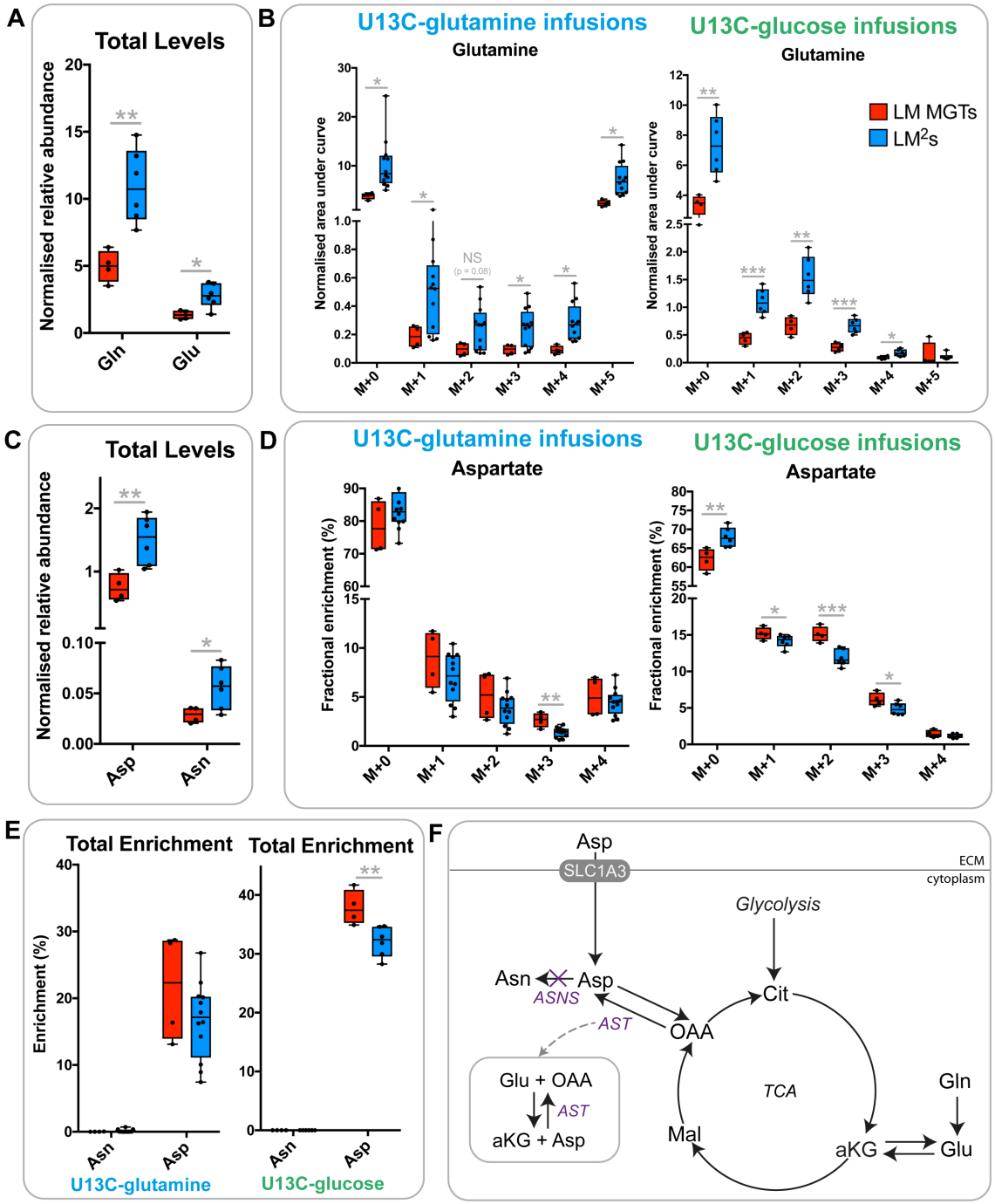


Figure 5-15. LC-MS metabolomics results comparing NEAAs.
Levels and fractional enrichment in LM MGTs and metastases derived from them (LM^{2}s). (A) Glutamine (Gln) and glutamate (Glu) total levels and (B) isotopologue fractional enrichment following $^{13}C_6$-glucose and $^{13}C_5$-glutamine infusions. (C) Aspartate (Asp) and asparagine (Asn) total levels and (D) isotopologue fractional enrichment following $^{13}C_6$-glucose and $^{13}C_5$-glutamine infusions. (E) Glucose-derived aspartate fractional enrichment is decreased in LM^{2}s, suggesting increased aspartate aminotransferase (AST) activity (F). Lack of labelling in asparagine suggests that asparagine synthestase (ASNS) is not active in LM MGTs or LM^{2}s. Significance calculated using an unpaired parametric t-test (* $p < 0.05$, ** $p < 0.01$, *** $p < 0.001$).

Isotope levels and glucose-derived fractional enrichment of another amino acid alanine were also increased in LM^{2}s in comparison with LM MGTs (Figure 5-16a-c). These results are consistent with recently reported observation that increased alanine synthesis from pyruvate via alanine aminotransferase is increased in breast cancer metastases for the production of alpha-KG, specifically due to elevated pyruvate levels in the lungs [165]. It is reported that alpha-KG produced in this reaction is needed for collagen hydroxylation via P4HA, which leads to ECM remodelling and increased migration of metastasis cells [165]. alpha-KG is also needed for the aspartate aminotransferase reaction in which aspartate carbons are incorporated into the TCA (Figure 5-15f).

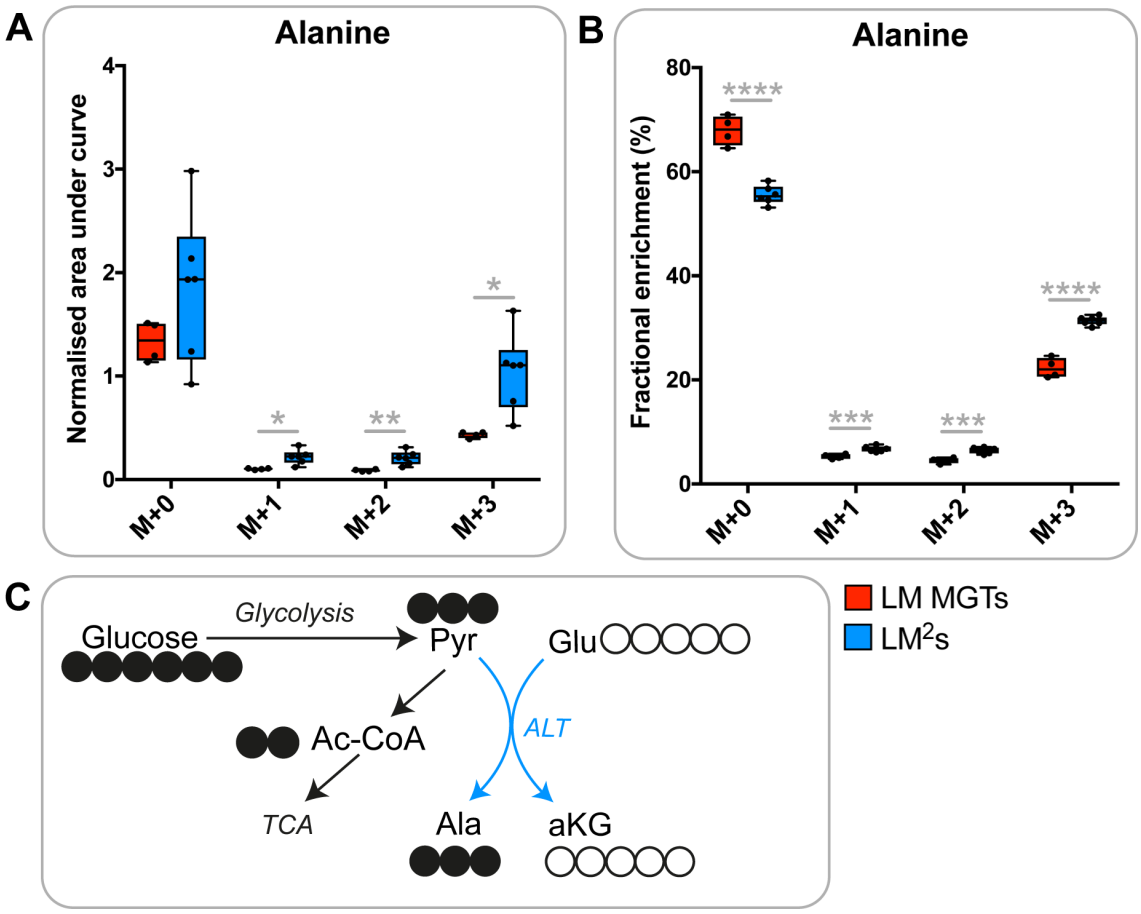


Figure 5-16. LC-MS metabolomics results comparing alanine.

Total levels (A) and fractional enrichment from $^{13}C_6$-glucose (B) in LM MGTs and metastases derived from them (LM^{2}s). Increased levels and glucose-derived enrichment suggests an increased alanine aminotransferase (ALT) activity in LM^{2}s (C). Significance calculated using an unpaired parametric t-test (* $p < 0.05$, ** $p < 0.01$, *** $p < 0.001$).

5.3.5 Essential amino acids

Similar to the Myc310 analysis (Chapter 4), the levels, and therefore import, of essential amino acids histidine, threonine and leucine were higher in LM^{2}s compared to LM MGTs (Figure 5-17a). Increased leucine levels suggest higher LAT1 transporter activity in LM^{2}S, and imported branched chain amino acids (BCAAs) contribute to the TCA cycle flux via branch chain aminotransferases (BCATs) (Figure 5-17b). Histidine and threonine can contribute carbons towards intermediates of the one carbon metabolism pathway (Figure 5-17c) [251], [255], [256], [743], which has been hypothesized to be upregulated in LMs in the context of this project, from findings discussed in the previous chapter.

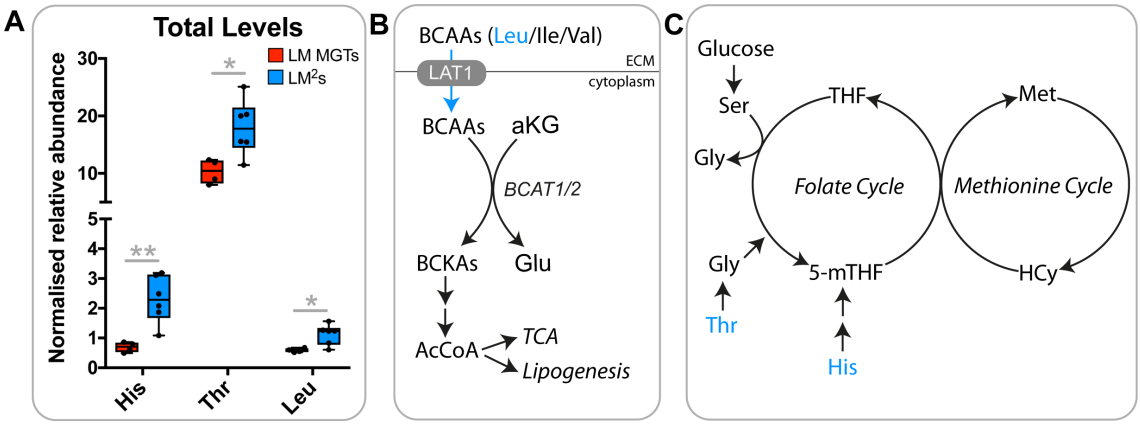


Figure 5-17. LC-MS metabolomics results comparing EAAs
Total levels (A) in LM MGTs and metastases derived from them (LM^{2}s). Increased levels of histidine (His), threonine (Thr) and leucine (Leu) in LM^{2}s suggests an increased activity of the LAT1 transporter and branched-chain amino acid (BCAA) catabolism (B), as well as increased carbon contribution to the one carbon metabolism pathway from threonine and histidine (C). Significance calculated using an unpaired parametric t-test (* $p < 0.05$, ** $p < 0.01$, *** $p < 0.001$).

5.3.6 One carbon metabolism

Consistently with the findings in the previous chapter, several intermediates of the one carbon metabolism pathway were increased in LM^2s compared to the MGTs from which they originate, including SAM, SAH, betaine and dimethylglycine, as well as the SAM/SAH ratio in LM^2s (Figure 5-18a,b). Furthermore, levels of both GSH and GSSG were significantly higher in LM^2s in comparison with LM MGTs, with a reduced GSH/GSSG ratio (Figure 5-18c,d), suggesting increased glutathione biosynthesis, and increased oxidative stress. Interestingly, the fractional enrichment from both glucose and glutamine, in both GSH and GSSG, was increased in LM MGTs. This suggests that in LM^2s, the precursors for glutathione biosynthesis, glutamate, glycine and cysteine, are either imported into the cells or synthesized from other metabolites.

Serine and subsequently glycine, the substrates for one carbon metabolism, can either be produced from glucose or taken up from the circulation. Glucose-derived enrichment of serine was not different while the enrichment of glycine isotopologues (M+1 and M+2) were lower in LM^2s in comparison with LM MGTs (Figure 5-18f, Figure 1-6). This suggested that the increased levels of one carbon metabolites and glutathione can be fuelled by the increased uptake of nutrients from the circulation.

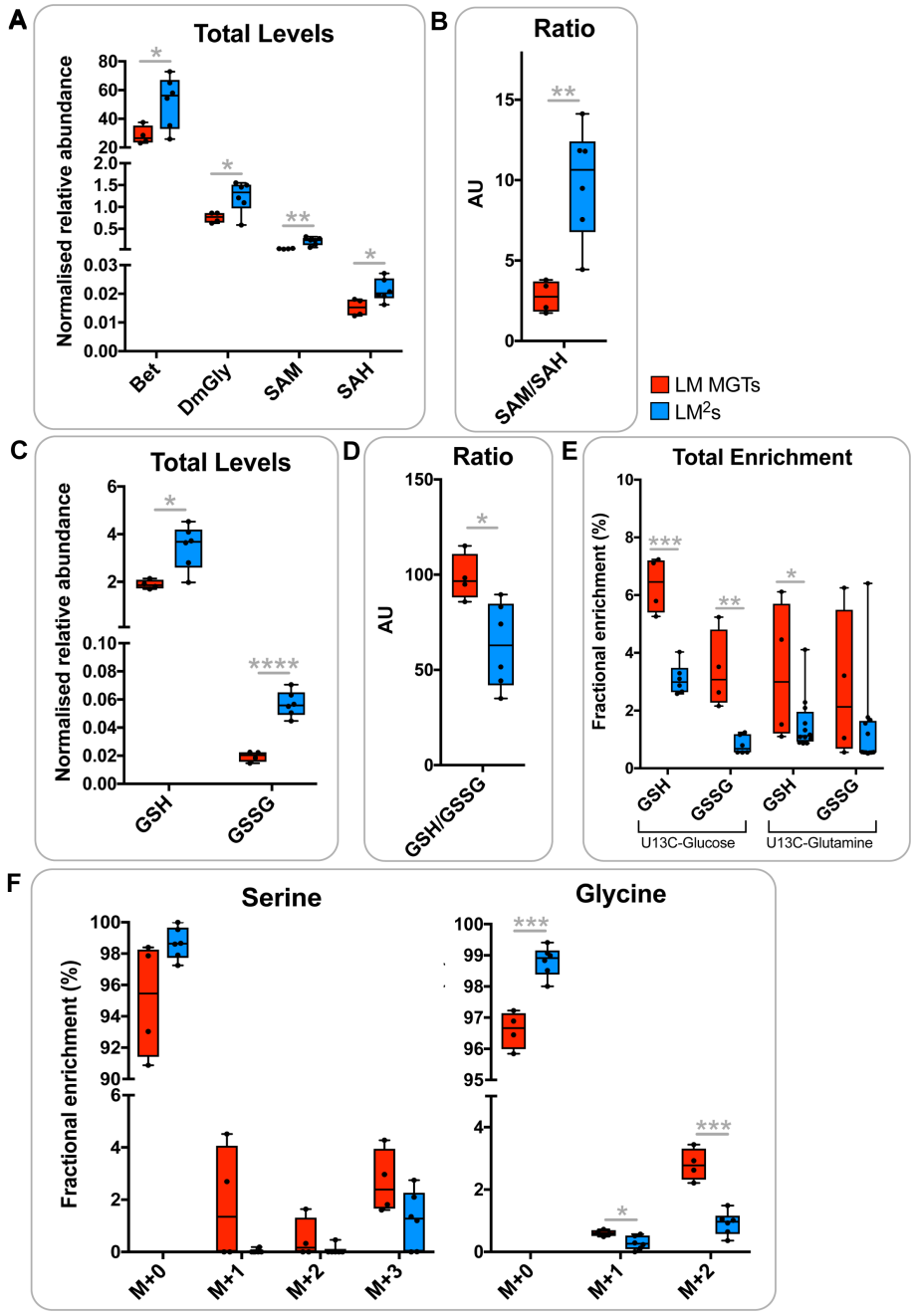


Figure 5-18. LC-MS metabolomics results comparing one carbon metabolism and contributing metabolites LM MGTs and metastases derived from them (LM²s).

(A) One carbon metabolism intermediates betaine (Bet), dimethylglycine (DmGly), S-adenosylmethionine (SAM) and S-adenosylhomocysteine (SAH) levels are increased in LM2s, as well as the ratio of SAM/SAH (B), suggesting a higher methylation capacity. (C) Elevated levels of both reduced (GSH) and oxidized (GSSG) glutathione in LM2s, as well as reduced ratio of GSH/GSSG (D), suggesting increased oxidative stress. (E) Decreased fractional enrichment in GSH and GSSG from $^{13}C_6$-glucose and $^{13}C_5$-glutamine in LM2s suggesting alternative external sources. (F) Fractional enrichment of serine and glycine from $^{13}C_6$-glucose is reduced in LM2s, in line with reduced labelling in glutathione. Significance calculated using an unpaired parametric t-test (* $p < 0.05$, ** $p < 0.01$, *** $p < 0.001$).

5.3.7 Consideration of whole body metabolism in *in vivo* stable isotope labelling studies.

While cancer metabolomics studies employing stable isotope labelling often focus on the incorporation into the tumour, or in this case the primary tumour and its secondary metastatic lesions, it is important to consider the metabolic functions of other organs in the body and how that may contribute to the patterns of stable isotope labelling that are observed. The fractional enrichment of labelled metabolites in the serum is an indication of the availability of these compounds to not only the tumour and metastases, but also to other vital organs that preferentially consume and are able to secrete certain metabolites [90], [744]. The metabolic steady state is achieved *in vivo* when the flux between the blood and other organs or tumours in the body are maintained at a constant [745], [746]. Isotopic steady state is only achieved after an initial increase in utilisation of the labelled substrate, and needs to account for a continuous flux of many metabolic intermediates between cells and organs of the body. Furthermore, the time it takes to reach isotopic steady state in different metabolic pathways depends on many factors, including metabolite flux, enzyme kinetics and alternative substrate availability[744], [745], [747]. Time-course labelling experiments are required to determine when exactly the steady state is reached, however in this study all labelling was performed for three hours due to potential isoflurane-induced toxicity following this time point [735].

Analysis of fractional enrichment serum from $^{13}C_6$-glucose labelling showed that the tumour and metastases consume more glucose and have a higher level of labelled glycolytic intermediates (Figure 5-19a). On the other hand, from $^{13}C_5$-glutamine fractional enrichment comparison to serum, there was a higher enrichment of labelled glutamine in serum than in the tumours or metastases (Figure 5-19b). Since the fractional enrichment from glutamine in downstream metabolites, such as NEAAs and TCA cycle intermediates is overall decreased in serum compared tumours and metastases, glutamine catabolism is active in these tissues. A higher fractional enrichment of labelled glutamine may be indicative of glutamine being secreted from the tumours, for example to accommodate LAT1 transporter activity [214], [748].

Fractional enrichment in serum can be used to compare the preferential substrate for different metabolic pathways in the tumours of interest compared to the rest of the body. In this study, the fractional enrichment of TCA cycle intermediates from $^{13}C_6$-glucose and from $^{13}C_5$-glutamine are relatively comparable, falling within the 5-20% range. In both MGTs and LMs, however, the glucose contribution to the TCA cycle falls in the range of 30-60% fractional enrichment, while contribution from glutamine is only 10-40%. Since the serum fractional enrichment is comparable from glucose and glutamine, this suggests that TCA cycle intermediates are not readily excreted from malignant tissues.

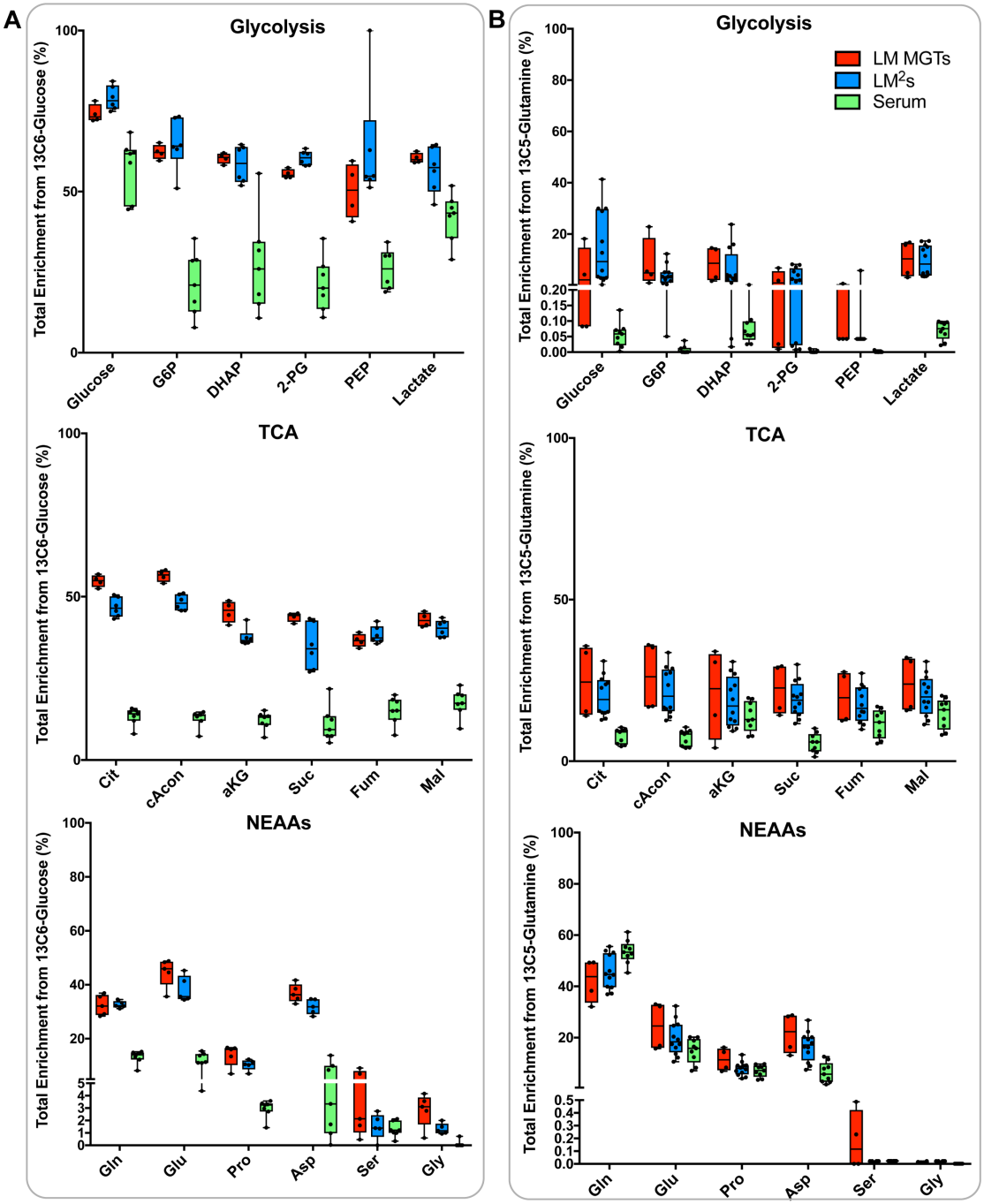


Figure 5-19. LC-MS metabolomics results comparing total fractional enrichment from in serum compared to LM MGT and LM2s.
Total fractional enrichment (%) from (A) $^{13}C_6$-glucose and (B) $^{13}C_5$-glutamine three hour infusions.

5.3.8 Chapter Discussion

By injecting Myc310 LM cells into the fat pad of wildtype FVB/NJ mice, I was able to create a robust metastatic model of MYC-driven breast cancer, and the increased number and size of lung metastases formed (compared to the initial Myc310-injected mice) allowed me to perform stable isotope labelling experiments and accurately dissect the formed LM^2s for LC-MS analysis.

Many of the metabolic differences in metabolite levels between LM MGTs and LM^2s reproduced the ones observed between the original Myc310 MGTs and their metastases, which instilled confidence that these changes are metastasis-specific. These included an increase in glycolysis and decrease in PPP in LM^2s. Stable isotope labelling showed that not only levels, but also enrichment from glucose was increased in glycolytic intermediates in LM_2s, and reduced in PPP intermediates R5P and S7P, although 6-phosphogluconate enrichment from glucose was higher in LM_2s. This finding demonstrates differential fates for glucose carbons between mammary gland tumours and their lung metastasis. Further investigation into the expression levels of PPP enzymes including G6PDH, 6PGDH and TKT, and of transcription factors modulating PPP such as nuclear erythroid 2-related factor 2 (NRF2) and the EMT transcription factors [730], [749], [750]. Several studies have reported upregulated PPP in more aggressive tumours, and have attributed NADPH production for maintenance of the antioxidant balance as the metabolic advantage for PPP upregulation [731], [751], [752]. Thus, despite increased levels of GSH and GSSG and a decreased GSH/GSSG ratio in LMs suggesting increased oxidative stress compared to MGTs, conflictingly LMs do not upregulate the PPP for NADPH production to support glutathione recycling. LM cells may rely on NADPH production from alternative pathways, including the TCA cycle, or the activity of malic enzyme or glutamate dehydrogenase [753].

Changes in the TCA cycle were consistent with the findings in the Myc310 model. Citrate, cis-aconitate and isocitrate levels were decreased in LM^2s, while fumarate and malate levels were increased, compared to LM MGTs. $^{13}C_5$-glutamine labelling revealed decreased reductive carboxylation of alpha-KG in LM^2s in comparison with LM MGTs, as seen by decreased levels of M+5 citrate, cis-aconitate and

isocitrate, as well as increased M+3 malate, fumarate and aspartate. Reductive carboxylation has been shown to support growth of cancer cells with mitochondrial defects or when oxygen availability is limited [150], [754], and may be downregulated in LM^2s since oxygen is abundant in the lung microenvironment [739]. Furthermore, the reductive IDH reaction requires NADPH, which supports ROS neutralisation by glutathione, therefore metastatic tumours may conserve NADPH for antioxidant pathways. Conversely, it has been reported that in an anchorage-independent tumour spheroid model, citrate and isocitrate produced by reductive carboxylation could be transferred into the mitochondria and fuel NADPH production for ROS protection [755]. The overarching role of reductive carboxylation in metastases, therefore, requires further investigation. Another method of stable-isotope labelling that can help confirm the activity of the reductive carboxylation pathway is through infusions of 1-13C-glutamine [150]. The first position carbon of glutamine will be excluded from the oxidative TCA pathway as carbon dioxide, however if reductive carboxylation is active, it will be incorporated onto citrate and downstream metabolites [150], [756].

Stable isotope labelling showed that the increased levels of malate and fumarate in LM^2s were not coupled with an increased fractional enrichment from either glucose or glutamine, suggesting alternative carbon sources in LM^2s for the TCA cycle. A possible metabolite which can feed into the TCA cycle is exogenous aspartate, imported into cells via the SLC1A3 transporter [179]. Notably, it has been shown that aspartate synthesis from asparagine via asparaginase was not possible in mammalian cancer cell lines, therefore an exogenous import of aspartate is the most likely alternative source [757]. Aspartate was still produced via the AST reaction, with enrichment from glucose significantly higher in the LM MGTs than LM^2s. Alpha-KG is required for the incorporation of aspartate into the TCA cycle via AST, and concurrently, alpha-KG is produced during the ALT reaction, in which alanine is synthesized from pyruvate. Alanine levels and enrichment from glucose were significantly higher in LM^2s, which is in line with recent work showing the importance of the ALT reaction for alpha-KG production and subsequent collagen hydroxylation in lung metastasis development [165].

Glucose- and glutamine-derived labelling was observed in aspartate, however no labelling was seen in asparagine (<0.001%), despite overall significantly higher levels in LM^2s suggesting that ASNS activity is either quite low or entirely downregulated in both LM MGTs and LM^2s and asparagine is taken up from the environment. A recent study described that asparagine levels and ASNS expression directly influenced metastatic burden in a breast cancer cell line [495]. Asparagine directly activates mTORC1 and regulates key cellular pathways including nucleotide biosynthesis and proliferation [177], [758]. In my model, no labelling from glucose or glutamine was observed in asparagine despite the incorporation of labelled carbons from both sources into aspartate, suggesting that ASNS activity is either quite low or entirely downregulated in both LM MGTs and LM^2s.

BCAAs can be another source of carbons for the TCA cycle, and indeed leucine levels were increased in LM^2s. Through the BCAT reaction, BCAAs are converted into branched chain keto-acids (BCKAs), which in turn can be used to produce acetyl-CoA for the TCA or lipogenesis [225], [759], [760]. Stable isotope leucine labelling and further inquiry into BCAA transporters such as LAT1 would be required to conclude the role of the increased leucine in LM^2s. LAT1 is also used in the import of other amino acids, including histidine and threonine, both of which were also increased in LM^2s and feed in to one carbon metabolism. Recently, LAT1 has been shown to be crucial for the development and survival of metastatic pancreatic cancer, playing a role in protein synthesis and amino acid metabolism [761].

In line with previous findings from the Myc310 LMs, there were increased levels of one carbon metabolism intermediates (betaine, dimethylglycine, SAM and SAH) in LM^2s, as well as increased levels of both reduced and oxidized glutathione, and a decreased GSH/GSSG ratio. As discussed in Chapter 4, the increased levels of intermediates of one carbon metabolism pathway, as well as the increased pools of both GSH and GSSG, support the hypothesis that tumour cells in the lung experience elevated levels of ROS [762] and therefore require metabolic adaptations to be able to neutralise these species and survive ([68], [504], [507]). Elevated levels of SAM also suggest an increased methylation capacity in the LM

cells, which may provide a functional link between metabolism and gene expression in the context of metastasis [658], [660], [694]–[696], [763]. A few recent works have demonstrated the role of serine and one carbon metabolism in metastasis [186], [263], [690], [764], [765], although the epigenetic implications remain unclear. The final part of my project focused on understanding the role of changes in the one carbon metabolism in LM cells further, with the overarching aim to potentially target this pathway and ultimately the ability of tumour cells to form metastasis.

The LC-MS experiments discussed in this and the previous chapters revealed a high degree of heterogeneity in metabolite levels with MGT and LM tumour sets, Furthermore, dissecting metastatic lesions from the surrounding lung introduces a high risk of non-tumour cells being included in the metabolite extraction, in addition to the known heterogeneous cell population within the metastatic niche, made up of connective tissue, immune cell infiltrates and lung pneumocytes in addition to tumour cells. In order to understand more clearly the distribution of metabolites within heterogeneous MGTs and the metastatic niche, a large proportion of my project was dedicated to developing mass spectrometry imaging methods using several technology platforms.

Chapter 6. Using DESI-MSI to analyse spatial distribution of polar metabolites in primary mammary gland tumours and their lung metastases.

6.1 Introduction

LC-MS metabolomics results showed several changes in polar metabolite pools between Myc310 MGTs and their LMs, especially when considering paired analysis between LMs and MGTs in the same animal. Many of these changes were also conserved between tumours generated by re-injection of LM cells into the fat pad (LM MGTs), and the metastases generated from them (LM^2s). However, a high degree of metabolic heterogeneity was observed within MGT and LM sample groups. One of the key focuses of my project was to establish methods to understand the origin of the observed metabolic heterogeneity, and to assess the limitations of traditional metabolomics techniques such as LC-MS when analysing complex tissue samples.

Indeed, several considerations should be taken into account when performing bulk tissue analysis in the lung metastasis model we use. First of all, grinding the entire tumour before extracting polar metabolites does not allow to discern any information about the distribution of metabolites within the tumours, which is especially pertinent given the histological heterogeneity of Myc-driven tumours [626], [766]. Secondly, most LMs were too small to accurately cryo-dissect prior to LC-MS analysis, without including some of the surrounding lung tissue. Closer histological evaluation by H&E and immunofluorescence stains also demonstrated that the metastatic lesions are very rarely composed of exclusively tumour cells and are often infiltrated by immune cells and pneumocytes (Figure 6-1). In fact, it has been shown in several recent studies that immune cells and other non-tumour cells in the metastatic niche and tumour microenvironment play an important role in metastasis development, survival and progression, often through metabolic crosstalk [486], [767]–[770].

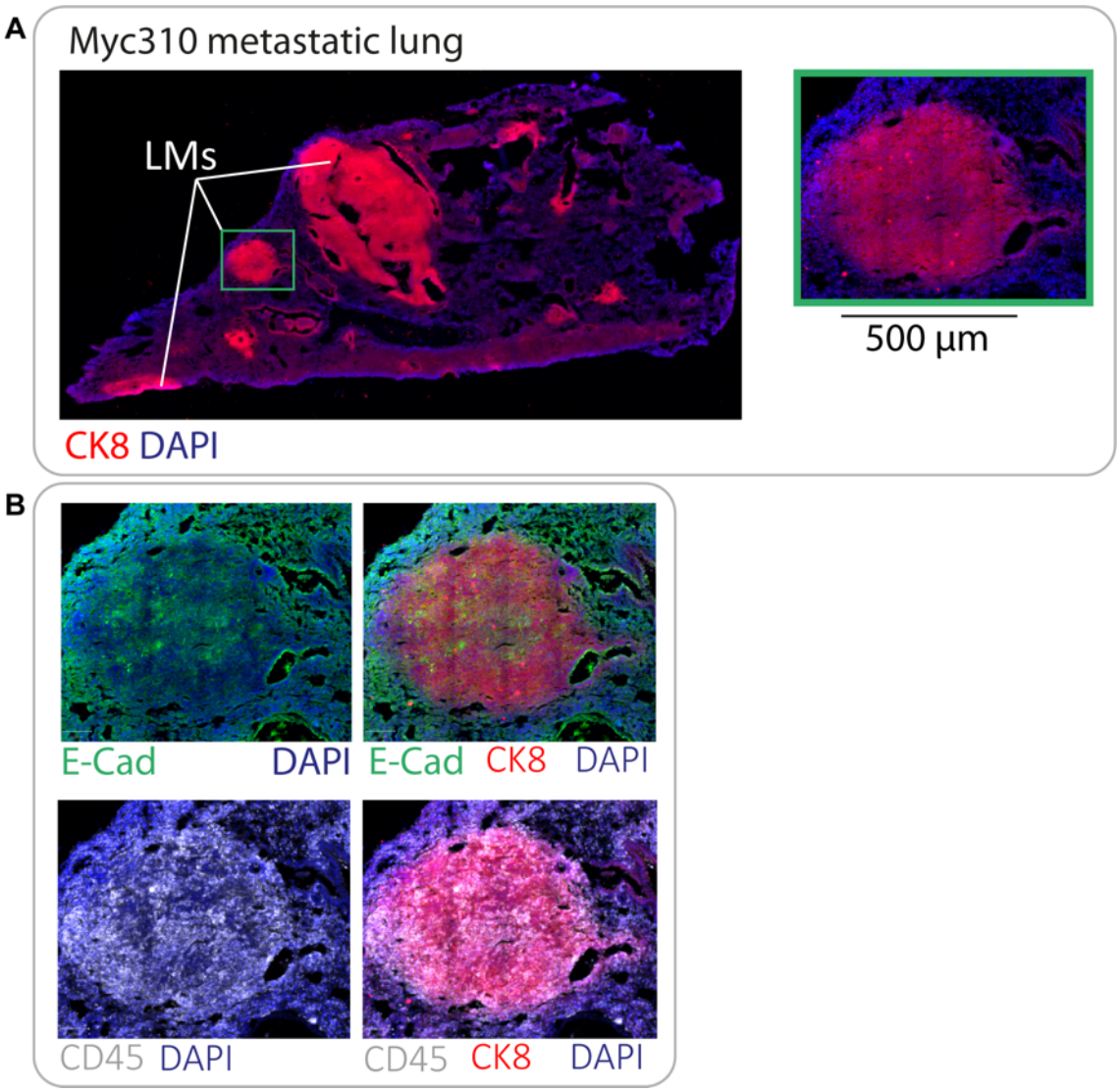


Figure 6-1. Immunofluorescent staining of a metastatic lung from a mouse that had a LM MGT.
(A) Cytokeratin 8 (CK8) staining for luminal epithelium highlighting the metastatic lesions (bronchial alveolar tissue also CK8+). (B) E-cadherin staining showed low expression in the metastatic lesions and high expression in the surrounding lung, with some pneumocytes infiltrating into the metastatic lesion. CD45 staining (pan-immune cell marker) revealed high degree of immune cell infiltration in the metastatic lesion.

These nuances must be kept in mind in order to identify metabolic requirements and vulnerabilities of the tumour cells and their interaction with the components of their environment. In order to elucidate how metabolites are distributed within tumours and metastatic lungs, I used mass spectrometry imaging (MSI). MSI allows the visualisation of the spatial distribution of metabolites within tissues without the need for dissection. Several MSI modalities are being developed for biological sample analysis, as reviewed in detail in the Introduction chapter. Throughout the length of my project I used two MSI platforms with different spatial resolutions, DESI-MSI (50-100 μm) and Orbi-SIMS (2 μm).

DESI-MSI allowed relatively quick whole-section imaging and detection of a wide range of polar metabolites within and between different tissue types, including primary tumours, lung metastasis and metastasis-surrounding lungs. First, I performed targeted analysis of DESI-MSI data and supervised clustering with histological segmentation of images into regions of interest (ROIs) to evaluate the localisation of metabolites detected by LC-MS in different histological regions. To obtain a more comprehensive picture of metabolite distribution, I have also performed untargeted analysis of DESI-MSI data using unsupervised multivariate analysis methods. Furthermore, Orbi-SIMS imaging allowed me to visualise metabolite distribution at a much higher lateral resolution than DESI-MSI, albeit with limited metabolite detection. In this chapter I will discuss how using MSI has enhanced our understanding of metabolic heterogeneity both within individual tumours and in the wider context of the whole organ in which metastatic tumours reside.

6.2 Experimental set-up and sample preparation

MGTs and whole lungs were cryo-sectioned for DESI-MSI sample analysis (sample preparation described in detail in the Methods chapter). Lungs from wildtype animals were prepared the same way and included on each slide for the comparison with the metastatic lungs. DESI-MSI images were acquired and pre-processed (see MSI Methods) prior to metabolite analysis. As discussed in the Methods section, negative ion polarity was used to acquire images due to a much

higher polar metabolite coverage as compared to the positive ion polarity. Possible adduct forms that were considered in negative ion mode were deprotonation ([M-H]-), loss of a water molecule and deprotonation ([M-H2O-H]-), and chlorination ([M+Cl]-). The pixel size of these DESI images was set to 100 µm, which in some cases was larger than the diameter of micro-metastases. While the DESI instrument can acquire images as low as 50 µm, lateral resolution is a trade off with image acquisition time and limited instrument availability. Images from several biological replicates of both Myc310 MGT and LM pairs, as well as LM MGT and LM^2 pairs are highlighted in the next two chapters to illustrate the advantages and findings of the DESI-MSI analysis. As described above, there was a range of sizes of LMs present in the lungs of mice with Myc310 MGTs, and while metabolite distribution is more reliably assessed in larger metastases, all detectable LMs were analysed to account for potential variations in the metabolic profile of metastases of different sizes.

6.3 Targeted DESI-MSI analysis: LMs vs. MGTs, comparison to LC-MS results.

The first analysis method that was applied to the DESI images is a targeted approach whereby the datasets were mined for all polar metabolites analysed in the LC-MS datasets. Central carbon metabolism has not been analysed using MSI in great detail to date. Historically, biological MSI was largely focused on lipid analysis [771]–[773], [392], [533], [774], and adapting the instrumentation to preserve and detect small polar metabolites is currently a novel and rapidly-growing interest [775]–[779]. Figure 6-2 shows the coverage of LC-MS matched polar metabolites across four DESI imaging sessions, and Table 10 below shows the exact metabolite identities, adducts and ppm error of ions identified from DESI-MSI that match with polar metabolites. The metabolite annotations were assigned based on putative matching of m/z values using the CEUMass Mediator database search [780], however as discussed throughout this section, *m/z* matching is often not sufficient to confidently assign ion identity when an ion matches multiple metabolites within the accepted mass resolving power (~15 ppm) and further confirmation by MS/MS is required. The figure shows the variability in metabolite

detection between imaging sessions that can be influenced by different external factors including room temperature and geometry of the sprayer and ion collection inlet. Nevertheless, it also shows that a significant number of ions were consistently detected in all biological replicates.

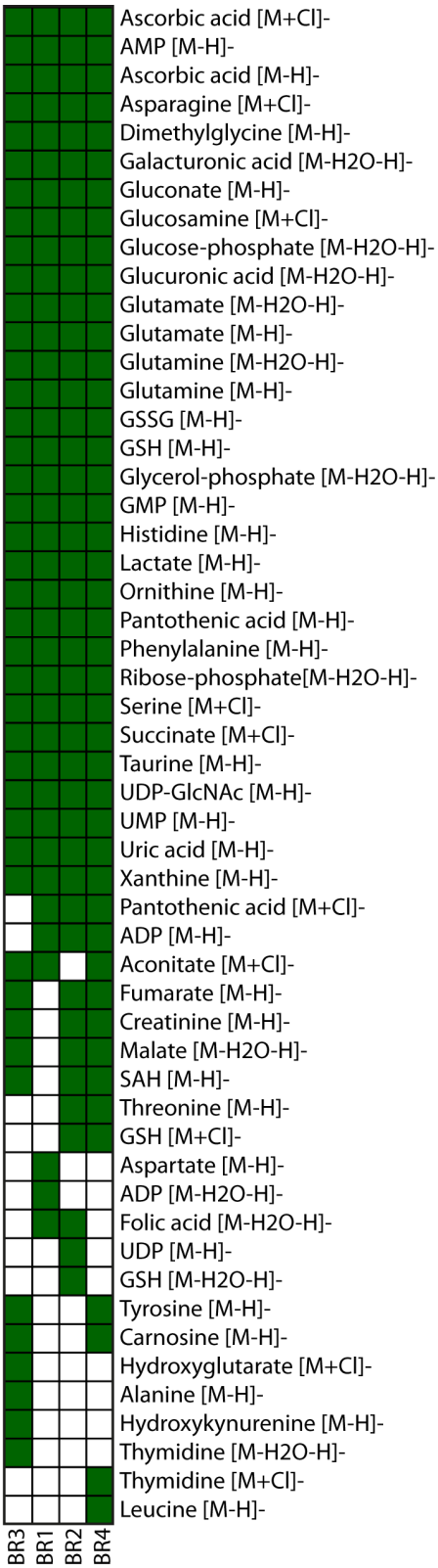


Figure 6-2. DESI-MSI coverage of polar metabolites.
DESI-MSI spectra were mined for polar metabolites typically analysed by LC-MS, across four biological replicates (BR). Each BR comprised of paired MGT and lung, as well as wildtype lung.

Table 10. DESI-MSI ion annotation to polar metabolites detected by LC-MS.
Isobaric species highlighted cannot be discerned based on *m/z* matching alone.

DESI m/z	Metabolite	Adduct	LC m/z	ppm	
89.024	Lactate	M-H	89.02445	5.1	
102.0551	Dimethylglycine	M-H	102.05605	9.3	
111.0198	Uracil	M-H	111.01995	1.4	
114.0568	Proline	M-H	114.05605	6.6	
115.0035	Fumarate	M-H	115.00365	1.3	isobaric
115.0035	Malate	M-H2O-H	115.00365	1.3	
116.0723	Betaine	M-H	116.07175	4.7	isobaric
116.0723	Valine	M-H	116.07175	4.7	
117.019	Succinate	M-H	117.01935	3.0	
118.0508	Threonine	M-H	118.05095	1.3	
124.0074	Taurine	M-H	124.00745	0.4	
127.0498	Glutamine	M-H2O-H	127.05125	11.4	
128.0352	Glutamate	M-H2O-H	128.03535	1.2	
130.0875	Isoleucine	M-H	130.08745	0.4	isobaric
130.0875	Leucine	M-H	130.08745	0.4	
131.0458	Asparagine	M-H	131.04615	2.7	
131.0825	Ornithine	M-H	131.08255	0.4	
132.0298	Aspartic acid	M-H	132.03025	3.4	
133.0141	Malate	M-H	133.01435	1.9	
133.0141	Xanthine	M-H2O-H	133.01555	10.9	
140.0117	Serine	M+Cl	140.01205	2.5	
145.0615	Glutamine	M-H	145.06185	2.4	
145.0964	Lysine	M-H	145.09825	12.7	
146.0458	Glutamate	M-H	146.04585	0.3	
151.0267	Xanthine	M-H	151.02615	3.6	
152.9962	Glycerol-phosphate	M-H2O-H	152.99595	1.6	
152.9962	Succinate	M+Cl	152.99605	1.0	
154.0621	Histidine	M-H	154.06215	0.3	
160.0637	Glucosamine	M-H2O-H	160.06155	13.4	
162.0572	Tyrosine	M-H2O-H	162.05605	7.1	
164.0723	Phenylalanine	M-H	164.07175	3.4	
167.0211	Uric acid	M-H	167.02105	0.3	
167.0211	Asparagine	M+Cl	167.02285	10.5	
171.0065	Glycerol-phosphate	M-H	171.00645	0.3	
173.0087	Aconitate	M-H	173.00925	3.2	isobaric
173.0087	Citrate	M-H2O-H	173.00925	3.2	
173.0087	Isocitrate	M-H2O-H	173.00925	3.2	
175.0247	Ascorbic acid	M-H	175.02485	0.9	isobaric
175.0247	Glucuronic acid	M-H2O-H	175.02485	0.9	
180.0664	Tyrosine	M-H	180.06665	1.4	
191.0198	Citrate	M-H	191.01975	0.3	isobaric
191.0198	Isocitrate	M-H	191.01975	0.3	

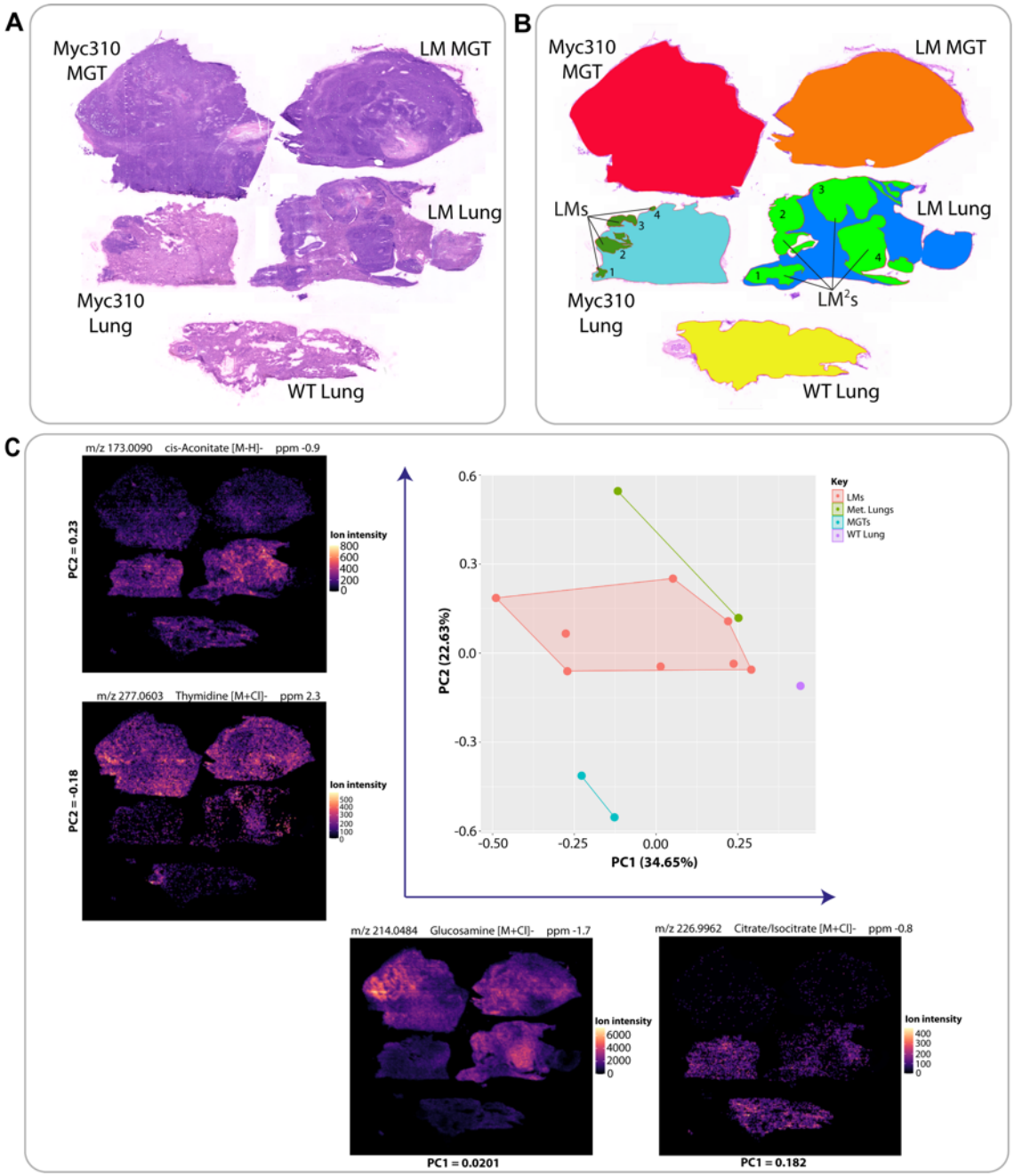
195.0507	Gluconate	M-H	195.05105	1.8	
202.9958	Uric acid	M+Cl	202.99775	9.6	
208.985	Aconitate	M+Cl	208.98595	4.5	
211.001	Ribose-phosphate	M-H2O-H	211.00135	1.7	
211.001	Ascorbic acid	M+Cl	211.00155	2.6	
214.0483	Glucosamine	M+Cl	214.04895	3.0	
216.0432	Tyrosine	M+Cl	216.04335	0.7	
218.1036	Pantothenic acid	M-H	218.10355	0.2	
223.0719	Thymidine	M-H2O-H	223.07235	2.0	
225.101	Carnosine	M-H	225.09935	7.3	
226.9965	Citrate	M+Cl	226.99645	0.2	isobaric
226.9965	Isocitrate	M+Cl	226.99645	0.2	
231.0274	Gluconate	M+Cl	231.02785	1.9	
241.0135	Fructose-phosphate	M-H2O-H	241.01195	6.4	isobaric
241.0135	Glucose-phosphate	M-H2O-H	241.01195	6.4	
254.0786	Pantothenic acid	M+Cl	254.08025	6.5	
275.0185	6-phosphogluconate	M-H	275.01745	3.8	
277.06	Thymidine	M+Cl	277.05975	0.9	
288.0653	GSH	M-H2O-H	288.06605	2.6	
306.0767	GSH	M-H	306.07665	0.2	
323.0288	UMP	M-H	323.02865	0.5	
346.0555	AMP	M-H	346.05585	1.0	
362.0497	GMP	M-H	362.05075	2.9	isobaric
362.0497	GMP	M-H	362.05075	2.9	
365.1002	SAH	M-H2O-H	365.10375	9.7	
383.1163	SAH	M-H	383.11445	4.8	
408.0133	ADP	M-H2O-H	408.01155	4.3	
422.1222	Folic acid	M-H2O-H	422.12195	0.6	
426.0221	ADP	M-H	426.02205	0.1	
440.1328	Folic acid	M-H	440.13245	0.8	
606.0746	UDP	M-H	606.07435	0.4	
611.1453	GSSG	M-H	611.14465	1.1	

6.3.1 Histological ROI Segmentation of DESI Images

Slides were stained with H&E following DESI image acquisition, and the H&E image was then scaled and overlaid with the DESI image in Matlab. Histological segmentation of the H&E images into areas of interest (LMs, MGT, metastatic lung, WT lung) were used to generate ROI masks, which were then applied onto the DESI image (Figure 6-3a,b). In order to facilitate image interpretation, especially in cases where ion counts are low, the mean intensity of a specific ion was calculated for selected ROIs. However, DESI ion intensities are not deemed truly quantitative due to potential differences in ion suppression and matrix effects across the sample. As shown in this chapter, representative images from two biological replicates revealed that there were both correlations and inconsistencies between certain metabolite levels between DESI and LC-MS experiments.

To evaluate the metabolite distribution between ROIs, intensities of ions matching in *m/z* values to LC-MS polar metabolites were first analysed by PCA (Figure 6-3c). Although in this instance the multivariate analysis is illustrative due to small sample size of each tissue type on a slide, clear segregation was observed between LMs, MGTs, metastatic and wildtype lungs. The loadings for each principal component were then used to select representative ions that contribute most strongly to the separation between principal components. In the example shown, high scores in PC1 represent ions most present in lung tissue. In PC2, lower scores represent ions highly localised to the MGTs, whereas higher scores depict ion signals localised in and around high-grade LMs. Furthermore, hierarchical clustering of metabolite intensities resulted in histology-based ROI separation (Figure 6-3), clustering grouped wildtype lung with the less-metastatic Myc310 lung. The two MGTs clustered together, and most of the metastasis clustered together as well.

These multivariate approaches instilled confidence that variations in polar metabolite distributions in DESI images were driven by histological regions and therefore specific cell types. Later in the chapter I will discuss how untargeted DESI image analysis can help elucidate even further metabolic heterogeneity, unrelated to histological features.


A
Myc310 MGT
LM MGT
LM Lung
Myc310 Lung
WT Lung
B
Myc310 MGT
LM MGT
LMs
LM Lung
Myc310 Lung
LM²s
WT Lung
C
m/z 173.0090 cis-Aconitate [M-H]- ppm -0.9
PC2 = 0.23
Ion intensity
800
600
400
200
0
m/z 277.0603 Thymidine [M+Cl]- ppm 2.3
PC2 = -0.18
Ion intensity
500
400
300
200
100
0
PC2 (22.63%)
0.6
0.3
0.0
-0.3
-0.6
-0.50
-0.25
0.00
0.25
PC1 (34.65%)
Key
LMs
Met. Lungs
MGTs
WT Lung
m/z 214.0484 Glucosamine [M+Cl]- ppm -1.7
Ion intensity
6000
4000
2000
0
PC1 = 0.0201
m/z 226.9962 Citrate/Isocitrate [M+Cl]- ppm -0.8
Ion intensity
400
300
200
100
0
PC1 = 0.182

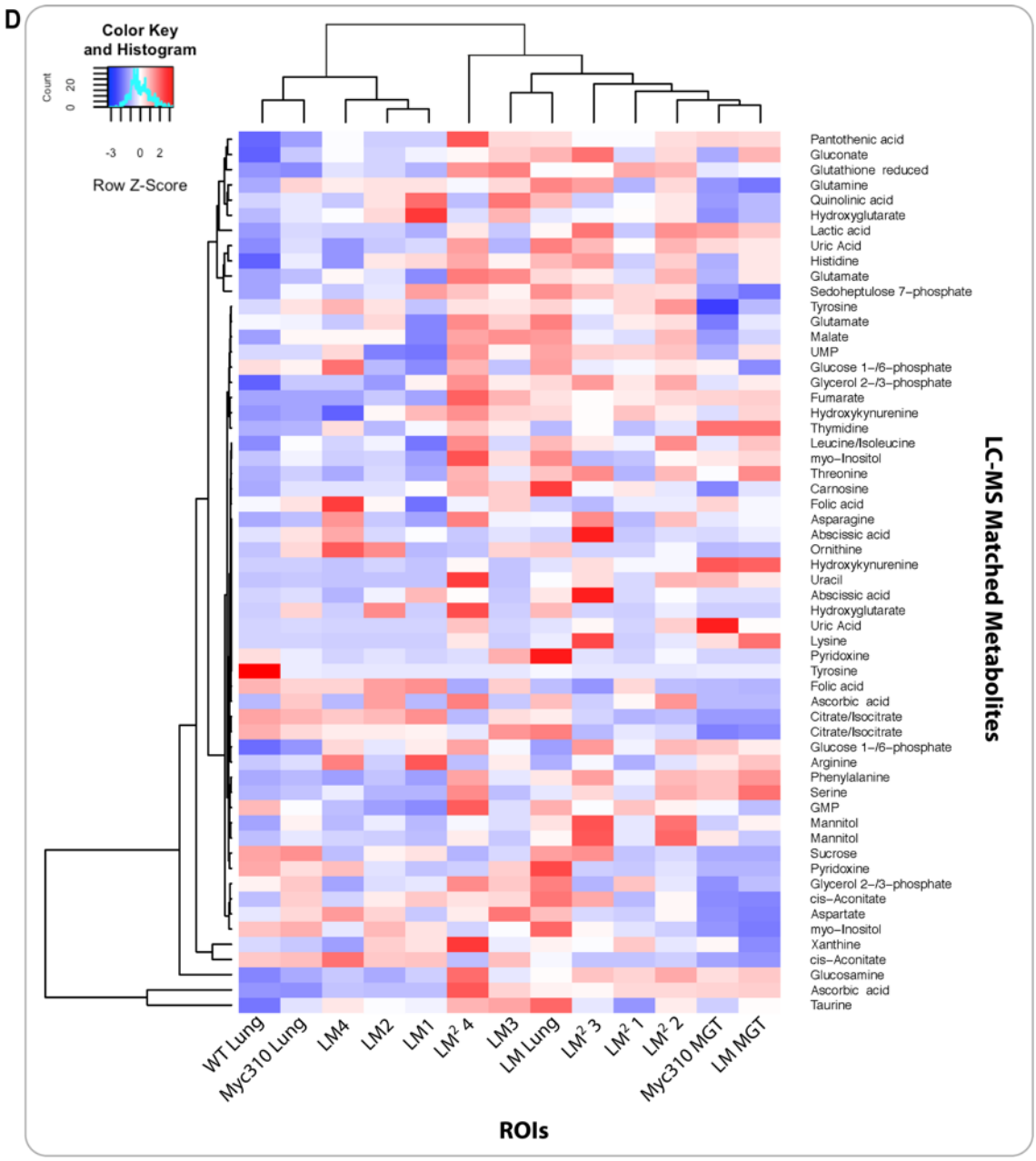


Figure 6-3. Histological segmentation of DESI-MSI images.
(A) Post-DESI whole slide H&E staining. (B) ROI segmentation based on post-DESI H&E stain. (C) Polar metabolites identified from all histology-based ROIs from a DESI-MSI image were sufficient to separate MGTs, LMs and lung tissues, indicating heterogeneous distribution between tissue types. (D) Heatmap showing hierarchical clustering of ROIs from the same DESI-MSI image with relative levels of the detected polar metabolites.

6.3.2 Glutamine, glutamate and TCA.

Glutamine and glutamate are two amino acids that are consistently detected with high confidence in DESI-MSI using our current method. Both of these metabolites were shown by LC-MS to be higher in LMs compared to MGTs (Figure 6-4).

However, DESI images of the distribution of these two ions revealed the remarkable advantage of MSI in analysing the spatial distribution of metabolites in different tissues non-invasively. DESI imaging of several biological replicates showed that the average glutamate signal was indeed higher in the LM ROIs compared to the MGT ROI consistent with LC-MS results (Figure 6-4b). However, it also demonstrated that glutamate is not uniformly distributed in MGTs; a feature that could not be identified by bulk tissue analysis using LC-MS. The higher levels of glutamate in some areas of MGTs and lower levels in others result in average levels that are overall lower than in LMs. DESI shows that the levels of glutamate are comparable between LMs and specific regions of histologically viable tumour cells in the MGT (Figure 6-4c).

Furthermore, while by LC-MS analysis glutamine levels were higher in LMs than in MGTs (Figure 3-9, Figure 5-15), DESI images show that the majority of the glutamine signal is localised to the metastasis-infiltrated lung, rather than in the LM lesions. These results suggest that some surrounding lung tissue may have been included in the LC-MS polar extract of the LMs contributing to higher glutamine levels in that samples. Lower levels of glutamine and higher levels of glutamate in metastasis versus metastasis-infiltrated lung suggest that metastasis have higher glutamine catabolism than the surrounding tissue.

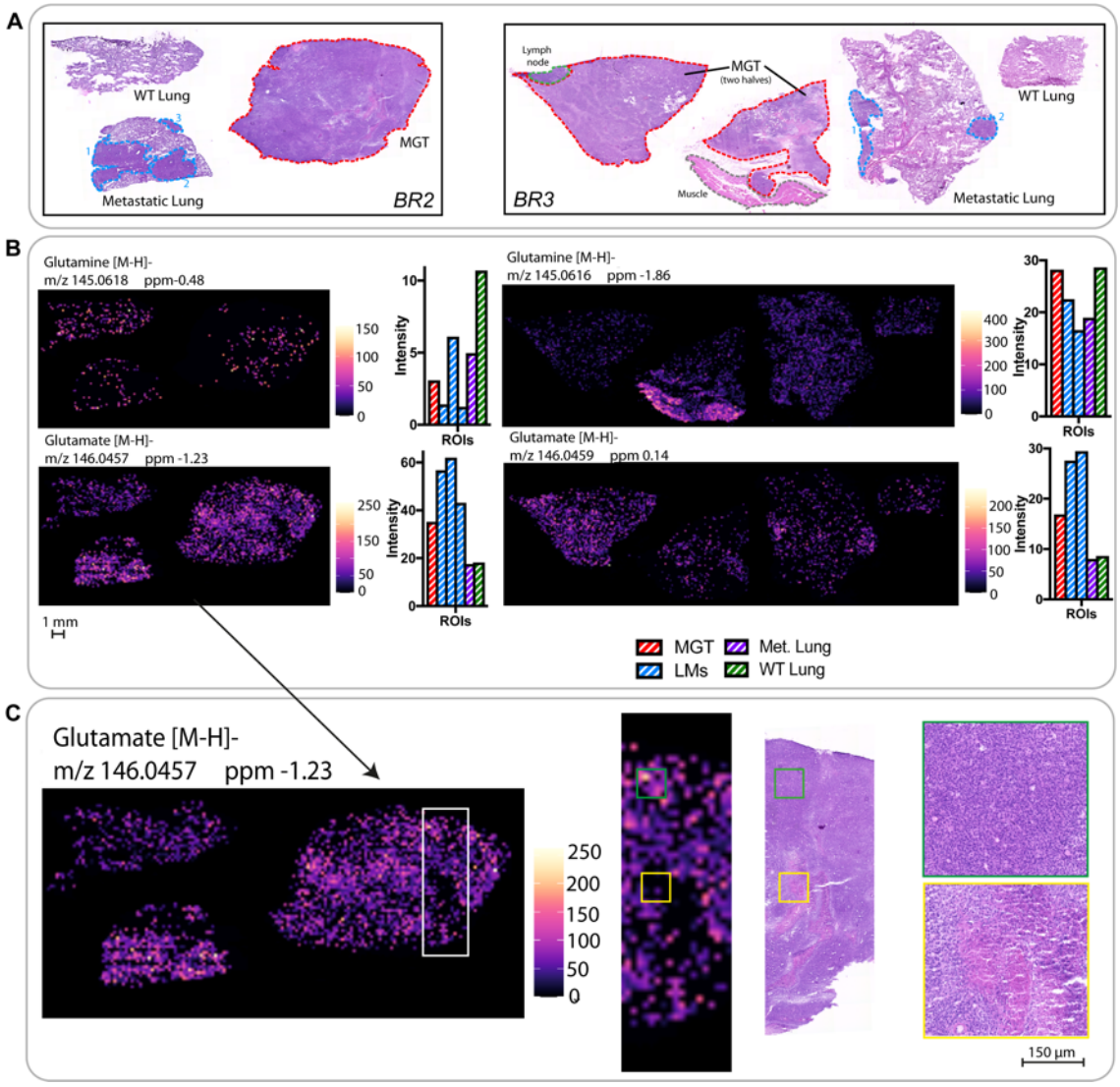


Figure 6-4. DESI-MSI imaging of glutamine and glutamate.
DESI-MSI of two biological sample (BR) slides, each containing a Myc310 MGT, metastatic lung from the same animal, and a wildtype lung for comparison. (A) Post-DESI H&E. (B) Spatial distribution of ions matching to glutamine and glutamate [M-H]- in two biological replicates, with relative intensities between histology-segmented ROIs shown in bar graph. Importantly, ion levels are relative and not considered quantitative. (C) Distribution of ion matching to glutamate [M-H]- shows differential distribution within the MGT between areas of proliferative tumour tissue and necrosis.

To confirm the differential distribution of glutamine and glutamate, I used stable isotope labelling, where mice bearing MGTs were infused with $^{13}C_5$-glutamine. DESI analysis confirmed the differential distribution of glutamine and glutamate between MGTs, LMs, metastatic and wildtype lungs (Figure 6-5 a-c). The M+5 isotopes of both amino acids were consistently detected using our DESI-MSI methods, and their distribution matched that of the unlabelled ions. The signal of glutamine M+5 was higher in metastasis than in MGTs and even further increased in the metastasis-infiltrated lung. The signal of glutamate M+5, on the other hand, was higher in most of the metastasis in comparison with the MGTs and surrounding lung. The distribution of both amino acids was heterogeneous within MGTs. These results confirmed that overall glutamine catabolism is increased in metastasis in comparison with primary tumours and there is glutamine accumulation in the metastasis-infiltrate lungs. Increased levels of glutamine in the metastatic lung surrounding the metastatic lesions may be a sign of a metastatic niche cell population which increases glutamine uptake, possibly as a pro-tumorigenic response. For example, glutamine availability has been shown to promote cancer-associated fibroblast (CAF) migration and tumour invasiveness [781], and CAFs also promote *de novo* glutamine biosynthesis in nutrient deplete conditions to promote tumour growth [782]. It has also recently been shown that lung fibroblasts require increased glutamine in the progression of fibrotic disease [783].

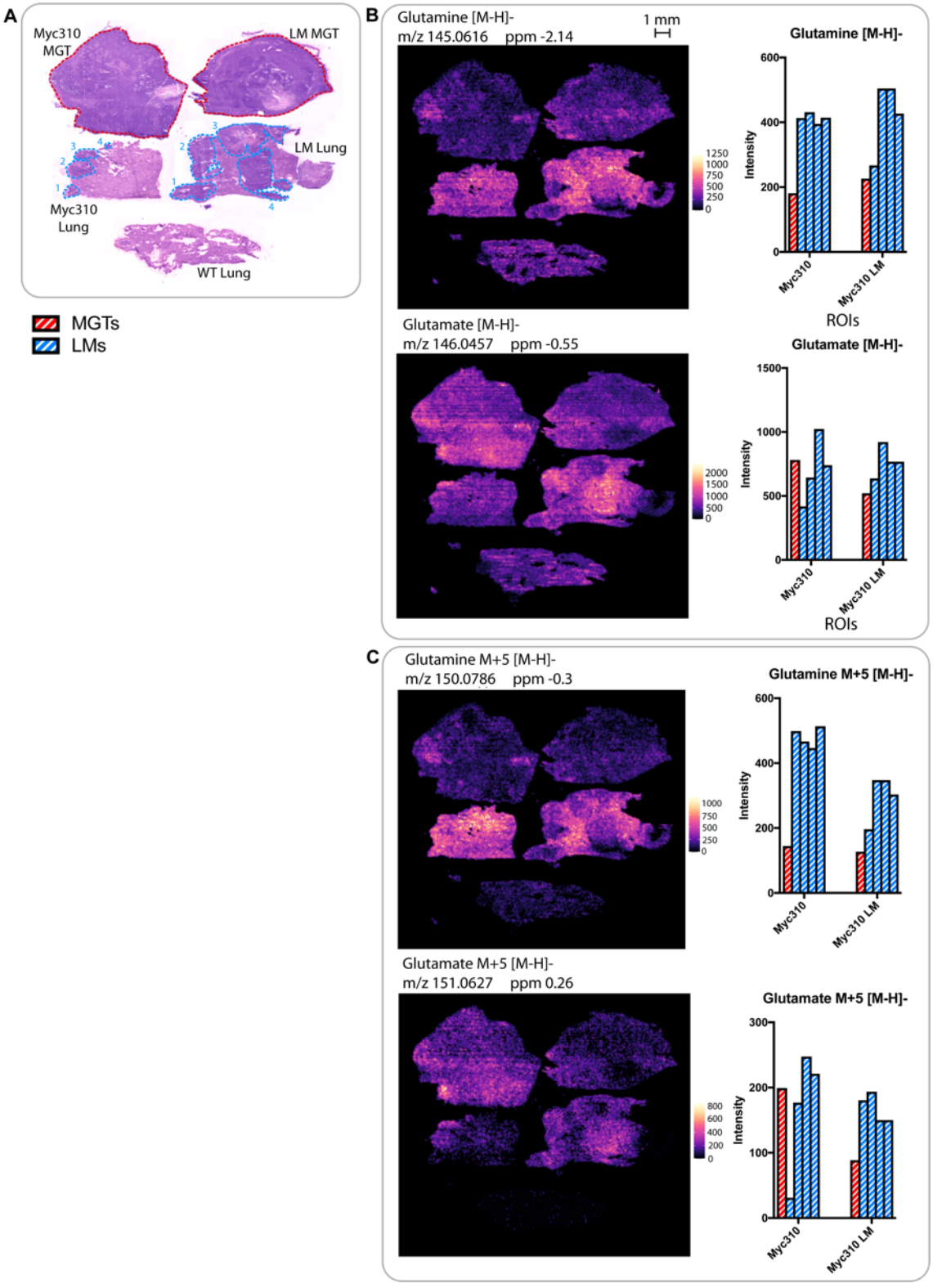

A
Myc310 MGT
LM MGT
LM Lung
Myc310 Lung
WT Lung
MGTs
LMs
B
Glutamine [M-H]-
m/z 145.0616 ppm -2.14
1 mm
Glutamine [M-H]-
Intensity
Myc310
Myc310 LM
ROIs
Glutamate [M-H]-
m/z 146.0457 ppm -0.55
Glutamate [M-H]-
C
Glutamine M+5 [M-H]-
m/z 150.0786 ppm -0.3
Glutamine M+5 [M-H]-
Glutamate M+5 [M-H]-
m/z 151.0627 ppm 0.26
Glutamate M+5 [M-H]-

Figure 6-5. DESI-MSI imaging of heavy isotope labelled glutamine and glutamate. DESI-MSI of one slide containing a Myc310 MGT and paired metastatic lung, a LM MGT and paired metastatic lung, and a wildtype lung for comparison. All animals were infused with $^{13}C_5$-glutamine for 3 hours prior to tissue collection. (A) Post-DESI H&E, metastases circled in blue. (B) Spatial distribution of ions matching to glutamine and glutamate [M-H]-, with relative intensities between histology-segmented ROIs shown ass bar graphs. (C) Spatial distribution of ions matching to glutamine [M+5-H]- and glutamate [M+5-H]-, with relative intensities between histology-segmented ROIs shown as bar graphs. Importantly, ion levels are relative and not considered quantitative.

Assigning peak identities to DESI-MSI peaks matching TCA metabolites proved difficult. Due to the deprotonation and loss of a water molecule that occurs during ionisation in DESI, the ions for fumarate [M-H]- and malate [M-H2O-H]- have the exact same chemical formula and therefore m/z value. In this case, since fumarate and malate are often found in equilibrium, this ion (*m/z* 116.0036) can be used as readout for both of these metabolites, with due caution. In line with LC-MS findings, DESI images of this ion were either comparable between LMs and MGTs, or elevated in LMs (Figure 6-6a,b). In the DESI BR3 slide it can be seen that this ion is distributed heterogeneously within the MGT, and post-DESI H&E stains showed that these areas were predominantly densely packed with, viable tumour cells.

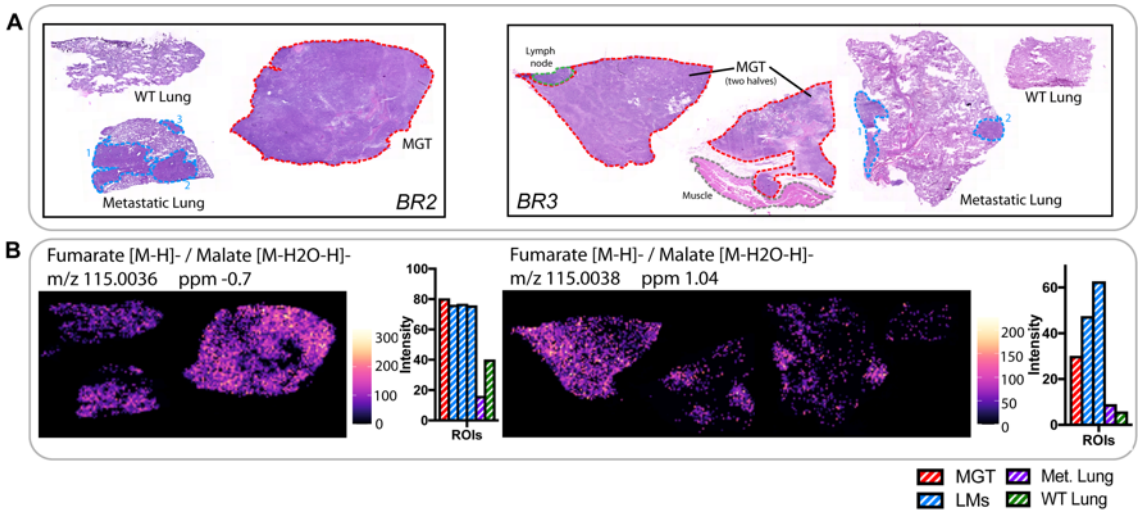


Figure 6-6. DESI-MSI imaging of TCA cycle intermediates.
DESI-MSI of two biological sample (BR) slides, each containing a Myc310 MGT, metastatic lung from the same animal, and a wildtype lung for comparison. (A) Post-DESI H&E. (B) Spatial distribution of ion matching to either fumarate [M-H]- or malate [M-H2O-H]- (or a combination of these two metabolites) in two biological replicates, with relative intensities between histology-segmented ROIs shown in bar graph. Importantly, ion levels are relative and not considered quantitative.

6.3.3 Nucleotides

When analysing nucleotide ions, individual ion peaks were annotated with a higher degree of certainty since there were no alternative database matches to these m/z values. However, only mono-phosphated nucleotides were detected consistently and sufficiently across all images. While LC-MS analysis demonstrated higher levels of ADP, ATP, GDP and GMP in some of the metastasis in comparison with MGTs (Figure 3-10), DESI showed elevated levels of AMP and GTP (Figure 6-7b). The absence of di- and triphosphate nucleotides in DESI images may be indicative of loss of phosphates from di- and tri-phosphate nucleotides during DESI image acquisition. Striking heterogeneity in nucleotide levels between LMs is shown very clearly by the BR3 image in which only one LM has elevated levels of GMP and AMP, while the other is comparable to the average signal in the MGT (Figure 6-7b). Since the true phosphate status of these nucleotides cannot be determined from this analysis, it is difficult to determine the exact biological significance of this observation, however upregulated nucleotide biosynthesis is vital for the bioenergetic demands of proliferation and metastatic colonisation [657], [784].

An ion matching to uric acid, a biomarker for nucleotide degradation and cell death [785], [786], showed severely different localisations between LMs and MGTs between biological replicates (Figure 6-7b). This may be determined by the number of dying cells in LMs, since the bigger LMs in the BR2 image show significantly higher levels of uric acid than the comparatively smaller LMs in the BR3 image.

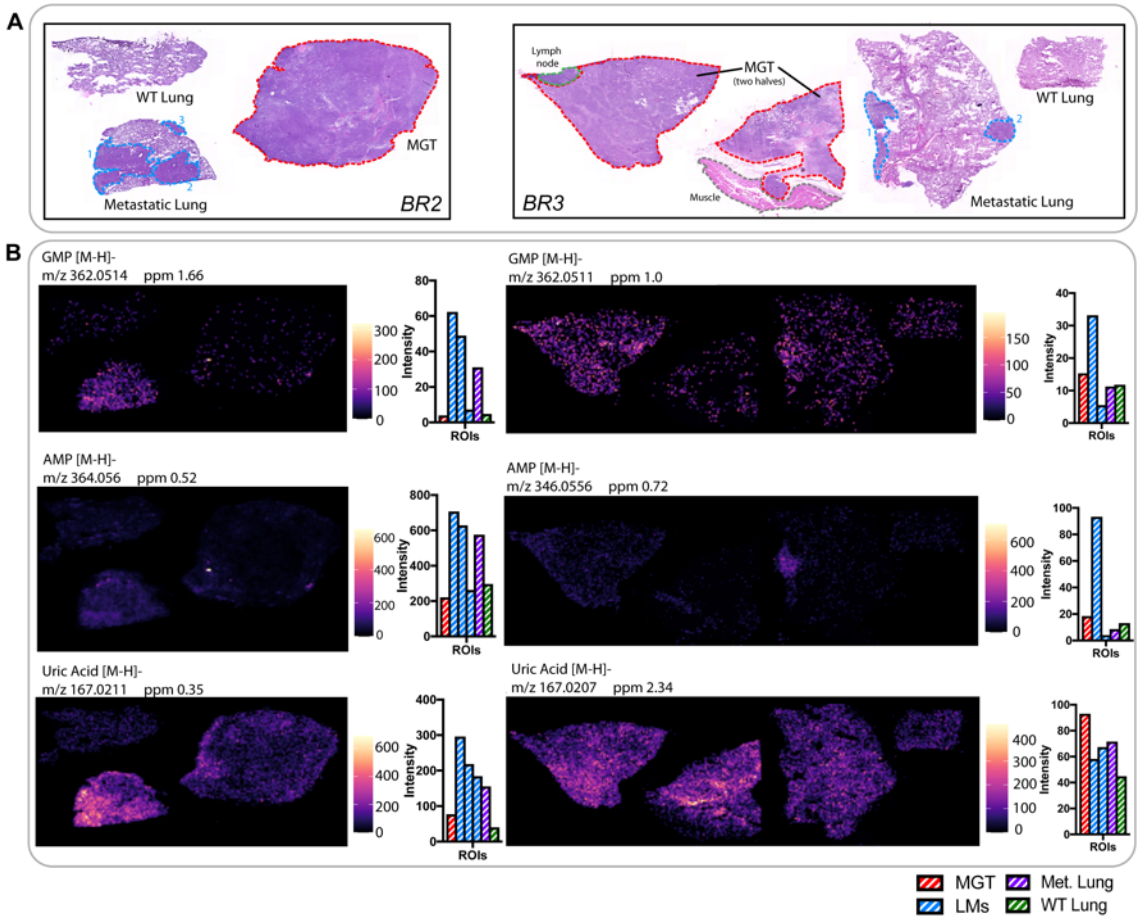


Figure 6-7. DESI-MSI imaging of nucleotides.
DESI-MSI of two biological sample (BR) slides, each containing a Myc310 MGT, metastatic lung from the same animal, and a wildtype lung for comparison. (A) Post-DESI H&E. (B) Spatial distribution of ions matching to nucleotides GMP, AMP and uric acid [M-H]- in two biological replicates, with relative intensities between histology-segmented ROIs shown in bar graph. Importantly, ion levels are relative and not considered quantitative.

6.3.4 GSH, GSSG and one carbon metabolism.

The only metabolite that was identified by DESI-MSI from the one carbon metabolism pathway was dimethylglycine. The ion images show clearly that this ion was detected at higher levels in the LMs compared to the MGTs, consistent with LC-MS findings (Figure 6-8). This finding is limited by dimethylglycine having the same chemical formula and therefore m/z value as gamma-aminobutyric acid (GABA), however may be indicative of the increase in one carbon intermediates in LMs as seen by LC-MS (Figure 6-8). Furthermore, both reduced (GSH) and oxidized glutathione (GSSG) were consistently detected and annotated with a high degree of confidence in the DESI-MSI images. GSH showed some heterogeneity in levels in different metastases (Figure 6-8d), however on average both GSH and GSSG intensities in LMs were higher than in MGTs across all biological replicates, consistent with LC-MS findings (Figure 3-11, Figure 5-18). Metastasis-infiltrated lungs had comparable signal intensity of GSSG as in LMs and significantly higher than in the normal lung (Figure 6-8b,d). These results demonstrate the highly oxidative environment of the metastatic niche, which is consistent with published observations [787], [788], and that LMs increase GSH production to be able to survive in it. This is consistent with recent findings demonstrating that increased oxidative stress due to inhibition of the glutathione cycle suppresses distant melanoma metastases [789]. These results, as well as the distribution of glutamine in LMs and the metastatic lung show that given correct and verified *m/z* annotation, DESI imaging can serve as an extremely valuable tool to understand metabolite distribution within complex tissue sections.

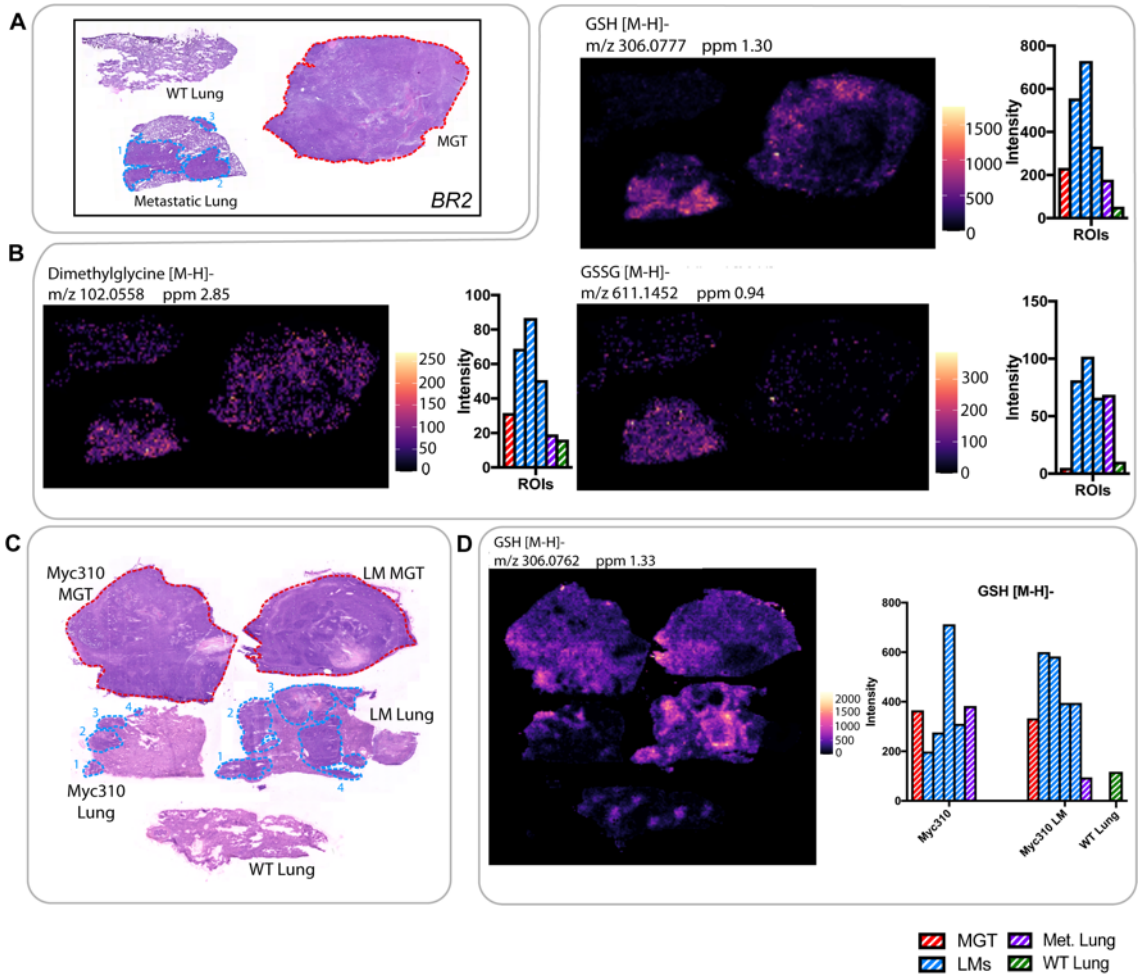


Figure 6-8. DESI-MSI distribution of glutathione and dimethylgycine.
(A) Post-DESI H&E of sample containing Myc310 MGT, paired metastatic lung and wildtype lung. (B) Spatial distribution of ions matching to dimethylgycine, reduced glutathione (GSH) and oxidized glutathione (GSSG) [M-H]-, with relative intensities between histology-segmented ROIs shown in bar graph. (C) Post-DESI H&E of sample containing a Myc310 MGT and paired metastatic lung, a LM MGT and paired metastatic lung, and a wildtype lung for comparison. (D) Spatial distribution of ion matching to reduced glutathione (GSH) [M-H]-, with relative intensities between histology-segmented ROIs shown in bar graph. Ions matching to dimethylglycine and GSSG [M-H]- were not detected in this imaging run. Importantly, ion levels are relative and not considered quantitative.

6.4 Intra-tumour heterogeneity revealed by DESI-MSI.

6.4.1 Introduction

Many LC-MS-matched DESI ions showed heterogeneous distribution within the same MGT ROI, highlighting the need to assess intra-tumour heterogeneity within a single tissue section using DESI-MSI. In this section I will discuss how MSI can be used to visualise heterogeneous metabolite distributions in complex tissue samples, and the potential complications that heterogeneity may introduce when comparing bulk tissue metabolites by LC-MS with DESI-MSI. I will also demonstrate how unsupervised multivariate analysis of DESI-MSI data can help identify specific regions of metabolic heterogeneity within a tissue section, and finally, demonstrate how higher lateral resolution MSI can be used to visualise metabolic differences between different cell types.

6.4.2 Metabolic heterogeneity in targeted DESI-MSI analysis

When mining the DESI-MSI datasets for specific polar metabolites that were analysed by LC-MS, there were often discrepancies between levels of metabolites in MGTs and LMs between the two techniques. For example, by LC-MS the levels of glycolytic intermediate G6P were significantly lower in LMs than in MGTs (Figure 6-9b), yet they appear to be comparable between MGT and LM ROIs in DESI, with the exception of the smallest LM in the DESI BR2 slide. Lactate levels were higher in LMs by LC-MS, but appeared to be clearly higher in MGTs by DESI-MSI (Figure 6-9b). Importantly, post-DESI H&E staining revealed that the lactate localisation correlates closely to necrotic areas within the tumour. There are several potential explanations for these discrepancies, which should be kept in mind throughout the comparisons between LC-MS and DESI images. First of all, DESI ion annotation relies exclusively on *m/z* matching, which means isobaric species which have the same chemical formula will not be distinguishable, and the ion image at a particular *m/z* can be the combination of several different ions. In this case, the *m/z* annotated as G6P will match with any hexose-phosphate (e.g. fructose-6-phosphate, glucose-1-phosphate), and the *m/z* for lactate also matches that of glyceraldehyde, which has the same chemical formula. This highlights an important

limitation of DESI-MSI due to lack of chromatographic separation, but MS/MS analysis may help to discern the true identity of the ion. Furthermore, the LC results showed a great degree of heterogeneity in MGTs and LMs as described in previous chapters, and more DESI images may need to be required to fully encompass potential variation in metabolic profiles. In the case of lactate, this heterogeneity might be explained by different amounts of necrosis within these tumours, but this was not confirmed.

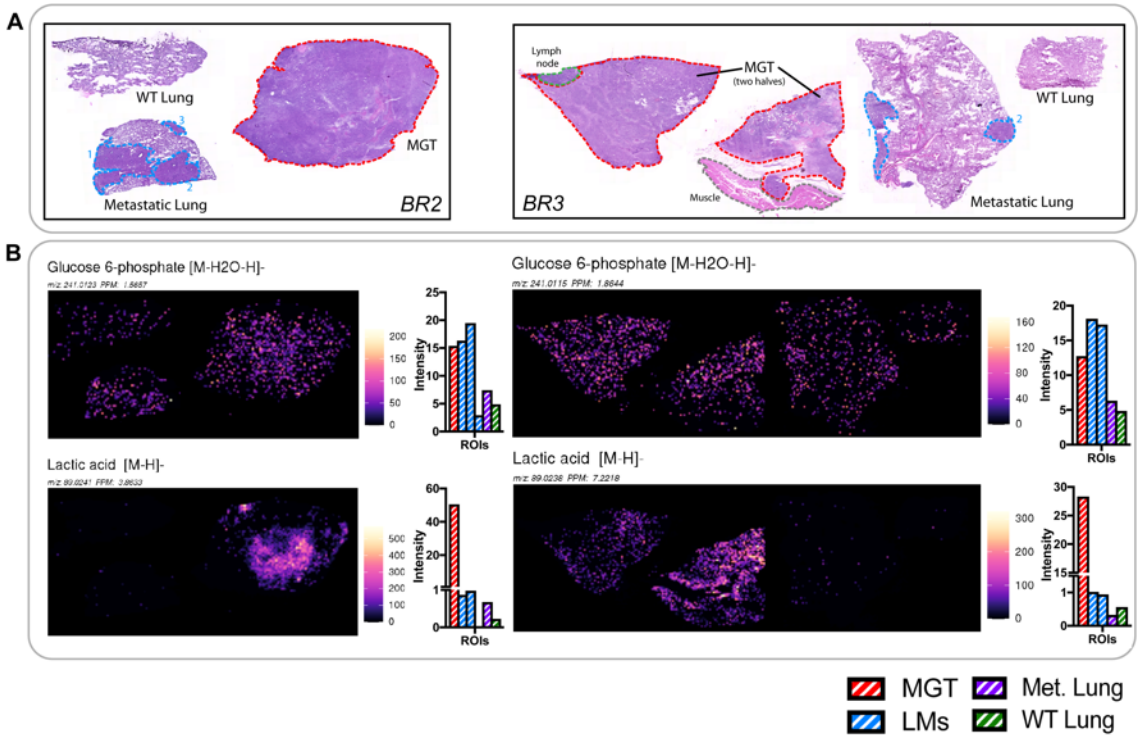


Figure 6-9. DESI-MSI imaging of glucose 6-phosphate and lactate.
DESI-MSI of two biological sample (BR) slides, each containing a Myc310 MGT, metastatic lung from the same animal, and a wildtype lung for comparison. (A) Post-DESI H&E. (B) Spatial distribution of ions matching to glucose-6-phosphate [M-H2O-H]- and lactic acid [M-H]- in two biological replicates, with relative intensities between histology-segmented ROIs shown in bar graph. Importantly, ion levels are relative and not considered quantitative.

Several amino acids, vitamins and related polar metabolites detected with DESI-MSI, showed heterogeneous distribution within MGT samples. Matching with LC-MS findings, taurine detected uniformly distributed between LMs and MGTs. Matching with LC-MS findings, taurine detected uniformly distributed between LMs and MGTs. Importantly, taurine is present at much higher levels in the peritoneal muscle that was attached to the tumour in DESI image BR3 (Figure 6-10b). This histology of this sample reveals that it has infiltrated into the muscle wall, and therefore it is probably that samples with higher taurine in LC-MS may contain some surrounding smooth muscle tissue. This muscle-specific localisation can also be seen in alanine, ornithine, carnosine and creatinine images by DESI-MSI, and these metabolites were either not detected or detected at very low levels in DESI image BR2 which did not have any muscle tissue identified by histology (Figure 6-10c). This example highlights a great advantage of DESI-MSI to identify the exact cell type in which a particular metabolite is overexpressed.

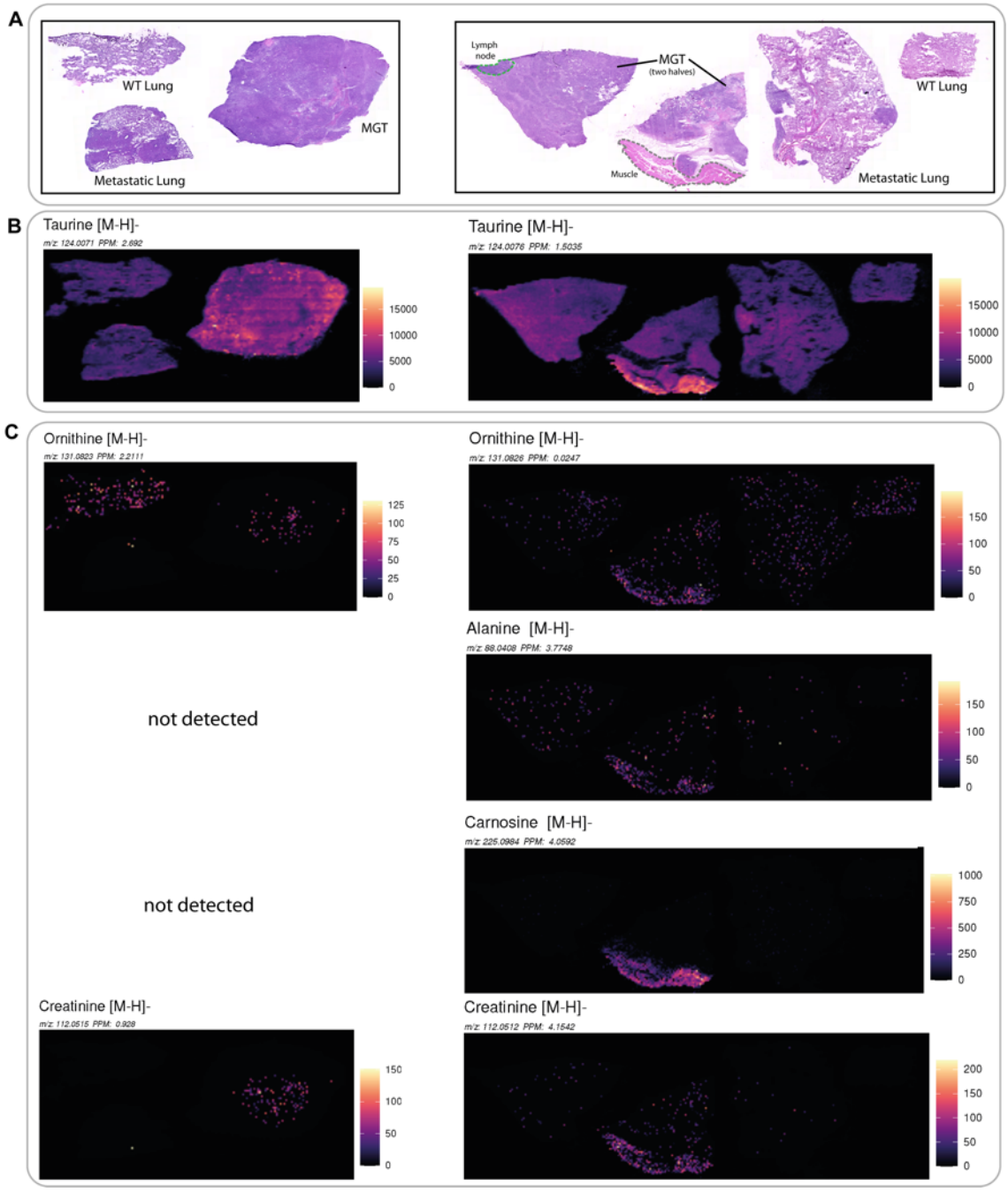


Figure 6-10. DESI-MSI imaging of other polar metabolites heterogeneously distributed in MGTs, in line with LC-MS findings.
DESI-MSI of two biological sample (BR) slides, each containing a Myc310 MGT, metastatic lung from the same animal, and a wildtype lung for comparison. (A) Post-DESI H&E. (B) Spatial distribution of ions matching to taurine [M-H]- in two biological replicates, showing predominant localisation in the peritoneal muscle attached to one MGT, and differential distribution between MGTs and LMs between biological replicates. (C) Spatial distribution of ions matching to ornithine, alanine, carnosine and creatinine [M-H]-, with alanine and carnosine [M-H]- detected only in one biological replicate, and localised mainly to peritoneal muscle adjacent to the MGT. Absence from other BRs may therefore be due to lack of peritoneal muscle and below-threshold levels of these metabolites in MGT and lung tissues.

Other metabolites which had no overall change between LMs and MGTs by LC-MS, were shown in DESI images to be localised to particular regions within MGTs. This can be seen in the distribution of ascorbic acid which is confined to the viable tumour regions and LMs, showing an opposite localisation pattern to lactate, which localised in necrotic tumour regions (Figure 6-11b). Ascorbic acid acts as an antioxidant and can be used by proliferating tumour cells to neutralise ROS accumulation due to an increased oxidative metabolism. Serine was detected as the chlorinated adduct and while its levels showed a differential distribution between LMs and MGTs (higher in some LMs, lower in others), it should be noted that this ion can also be annotated as O-phosphoethanolamine [M-H]- (Figure 6-11c). Similarly, glucosamine [M+Cl]- shows interesting heterogeneous distribution within MGTs and between LMs, however the ion also matches to glycerylphosphoryl-ethanolamine [M-H]- (Figure 6-10d). An ion matching in m/z value to histidine [M-H]- was identified across DESI images, however while LC-MS shows histidine as elevated in LMs, the DESI image of this ion shows the opposite localisation, mainly in MGTs (Figure 6-11d). A potential explanation is that this m/z matches also to 2-oxoarginine, a metabolite that has been identified as a biomarker for urea cycle disfunction [790], [791]. Robust and trustworthy ion identification is a priority that has been raised due to the findings in this study.

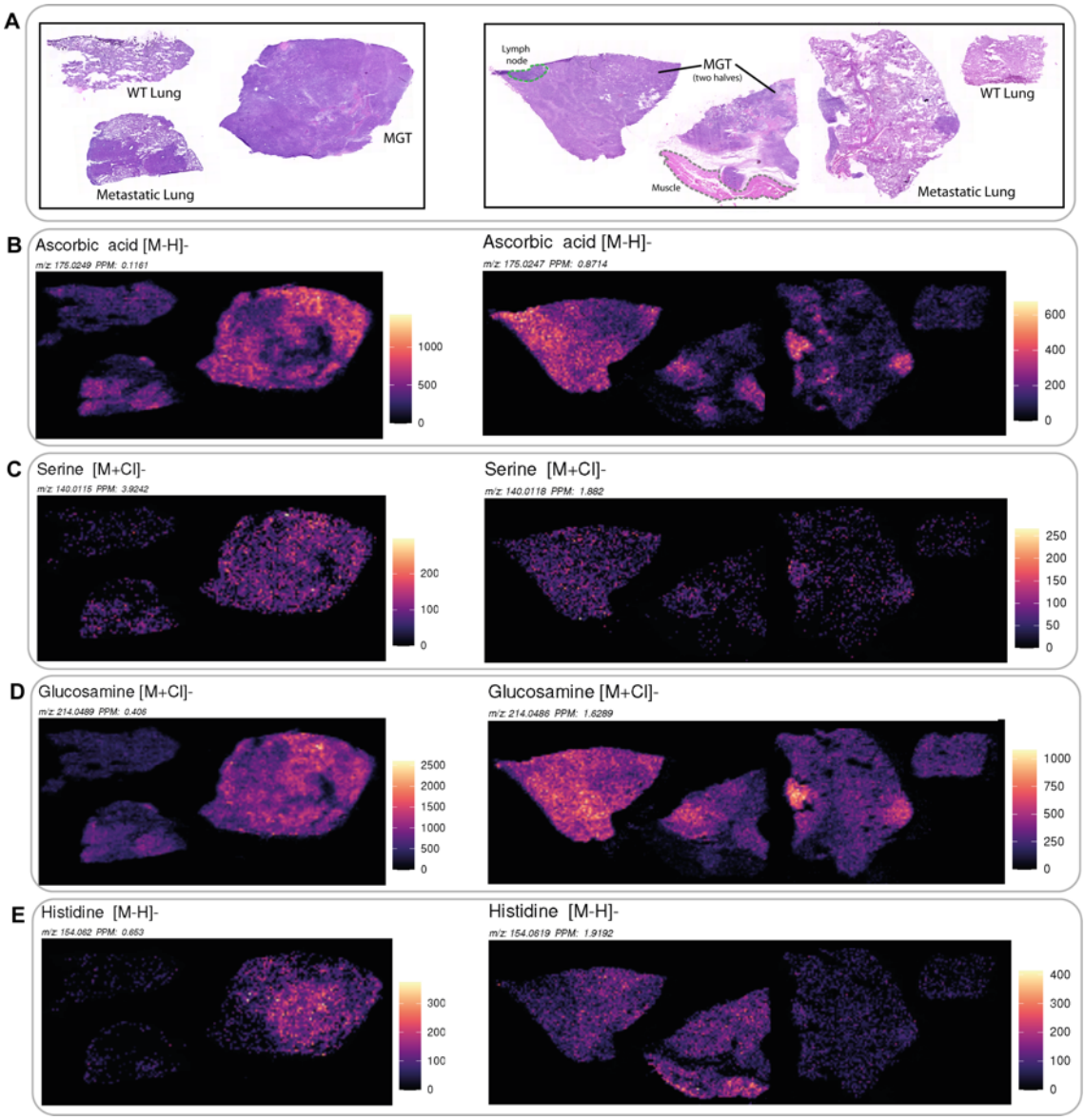


Figure 6-11. DESI-MSI imaging of other polar metabolites heterogeneously distributed in MGTs, in contrast to LC-MS findings.
DESI-MSI of two biological sample (BR) slides, each containing a Myc310 MGT, metastatic lung from the same animal, and a wildtype lung for comparison. (A) Post-DESI H&E. (B) Spatial distribution of ions matching to ascorbic acid [M-H]-, (C) serine [M+Cl]-, (D) glucosamine [M+Cl]- and (E) histidine [M-H]- in two biological replicates.

6.4.3 Metabolic heterogeneity in untargeted DESI-MSI analysis

Targeted analysis of DESI images was used to compare metabolite coverage between DESI and LC-MS, however DESI-MSI detects several thousand of peaks per pixel. In order to determine ions that are heterogeneously localised in different regions of the samples beyond central carbon metabolism, untargeted analysis was performed. MSI data are largely analysed using unsupervised clustering methods such as k-means clustering [792], NMF or PCA [793]–[795], or more recently, more complex neural-network assisted nonlinear dimensionality reduction techniques such as tSNE in order to dissect the images into chemically similar regions [796]. These techniques are useful for detecting differential metabolic patterns between areas with known histological difference, but also the metabolically-different areas that may otherwise be indistinguishable by post-DESI histological analysis.

Untargeted DESI image analysis revealed that there were many chemically-distinct regions within the same MGT, which adds complexity to the comparison between LMs and MGTs. The BR2 image was again used as an example in figures in this section, however similar heterogeneity was observed in all analysed MGTs. It should be noted that intra-tumour heterogeneity was not the primary focus of this project due to time constraints, and further in-depth exploration of these DESI results is needed. However, here I aim to demonstrate the degree of metabolic heterogeneity in MGTs and how some of it may be explained by distinct histological regions, while other regions may be histologically-comparable but chemically distinct.

The ions that were identified as significantly enriched in the MGT compared to LMs localised in several distinct patterns within the tumour. Representative ion images from five of the most prominent areas are shown (Figure 6-11). Ion images were aligned to post-DESI H&E staining to determine if any distinct histological characteristics may be responsible for the metabolic profiles. Four 200 um^2 areas were randomly selected from regions where representative ion intensity was highest, in order to closely visualise the histological features (Figure 6-12).

Area 1 contained ions that showed a localisation similar to lactate, matching to necrotic regions in the tumour (Figure 6-12). Area 2 contained hotspots of lipid-laden cells (closely resembling lipid-laden macrophages), and the majority of ions localising to this region were annotated as lipids (Figure 6-12). The histology of Area 3 was even more heterogeneous, however stromal infiltrates were observed in all four selected areas so ions with highest levels in this area may be originating from the stroma (Figure 6-12). Further analysis of the post-DESI H&E stain in relation to each chemically distinct region was harder to link to a particular cell type without further histological staining.

It is highly important to consider this degree of heterogeneity when analysing such complex tumours with traditional metabolomics approaches such as LC-MS, keeping in mind that the mean signal of a particular metabolite may not accurately represent the levels across the whole tumour.

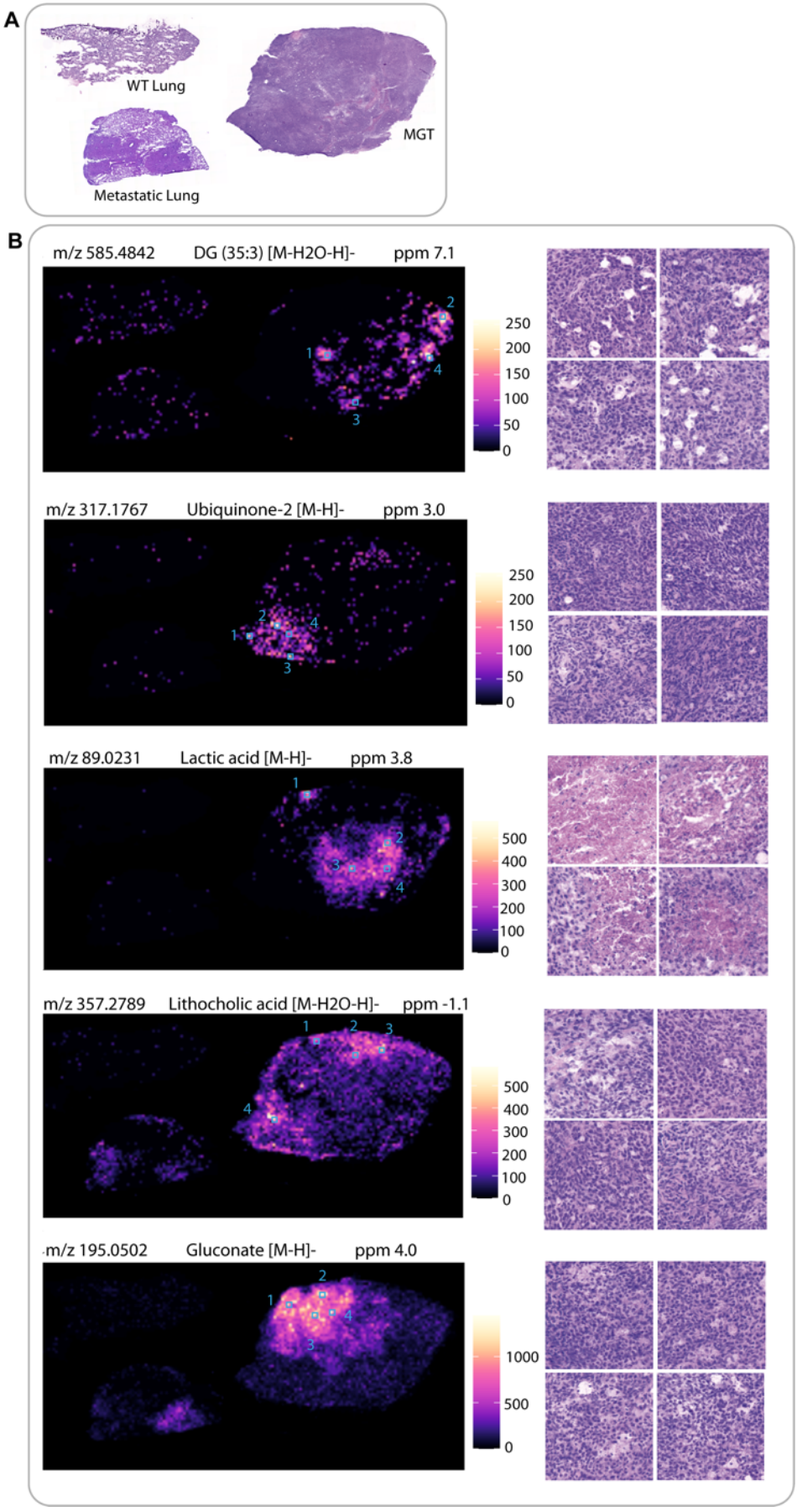

A
WT Lung
MGT
Metastatic Lung
B
m/z 585.4842 DG (35:3) [M-H2O-H]- ppm 7.1
250
200
150
100
50
0
m/z 317.1767 Ubiquinone-2 [M-H]- ppm 3.0
250
200
150
100
50
0
m/z 89.0231 Lactic acid [M-H]- ppm 3.8
500
400
300
200
100
0
m/z 357.2789 Lithocholic acid [M-H2O-H]- ppm -1.1
500
400
300
200
100
0
m/z 195.0502 Gluconate [M-H]- ppm 4.0
1000
500
0

Figure 6-12. Intra-tumour metabolic heterogeneity linked to histological phenotypes. (A) Post-DESI H&E of sample containing a Myc310 MGT, metastatic lung from the same animal, and a wildtype lung for comparison. (B) Representative DESI-MSI ions with matched metabolite identities, which show the five predominant localisation patterns of metabolites within a MGT. Four regions were randomly selected from high intensity areas of each representative ion image, and the post-DESI H&E was used to map the histological profile of these regions. Importantly, only the last two regions in the MGT express ions that are also present, notably heterogeneously, in LMs (m/z 357.2789 and m/z 195.0502).

6.4.4 Network analysis of DESI-MSI imaging.

DESI-MSI generates huge datasets due to the abundance of chemical information acquired at each pixel of the image. Developing multivariate analysis method for DESI-MSI data has been the focus of several projects both in our lab and with several collaborators. To help discern the full extent of metabolic heterogeneity observed in my samples, with the help of Dr. Avinash Ghanate in our lab, my DESI images were subjected to a multivariate analysis technique that has been developed and described by Dr. Paolo Inglese at Imperial College London. Briefly, the method uses weighted co-expression network analysis (WGCNA) to separate DESI-MSI images into regions of similar metabolic composition. When grouping areas of the DESI image into distinct metabolic "modules", WGCNA groups together ions that are often co-localised. This proximity-based approach produces circle plots of ions that contribute to each module, highlighting the colocalization instances. We can then use metabolite databases to assign identities to the *m/z* values and gain an understanding of the possible biological significance of each module.

For the purpose of my project, network analysis was used to demonstrate the degree of metabolic heterogeneity and introducing a robust DESI data analysis tool for future work. The results of this analysis have not been further mined for specific metabolite annotations, however this analysis presents a new avenue for the future analysis of metabolic heterogeneity in these and other samples. Network analysis of one DESI image generated 32 modules, six of which are shown in Figure 6-13 and demonstrate the most strikingly different metabolite distributions across the sample. It can be seen how some modules correlate to histological tissue identities, such as Module 1 localised in WT and less-metastatic lung, and Module 2

highlighting all lung tissue. Module 3 highlights a particular region in both MGTs but is absent from lung tissues. On the other hand, Modules 4, 7 and 29 demonstrate ions that are present both in LMs and MGTs, however their distribution varies greatly, especially within MGTs. Annotating the ions of each module and immunohistochemical staining for different cell populations in MGTs and lungs will help link metabolic observations with biological function in future work. Network analysis demonstrates the wealth of novel information that can be generated from DESI-MSI images and introduces a robust method for analysing such complex data sets in the future.

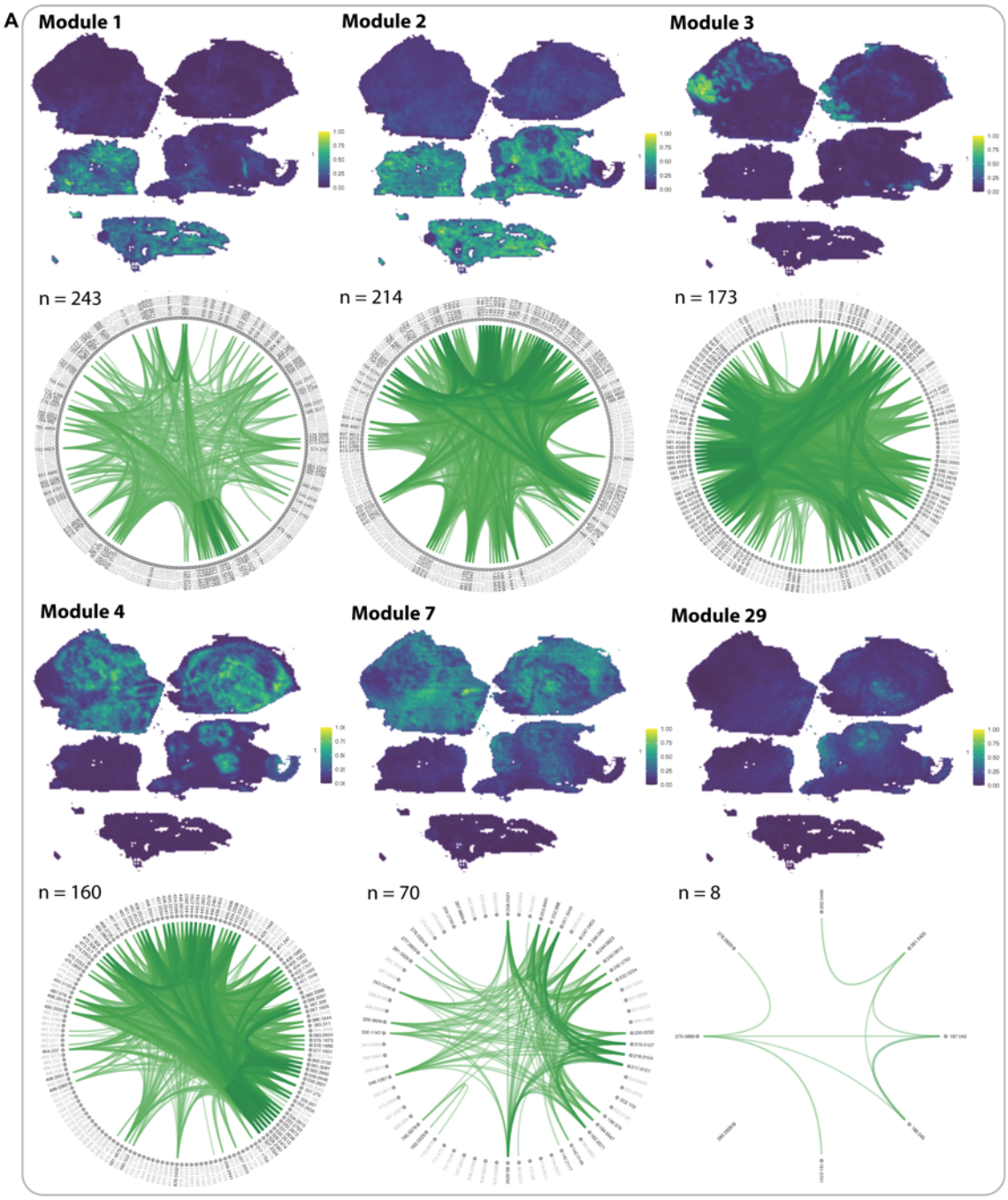


Figure 6-13. Module analysis of DESI-MSI data to assess metabolic heterogeneity. WCGNA module analysis of DESI-MSI image containing a Myc310 MGT and paired metastatic lung, a LM MGT and paired metastatic lung, and a wildtype lung for comparison (see Figure 6-12 for post-DESI H&E). Representative images of ion localisation in a selection of 6 modules that had the most heterogeneous distribution among tissue types: Module 1 – WT and less-metastatic lung, Module 2 – all lung tissue, Module 3 – MGT-specific localisation in distinct areas of the tumour, Module 4/7/29 – comparable distributions between different areas of MGTs and LMs. Circle plots show co-expressed ions that contribute to each module.

6.5 Exploring inter-tumour metabolic heterogeneity further with a higher spatial resolution modality, the Orbi-SIMS

So far, I have demonstrated whole-section metabolic heterogeneity in MGTs using DESI-MSI. One limitation of this platform is limited lateral resolution, and therefore the size of histological features that can be accurately detected. With the DESI pixel size diameter of 100 um, histological segmentation is limited to macro features such as metastases, necrotic pools or areas of desmoplasia. In order to look closer at the metabolic differences between individual cell types, I set out to optimise methods using a state-of-the-art MSI platform, the Orbi-SIMS.

The advantages and limitations of different MSI modalities must be considered when choosing a particular platform for analysis. In DESI-MSI, polar metabolites can be detected and analysed with confidence due to the minimal ion fragmentation in the proses of desorption and ionisation with a charged, methanol-based electrospray [773], [797], [798]. However, the ionisation source in the OrbiSIMS is an argon gas cluster ion beam (GCIB), which has been shown to cause metabolite fragmentation upon impact [799]. On the other hand, the crater size of the GCIB permits the acquisition of metabolite images with pixel size as low as 2 um [534]. Furthermore, the Orbitrap mass analyser in the OrbiSIMS provides a mass resolving power of up to 240,000, facilitating ion separation in the mass spectrum and therefore more accurate ion annotation. The chemical formulae of ions determined from the *m/z* can match to polar metabolites through database searches, however there is no way to determine if the ion represents an intact metabolite due to high in-source fragmentation.

OrbiSIMS images were acquired in different regions of Myc310 MGTs in order to observe metabolic heterogeneity at a single cell level. Post-OrbiSIMS H&E stains were performed to gain understanding of the histological subtype of cells in the imaged areas. Due to the low pixel size of 2 um in the OrbiSIMS, it was important to develop a method for accurately aligning the imaged area with the post-OrbiSIMS H&E stain. Since the OrbiSIMS is a hybrid instrument, it has retained features of TOF-SIMS MSI instruments, which are more widely used for surface chemistry analysis both in and outside of biological research. One of these features

is a high-energy caesium focused ion beam (FIB), which can be used to rapidly cut into the sample to study the chemical composition of multiple planes. For my analysis, following GCIB imaging, I used the FIB to completely remove tissue outside of each corner of the imaged area, without disturbing any tissue that was imaged (Figure 6-14a). The exact area that was imaged can be detected by taking a secondary electron image directly after GCIB imaging, and this can then be used as a guide for the FIB. The fiduciary markers were then used to align post-OrbiSIMS H&E stains and revealed bands of stromal fibroblasts closely interknit between tumour cells. PCA was performed on the image using the full spectrum collected by OrbiSIMS (Figure 6-14b), revealing a segmentation between tumour and stromal cells. Representative ions from PC1 loadings show ions matching to purine metabolites adenine and hypoxanthine in the tumour cells, representative of more proliferative cells. The stromal region was similarly defined by ions matching to sulphuric acid (likely a fragment of chondroitin sulphate), and arachidonic acid, a primary metabolite in immune cell signalling.

The OrbiSIMS instrument is still in development stages and further work is required to minimise ion fragmentation and maximise ion detection for robust analysis of biological samples. However, during my project I was able to contribute to the development of preliminary methods for imaging metabolic heterogeneity in mouse tissue samples at a cellular level.

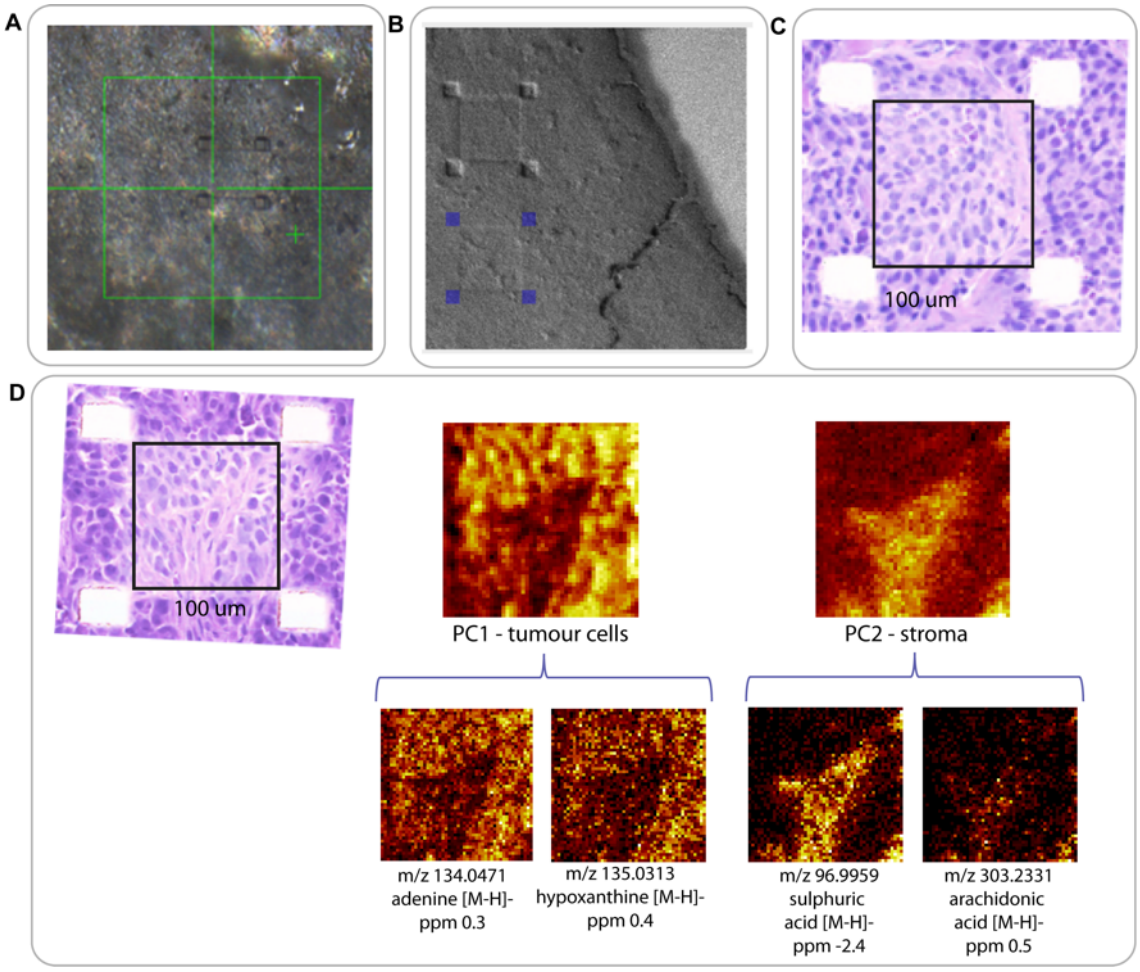


Figure 6-14. Orbi-SIMS imaging shows heterogeneous metabolite distribution between tumour cells and stromal infiltrate in a Myc310 MGT.
(A) Optical image and (B) secondary electron image of the tumour areas imaged by Orbi-SIMS, highlighting the fiduciary markers used for post-MSI histology co-localisation (C). (D) PCA of Orbi-SIMS image revealed separation between tumour and stroma cells in PC1 and PC2, respectfully. Representative ions obtained from the PC loadings of each component match to adenine [M-H]- and hypoxanthine [M-H]- in the tumour cells, and sulphuric acid [M-H]- and arachidonic acid [M-H]- in the stroma.

6.6 Metabolic heterogeneity in the metastatic lung

6.6.1 Polar metabolic heterogeneity between metastases

Our LC and targeted DESI analysis demonstrated that the intensity of signals for some of the polar metabolites differed between different lung metastases even in the same lung lobe. DESI images allow an accurate comparison of metabolite levels between different ROIs on the same slide image with a high degree of certainty. In this section I will highlight an example of extreme metabolic heterogeneity between two metastases in the same lung lobe. Notably, the larger LM from this lung was successfully dissected out for LC-MS analysis after DESI slides were made. However, it was not possible to analyse the smaller LM by LC-MS because of its size and tight integration into the surrounding lung. Therefore, DESI-MSI played an integral role in visualising the distinct metabolic profiles between these two LMs, within their *in vivo* micro-environment.

Before starting the ROI-based analysis, the DESI BR3 image was subjected to NN-tSNE analysis in order to determine if the two metastases have a significantly distinct metabolic profile. This analysis projects pixels with similar chemical compositions into an RGB colour space, and then the image is reconstructed using those colour assignments. The tSNE image shows a distinct metabolic profile between LMa and LMb (Figure 6-15b). The tSNE also shows that each of the two LMs has a similar metabolic composition to distinct regions within the MGT. This finding demonstrates the entirely novel dimension of metabolism analysis that is provided exclusively by MSI. The distinct heterogeneous metabolite distribution supported the need for a more detailed study of the specific metabolic differences between the two LMs.

For each LM in the BR3 image (LMa and LMb), individual ROIs were drawn using the colocalised post-DESI H&E stain (Figure 6-15a). Average ROI intensities were compared between the two LMs, and a threshold of average intensity of 1 was applied to select for the more abundant ions. There were 353 ions which were significantly ($\log_2(FC) > 1$) higher expressed in LMa, and 424 ions higher expressed in LMb. In order to gain insight into the metabolites behind these

changes, database mining was conducted for the m/z values in each significant group.

First, to identify polar metabolites that differed between the two LMs, ion annotation was restricted to metabolites found in mammalian metabolic pathways using CEUMass Mediator to mine the KEGG database (pathways included specified in Table 9 (Methods)). All annotations are putative, and the identity of metabolites of interest need to be confirmed using MS/MS. Of the ions significantly upregulated in each LM, there were positive matches for 47 out of 353 ions in LMa, and 42 out of 424 ions in LMb. For many m/z values there were several possible metabolites identified for the same ion, either due to isobaric species or different adduct forms falling within the accepted ppm threshold. In particular, specific pathways including the 'Alpha Linolenic Acid and Linoleic Acid Metabolism', 'Steroidogenesis', 'Arachidonic Acid Metabolism' and 'Bile Acid Biosynthesis' pathways contained multiple intermediates that have the same chemical formula and therefore many possible metabolites were matched to a particular *m/z* value. However, when the matches were limited to a specific pathway, the ion image may be composed of several ion species and higher intensity of this particular ion peak may be the result of upregulated activity of the whole pathway.

Figure 6-15c shows selected ion images of the most prominent metabolites from the analysis comparing ions enriched in each of the LMs in the DESI BR3 image, matching to KEGG mammalian metabolite pathways. LMa had increased signals of pantothenic acid, required for acetyl CoA biosynthesis, in comparison with LMb. The signals of some nucleotides including AMP, GMP and UMP, as well as free adenine, were also higher in LMa than in LMb. The signals of many free fatty acids, including palmitic, oleic, linoleic and stearic acid, were also enriched in LMa in comparison with LMb. In LMb on the other hand, there was an increase in metabolite signals from the arachidonic acid metabolism pathway, which contains prostaglandins and other immune signalling molecules. There was also an increase in nucleotide degradation metabolites xanthine and xanthosine, as well as inosine which plays a role in both nucleotide synthesis and breakdown. There were also several intermediates of linolenic acid metabolism higher in LMb, such as DHA, THA and lithocholic acid, as well as the glycerophospholipid biosynthesis

intermediate glycerol 3-phosphate. Another interesting metabolite that was significantly enriched in LMb was S-lactoylglutathione, an intermediate of glyoxylate metabolism which has been shown to be an alternative source of glutathione in the mitochondria [800].

Overall, these ROI-based comparisons using the KEGG database revealed that the two metastases showed biologically-relevant metabolic distinctions. LMa had higher levels of nucleotides, fatty acids and pantothenic acid, which is suggestive of a more proliferative state. On the other hand, the multiple upregulated immune signalling metabolites seen in LMb, in line with its deeper integration into the lung, suggests a higher degree of interaction of LMb with immune cells in the metastatic niche. As seen with the NN-tSNE analysis, most of the metabolites that are upregulated in one of the LMs are also expressed at higher levels in particular regions of the MGT.

Importantly, metabolic distinction between the two LMs discussed here is not limited to polar metabolites. In the next chapter, I will revisit this dataset and explore changes in distribution of lipid species.

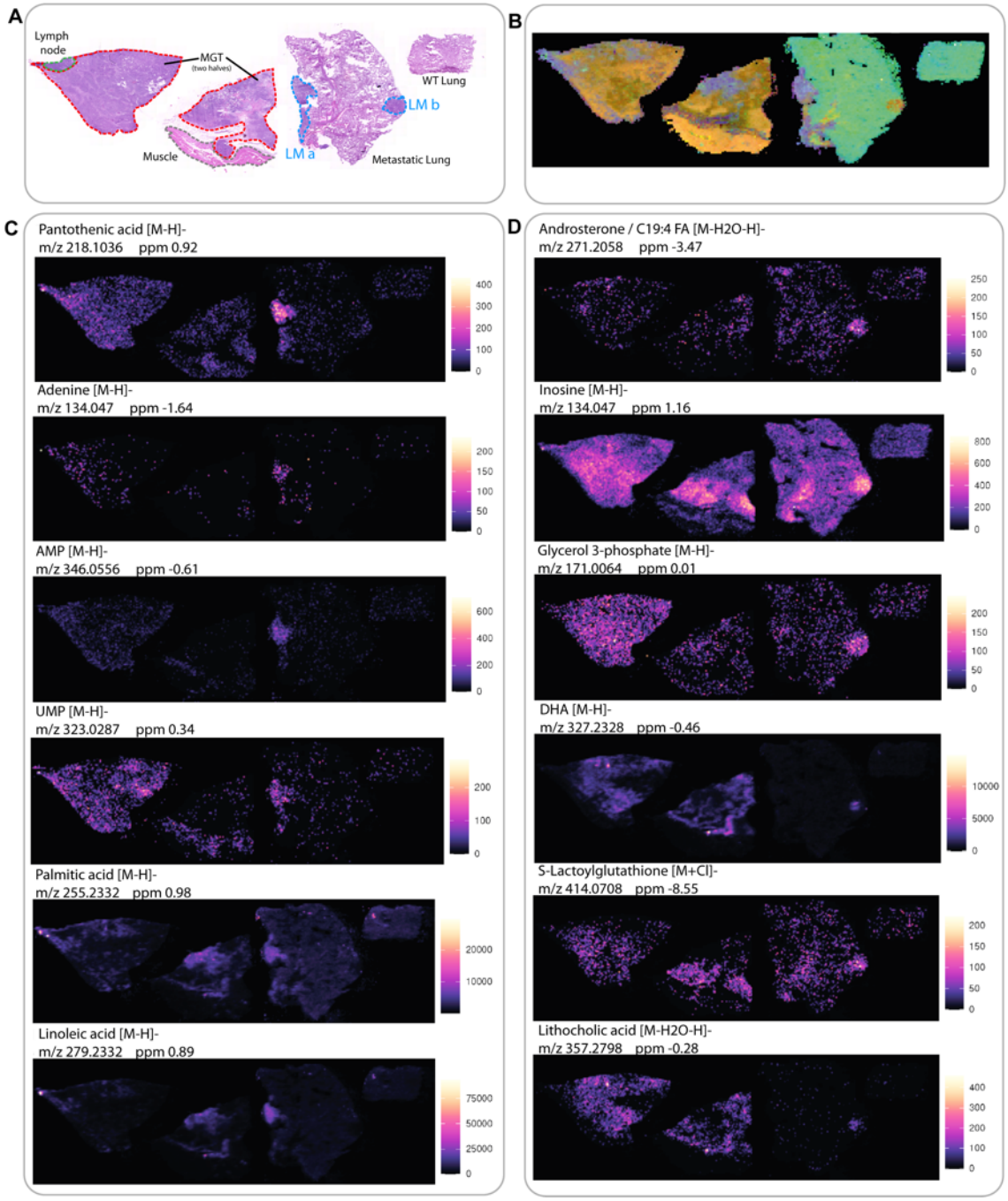


Figure 6-15. Metabolic heterogeneity between two metastatic lesions in the same lung lobe shown by DESI-MSI.
(A) Post-DESI H&E of sample containing a Myc310 MGT, metastatic lung from the same animal, and a wildtype lung for comparison. (B) k-means clustering of the DESI-MSI image revealing that the two LM lesions belong to separate clusters, each correlating in metabolite expression to different regions in the MGT. The ROIs from two LMs (LMa and LMb, highlighted in (A)) were used to compare metabolite levels upregulated in each LM. (C) Ions present at higher levels in LM1 and (D) LMb that were matched to known polar and lipid metabolites.

6.6.2 Polar metabolic heterogeneity between wildtype and metastatic lung

DESI analysis allows the comparison of metabolite distributions between any regions on the same slide, therefore it was also possible to observe chemical differences between normal and metastasis-infiltrated lungs (Figure 6-17). Once again post-DESI H&E stains were used to generate ROIs for each region. While the ROI segmentation of metastatic lung away from the LMs was profoundly more accurate than cryo-dissection of the metastatic tumours for LC-MS analysis, there was still a limitation due to an inter-mixed population of cells within the metastatic lesion, and potential individual tumour cells present in the metastatic lung.

The metabolite species that were upregulated in the metastatic lung in comparison with the normal lung based on KEGG database matching included oxidized glutathione and GMP, as well as several lipid species which will be described in the next chapter. Next, I analysed which ions were downregulated in the lungs in the presence of metastases. Ions that were significantly higher in the wildtype lung were selected. KEGG-annotated ions included 2-hydroxethanesulfonate (taurine metabolism), hydroxy-oxoglutarate (vitamin B6 metabolism), pantothenic acid, and an ion matching either fumarate [M-H]- or malate [M-H2O-H]-, suggesting a potentially increased central carbon metabolism. The presence of metastases in the lung may therefore compromise healthy metabolism of the cells in the lung, potentially due to physically obstructed oxygenation or elevated nutrient uptake by the tumour cells. Indeed, the fumarate and pantothenic acid images demonstrate that the levels of these metabolites are comparable between the wildtype lung, the metastases and specific areas of the MGT, however present at much lower levels in the surrounding metastatic lung.

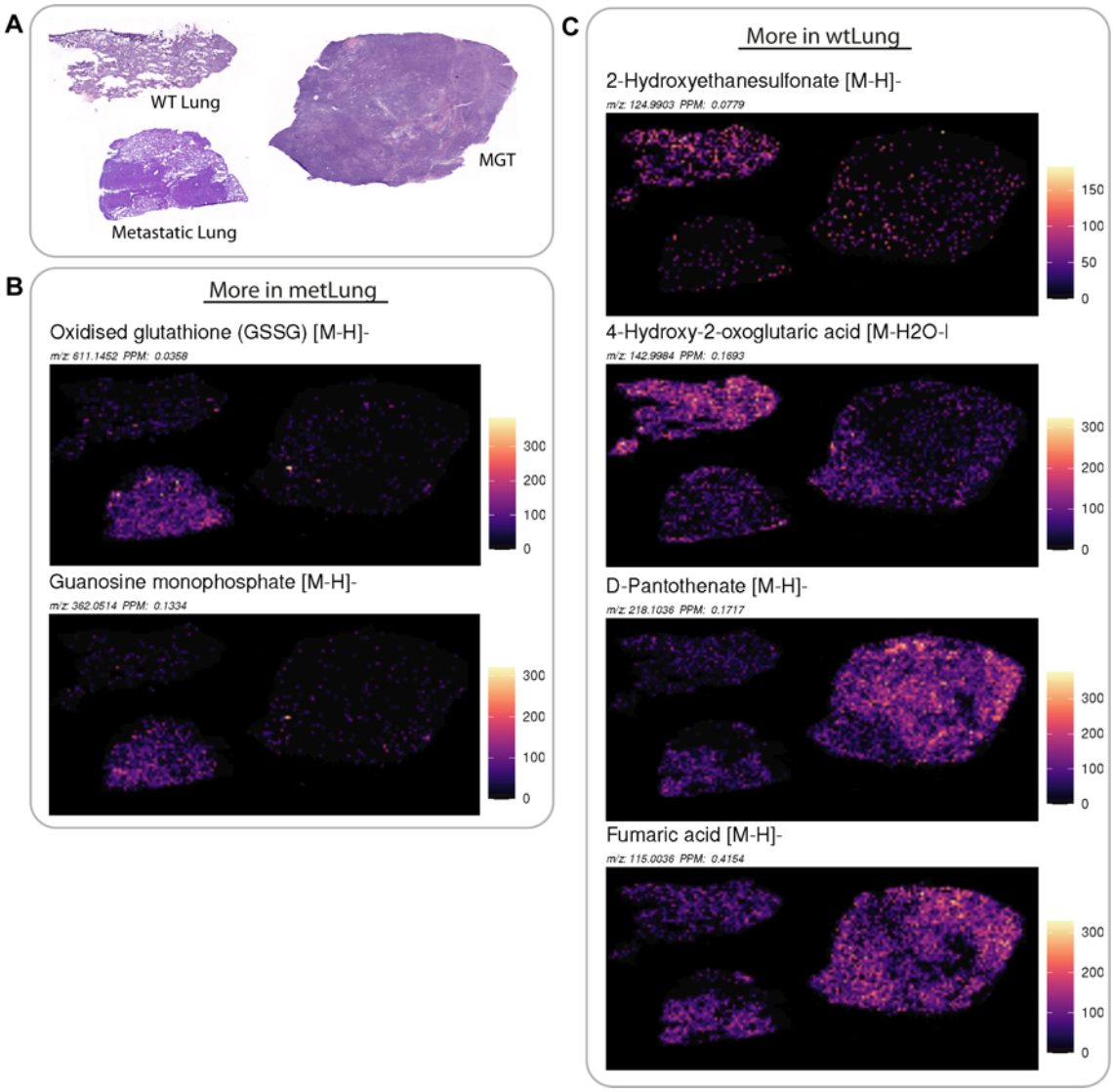


Figure 6-17. Metabolic heterogeneity between metastatic and wildtype lungs by DESI-MSI.
(A) Post-DESI H&E of sample containing a Myc310 MGT, metastatic lung from the same animal, and a wildtype lung for comparison. (B) Ions present at higher levels in the wildtype lung and (D) metastatic lung that were identified as polar metabolites.

6.7 Chapter Discussion

MSI as a field is still in the beginning stages for biological sample analysis, however it has already proven to be a highly useful tool to bring another dimension of information that we can discern from a variety of samples. In comparison with other MSI methods, DESI-MSI in particular allows minimal sample preparation and the acquisition of chemical images of multiple tissues in one imaging run. While metabolite coverage and ion identification from DESI-MSI runs still pose difficulties at times, it has been shown in this and other projects recently that many key polar and lipid metabolites can be detected consistently. With this technology it is possible to visualise the metabolite distribution without disturbing the morphology and structure of the samples. This is particularly valuable when looking at the metabolism of metastases in the context of the organ they are residing in. Only with MSI can the metabolite distributions be captured between different cell types and across various environmental gradients such as hypoxia and nutrient bioavailability. Furthermore, as part of this study, I was able to assess the capability of DESI-MSI to visualise the distribution of heavy isotope labelled compounds within MGTs and metastatic lungs. Visualising metabolic flux *in situ* presents a truly state-of-the-art approach for assessing metabolic heterogeneity.

As seen in the comparison between two metabolically distinct metastatic lesions in the same lung lobe, from one DESI image it is possible to not only study the metabolite distributions between different tumours and the lung in which they reside, but also trace those metabolic profiles to distinct metabolically heterogeneous zones within the MGT. More work is needed to determine whether these similar chemical profiles between areas in the MGT and specific LMs highlight the tumour regions from which those LMs may have originated, or whether environmental factors such as oxygen or nutrient availability is what governs these metabolic differences. An important limitation in MSI is determining the effect of matrix effects on the ionisation potential of different metabolite species. It has been shown that differential chemical and physical properties of tissues can promote or suppress ionisation of certain metabolites. To further assess differences in ion abundance in particular regions, a metabolite standard can be uniformly sprayed

across tissue samples to determine whether matrix effects may be interfering with accurately visualising *in situ* metabolite distribution.

I have shown that many polar metabolites that are traditionally analysed by LC-MS can be detected using DESI-MSI, however reliable ion annotation remains a challenge. A majority of the ions that emerge from various untargeted data analysis methods, including histological ROI segmentation and unsupervised clustering, did not match any metabolites in the database searches. Furthermore, it is a common instance that a m/z value matches to several different metabolites given the mass resolving power and ppm threshold. Ion annotation and the possibility of alternative fragmentation or adduct formation in DESI-MSI is currently an active area of interest in the community, and further work is needed to accurately identify metabolites of interest from the DESI images. Nonetheless, the example discussed in this section highlights a prominent advantage that MSI can provide when exploring the metabolism of metastases in the context of the organ in which they reside.

Chapter 7. Using MSI to analyse spatial distribution of lipid metabolites in lung metastases and the metastatic niche.

7.1 Introduction

So far, the focus of my investigation has been focused on polar metabolite analysis between LM MGTs and LM^2s using LC-MS and DESI-MSI. Since MSI does not require any metabolite extraction procedures, both polar and lipid metabolites are collected and detected within the same imaging run. Many of the species identified as differentially distributed between MGTs and LMs in DESI analysis were identified by database m/z matching to lipid species. In this chapter, I will discuss some of the observations of apolar metabolite heterogeneity that was observed. Furthermore, to draw parallels between DESI and LC-MS comparisons, I extracted apolar metabolites from the same MGT and LM samples that were used for polar metabolites (see LC-MS Methods). Due to the already large scope of my project, data analysis of apolar LC-MS data was performed by a visiting Master's student, Mia Cabantous, with the help of Dr. Avinash Ghanate in our lab.

7.2 Distinctions in lipid metabolites between two LMs localised in the same lung lobe by DESI-MSI.

In the previous chapter, I have described polar metabolite distinctions between two LMs in the same lung lobe. I used the KEGG database to assign annotations to ions which were significantly changing between the two LMs, however a large proportion of the differentially-distributed ion peaks had higher m/z values (> 500 m/z), suggestive of lipid species.

To annotate heavier ions, I used CEUMass Mediator to search the LipidMaps and HMDB databases in order to curate ions matching with lipid species that were present at different levels between the two LMs. Lipid analysis by database m/z

value matching alone can be misleading due to many metabolites from different lipid classes having the same chemical formula, especially when taking different adduct formation into account. From the 353 ions that had significantly higher average intensity in LMa compared to LMb, there were 3045 matches for possible lipid species. These results were used to quantify the number of metabolites from the same lipid class which were detected at higher levels in one of the LMs. For the purpose of this analysis, if a m/z value matched within the ppm threshold several metabolites of different classes, that ion was counted as both lipid groups. To add to the complexity, without MS/MS it is impossible to know the exact fatty acyl chain lengths of lipid groups, therefore all the possible combinations of chain lengths in a particular lipid were returned by the database search. All lipids were therefore putatively annotated with the name of the lipid class, total chain length and number of unsaturated bonds. Any lipid annotations which contained odd chain length fatty acyls were excluded from the analysis, since the formation of odd chain lengths is unlikely in mammalian species. It is possible that these ions formed as a result of fragmentation of larger lipid species during desorption or while travelling through the DESI instrument.

Representative images from each lipid class that was overall enriched in one of the LMs are shown in Figure 7-1c,d. DG and TG species were significantly enriched in LMa, as well as the majority of PC and PE species. On the other hand, in LMb there were more PG, PS and PI lipids observed. In the previous chapter, I discussed the polar metabolic differences between these two LM lesions, which suggested that LMa has a more proliferative phenotype, while LMb has more immune signalling metabolites (Figure 6-15). The distinctions in lipid classes between these two LMs are in line with these findings.

The cell membrane phospholipid composition can play an important role in motility and proliferation, and upregulated synthesis of a particular lipid class in metastatic cells may be necessary for their survival and development in the lung. PC and PE lipids are the two most abundant lipids in the cell membrane [801], [802] and increased PC lipid levels have been reported in malignant tissues [406]–[408], [803]. PC lipids can be produced from PE lipids via phosphatidylethanolamine N-methyltransferase enzyme (PEMT), which requires SAM as a methyl group donor

and is a poor prognosis marker in cancer [804]. Apart from their role in phospholipid membrane synthesis, PE lipids regulate membrane rigidity and ferroptosis [400], [402]. Increased pools of stored di- and triglycerides have been shown to protect cells from stress by providing unsaturated fatty acids to counteract the build-up of toxic saturated lipid species in hypoxic conditions [805].

PS lipids, upregulated in LMb, play a role in ROS signalling, therefore oxidative stress may be elevated in this metastasis [396]. Furthermore, a recent study demonstrated a link between MYC expression and PG lipid biosynthesis, therefore higher expression of these lipids in LMb and specific regions of the MGT may be related to higher MYC activity [379], and this hypothesis needs to be further explored using immunohistochemistry.

Apart from revealing differential functions in cancer cells, lipids may be used as biomarkers of a particular cell type in the metastatic niche [513], [806], [807]. This summary analysis requires closer inspection of the exact lipid species detected and their biological significance. In the next chapter I will further explore the differences in apolar metabolites in the metastatic niche and between LMs and MGTs.

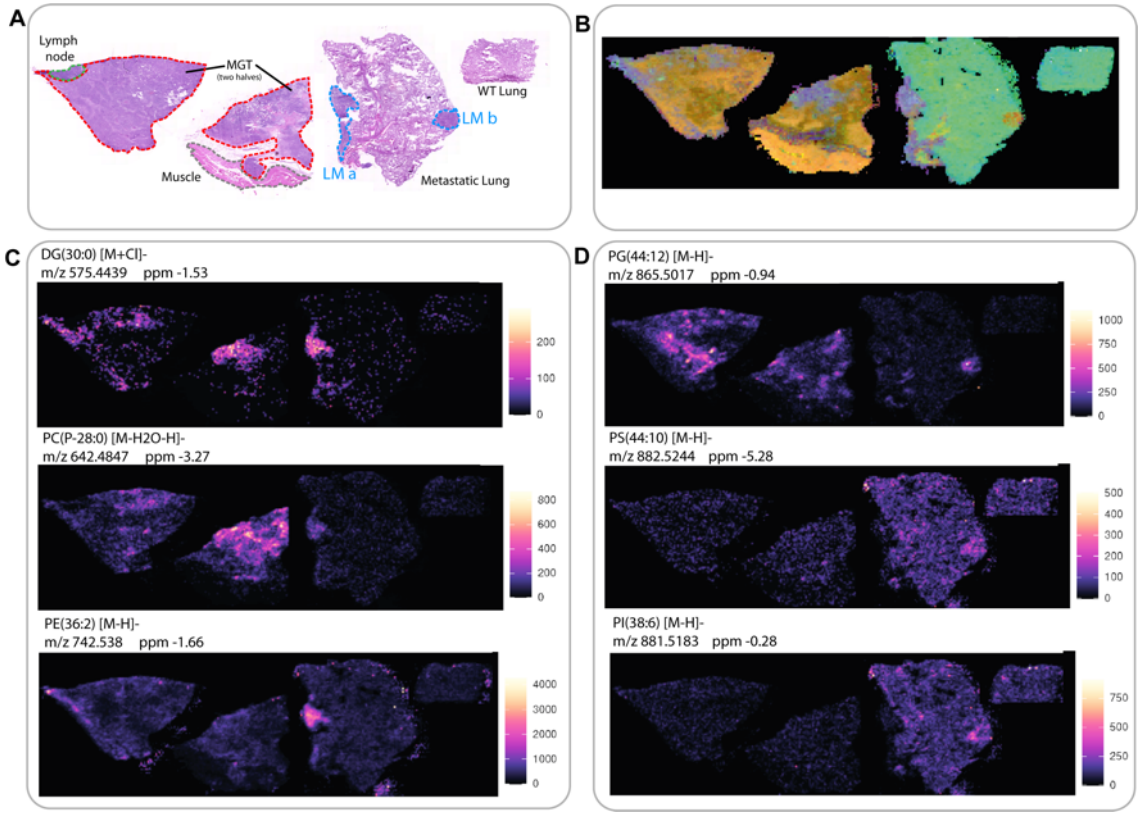


Figure 7-1. Metabolic heterogeneity between two metastatic lesions in the same lung lobe shown by DESI-MSI.
(A) Post-DESI H&E of sample containing a Myc310 MGT, metastatic lung from the same animal, and a wildtype lung for comparison. (B) k-means clustering of the DESI-MSI image revealing that the two LM lesions belong to separate clusters, each correlating in metabolite expression to different regions in the MGT. The ROIs from two LMs (LMa and LMb, highlighted in (A)) were used to compare metabolite levels upregulated in each LM. (C) Ions matching to lipid metabolites from different lipid classes present at higher levels in LMa and (D) LMb that were matched to known polar and lipid metabolites.

7.3 Analysing lipid metabolite distribution in metastatic and WT lungs by DESI-MS.

In the previous chapter I discussed polar metabolite differences between the metastatic and wildtype lung as revealed by DESI-MSI (Figure 6-17). A database search of the ions upregulated in the two tissue types using LipidMaps revealed members of different phospholipid classes, including PI-Cer, PI, PA, PG, PS and PE lipids, present at higher levels in the metastatic lung compared to the wildtype lung (Figure 7-2c). These findings are in line with the previously published works demonstrating that the metastatic lung is higher infiltrated with immune cells which produce lipid signalling molecules and may be composed of lipid species distinct from those that make up pneumocytes or tumour cells [787], [808]–[812]. Interestingly, a distinct pattern of lipid species was detected on the periphery of the large LM (Figure 7-2c). and this was a phenomenon observed across multiple DESI images analysed. Further investigation of these lipid-rich peri-metastatic regions is discussed below, combining DESI-MSI, immunofluorescence and OrbiSIMS.

LipidMaps database mining also identified ions matching to DG, TG and PC lipid species, which were downregulated in the metastatic lung in comparison to the wildtype lung (Figure 7-2b). PC is the major phospholipid class which comprises pulmonary surfactant, which in turn has been shown to reduce progression of lung tumours via inhibition of immune signalling [813]. Therefore, the observed reduction of PC species the metastatic lung may play a role in metastasis progression.

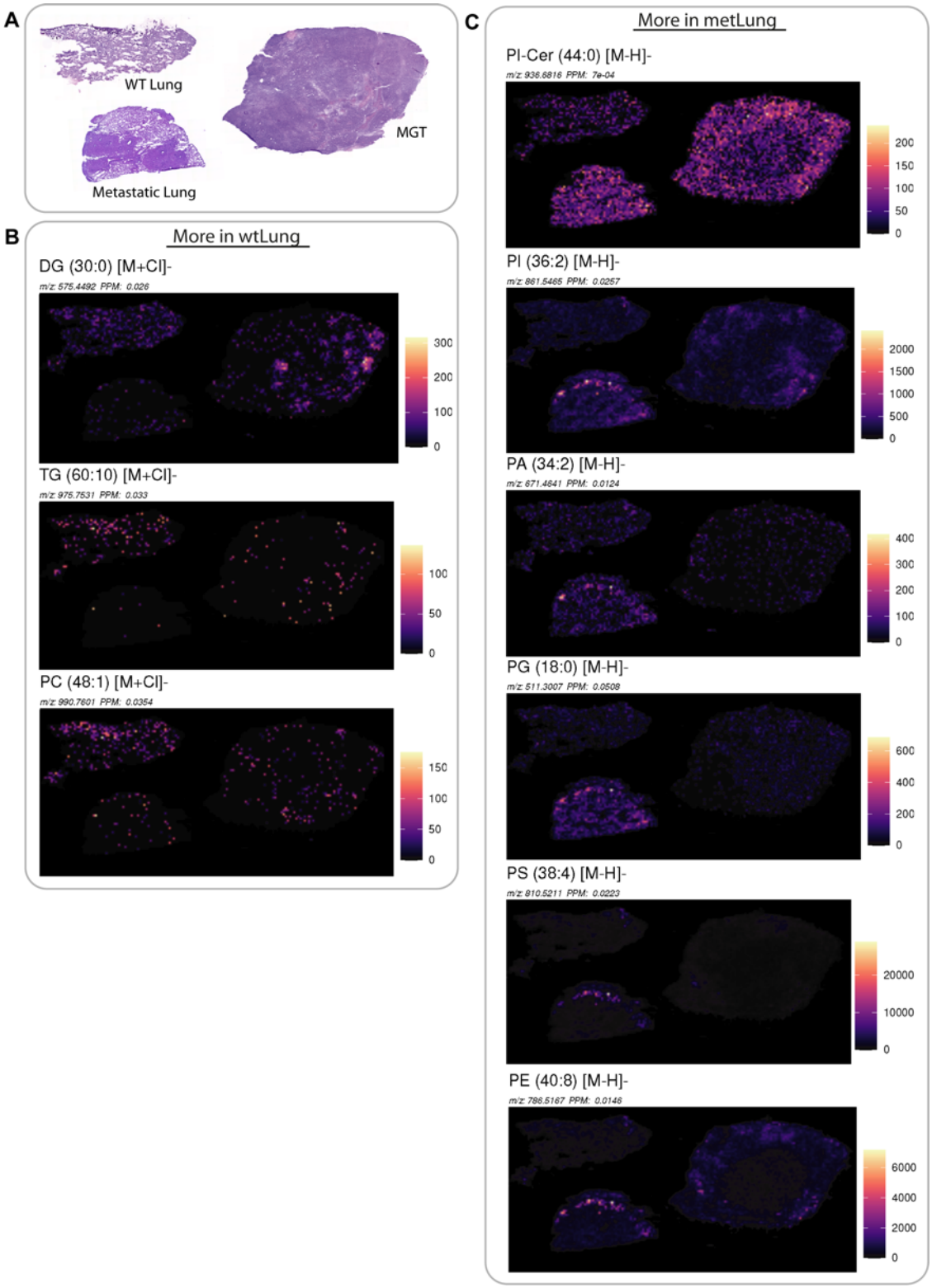


Figure 7-2. Metabolic heterogeneity between metastatic and wildtype by DESI-MSI. (A) Post-DESI H&E of sample containing a Myc310 MGT, metastatic lung from the same animal, and a wildtype lung for comparison. (C) Ions present at higher levels in wildtype and (D) metastatic that were matched to known polar and lipid metabolites.

7.4 Comparing changes in lipid classes between Myc310 MGTs and LMs using LC-MS and DESI-MSI.

7.4.1 Apolar LC-MS

Apolar metabolites from LM MGTs and LM^2s were analysed using untargeted LC-MS (see Methods). Untargeted lipid class analysis was used to identify 2447 lipid metabolites in the entire dataset. Fold change analysis further determined that 370 of these metabolites were significantly ($\log2(FC) \geq 2$), enriched in LM^2s compared to MGTs, of which 55 ions were annotated to specific lipid species using an R-based workflow, LipidMatch [814]. There were 349 apolar metabolites significantly enriched in MGTs, out of which 150 ions were successfully annotated using LipidMatch. Importantly, LipidMatch uses not only m/z values, but also LC-MS retention times and summed fragment intensities based on *in silico* predicted fragmentation patterns to assign ion identities.

Figure 7-3a shows a volcano plot distribution of detected lipid species between LM^2s and LM MGTs, and Figure 7-3b shows a dot plot of intensity fold changes between metabolites belonging to different lipid classes. Di- and triacylglycerols (DG, TG) were significantly higher in LM MGTs than in LM^2s. In LM^2s, specific ceramides and sphingomyelin lipids were present at significantly higher levels than in LM MGTs. The distribution of intensity fold changes between other lipid classes either varied within a class, or there were very few species identified per class.

Due to the large variety of lipid species and classes found in biological samples, an exploratory analysis is the first step of understanding changes in lipid species. A more detailed lipidomics analysis, using metabolite standards and MS/MS of ions with significantly distinct intensities is needed to draw further conclusions.

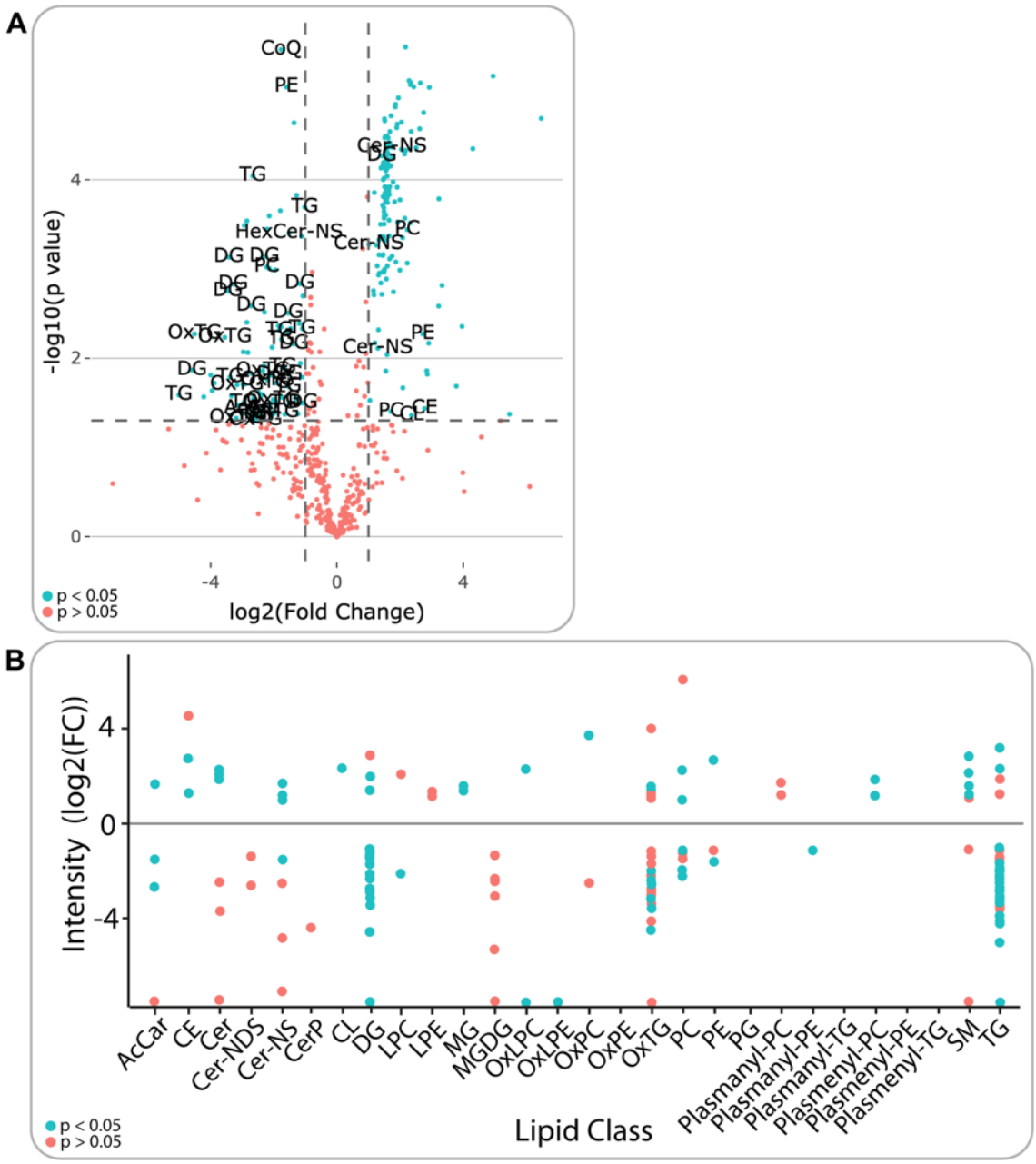


Figure 7-3. Apolar LC-MS analysis of lipid classes between LM^{2}s and LM MGTs – higher fold change represents enrichment in LM^{2}s.
(A) Volcano plot showing lipid metabolites differentially expressed between LM^{2}s and LM MGTs, with lipid classes labelled. (B) Fold change analysis of metabolites in each lipid class significantly changing between LM^{2}s and LM MGTs. Higher $\log_2$(FC) signifies higher levels in LMs. Point colours represent parametric t-test significance (* $p < 0.05$, ** $p < 0.01$, *** $p < 0.001$). Lipid classes: AcCar = acyl carnitine, CE = cholesterol ester, Cer = ceramide, Cer-NDS = ceramides containing non-hydroxy FA-dihydrosphingosine, Cer-NS = ceramide containing non-hydroxy FA-sphingosine, CL = cardiolipin, DG = diacylglycerol, LPC/PE = lyso-PC/PE, MG = monoacylglycerol, OxPC/PE/TG = oxidized PC/PE/TG, PC = phosphatidylcholine, PE = phosphatidylethanolamine, PG = phosphatidylglycerol, SM = sphingomyelin, TG = triacylclycerol.

7.4.2 Apolar DESI-MSI

Following identification of metabolic heterogeneity between LMs and MGTs using apolar LC-MS, DESI-MSI images were subjected to untargeted lipid metabolite analysis using the LipidMaps database. Both DGs and TGs were enriched in MGTs in comparison with LMs. By DESI, TG ions were rarely identified, and those that matched to TG species had a homogenous distribution between all tissue samples (Figure 7-4c). On the other hand, many DG species were seen in DESI-MSI images, localised to specific areas of MGTs, and not present at all in lungs or LMs. The particular DG-high areas contained lipid-laden cells in post-DESI H&E stains (Figure 7-4b,c). These cells are likely to be adipocytes remaining from the mammary fat pad; they are more likely to be found in mammary tissue than the lung, and they are known to be sites of TG synthesis from DGs [815], [816]. TGs may not be accurately detected in MSI due to possible fragmentation or lack of ionisation potential. Notably, while DESI-MSI analysis was performed in negative ion polarity for maximising polar metabolite coverage, lipid metabolite detection may be improved in the positive polarity [817].

In accordance with LC-MS findings (Figure 7-3), several ions matching to ceramide and sphingolipid species were upregulated in LMs (Figure 7-4d). Interestingly, Myc310 LMs have strikingly higher signals of these lipid species than LM^2s. However, this may also be related to metastasis size, since Myc310 LMs were on average smaller than LM^2s. Recently, it has been shown that sphingolipid and ceramide metabolism has been implicated in metastatic progression in breast cancer, through TGFb signalling and EMT initiation [443]. DESI-MSI in combination with LC-MS confirmed the exact localisation of ions matching to these lipid classes, but understanding their biological role in metastatic progression requires further inquiry.

Untargeted DESI-MSI also revealed heterogeneous distributions of ions matching to several other lipid classes, shown with representative images in Figure 7-4e, between MGTs, LMs and lungs. Several PG lipids were found exclusively in lung tissue, regardless of the presence of metastases (Figure 7-4e, top left). On the other hand, ions annotated as cardiolipin species were present in wildtype lungs

but their intensity reduced with increasing metastatic burden in the lung (Figure 7-4e, top right). Furthermore, there were several PE lipids that localised within Myc310 LMs, however were excluded from larger LM^2 lesions (Figure 7-4e, bottom, left). Finally, an ion matching the chemical formula of a PIP lipid showed specific localisation within all LMs, and distinct areas of MGTs (Figure 7-4e, bottom, right).

Untargeted apolar DESI-MSI analysis provided annotations for many ions which did not match to any polar metabolites, and revealed yet another dimension of metabolic heterogeneity in these complex samples. Lipids are involved in multiple vital process in tumour progression and metastasis, including proliferation, migration, vascular permeability, immune signalling and bioenergetics [818], [819]. Further work is needed to understand the role of lipids in MGTs and the metastatic niche.

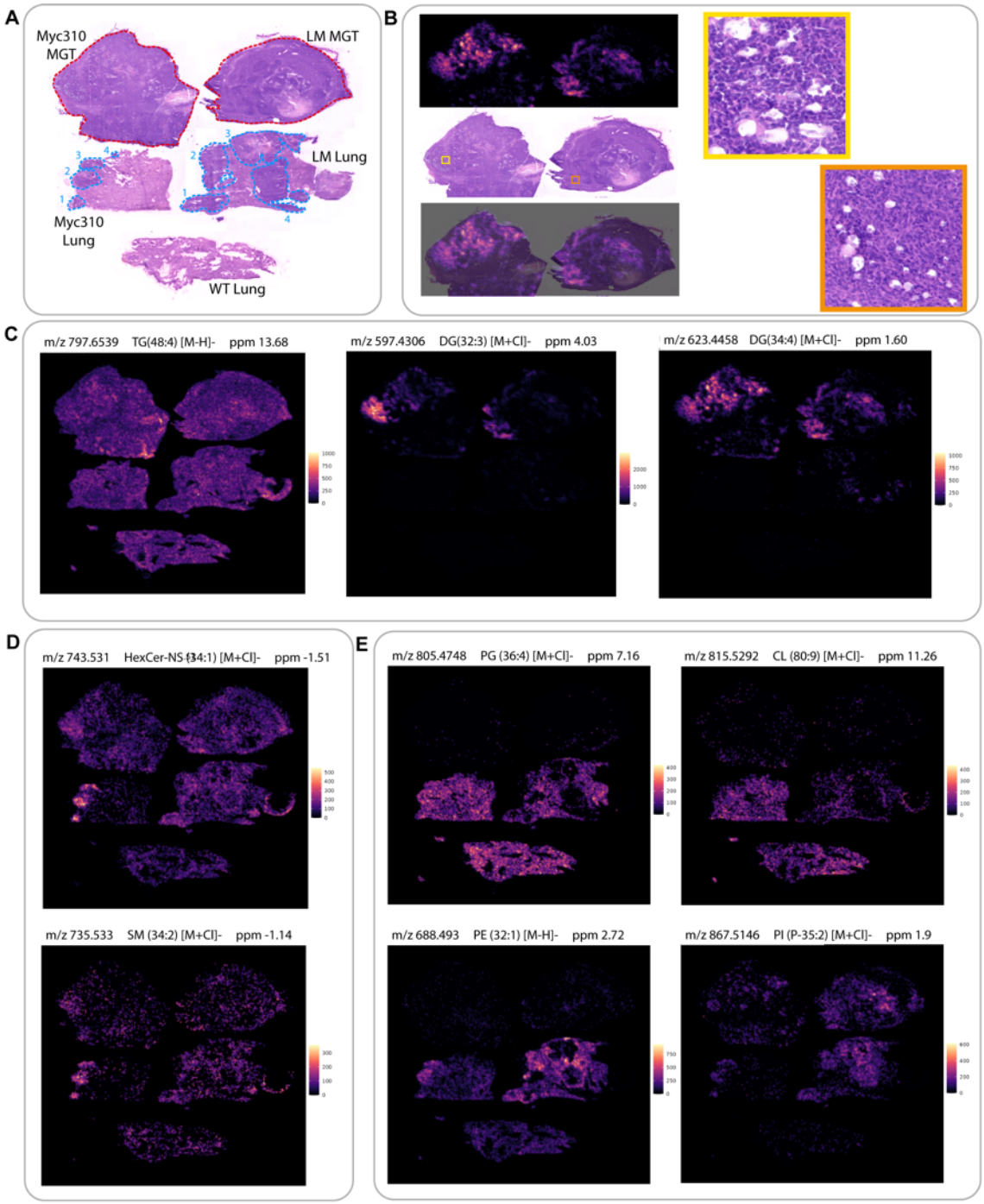


Figure 7-4. Assessing lipid heterogeneity between MGTs and the metastases derived from them, by DESI-MSI. (A) Post-DESI H&E of sample containing a Myc310 MGT and paired metastatic lungs, LM MGT and paired metastatic lungs, and a wildtype lung for comparison. (B) Overlay of DESI-MSI image of m/z 623.4458, matching to DG(34:4) [M+Cl]-, with post-DESI H&E, revealing co-localisation of glycerolipid metabolites with cells that phenotypically resemble adipocytes. Heterogeneous distribution of (C) glycerolipid, (D) sphingolipids and (E) phospholipids between MGTs, LMs and lung tissue.

7.5 Exploring peri-metastatic lipid accumulation using the Orbi-SIMS.

In the previous chapter I described how Orbi-SIMS MSI allows the acquisition of metabolite images with a high lateral resolution (2 um pixel size). However, peak annotation is a challenge due to potential metabolite fragmentation upon impact of the GCIB ionisation source and during ion transfer. The predecessors of OrbiSIMS is ToF-SIMS, which has been used consistently to image lipid metabolite distribution in biological samples [582], [585], [583]. Since apolar metabolite detection has been well characterised by SIMS techniques, and following the observations of heterogeneous lipid distribution between LMs and the metastatic lung as seen by DESI-MSI, I wanted to more closely explore the metastatic niche using the Orbi-SIMS.

Due to high ion fragmentation, negative ion polarity and low collisional cooling during ion transfer, intact lipid species were not abundantly detected using the Orbi-SIMS. However, I observed distinct hotspots of fatty acid accumulation on the periphery of a metastatic tumour (Figure 7-5). The ion signal matching to adenine was localised in the metastasis, with lower signals originating from surrounding lung epithelium. From previous Orbi-SIMS images of MGT heterogeneity (Figure 6-14), the ion annotated as adenine was consistently upregulated in specifically the tumour cells compared to the stroma, and hence was considered a chemical marker of tumour cells in our Orbi-SIMS images. This may be a read-out for high nuclear density of these cells as adenine can be fragmented from nucleotides. Alignment of post-SIMS H&E staining confirmed that there was a specific lipid-laden cell type that co-localised perfectly with the areas of increased fatty acid accumulation as seen with OrbiSIMS imaging. Taken together with the specific lipid accumulation in the whole metastatic lung as seen by DESI-MSI (Figure 7-2), this observation demonstrates the novel perspective that MSI provides the link between specific histological features with metabolic signatures.

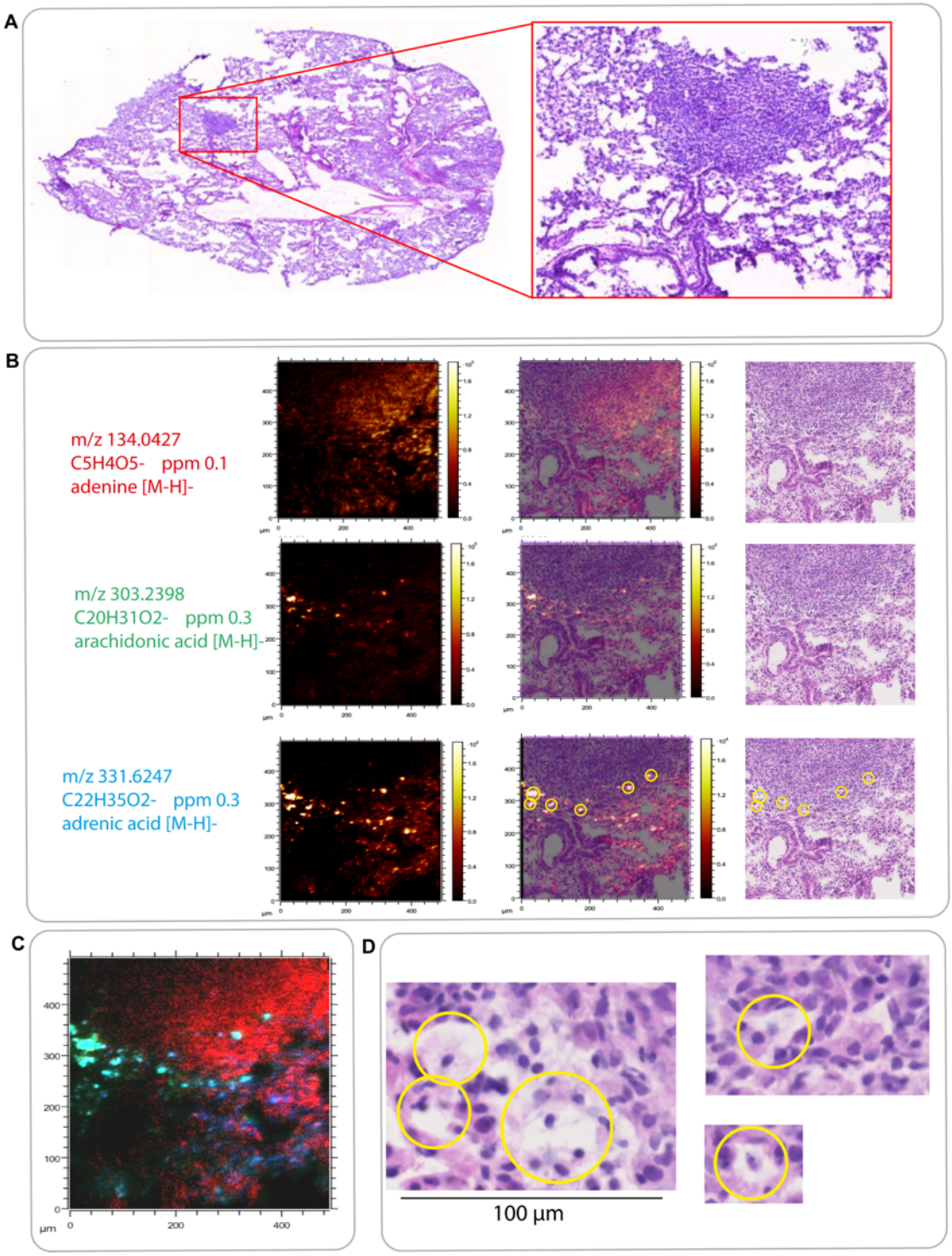


Figure 7-5. Peri-metastatic lipid accumulation in metastatic lung identified by Orbi-SIMS imaging.
(A) Post-MSI H&E stain highlighting metastatic lesion. (B) Ions identified by database mining using Orbi-SIMS *m/z* values: ion matched to adenine [M-H]- localised in the metastatic lesion, whereas ions matching to arachidonic acid [M-H]- and its derivative, adrenic acid [M-H]- are localised on the metastatic periphery. (C) RGB overlay of the three ion images in (B). (D) Magnified H&E stain from (B) lower-right panel revealing exact co-localisation of lipid-rich areas with lipid-laden cells; yellow circles represent areas of high lipid accumulation from (B).

7.6 Identifying the cell population within the metastatic niche that accumulates lipids on the metastatic border.

Following my observation of specific cells accumulating lipids at the periphery of lung metastasis, I first wanted to determine if there was an increase in expression of enzymes involved in lipid biosynthesis in these areas. Immunofluorescence staining for fatty acid synthase (FASN) revealed that its expression was increased in a specific cell sub-population in the metastatic lung, compared to MGT and WT lung (Figure 7-6b,c).

Next, I aimed to identify the cell type that is responsible for this phenotype. By Orbi-SIMS, one of the identified ions localised to these lipid hotspots was arachidonic acid, which is a key signalling molecule in immune cell activation [820]–[822]. I used immunofluorescent staining on consecutive metastatic lung sections to evaluate if there was an accumulation of a particular immune cell type around lung metastases that would have increased FASN expression. Co-staining for FASN and CD45 highlighted the high degree of immune cells infiltrating both the metastatic lung and the LM (Figure 7-6d). Independent co-localisation staining against FASN and M1 macrophages (CD68) showed that macrophages mainly reside within the LM lesion, and are not the cells overexpressing FASN (Figure 7-6e). Staining for T-cells (CD3) and B cells (B220) showed that while there are abundant populations of both of these cell types specifically in the metastatic lung, there was no co-expression of these markers with FASN (Figure 7-6f,g).

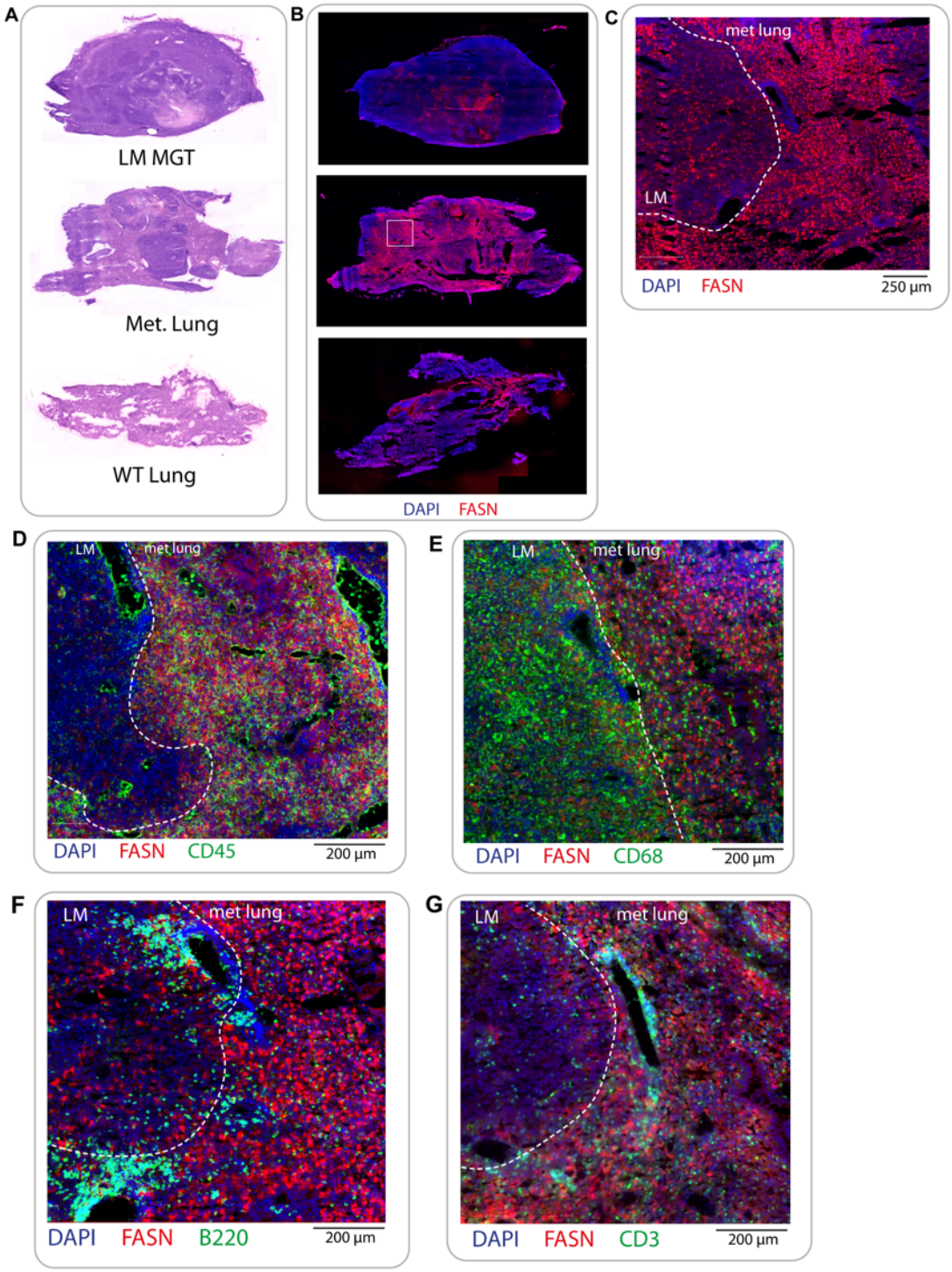


Figure 7-6. Analysis of FASN distribution in the metastatic lung.
Immunofluorescent staining of an LM MGT, the metastatic lung from the same animal and a wildtype lung reveals upregulation of fatty acid synthase (FASN) in the metastatic lung. (A) H&E stain of near-adjacent tissue slices to those imaged by IF. (B) IF staining of FASN and DAPI across the three tissues. (C) Magnified image of the region surrounding the LM lesion, showing upregulation of in the metastatic lung but not within the LM itself. (D)-(G) Co-staining of FASN and immune cell markers on adjacent slices of the metastatic lung. CD45 = pan-immune marker (D), CD68 = M1 macrophage marker (E), B220 = B-cell marker (F), CD3 = T-cell marker (G).

During the course of my immunofluorescence experiments, while determining a robust IF marker for metastases, I discovered that Myc310 LMs and LM^2s are E-cadherin low, suggesting a more mesenchymal phenotype. The lung epithelium, however, was E-cadherin high, with virtually every pneumocyte clearly expressing a high level of E-cadherin in comparison to other cell types in the lung (Figure 7-7a). Co-staining of E-cadherin and FASN was performed to determine whether it is the lung cells that are upregulating *de novo* lipid biosynthesis in response to the presence of an LM tumour in the lung (Figure 7-7a). Due to time limitations and the lack of metastatic lung consecutive sections, the FASN and E-cadherin co-localisation was evaluated in a new set of LM MGTs and their metastatic lungs. Indeed, clear co-localisation of the FASN signal was observed when co-stained with E-cadherin. A fascinating discovery was that some LMs had a high degree of E-cadherin-positive lung cells inside the LM lesion, suggesting that the tumour cells were able to migrate between and around pneumocytes as they colonise the lungs (Figure 7-7b,c). FASN-high lung cells included within the LM region would be impossible to dissect and are inevitably included in any bulk tissue analysis by LC-MS. On the other hand, many LM lesions, even in the same lung lobe, were not able to penetrate into the lung and are therefore clear of pneumocytes and subsequently, are predicted to have lower lipid accumulation due to low expression of FASN (Figure 7-7).

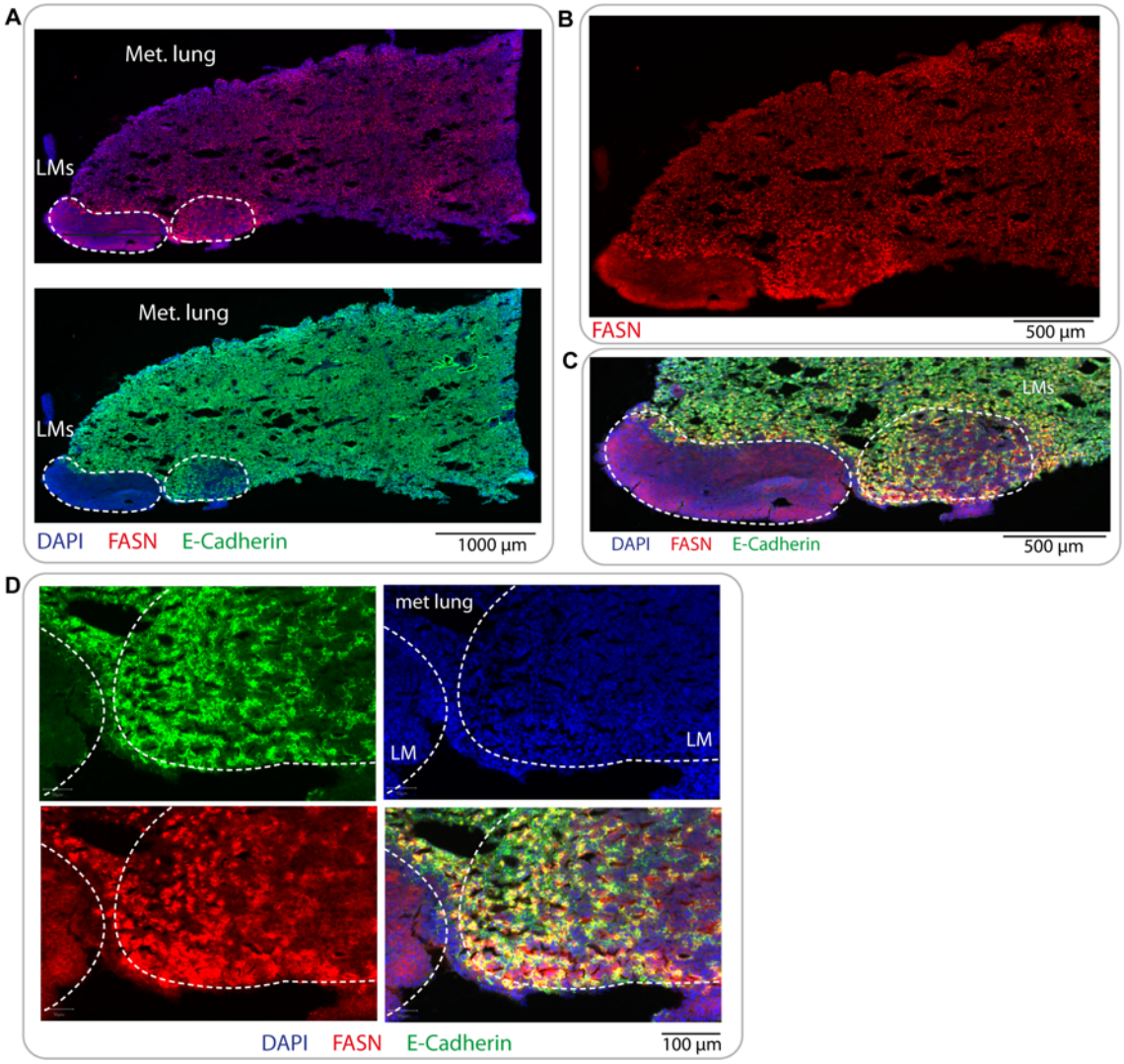


Figure 7-7. Immunofluorescence staining to identify which cells in the metastatic lung upregulate FASN.
(A) E-cadherin (green) epithelial cell marker is not expressed in the LM lesions, suggesting a mesenchymal phenotype. Lung epithelium is E-cadherin positive. FASN (red) is expressed in the LMs and at a higher level in the surrounding lung, especially in the per-metastatic region. (B) Magnification of the FASN stain demonstrating that FASN expression is upregulated at the metastatic boundary and inside the invasive LM lesion. (C) Overlay of E-cadherin, FASN and DAPI IF shows that two different LM lesions differ in invasiveness: the left lesion has not yet penetrated into the lung epithelium, whereas the right lesion is heavily infiltrated with pneumocytes. (D) Magnified IF images show co-localisation of FASN-high cells with E-cadherin positive lung cells at the periphery of the LM lesion.

7.7 Chapter Discussion

Lipid metabolism plays multiple vital roles in tumour progression and metastases, including proliferation, maintenance of bioenergetic reactions, remodelling of the tumour microenvironment, immune cell signalling and coping with increased oxidative stress [819]. Specifically in the context of breast cancer, due to the surrounding adipocyte-rich environment of the mammary fat pad, lipid metabolism provides additional nutrients that support tumour development [823], [824], [197]. The scope of my project did not allow for a detailed study of lipid metabolism in MGTs and LMs, however MSI revealed notable changes in specifically lipid metabolites in the metastatic niche and therefore it was important to explore this finding further.

Apolar LC-MS analysis showed the enrichment of DG and TG species in the MGTs compared to LMs, and in turn, several species of sphingolipids and ceramides were enriched consistently in the metastases. As with the polar LC-MS analysis, crude dissection of metastases remains a limitation to bulk tissue analysis, especially when considering the immense diversity of immune and lung cells which were found within LM tumours. DESI-MSI and OrbiSIMS imaging allowed me to trace the exact location of lipids in the same classes as shown to be significantly changing between LMs and MGTs by LC-MS. Heterogeneous distribution of DG species was seen within MGTs, located in regions which appear to be populated by adipocytes or other lipid-laden cells. Lipid-laden cells in areas of the metastatic lungs surrounding LMs were also observed by OrbiSIMS and confirmed by H&E staining. Even though OrbiSIMS ion annotations must be taken with caution due to a high degree of in-source fragmentation, this approach allowed me to discover an accumulation of cells in the metastatic niche that upregulate *de novo* lipogenesis through FASN overexpression. It is still unknown whether the FASN-high cells have a lipid-laden phenotype, and further immunohistochemistry studies are required to determine this.

Combining MSI and immunofluorescent staining I was able to determine that the cells upregulating FASN in the metastatic lung are a population of E-cadherin positive lung epithelial cells. These cells are not suspected to be tumour cells

undergoing mesenchymal-to-epithelial transition due to the complete absence of the MYC oncogene in these cells. The particularly intriguing finding is that only lung cells which have been infiltrated by metastatic tumour cells show an upregulated level of FASN, and is absent in lung cells that are located near metastatic lesions that has not yet penetrated into the lung organ. This observation suggests the upregulation of lipid biosynthesis by lung cells is instigated by direct contact or signalling of migrating tumour cells, but future investigation is required. Interestingly, a recent study demonstrated how lung metastases stimulate the remodelling of the lung epithelium, provoking a cancer-associated phenotype which supports metastatic cell growth [787]. Changes in lipid metabolism in the lung epithelium in response to metastasis has not yet been reported and understanding the mechanism of this phenotype remains a key interest in the lab.

Taken together, MSI as a multimodal approach to exploring metabolic heterogeneity is increasingly proving to be a requirement to understand the full scope of complex metabolic crosstalk between different cell types, both within tumours and in the context of metastasis.

Chapter 8. Discussion

The primary aim of this project was to establish a robust methodology to study metabolic heterogeneity in the context of metastatic disease. During the course of my work I was able to develop a model to study the metabolism of MYC-driven mammary gland tumours and their lung metastases, and determine the environmental impact of the surrounding organ on metabolic transformation and plasticity. Using several mass spectrometry imaging platforms, I was able to study metabolite distribution *in situ*, uncovering metabolic heterogeneity within individual MGTs, between MGTs and the LMs derived from them, and also importantly in the unperturbed metastatic niche. My work has demonstrated the unique and powerful advantages that MSI modalities bring into the field of cancer metabolomics, although numerous limitations remain in these still relatively new and developing techniques.

The results of LC-MS and DESI-MSI experiments and their significance in the context of metabolic vulnerabilities of metastatic development and survival have been discussed at the end of each chapter. In this chapter, I will discuss the model used in this thesis to study metastasis, briefly summarize the key changes in metabolism between MGTs and their lung metastases, and will then focus in greater detail on the advantages and limitations of using a combination of traditional LC-MS with the novel MSI technology platforms for studying metabolic heterogeneity in cancer. I will conclude with an outline of the future directions that will be pursued in the lab as a result of my findings.

8.1 Developing a method to study the metabolism of lung metastases.

Incidence of metastasis of transgenic MMTV-MYC tumours has previously been observed by Dr. Emma Still in our lab, however transgenic tumour lung metastases were too small to dissect for LC-MS metabolomic analysis. In my project, I used the Myc310 cell line, originally derived from a transgenic MMTV-MYC tumour and passaged *in vitro* more than thirty times. When injected into the mammary fat pad of wildtype mice, the Myc310 cell line yielded metastases to the lungs that were visibly detectable, albeit still periodically too small for dissection. Several metastatic breast cancer mouse models have been established and are widely used in various studies of metabolism, such as the MMTV-PyMT and 4T1 models. For my project I wanted to focus specifically on MYC-driven metastatic mammary gland tumours, given the poor prognosis in patients with triple negative breast cancer driven by MYC amplification [484], [607], [825], [826]. Apart from MYC as the driver oncogene, the advantages of the Myc310 model include the reproducibility and relatively fast tumour development *in vivo*. Gene expression analysis for additional oncogenic drivers, such as RAS, PI3K and p53, as well as EMT transcription factors, will help elucidate the underlying mechanisms of metastatic progression in these cells.

The mechanism behind the increased metastatic potential of tumours generated by injection of the Myc310 cell line, compared to transgenic MMTV-MYC tumours, requires further investigation, and will be pursued in future work. Initial metabolomic comparison of transgenic MMTV-MYC MGTs to Myc310 MGTs revealed several metabolic pathways which may be associated with a higher propensity for metastasis. Myc310 MGTs had increased levels of glycolytic and TCA cycle intermediates, as well as increased levels of nucleotides. Furthermore, the increased levels of PPP intermediates, as well as increased glutathione biosynthesis could be attributed to a metabolic signature that facilitates metastatic progression, since antioxidant pathways have been shown to be upregulated in higher grade tumours and metastases [731].

As part of my project I wanted to understand if the observed metabolic differences between Myc310 MGTs and their LMs were dictated by the surrounding lung environment. The isolation, *in vitro* propagation and re-injection of LM cells into the mammary fat pad of wildtype mice generated significantly more metastatic tumours in both incidence and size of lung metastasis lesions. However, LM MGTs were comparable in proliferation rates and metabolism to less-metastatic Myc310 MGTs. This model allowed me to observe the plasticity of metabolic reprogramming in these cells, although the mechanism behind the increased aggressiveness has not yet been explored. As discussed in Chapter 5, the LM cells are likely a selected clonal sub-population of Myc310 cells that are more prone to migration, survival in circulation and the lung, immunosuppression or apoptotic resistance. The metabolic distinctions between LMs and MGTs are maintained in both Myc310 LMs and LM^2s, and are discussed below and in detail in Chapters 4 and 5. Overall the majority of metabolic changes exhibited by LMs are absent when comparing LM MGTs to Myc310 MGTs, suggesting flexible metabolic reprogramming that is governed by the environment of the tumour cells. Given the preservation of metastasis-specific metabolic characteristics, it would be worthwhile to assess the same metabolic reprogramming in other models of metastatic breast cancer, as well as metastatic patient-derived xenografts (PDXs). Elucidating overarching metabolic vulnerabilities of lung metastasis would allow for more wide-ranging therapeutic approaches that may be beneficial irrespective of primary tumour origin or genetic lesion.

8.2 Metabolic changes between MYC-driven mammary gland tumours and their metastases to the lung.

The MYC oncogene has been widely characterised as a metabolic regulator in cancer development and progression [142], [827], however most studies involving MYC-induced metabolic changes have been focused on comparing tumour cells with normal cells [130], [143], [144]. At the same time, MYC has been identified as a marker of poor prognosis and metastatic disease [825]. Therefore, one of the aims of this project was to assess changes in metabolism between MYC-driven mammary gland tumours and their metastases to the lung.

8.2.1 Lung metastases have increased bioenergetic demands than mammary gland tumours, as demonstrated by increased glycolysis, amino acid metabolism and nucleotide biosynthesis.

LC-MS analysis revealed that LMs had higher levels of glycolytic intermediates and non-essential amino acids, including alanine, glutamine, glutamate, aspartate and asparagine. Furthermore, levels of nucleotides and the ATP/AMP ratio were also increased in some LM lesions, suggesting a degree of bioenergetic heterogeneity between them. Experiments using $^{13}C_6$-glucose labelling showed that LMs also had higher enrichment in glycolytic intermediates, alanine, glutamate, and glutamine. The increased alanine production in metastases is in line with recent findings that lung metastases upregulate the alanine aminotransferase reaction in order to produce alpha-ketoglutarate, which in turn drives ECM remodelling and metastasis progression [165]. The TCA intermediates fumarate and malate were elevated in LMs, however levels and labelling from glucose of citrate, cis-aconitate and alpha-ketoglutarate was decreased. These findings suggest that acetyl-CoA in LMs may be redirected towards lipid biosynthesis, and also that LMs have reduced reductive carboxylation of alpha-ketoglutarate than MGTs. $^{13}C_5$-glutamine labelling supported this finding with reduced M+5 enrichment in these metabolites in LMs. A possible explanation for this shift is that LM cells require NADPH for antioxidant metabolism and therefore downregulate other pathways that require this cofactor, including the reductive carboxylation of alpha-ketoglutarate by IDH.

The observation that the PPP is reduced in LMs compared to MGTs is conflicting with the hypothesis that LMs require increase protection against ROS, since PPP is the primary source of intracellular NADPH production, and has been shown in other models to be upregulated in more aggressive tumours [115], [741], [828], [829]. The underlying mechanism for a downregulation of the PPP in LMs requires further inquiry. Since EMT transcription factors signal directly to upregulate PPP enzymes, the reduced activity of this pathway in LMs may signify that the metastatic cells are undergoing the reverse, mesenchymal-to-epithelial transition (MET), and therefore EMT-derived metabolic signalling is reduced. In Chapter 7, however, I showed that LM lesions have low expression of the epithelial marker E-cadherin, therefore it is unlikely that these cells reverted back to an entirely epithelial state at the point of resection. Further investigation into EMT transcription factor levels and signalling and PPP enzyme expression levels in LMs and MGTs is needed to draw final conclusions about the mechanism behind reduced levels of PPP intermediates in LMs.

8.2.2 Lung metastases have an upregulated one carbon metabolism and glutathione biosynthesis.

The increase in one carbon metabolism intermediates SAM and SAH were consistently significant in Myc310 LMs and LM^2s, compared to the MGTs that they originated from. The SAM/SAH ratio was also increased, suggesting a higher methylation capacity in LMs. This link between metabolism and epigenetic regulation is an extremely interesting and novel observation to date. A primary focus of future work will be assessing the methylation status of histones, DNA and proteins in LMs and MGTs, in order to identify the mechanistic purpose of this observation. As discussed in chapter 5, SAM is a global methyl donor that is used by numerous methyltransferases, not only in epigenetic regulation reactions but also in phospholipid and polyamine biosynthesis and regulation of nutrient sensing by mTOR. Therefore, this metabolic phenotype is likely to directly link to other processes driving metastatic progression and therefore SAM production presents an appealing therapeutic target against metastasis development in our model.

Importantly, many intermediates of the one carbon metabolism, including most of the folate cycle metabolites were not detectable using our current LC-MS analysis method. Upregulated levels of the essential amino acids threonine and histidine in LMs hint towards an upregulated folate cycle, however this has to be confirmed with enzyme expression and activity assays. In order to fully understand the one carbon metabolism upregulation in LMs, future work will focus on tailoring the metabolite extraction and LC-MS analysis method for better detection of these species. Furthermore, $^{13}C_5$-methionine labelling in the diet can be used to assess the flux into SAM, SAH and other one carbon metabolism intermediates.

Both reduced and oxidized forms of glutathione were consistently upregulated in LMs, and the GSH/GSSG ratio was reduced, suggesting elevated oxidative stress in LMs. This observation supports established findings regarding elevated ROS in highly proliferative tumours, especially in the highly-oxygenated lung microenvironment. Given the upregulation in one carbon metabolism intermediates, we hypothesized that glutathione synthesis from homocysteine through the transsulfuration pathway is likely. Glutathione production via the transsulfuration pathway requires glutamine, however $^{13}C_5$-glutamine-derived enrichment in GSH and GSSG was significantly reduced in LMs compared to MGTs. This finding was surprising, however it may indicate that LMs upregulate glutathione recycling rather than *de novo* biosynthesis, conserving glutamine for other catabolic pathways such as nucleotide biosynthesis. Overall the fate of glutamine-derived carbons in LMs remains unclear, due to a lack of significant increase in $^{13}C_5$-glutamine-derived flux into the TCA, aspartate or other downstream pathways. However, glutamine efflux through the LAT1 transporter plays an important role in essential amino acid influx, and upregulated levels of EAAs were observed in LMs. EAAs can be catabolised in the mitochondria for energy and biomass production, and leucine regulated mTOR activation, which drives metabolic reprogramming and proliferation. Furthermore, efflux of glutamine-derived glutamate through the xCT transporter drives cystine import, which yields cysteine and contributes to glutathione biosynthesis. Therefore, the role of glutamine in LMs needs to be further investigated by assessing the expression status of the LAT1, xCT and ASCT2 receptors, as well as downstream enzymes involved in EAA catabolism and glutathione synthesis in the transsulfuration pathway.

With regards to glutathione, the expression and activation of glutathione peroxidase, the enzyme that recycles GSSG back to GSH, also needs to be assessed. Given that NADPH is required for this reaction, it will be beneficial to measure NAD(P)+ and NAD(P)H using LC-MS metabolomics, however this remains a challenge due to spontaneous oxidation of the reduced species during extraction.

8.2.3 Limitations of LC-MS for assessing metabolism of metastasis

Traditional metabolomics techniques such as LC-MS require accurate tumour dissection from the surrounding organ for bulk analysis of the metabolome. This approach is advantageous due to the reputable polar and lipid metabolite detection and quantification methods. However, the crude dissection of metastatic lesions from the frozen lung in this project presented a substantial limitation, and the LC-MS results presented in this body of work are limited by the likely presence of some surrounding lung tissue in the LM samples.

To date, the vast majority of studies of metastatic metabolism rely on *in vitro* models such as 3D tumourspheres and suspension cultures to mimic the anchorage-independent growth of metastatic lesions. These methods have profound limitations due to the influence of *in vitro* media composition and oxygen levels, as well as lack of non-tumour cells that normally contribute to metastasis growth, signalling and metabolism. The reason for using such models lies in the difficulty of isolating individual metastatic lesions from the surrounding organ. As shown in this and other studies, metastatic lesions are composed of a heterogeneous population of cells, which include not only tumour cells but also various immune infiltrates and cells from the organ that is being colonised. Furthermore, metastatic dissemination begins with single cells that extravasate into distal organs, and it is often impossible to accurately resect these lesions for metabolomics analysis. Recently, advances in laser capture microdissection have demonstrated the ability to perform genome, transcriptome and proteome analysis on specific cell populations in complex tissue samples, however this technique relies heavily on tissue fixation, which is problematic for metabolomic studies [830]–[833]. Taken together, there is a clear need for spatially-resolved metabolomics methods that could assess metabolite distribution in heterogenous

tissues such as metastatic lesions. In this work I demonstrate how mass spectrometry imaging can be used for this purpose and introduce several metabolic vulnerabilities of metastasis that were observed using these techniques.

8.3 Advantages and limitations of MSI for studying metabolic heterogeneity in complex tissues.

MSI is a powerful analytical tool for visualising metabolite distribution *in situ* without the need for dissection. Using immunofluorescent staining I have demonstrated the diverse cell populations in MGTs and within the metastatic niche, and highlighted that understanding how different components of these tissues contribute to metabolism is vital for successful therapeutic strategies.

8.3.1 DESI-MSI reveals heterogeneous distribution of metabolites within MGTs and in the metastatic lung.

DESI-MSI image segmentation into histological ROIs revealed heterogeneous distribution of LC-MS-matched polar metabolites between MGTs, LMs, metastatic and wildtype lungs. Hierarchical clustering of polar metabolite ions revealed similarities between larger LMs and MGTs, while smaller metastatic lesions were clustered closer to the metastatic lungs. The limitations of histological ROI segmentation are similar to those present with dissection for LC-MS, since diverse cell types are analysed together. However, images of ions upregulated in specific ROIs can then be closer inspected and combined with post-MSI histological staining to determine specific cell sub-populations that co-localise with the metabolic signals. Furthermore, I have briefly introduced the WCGNA module analysis method that reveals metabolically distinct regions in DESI-MSI images, factoring in proximity and underlying biological pathways of metabolite species [600], [834]. This and other multivariate data analysis techniques, such as the neural network tSNE approach, are methods by which the true complexity of chemical mapping by MSI can be assessed [796]. For the purpose of my investigation I focused on coupling DESI-MSI findings with LC-MS, however further data analysis efforts are required for a more encompassing, untargeted data analysis of the DESI-MSI data sets.

DESI-MSI results were complimentary to LC-MS findings in demonstrating the increased levels of glutathione and the one carbon metabolism intermediate dimethylglycine in LMs compared to MGTs. Imaging of GSSG distribution further revealed that the metastatic lungs had similarly high levels compared to LMs, suggesting that LM presence causes ROS accumulation in the entire organ.
On the other hand, DESI-MSI revealed new information that was conflicting with LC-MS findings, highlighting the limitations behind bulk tissue analysis by LC-MS. Glutamine was consistently enriched in the LMs by LC-MS, however DESI-MSI revealed it's upregulation in the metastatic lung, rather than in the LM itself. Furthermore, I was able to acquire DESI-MSI images of $^{13}C_5$-glutamine and glutamate following stable isotope infusions, and the localisation of the labelled metabolites was consistent with higher glutamine in the metastatic lung. Upregulated glutamate in the LM lesion is a visual demonstration of glutamine catabolism in the LM. The increased levels of glutamine in the metastatic lungs requires further investigation to understand if the presence of a metastatic lesion stimulates increased glutamine uptake in the entire organ, and potentially support metastatic growth.

Both targeted and untargeted DESI image analysis showed that in many cases, metabolites that were deemed to be present at higher levels in LMs were actually present at comparable levels in specific regions of the MGT. In some cases, absence of polar metabolites can be traced to areas of necrosis in the post-DESI H&E staining, however in other cases it remained unclear why certain metabolites localised to certain tumour regions. LMs often chemically resembled particular regions within the MGT. These regions of the tumour may contain cells with metastatic properties and undergoing EMT. Furthermore, such comparative metabolic profiles may represent regions of comparable oxygen availability and therefore ROS, or simply regions of comparable proliferation rates. Indeed, in post-DESI H&E stains, both LMs and the MGT regions which express a similar metabolic profile are mostly made up of de-differentiated, proliferating tumour cells. Further histological analysis of the tumours imaged by DESI-MSI is needed to identify the drivers of similar metabolic profiles between certain regions in the MGT and the LMs derived from it.

Intra-tumour heterogeneity was addressed in this study using DESI-MSI and also the relatively novel MSI modality, the OrbiSIMS. Method development for biological tissue analysis by OrbiSIMS is still in development, however as part of this project I was able to demonstrate metabolic differences between tumour and stroma cells. The harsh ionising conditions of the gas cluster ion beam of the OrbiSIMS instrument and in-source ion fragmentation present a difficulty in accurately assigning metabolite identities to specific ions. However, I was able to see enriched arachidonic acid in the tumour stroma. Whether this is a free fatty acid or a cleaved head-group from eicosanoid lipids is yet to be determined, however in this case, regardless of fragmentation this signal is suggestive of increased immune signalling. The high-vacuum conditions of the OrbiSIMS are also problematic for biological tissue analysis due to tissue desiccation and ion suppression effects. Recently, a method was developed to analyse biological samples in the OrbiSIMS in their native state using high-pressure freezing and cryogenic imaging at -150°C, which significantly improved polar metabolite detection and tissue morphology preservation [542], as well as detection of lipids and hydrocarbons that are typically volatile under high vacuum [835]. Such impactful developments in the methodology for biological tissue analysis are continuously advancing the MSI field.

8.3.2 Lipid biosynthesis is upregulated by lung cells in close proximity to invasive metastatic lesions.

One of the key findings resulting from OrbiSIMS studies was the observation of lipid accumulation in specific spherical regions on the periphery of the metastatic lesion, resembling individual cells in shape and size. Co-localisation with post-MSI H&E stains indeed revealed individual lipid-laden cells in the vicinity of LM tumours. The high spatial resolution of the OrbiSIMS, therefore, allowed the visualisation of a metabolic signature in a particular cell type in the innate *in situ* context. The lipid accumulation around metastases was also seen by DESI-MSI, although at a much lower spatial resolution, showing a more global accumulation of lipids surrounding LMs. These findings were followed up with immunofluorescent stains against the rate limiting enzyme of *de novo* fatty acid biosynthesis, FASN. In accordance with OrbiSIMS and DESI-MSI images, FASN expression was also upregulated in the

peri-metastatic regions. Further immunohistological probing revealed that the FASN-expressing cells were E-cadherin positive lung cells, and not an immune cell sub-population as initially hypothesized. This finding is crucial in demonstrating how MSI can drive novel therapeutic target identification, and investigating the impact of lipid accumulation in the lung cells on metastatic progression remains a key interest in the lab.

Recently it has been showed that lung pneumocytes play a key role in driving progression and supporting growth of metastases, however the underlying metabolic reprogramming remains unknown [787]. The role of lipid metabolism upregulation in neutrophils to support metastasis has also been recently demonstrated [767], [807]. Eicosanoid biosynthesis supports metabolism and vascular remodelling in the context of metastasis and the pre-metastatic niche, however these findings have only been shown in tumour and immune cells [836]–[838]. Furthermore, increased ROS were shown to induce lipid accumulation in lipid droplets in hepatocytes and cancer cells [839]–[841], and lipid droplet formation protects the cell from ROS induced by lipid-peroxidation [842]–[844]. Also, while increased fatty acid oxidation is a known source of ROS [134], [845]–[847], long-chain poly-unsaturated fatty acids (PUFAs) have been identified as potent antioxidants and anti-inflammatory mediators [848]–[853]. Therefore, identifying the exact fatty acid and lipid species that are enriched in the metastatic lung is required to better our understanding of the mechanistic importance of this observation.

There are several possible reasons for FASN upregulation in lung cells in proximity to invasive metastatic lesions. Fatty acid production can support fatty oxidation for ATP production, which has been shown to drive triple negative cancer metastasis [854]. Furthermore, FASN inhibition has been shown to reduce growth of breast, lung and ovarian cancers [855]–[857], and to support the transition to anchorage-independent growth [858]. Interestingly, the IF staining of FASN in my metastatic model does not show a FASN upregulation in the metastases themselves, but rather in the adjacent lung cells. *De novo* fatty acid biosynthesis consumed NADPH, limiting the cell's reductive capacity, and therefore the metastasis cells may be downregulating this pathway to preserve NADPH for glutathione recycling [107], [859]. It remains unclear if the metastasis cells are able to induce

upregulation of FASN in pneumocytes, or if there is a lipid transfer between lung cells and metastasis cells that support metastatic tumour growth. These questions can be addressed through selective knockdowns of FASN in pneumocytes, and measuring the expression of FA transporters such as CD36 in LM cells.

Increased lipid production in the lung may be a mechanistic response to metastatic invasion. A recent study demonstrated that upon lung injury by bleomycin, FASN is needed to support ATP production in the context of mitochondrial damage and maintain surfactant lipid synthesis [860]. In this study, targeted FASN knockdown in alveolar epithelial cells mediated critical lung fibrosis following bleomycin-induced cell damage. Therefore, in the context of lung metastases, FASN upregulation may relate to lung cell damage as a result of metastatic cell invasion, or local elevated ROS production. Conversely, another study showed that pharmacological FASN inhibition in fibroblasts reduced pro-fibrotic signalling and improved lung function following bleomycin treatment [861]. Future work will focus on confirming the exact subtype of lung cells that are overexpressing FASN in response to metastasis, and determining the mechanism and function of this upregulation.

8.3.3 Future challenges for MSI analysis of complex biological tissues.

I have demonstrated how MSI techniques can be used to complement findings by traditional metabolomics methods, and also unveil a new dimension of spatially-resolved metabolic heterogeneity. However, MSI for biological sample analysis is a relatively novel field, and many limitations and complications remain. As discussed in chapters 6 and 7, MSI modalities are more robust and routinely used for imaging of lipid species and exogenous drug compounds [579], [773], [862], [863], and therefore polar metabolite detection is at times limited, although DESI-MSI maintains a comparatively broad metabolite coverage compared to other modalities [862], [864], [865]. Factors that have been shown to affect ionisation include sprayer geometry, solvent composition, ion transfer and surface wettability, and modulating these parameters may help increase sensitivity [553], [556], [798], [866]. Furthermore, attributing metabolite identities to ions based on purely *m/z* values is problematic due to isobaric species, varied adduct formation and to a lesser extent in ambient metabolomics such as DESI, chemical fragmentation

[867]. Future method development strategies should focus on confirming ion annotations through the use of MS/MS and metabolite standards, which can be uniformly sprayed across a sample to investigate potential heterogeneous ion suppression effects of diverse biological tissues [868]–[870]. Developing reliable ion annotation strategies is particularly relevant in lipidomics studies, since many lipids share common fragments and identical chemical formulae.

It is important to note that the sheer volume of data generated from a single MSI experiment is profound, and while this work focuses on parallels between MSI and LC-MS findings, there remains a plethora of information that can be extracted from these datasets using multivariate data analysis approaches. Unlike LC- and GC-MS, MSI modalities are able to simultaneously extract spatial information of polar and lipid metabolites, providing a more thorough coverage of the sample metabolome. Current work in the field is advancing MSI data analysis pipelines and several MSI-specific databases for ion annotation have been curated [871]–[873].

8.4 Conclusion

In the scope of this work, I was able to establish novel methods for biological sample analysis by MSI, including detection of stable isotope labelled compounds. I have also highlight how MSI can be used to complement and enhance findings from traditional metabolomics techniques, and uncovered specific metabolic changes within the metastatic niche that may provide new targets for therapeutic intervention in treatment of metastatic breast cancer. While many challenges in biological analysis by MSI still remain, this work has advanced our understanding of metabolite coverage by MSI modalities, and provided novel insight into the distribution of these metabolites within heterogeneous biological samples. Further method development and biological metabolic studies continue in Professor Zoltan Takáts's and Professor Ian Gilmore's lab to advance the use of DESI-MSI and OrbiSIMS modalities for cancer research. In future work, I and others in Dr. Mariia Yuneva's lab will pursue the role of increased methylation capacity via SAM in lung metastases originating from MYC-driven mammary gland tumours. We aim to identify the enzymes and methylation targets that are involved in the metabolic regulation of metastasis in this model, with the overarching aim of identifying a potential therapeutic target that can mediate a reduction in metastasis tumour incidence and growth. Furthermore, the role of FASN and lipid biosynthesis upregulation in the metastatic lung is another exciting avenue for further investigation.

References

[1] H. Sung *et al.*, 'Global cancer statistics 2020: GLOBOCAN estimates of incidence and mortality worldwide for 36 cancers in 185 countries', *CA: A Cancer Journal for Clinicians*, vol. n/a, no. n/a, doi: https://doi.org/10.3322/caac.21660.

[2] C. R. Smittenaar, K. A. Petersen, K. Stewart, and N. Moitt, 'Cancer incidence and mortality projections in the UK until 2035', *Br J Cancer*, vol. 115, no. 9, pp. 1147–1155, Oct. 2016, doi: 10.1038/bjc.2016.304.

[3] D. Hanahan and R. A. Weinberg, 'The hallmarks of cancer', *Cell*, vol. 100, no. 1, pp. 57–70, Jan. 2000, doi: 10.1016/s0092-8674(00)81683-9.

[4] D. Hanahan and R. A. Weinberg, 'Hallmarks of cancer: the next generation', *Cell*, vol. 144, no. 5, pp. 646–674, Mar. 2011, doi: 10.1016/j.cell.2011.02.013.

[5] D. L. Burkhart and J. Sage, 'Cellular mechanisms of tumour suppression by the retinoblastoma gene', *Nat Rev Cancer*, vol. 8, no. 9, pp. 671–682, Sep. 2008, doi: 10.1038/nrc2399.

[6] L. K. Boroughs and R. J. DeBerardinis, 'Metabolic pathways promoting cancer cell survival and growth', *Nat Cell Biol*, vol. 17, no. 4, pp. 351–359, Apr. 2015, doi: 10.1038/ncb3124.

[7] V. Fritz and L. Fajas, 'Metabolism and proliferation share common regulatory pathways in cancer cells', *Oncogene*, vol. 29, no. 31, Art. no. 31, Aug. 2010, doi: 10.1038/onc.2010.182.

[8] M. A. Keibler, T. M. Wasylenko, J. K. Kelleher, O. Iliopoulos, M. G. Vander Heiden, and G. Stephanopoulos, 'Metabolic requirements for cancer cell proliferation', *Cancer & Metabolism*, vol. 4, no. 1, p. 16, Aug. 2016, doi: 10.1186/s40170-016-0156-6.

[9] V. R. Muthukkaruppan, L. Kubai, and R. Auerbach, 'Tumor-induced neovascularization in the mouse eye', *J Natl Cancer Inst*, vol. 69, no. 3, pp. 699–708, Sep. 1982.

[10] B. Cruys *et al.*, 'Glycolytic regulation of cell rearrangement in angiogenesis', *Nat Commun*, vol. 7, p. 12240, Jul. 2016, doi: 10.1038/ncomms12240.

[11] H. Huang *et al.*, 'Role of glutamine and interlinked asparagine metabolism in vessel formation', *EMBO J*, vol. 36, no. 16, pp. 2334–2352, Aug. 2017, doi: 10.15252/embj.201695518.

[12] N. Draoui, P. de Zeeuw, and P. Carmeliet, 'Angiogenesis revisited from a metabolic perspective: role and therapeutic implications of endothelial cell metabolism', *Open Biol*, vol. 7, no. 12, Dec. 2017, doi: 10.1098/rsob.170219.

[13] A. Méndez-Lucas *et al.*, 'Identifying strategies to target the metabolic flexibility of tumours', *Nat Metab*, vol. 2, no. 4, pp. 335–350, Apr. 2020, doi: 10.1038/s42255-020-0195-8.

[14] K. S. Albain *et al.*, 'Gemcitabine plus Paclitaxel versus Paclitaxel monotherapy in patients with metastatic breast cancer and prior anthracycline treatment', *J Clin Oncol*, vol. 26, no. 24, pp. 3950–3957, Aug. 2008, doi: 10.1200/JCO.2007.11.9362.

[15] T. A. Yap, A. Omlin, and J. S. de Bono, 'Development of therapeutic combinations targeting major cancer signaling pathways', *J Clin Oncol*, vol. 31, no. 12, pp. 1592–1605, Apr. 2013, doi: 10.1200/JCO.2011.37.6418.

[16] I. Dagogo-Jack and A. T. Shaw, ‘Tumour heterogeneity and resistance to cancer therapies’, *Nat Rev Clin Oncol*, vol. 15, no. 2, pp. 81–94, Feb. 2018, doi: 10.1038/nrclinonc.2017.166.
[17] Z.-F. Lim and P. C. Ma, ‘Emerging insights of tumor heterogeneity and drug resistance mechanisms in lung cancer targeted therapy’, *J Hematol Oncol*, vol. 12, no. 1, p. 134, Dec. 2019, doi: 10.1186/s13045-019-0818-2.
[18] ‘Cancer statistics’, *World Cancer Research Fund*, Aug. 27, 2014. https://www.wcrf-uk.org/uk/preventing-cancer/cancer-preventability-statistics (accessed Mar. 25, 2021).
[19] ‘Breast cancer statistics’, *Cancer Research UK*, May 14, 2015. https://www.cancerresearchuk.org/health-professional/cancer-statistics/statistics-by-cancer-type/breast-cancer (accessed Mar. 25, 2021).
[20] ‘Survival for breast cancer | Breast Cancer | Cancer Research UK’. https://www.cancerresearchuk.org/about-cancer/breast-cancer/survival (accessed Mar. 25, 2021).
[21] E. Rivera and H. Gomez, ‘Chemotherapy resistance in metastatic breast cancer: the evolving role of ixabepilone’, *Breast Cancer Res*, vol. 12, no. Suppl 2, p. S2, 2010, doi: 10.1186/bcr2573.
[22] H. Peinado *et al.*, ‘Melanoma exosomes educate bone marrow progenitor cells toward a pro-metastatic phenotype through MET’, *Nature Medicine*, vol. 18, no. 6, Art. no. 6, Jun. 2012, doi: 10.1038/nm.2753.
[23] C. M. Perou *et al.*, ‘Molecular portraits of human breast tumours’, *Nature*, vol. 406, no. 6797, pp. 747–752, Aug. 2000, doi: 10.1038/35021093.
[24] X. Dai *et al.*, ‘Breast cancer intrinsic subtype classification, clinical use and future trends’, *Am J Cancer Res*, vol. 5, no. 10, pp. 2929–2943, Sep. 2015.
[25] R. Sandhu, J. S. Parker, W. D. Jones, C. A. Livasy, and W. B. Coleman, ‘Microarray-Based Gene Expression Profiling for Molecular Classification of Breast Cancer and Identification of New Targets for Therapy’, *Laboratory Medicine*, vol. 41, no. 6, pp. 364–372, Jun. 2010, doi: 10.1309/LMLIK0VIE3CJK0WD.
[26] O. Yersal and S. Barutca, ‘Biological subtypes of breast cancer: Prognostic and therapeutic implications’, *World J Clin Oncol*, vol. 5, no. 3, pp. 412–424, Aug. 2014, doi: 10.5306/wjco.v5.i3.412.
[27] N. Howlader, K. A. Cronin, A. W. Kurian, and R. Andridge, ‘Differences in Breast Cancer Survival by Molecular Subtypes in the United States’, *Cancer Epidemiol Biomarkers Prev*, vol. 27, no. 6, pp. 619–626, Jun. 2018, doi: 10.1158/1055-9965.EPI-17-0627.
[28] M. Smid *et al.*, ‘Subtypes of Breast Cancer Show Preferential Site of Relapse’, *Cancer Res*, vol. 68, no. 9, pp. 3108–3114, May 2008, doi: 10.1158/0008-5472.CAN-07-5644.
[29] M. C. U. Cheang *et al.*, ‘Ki67 index, HER2 status, and prognosis of patients with luminal B breast cancer’, *J Natl Cancer Inst*, vol. 101, no. 10, pp. 736–750, May 2009, doi: 10.1093/jnci/djp082.
[30] A. A. Hashmi *et al.*, ‘Ki67 index in intrinsic breast cancer subtypes and its association with prognostic parameters’, *BMC Res Notes*, vol. 12, Sep. 2019, doi: 10.1186/s13104-019-4653-x.
[31] J.-M. Tian, B. Ran, C.-L. Zhang, D.-M. Yan, and X.-H. LI, ‘Estrogen and progesterone promote breast cancer cell proliferation by inducing cyclin G1 expression’, *Braz J Med Biol Res*, vol. 51, no. 3, Mar. 2018, doi: 10.1590/1414-431X20175612.

[32] T. Holbro, R. R. Beerli, F. Maurer, M. Koziczak, C. F. Barbas, and N. E. Hynes, 'The ErbB2/ErbB3 heterodimer functions as an oncogenic unit: ErbB2 requires ErbB3 to drive breast tumor cell proliferation', *Proc Natl Acad Sci U S A*, vol. 100, no. 15, pp. 8933–8938, Jul. 2003, doi: 10.1073/pnas.1537685100.
[33] S. Oesterreich *et al.*, 'Estrogen-mediated down-regulation of E-cadherin in breast cancer cells', *Cancer Res*, vol. 63, no. 17, pp. 5203–5208, Sep. 2003.
[34] N. Fujita, D. L. Jaye, M. Kajita, C. Geigerman, C. S. Moreno, and P. A. Wade, 'MTA3, a Mi-2/NuRD complex subunit, regulates an invasive growth pathway in breast cancer', *Cell*, vol. 113, no. 2, pp. 207–219, Apr. 2003, doi: 10.1016/s0092-8674(03)00234-4.
[35] Y. Ye, Y. Xiao, W. Wang, K. Yearsley, J.-X. Gao, and S. H. Barsky, 'ERα suppresses slug expression directly by transcriptional repression', *Biochem J*, vol. 416, no. Pt 2, pp. 179–187, Dec. 2008, doi: 10.1042/BJ20080328.
[36] S. T. Bailey, H. Shin, T. Westerling, X. S. Liu, and M. Brown, 'Estrogen receptor prevents p53-dependent apoptosis in breast cancer', *Proceedings of the National Academy of Sciences*, vol. 109, no. 44, pp. 18060–18065, Oct. 2012, doi: 10.1073/pnas.1018858109.
[37] S. J. Han *et al.*, 'Estrogen Receptor β Modulates Apoptosis Complexes and the Inflammasome to Drive the Pathogenesis of Endometriosis', *Cell*, vol. 163, no. 4, pp. 960–974, Nov. 2015, doi: 10.1016/j.cell.2015.10.034.
[38] L. Björnström and M. Sjöberg, 'Mechanisms of Estrogen Receptor Signaling: Convergence of Genomic and Nongenomic Actions on Target Genes', *Molecular Endocrinology*, vol. 19, no. 4, pp. 833–842, Apr. 2005, doi: 10.1210/me.2004-0486.
[39] V. Craig Jordan, 'The role of tamoxifen in the treatment and prevention of breast cancer', *Current Problems in Cancer*, vol. 16, no. 3, pp. 134–176, May 1992, doi: 10.1016/0147-0272(92)90002-6.
[40] null Shagufta and I. Ahmad, 'Tamoxifen a pioneering drug: An update on the therapeutic potential of tamoxifen derivatives', *Eur J Med Chem*, vol. 143, pp. 515–531, Jan. 2018, doi: 10.1016/j.ejmech.2017.11.056.
[41] M. Fan, E. L. Rickert, L. Chen, S. A. Aftab, K. P. Nephew, and R. V. Weatherman, 'Characterization of molecular and structural determinants of selective estrogen receptor downregulators', *Breast Cancer Res Treat*, vol. 103, no. 1, pp. 37–44, May 2007, doi: 10.1007/s10549-006-9353-2.
[42] J. F. R. Robertson *et al.*, 'Fulvestrant versus anastrozole for the treatment of advanced breast carcinoma in postmenopausal women: a prospective combined analysis of two multicenter trials', *Cancer*, vol. 98, no. 2, pp. 229–238, Jul. 2003, doi: 10.1002/cncr.11468.
[43] M. A. Molina, J. Codony-Servat, J. Albanell, F. Rojo, J. Arribas, and J. Baselga, 'Trastuzumab (herceptin), a humanized anti-Her2 receptor monoclonal antibody, inhibits basal and activated Her2 ectodomain cleavage in breast cancer cells', *Cancer Res*, vol. 61, no. 12, pp. 4744–4749, Jun. 2001.
[44] D. Gajria and S. Chandarlapaty, 'HER2-amplified breast cancer: mechanisms of trastuzumab resistance and novel targeted therapies', *Expert Rev Anticancer Ther*, vol. 11, no. 2, pp. 263–275, Feb. 2011, doi: 10.1586/era.10.226.

[45] E. Senkus *et al.*, 'Primary breast cancer: ESMO Clinical Practice Guidelines for diagnosis, treatment and follow-up', *Ann Oncol*, vol. 26 Suppl 5, pp. v8-30, Sep. 2015, doi: 10.1093/annonc/mdv298.
[46] N. U. Lin *et al.*, 'Clinicopathologic features, patterns of recurrence, and survival among women with triple-negative breast cancer in the National Comprehensive Cancer Network', *Cancer*, vol. 118, no. 22, pp. 5463–5472, Nov. 2012, doi: 10.1002/cncr.27581.
[47] T. Sørlie *et al.*, 'Repeated observation of breast tumor subtypes in independent gene expression data sets', *PNAS*, vol. 100, no. 14, pp. 8418–8423, Jul. 2003, doi: 10.1073/pnas.0932692100.
[48] J. S. Parker *et al.*, 'Supervised Risk Predictor of Breast Cancer Based on Intrinsic Subtypes', *J Clin Oncol*, vol. 27, no. 8, pp. 1160–1167, Mar. 2009, doi: 10.1200/JCO.2008.18.1370.
[49] M. L. Gatza *et al.*, 'A pathway-based classification of human breast cancer', *PNAS*, vol. 107, no. 15, pp. 6994–6999, Apr. 2010, doi: 10.1073/pnas.0912708107.
[50] A. R. Green *et al.*, 'Identification of key clinical phenotypes of breast cancer using a reduced panel of protein biomarkers', *British Journal of Cancer*, vol. 109, no. 7, Art. no. 7, Oct. 2013, doi: 10.1038/bjc.2013.528.
[51] V. Cappelletti, E. Iorio, P. Miodini, M. Silvestri, M. Dugo, and M. G. Daidone, 'Metabolic Footprints and Molecular Subtypes in Breast Cancer', *Disease Markers*, vol. 2017, p. e7687851, Dec. 2017, doi: 10.1155/2017/7687851.
[52] Z. Wang *et al.*, 'Blocking autophagy enhanced cytotoxicity induced by recombinant human arginase in triple-negative breast cancer cells', *Cell Death Dis*, vol. 5, no. 12, p. e1563, Dec. 2014, doi: 10.1038/cddis.2014.503.
[53] S. Noh, D. H. Kim, W. H. Jung, and J. S. Koo, 'Expression levels of serine/glycine metabolism-related proteins in triple negative breast cancer tissues', *Tumour Biol*, vol. 35, no. 5, pp. 4457–4468, May 2014, doi: 10.1007/s13277-013-1588-z.
[54] E. Mullarky *et al.*, 'Identification of a small molecule inhibitor of 3-phosphoglycerate dehydrogenase to target serine biosynthesis in cancers', *Proc Natl Acad Sci U S A*, vol. 113, no. 7, pp. 1778–1783, Feb. 2016, doi: 10.1073/pnas.1521548113.
[55] X. Sun *et al.*, 'Metabolic Reprogramming in Triple-Negative Breast Cancer', *Front. Oncol.*, vol. 10, 2020, doi: 10.3389/fonc.2020.00428.
[56] M. E. Monaco, 'Fatty acid metabolism in breast cancer subtypes', *Oncotarget*, vol. 8, no. 17, pp. 29487–29500, Feb. 2017, doi: 10.18632/oncotarget.15494.
[57] J. Garcia-Bermudez, R. T. Williams, R. Guarecuco, and K. Birsoy, 'Targeting extracellular nutrient dependencies of cancer cells', *Molecular Metabolism*, vol. 33, pp. 67–82, Mar. 2020, doi: 10.1016/j.molmet.2019.11.011.
[58] M. G. Vander Heiden and R. J. DeBerardinis, 'Understanding the Intersections between Metabolism and Cancer Biology', *Cell*, vol. 168, no. 4, pp. 657–669, Feb. 2017, doi: 10.1016/j.cell.2016.12.039.
[59] F. Hillen and A. W. Griffioen, 'Tumour vascularization: sprouting angiogenesis and beyond', *Cancer Metastasis Rev*, vol. 26, no. 3–4, pp. 489–502, Dec. 2007, doi: 10.1007/s10555-007-9094-7.
[60] H. Saman, S. S. Raza, S. Uddin, and K. Rasul, 'Inducing Angiogenesis, a Key Step in Cancer Vascularization, and Treatment Approaches', *Cancers (Basel)*, vol. 12, no. 5, May 2020, doi: 10.3390/cancers12051172.

[61] J. Kim, P. Gao, Y.-C. Liu, G. L. Semenza, and C. V. Dang, 'Hypoxia-inducible factor 1 and dysregulated c-Myc cooperatively induce vascular endothelial growth factor and metabolic switches hexokinase 2 and pyruvate dehydrogenase kinase 1', *Mol Cell Biol*, vol. 27, no. 21, pp. 7381–7393, Nov. 2007, doi: 10.1128/MCB.00440-07.
[62] M. Wolff, F. K. Kosyna, J. Dunst, W. Jelkmann, and R. Depping, 'Impact of hypoxia inducible factors on estrogen receptor expression in breast cancer cells', *Archives of Biochemistry and Biophysics*, vol. 613, pp. 23–30, Jan. 2017, doi: 10.1016/j.abb.2016.11.002.
[63] S.-M. Fendt, C. Frezza, and A. Erez, 'Targeting metabolic plasticity and flexibility dynamics for cancer therapy', *Cancer Discov*, vol. 10, no. 12, pp. 1797–1807, Dec. 2020, doi: 10.1158/2159-8290.CD-20-0844.
[64] C. T. Hensley *et al.*, 'Metabolic Heterogeneity in Human Lung Tumors', *Cell*, vol. 164, no. 4, pp. 681–694, Feb. 2016, doi: 10.1016/j.cell.2015.12.034.
[65] S. M. Davidson *et al.*, 'Environment Impacts the Metabolic Dependencies of Ras-Driven Non-Small Cell Lung Cancer', *Cell Metab*, vol. 23, no. 3, pp. 517–528, Mar. 2016, doi: 10.1016/j.cmet.2016.01.007.
[66] S. Christen *et al.*, 'Breast Cancer-Derived Lung Metastases Show Increased Pyruvate Carboxylase-Dependent Anaplerosis', *Cell Reports*, vol. 17, no. 3, pp. 837–848, Oct. 2016, doi: 10.1016/j.celrep.2016.09.042.
[67] S. Andrzejewski *et al.*, 'PGC-1α Promotes Breast Cancer Metastasis and Confers Bioenergetic Flexibility against Metabolic Drugs', *Cell Metab*, vol. 26, no. 5, pp. 778-787.e5, Nov. 2017, doi: 10.1016/j.cmet.2017.09.006.
[68] F. Dupuy *et al.*, 'PDK1-Dependent Metabolic Reprogramming Dictates Metastatic Potential in Breast Cancer', *Cell Metabolism*, vol. 22, no. 4, pp. 577–589, Oct. 2015, doi: 10.1016/j.cmet.2015.08.007.
[69] D. Anastasiou *et al.*, 'Pyruvate kinase M2 activators promote tetramer formation and suppress tumorigenesis', *Nat Chem Biol*, vol. 8, no. 10, pp. 839–847, Oct. 2012, doi: 10.1038/nchembio.1060.
[70] D. Rohle *et al.*, 'An inhibitor of mutant IDH1 delays growth and promotes differentiation of glioma cells', *Science*, vol. 340, no. 6132, pp. 626–630, May 2013, doi: 10.1126/science.1236062.
[71] D. Zhang, J. Li, F. Wang, J. Hu, S. Wang, and Y. Sun, '2-Deoxy-D-glucose targeting of glucose metabolism in cancer cells as a potential therapy', *Cancer Lett*, vol. 355, no. 2, pp. 176–183, Dec. 2014, doi: 10.1016/j.canlet.2014.09.003.
[72] M. I. Gross *et al.*, 'Antitumor activity of the glutaminase inhibitor CB-839 in triple-negative breast cancer', *Mol Cancer Ther*, vol. 13, no. 4, pp. 890–901, Apr. 2014, doi: 10.1158/1535-7163.MCT-13-0870.
[73] C. A. Klein, 'Parallel progression of primary tumours and metastases', *Nat Rev Cancer*, vol. 9, no. 4, pp. 302–312, Apr. 2009, doi: 10.1038/nrc2627.
[74] R. A. Cairns, I. S. Harris, and T. W. Mak, 'Regulation of cancer cell metabolism', *Nature Reviews Cancer*, vol. 11, no. 2, Art. no. 2, Feb. 2011, doi: 10.1038/nrc2981.
[75] M. O. Yuneva *et al.*, 'The metabolic profile of tumors depends on both the responsible genetic lesion and tissue type', *Cell Metab*, vol. 15, no. 2, pp. 157–170, Feb. 2012, doi: 10.1016/j.cmet.2011.12.015.
[76] E. Gaude and C. Frezza, 'Defects in mitochondrial metabolism and cancer', *Cancer Metab*, vol. 2, p. 10, 2014, doi: 10.1186/2049-3002-2-10.

[77] B. C. Bergman *et al.*, ‘Active muscle and whole body lactate kinetics after endurance training in men’, *J Appl Physiol (1985)*, vol. 87, no. 5, pp. 1684–1696, Nov. 1999, doi: 10.1152/jappl.1999.87.5.1684.
[78] C. B. Peek *et al.*, ‘Circadian Clock Interaction with HIF1α Mediates Oxygenic Metabolism and Anaerobic Glycolysis in Skeletal Muscle’, *Cell Metab*, vol. 25, no. 1, pp. 86–92, Jan. 2017, doi: 10.1016/j.cmet.2016.09.010.
[79] G. Mithieux, ‘New data and concepts on glutamine and glucose metabolism in the gut’, *Curr Opin Clin Nutr Metab Care*, vol. 4, no. 4, pp. 267–271, Jul. 2001, doi: 10.1097/00075197-200107000-00004.
[80] C. Granchi, S. Bertini, M. Macchia, and F. Minutolo, ‘Inhibitors of lactate dehydrogenase isoforms and their therapeutic potentials’, *Curr Med Chem*, vol. 17, no. 7, pp. 672–697, 2010, doi: 10.2174/092986710790416263.
[81] E. A. Melkonian and M. P. Schury, ‘Biochemistry, Anaerobic Glycolysis’, in *StatPearls*, Treasure Island (FL): StatPearls Publishing, 2021. Accessed: Apr. 11, 2021. [Online]. Available: http://www.ncbi.nlm.nih.gov/books/NBK546695/
[82] O. Warburg, F. Wind, and E. Negelein, ‘THE METABOLISM OF TUMORS IN THE BODY’, *J Gen Physiol*, vol. 8, no. 6, pp. 519–530, Mar. 1927, doi: 10.1085/jgp.8.6.519.
[83] E. Racker, ‘Bioenergetics and the problem of tumor growth’, *Am Sci*, vol. 60, no. 1, pp. 56–63, Feb. 1972.
[84] D.L. Nelson and M.M. Cox, *Lehninger principles of biochemistry.*, 7th ed. 2017.
[85] J. W. Locasale and L. C. Cantley, ‘Metabolic Flux and the Regulation of Mammalian Cell Growth’, *Cell Metabolism*, vol. 14, no. 4, pp. 443–451, Oct. 2011, doi: 10.1016/j.cmet.2011.07.014.
[86] A. A. Shestov *et al.*, ‘Quantitative determinants of aerobic glycolysis identify flux through the enzyme GAPDH as a limiting step’, *Elife*, vol. 3, Jul. 2014, doi: 10.7554/eLife.03342.
[87] P. Sonveaux *et al.*, ‘Targeting lactate-fueled respiration selectively kills hypoxic tumor cells in mice’, *J Clin Invest*, vol. 118, no. 12, pp. 3930–3942, Dec. 2008, doi: 10.1172/JCI36843.
[88] B. Faubert *et al.*, ‘Lactate Metabolism in Human Lung Tumors’, *Cell*, vol. 171, no. 2, pp. 358-371.e9, Oct. 2017, doi: 10.1016/j.cell.2017.09.019.
[89] K. G. de la Cruz-López, L. J. Castro-Muñoz, D. O. Reyes-Hernández, A. García-Carrancá, and J. Manzo-Merino, ‘Lactate in the Regulation of Tumor Microenvironment and Therapeutic Approaches’, *Front Oncol*, vol. 9, p. 1143, Nov. 2019, doi: 10.3389/fonc.2019.01143.
[90] S. Hui *et al.*, ‘Glucose feeds the TCA cycle via circulating lactate’, *Nature*, vol. 551, no. 7678, pp. 115–118, Nov. 2017, doi: 10.1038/nature24057.
[91] S. Liu, Z. Dai, D. E. Cooper, D. G. Kirsch, and J. W. Locasale, ‘Quantitative Analysis of the Physiological Contributions of Glucose to the TCA Cycle’, *Cell Metabolism*, vol. 32, no. 4, pp. 619-628.e21, Oct. 2020, doi: 10.1016/j.cmet.2020.09.005.
[92] T. Yamamoto *et al.*, ‘Over-expression of facilitative glucose transporter genes in human cancer’, *Biochem Biophys Res Commun*, vol. 170, no. 1, pp. 223–230, Jul. 1990, doi: 10.1016/0006-291x(90)91263-r.
[93] R. S. Brown and R. L. Wahl, ‘Overexpression of Glut-1 glucose transporter in human breast cancer. An immunohistochemical study’, *Cancer*, vol. 72, no.

10, pp. 2979–2985, Nov. 1993, doi: 10.1002/1097-0142(19931115)72:10<2979::aid-cncr2820721020>3.0.co;2-x.
[94] B. Thorens and M. Mueckler, ‘Glucose transporters in the 21st Century’, *Am J Physiol Endocrinol Metab*, vol. 298, no. 2, pp. E141-145, Feb. 2010, doi: 10.1152/ajpendo.00712.2009.
[95] C. Spick, K. Herrmann, and J. Czernin, ‘18F-FDG PET/CT and PET/MRI Perform Equally Well in Cancer: Evidence from Studies on More Than 2,300 Patients’, *J Nucl Med*, vol. 57, no. 3, pp. 420–430, Mar. 2016, doi: 10.2967/jnumed.115.158808.
[96] M. G. Vander Heiden, L. C. Cantley, and C. B. Thompson, ‘Understanding the Warburg Effect: The Metabolic Requirements of Cell Proliferation’, *Science*, vol. 324, no. 5930, pp. 1029–1033, May 2009, doi: 10.1126/science.1160809.
[97] I. San-Millán and G. A. Brooks, ‘Reexamining cancer metabolism: lactate production for carcinogenesis could be the purpose and explanation of the Warburg Effect’, *Carcinogenesis*, vol. 38, no. 2, pp. 119–133, Feb. 2017, doi: 10.1093/carcin/bgw127.
[98] V. Estrella *et al.*, ‘Acidity generated by the tumor microenvironment drives local invasion’, *Cancer Res*, vol. 73, no. 5, pp. 1524–1535, Mar. 2013, doi: 10.1158/0008-5472.CAN-12-2796.
[99] C. Ward *et al.*, ‘The impact of tumour pH on cancer progression: strategies for clinical intervention’, *Explor Target Antitumor Ther.*, vol. 1, no. 2, pp. 71–100, Apr. 2020, doi: 10.37349/etat.2020.00005.
[100] Y. Kato *et al.*, ‘Acidic extracellular pH increases calcium influx-triggered phospholipase D activity along with acidic sphingomyelinase activation to induce matrix metalloproteinase-9 expression in mouse metastatic melanoma’, *The FEBS Journal*, vol. 274, no. 12, pp. 3171–3183, 2007, doi: https://doi.org/10.1111/j.1742-4658.2007.05848.x.
[101] D. Fukumura, L. Xu, Y. Chen, T. Gohongi, B. Seed, and R. K. Jain, ‘Hypoxia and acidosis independently up-regulate vascular endothelial growth factor transcription in brain tumors in vivo’, *Cancer Res*, vol. 61, no. 16, pp. 6020–6024, Aug. 2001.
[102] S. Beckert *et al.*, ‘Lactate stimulates endothelial cell migration’, *Wound Repair Regen*, vol. 14, no. 3, pp. 321–324, Jun. 2006, doi: 10.1111/j.1743-6109.2006.00127.x.
[103] A. Calcinotto *et al.*, ‘Modulation of microenvironment acidity reverses anergy in human and murine tumor-infiltrating T lymphocytes’, *Cancer Res*, vol. 72, no. 11, pp. 2746–2756, Jun. 2012, doi: 10.1158/0008-5472.CAN-11-1272.
[104] M. Bellone, A. Calcinotto, P. Filipazzi, A. De Milito, S. Fais, and L. Rivoltini, ‘The acidity of the tumor microenvironment is a mechanism of immune escape that can be overcome by proton pump inhibitors’, *Oncoimmunology*, vol. 2, no. 1, Jan. 2013, doi: 10.4161/onci.22058.
[105] A. El-Kenawi *et al.*, ‘Acidity promotes tumour progression by altering macrophage phenotype in prostate cancer’, *British Journal of Cancer*, vol. 121, no. 7, Art. no. 7, Oct. 2019, doi: 10.1038/s41416-019-0542-2.
[106] G.-Y. Liou and P. Storz, ‘Reactive oxygen species in cancer’, *Free Radic Res*, vol. 44, no. 5, May 2010, doi: 10.3109/10715761003667554.
[107] H.-Q. Ju, J.-F. Lin, T. Tian, D. Xie, and R.-H. Xu, ‘NADPH homeostasis in cancer: functions, mechanisms and therapeutic implications’, *Signal*

Transduct Target Ther, vol. 5, no. 1, p. 231, Oct. 2020, doi: 10.1038/s41392-020-00326-0.
[108] D. Han, E. Williams, and E. Cadenas, 'Mitochondrial respiratory chain-dependent generation of superoxide anion and its release into the intermembrane space', *Biochem J*, vol. 353, no. Pt 2, pp. 411–416, Jan. 2001, doi: 10.1042/0264-6021:3530411.
[109] J. F. Turrens, 'Mitochondrial formation of reactive oxygen species', *J Physiol*, vol. 552, no. Pt 2, pp. 335–344, Oct. 2003, doi: 10.1113/jphysiol.2003.049478.
[110] M. Ushio-Fukai and Y. Nakamura, 'Reactive Oxygen Species and Angiogenesis: NADPH Oxidase as Target for Cancer Therapy', *Cancer Lett*, vol. 266, no. 1, pp. 37–52, Jul. 2008, doi: 10.1016/j.canlet.2008.02.044.
[111] A. Guerra-Castellano *et al.*, 'Oxidative stress is tightly regulated by cytochrome c phosphorylation and respirasome factors in mitochondria', *PNAS*, vol. 115, no. 31, pp. 7955–7960, Jul. 2018, doi: 10.1073/pnas.1806833115.
[112] R.-Z. Zhao, S. Jiang, L. Zhang, and Z.-B. Yu, 'Mitochondrial electron transport chain, ROS generation and uncoupling (Review)', *International Journal of Molecular Medicine*, vol. 44, no. 1, pp. 3–15, Jul. 2019, doi: 10.3892/ijmm.2019.4188.
[113] E. Przybytkowski and D. A. Averill-Bates, 'Correlation between glutathione and stimulation of the pentose phosphate cycle in situ in Chinese hamster ovary cells exposed to hydrogen peroxide', *Arch Biochem Biophys*, vol. 325, no. 1, pp. 91–98, Jan. 1996, doi: 10.1006/abbi.1996.0011.
[114] N. S. Brown and R. Bicknell, 'Hypoxia and oxidative stress in breast cancer. Oxidative stress: its effects on the growth, metastatic potential and response to therapy of breast cancer', *Breast Cancer Res*, vol. 3, no. 5, pp. 323–327, 2001, doi: 10.1186/bcr315.
[115] C.-L. Liu *et al.*, 'Targeting the pentose phosphate pathway increases reactive oxygen species and induces apoptosis in thyroid cancer cells', *Mol Cell Endocrinol*, vol. 499, p. 110595, Jan. 2020, doi: 10.1016/j.mce.2019.110595.
[116] Z. T. Schafer *et al.*, 'Antioxidant and oncogene rescue of metabolic defects caused by loss of matrix attachment', *Nature*, vol. 461, no. 7260, Art. no. 7260, Sep. 2009, doi: 10.1038/nature08268.
[117] J. Yu *et al.*, 'Snail Enhances Glycolysis in the Epithelial-Mesenchymal Transition Process by Targeting FBP1 in Gastric Cancer', *Cell Physiol Biochem*, vol. 43, no. 1, pp. 31–38, 2017, doi: 10.1159/000480314.
[118] L. J. Reitzer, B. M. Wice, and D. Kennell, 'Evidence that glutamine, not sugar, is the major energy source for cultured HeLa cells', *J Biol Chem*, vol. 254, no. 8, pp. 2669–2676, Apr. 1979.
[119] R. J. DeBerardinis *et al.*, 'Beyond aerobic glycolysis: transformed cells can engage in glutamine metabolism that exceeds the requirement for protein and nucleotide synthesis', *Proc Natl Acad Sci U S A*, vol. 104, no. 49, pp. 19345–19350, Dec. 2007, doi: 10.1073/pnas.0709747104.
[120] D. R. Wise *et al.*, 'Myc regulates a transcriptional program that stimulates mitochondrial glutaminolysis and leads to glutamine addiction', *PNAS*, vol. 105, no. 48, pp. 18782–18787, Dec. 2008, doi: 10.1073/pnas.0810199105.
[121] T. Migita *et al.*, 'ATP citrate lyase: activation and therapeutic implications in non-small cell lung cancer', *Cancer Res*, vol. 68, no. 20, pp. 8547–8554, Oct. 2008, doi: 10.1158/0008-5472.CAN-08-1235.

[122] A. Carracedo, L. C. Cantley, and P. P. Pandolfi, ‘Cancer metabolism: fatty acid oxidation in the limelight’, *Nat Rev Cancer*, vol. 13, no. 4, pp. 227–232, Apr. 2013, doi: 10.1038/nrc3483.
[123] N. Koundouros and G. Poulogiannis, ‘Reprogramming of fatty acid metabolism in cancer’, *British Journal of Cancer*, vol. 122, no. 1, Art. no. 1, Jan. 2020, doi: 10.1038/s41416-019-0650-z.
[124] J. M. Berg, J. L. Tymoczko, and L. Stryer, ‘Amino Acids Are Made from Intermediates of the Citric Acid Cycle and Other Major Pathways’, *Biochemistry. 5th edition*, 2002, Accessed: Apr. 13, 2021. [Online]. Available: https://www.ncbi.nlm.nih.gov/books/NBK22459/
[125] B.-H. Choi and J. L. Coloff, ‘The Diverse Functions of Non-Essential Amino Acids in Cancer’, *Cancers (Basel)*, vol. 11, no. 5, May 2019, doi: 10.3390/cancers11050675.
[126] Y. W. Yap *et al.*, ‘Restriction of essential amino acids dictates the systemic metabolic response to dietary protein dilution’, *Nature Communications*, vol. 11, no. 1, Art. no. 1, Jun. 2020, doi: 10.1038/s41467-020-16568-z.
[127] M. Yue, J. Jiang, P. Gao, H. Liu, and G. Qing, ‘Oncogenic MYC Activates a Feedforward Regulatory Loop Promoting Essential Amino Acid Metabolism and Tumorigenesis’, *Cell Rep*, vol. 21, no. 13, pp. 3819–3832, Dec. 2017, doi: 10.1016/j.celrep.2017.12.002.
[128] A. Hattori *et al.*, ‘Cancer progression by reprogrammed BCAA metabolism in myeloid leukaemia’, *Nature*, vol. 545, no. 7655, pp. 500–504, May 2017, doi: 10.1038/nature22314.
[129] J. M. Thornburg *et al.*, ‘Targeting aspartate aminotransferase in breast cancer’, *Breast Cancer Research*, vol. 10, no. 5, p. R84, Oct. 2008, doi: 10.1186/bcr2154.
[130] W. Liu *et al.*, ‘Reprogramming of proline and glutamine metabolism contributes to the proliferative and metabolic responses regulated by oncogenic transcription factor c-MYC’, *PNAS*, vol. 109, no. 23, pp. 8983–8988, Jun. 2012, doi: 10.1073/pnas.1203244109.
[131] S. Sookoian and C. J. Pirola, ‘Alanine and aspartate aminotransferase and glutamine-cycling pathway: Their roles in pathogenesis of metabolic syndrome’, *World J Gastroenterol*, vol. 18, no. 29, pp. 3775–3781, Aug. 2012, doi: 10.3748/wjg.v18.i29.3775.
[132] B. Ratnikov, P. Aza-Blanc, Z. A. Ronai, J. W. Smith, A. L. Osterman, and D. A. Scott, ‘Glutamate and asparagine cataplerosis underlie glutamine addiction in melanoma’, *Oncotarget*, vol. 6, no. 10, pp. 7379–7389, Feb. 2015.
[133] N. M. Anderson, P. Mucka, J. G. Kern, and H. Feng, ‘The emerging role and targetability of the TCA cycle in cancer metabolism’, *Protein Cell*, vol. 9, no. 2, pp. 216–237, Feb. 2018, doi: 10.1007/s13238-017-0451-1.
[134] C. Quijano, M. Trujillo, L. Castro, and A. Trostchansky, ‘Interplay between oxidant species and energy metabolism’, *Redox Biol*, vol. 8, pp. 28–42, Nov. 2015, doi: 10.1016/j.redox.2015.11.010.
[135] I. Martínez-Reyes and N. S. Chandel, ‘Mitochondrial TCA cycle metabolites control physiology and disease’, *Nature Communications*, vol. 11, no. 1, Art. no. 1, Jan. 2020, doi: 10.1038/s41467-019-13668-3.
[136] N. Burnichon *et al.*, ‘SDHA is a tumor suppressor gene causing paraganglioma’, *Hum Mol Genet*, vol. 19, no. 15, pp. 3011–3020, Aug. 2010, doi: 10.1093/hmg/ddq206.

[137] I. P. M. Tomlinson *et al.*, 'Germline mutations in FH predispose to dominantly inherited uterine fibroids, skin leiomyomata and papillary renal cell cancer', *Nat Genet*, vol. 30, no. 4, pp. 406–410, Apr. 2002, doi: 10.1038/ng849.
[138] L. Dang *et al.*, 'Cancer-associated IDH1 mutations produce 2-hydroxyglutarate', *Nature*, vol. 462, no. 7274, pp. 739–744, Dec. 2009, doi: 10.1038/nature08617.
[139] L. Chen *et al.*, 'Citrate synthase expression affects tumor phenotype and drug resistance in human ovarian carcinoma', *PLoS One*, vol. 9, no. 12, p. e115708, 2014, doi: 10.1371/journal.pone.0115708.
[140] M.-D. Wang *et al.*, 'Acetyl-coenzyme A carboxylase alpha promotion of glucose-mediated fatty acid synthesis enhances survival of hepatocellular carcinoma in mice and patients', *Hepatology*, vol. 63, no. 4, pp. 1272–1286, Apr. 2016, doi: 10.1002/hep.28415.
[141] A. V. Snezhkina *et al.*, 'Differential expression of alternatively spliced transcripts related to energy metabolism in colorectal cancer', *BMC Genomics*, vol. 17, no. Suppl 14, p. 1011, Dec. 2016, doi: 10.1186/s12864-016-3351-5.
[142] C. V. Dang, 'MYC, metabolism, cell growth, and tumorigenesis', *Cold Spring Harb Perspect Med*, vol. 3, no. 8, Aug. 2013, doi: 10.1101/cshperspect.a014217.
[143] A. J. Bott *et al.*, 'Oncogenic Myc induces expression of glutamine synthetase through promoter demethylation', *Cell Metab*, vol. 22, no. 6, pp. 1068–1077, Dec. 2015, doi: 10.1016/j.cmet.2015.09.025.
[144] L. R. Edmunds *et al.*, 'c-Myc programs fatty acid metabolism and dictates acetyl-CoA abundance and fate', *J Biol Chem*, vol. 290, no. 33, p. 20100, Aug. 2015, doi: 10.1074/jbc.A114.580662.
[145] J. Y. Guo *et al.*, 'Activated Ras requires autophagy to maintain oxidative metabolism and tumorigenesis', *Genes Dev*, vol. 25, no. 5, pp. 460–470, Mar. 2011, doi: 10.1101/gad.2016311.
[146] M. Saqcena, S. Mukhopadhyay, C. Hosny, A. Alhamed, A. Chatterjee, and D. A. Foster, 'Blocking anaplerotic entry of glutamine into the TCA cycle sensitizes K-Ras mutant cancer cells to cytotoxic drugs', *Oncogene*, vol. 34, no. 20, pp. 2672–2680, May 2015, doi: 10.1038/onc.2014.207.
[147] J. J. Kamphorst *et al.*, 'Human pancreatic cancer tumors are nutrient poor and tumor cells actively scavenge extracellular protein', *Cancer Res*, vol. 75, no. 3, pp. 544–553, Feb. 2015, doi: 10.1158/0008-5472.CAN-14-2211.
[148] J. Kim, I. Tchernyshyov, G. L. Semenza, and C. V. Dang, 'HIF-1-mediated expression of pyruvate dehydrogenase kinase: a metabolic switch required for cellular adaptation to hypoxia', *Cell Metab*, vol. 3, no. 3, pp. 177–185, Mar. 2006, doi: 10.1016/j.cmet.2006.02.002.
[149] P. A. Gameiro *et al.*, 'In vivo HIF-mediated reductive carboxylation is regulated by citrate levels and sensitizes VHL-deficient cells to glutamine deprivation', *Cell Metab*, vol. 17, no. 3, pp. 372–385, Mar. 2013, doi: 10.1016/j.cmet.2013.02.002.
[150] C. M. Metallo *et al.*, 'Reductive glutamine metabolism by IDH1 mediates lipogenesis under hypoxia', *Nature*, vol. 481, no. 7381, pp. 380–384, Nov. 2011, doi: 10.1038/nature10602.
[151] A. D. Marshall *et al.*, 'ASCT2 regulates glutamine uptake and cell growth in endometrial carcinoma', *Oncogenesis*, vol. 6, no. 7, Art. no. 7, Jul. 2017, doi: 10.1038/oncsis.2017.70.

[152] M. van Geldermalsen *et al.*, 'ASCT2/SLC1A5 controls glutamine uptake and tumour growth in triple-negative basal-like breast cancer', *Oncogene*, vol. 35, no. 24, pp. 3201–3208, Jun. 2016, doi: 10.1038/onc.2015.381.
[153] M. L. Schulte *et al.*, 'Pharmacological blockade of ASCT2-dependent glutamine transport leads to antitumor efficacy in preclinical models', *Nat Med*, vol. 24, no. 2, pp. 194–202, Feb. 2018, doi: 10.1038/nm.4464.
[154] X. Tong, F. Zhao, and C. B. Thompson, 'The molecular determinants of de novo nucleotide biosynthesis in cancer cells', *Curr Opin Genet Dev*, vol. 19, no. 1, pp. 32–37, Feb. 2009, doi: 10.1016/j.gde.2009.01.002.
[155] B. A. Moffatt and H. Ashihara, 'Purine and Pyrimidine Nucleotide Synthesis and Metabolism', *Arabidopsis Book*, vol. 1, Apr. 2002, doi: 10.1199/tab.0018.
[156] J. G. Moloughney *et al.*, 'mTORC2 Responds to Glutamine Catabolite Levels to Modulate the Hexosamine Biosynthesis Enzyme GFAT1', *Mol Cell*, vol. 63, no. 5, pp. 811–826, Sep. 2016, doi: 10.1016/j.molcel.2016.07.015.
[157] Y. Wang *et al.*, 'Coordinative metabolism of glutamine carbon and nitrogen in proliferating cancer cells under hypoxia', *Nature Communications*, vol. 10, no. 1, Art. no. 1, Jan. 2019, doi: 10.1038/s41467-018-08033-9.
[158] M. Meng, S. Chen, T. Lao, D. Liang, and N. Sang, 'Nitrogen anabolism underlies the importance of glutaminolysis in proliferating cells', *Cell Cycle*, vol. 9, no. 19, pp. 3921–3932, Oct. 2010, doi: 10.4161/cc.9.19.13139.
[159] L. B. Sullivan, D. Y. Gui, A. M. Hosios, L. N. Bush, E. Freinkman, and M. G. Vander Heiden, 'Supporting Aspartate Biosynthesis Is an Essential Function of Respiration in Proliferating Cells', *Cell*, vol. 162, no. 3, pp. 552–563, Jul. 2015, doi: 10.1016/j.cell.2015.07.017.
[160] M. M. Robinson *et al.*, 'Novel mechanism of inhibition of rat kidney-type glutaminase by bis-2-(5-phenylacetamido-1,2,4-thiadiazol-2-yl)ethyl sulfide (BPTES)', *Biochem J*, vol. 406, no. 3, pp. 407–414, Sep. 2007, doi: 10.1042/BJ20070039.
[161] J.-B. Wang *et al.*, 'Targeting mitochondrial glutaminase activity inhibits oncogenic transformation', *Cancer Cell*, vol. 18, no. 3, pp. 207–219, Sep. 2010, doi: 10.1016/j.ccr.2010.08.009.
[162] J. L. Coloff *et al.*, 'Differential Glutamate Metabolism in Proliferating and Quiescent Mammary Epithelial Cells', *Cell Metab*, vol. 23, no. 5, pp. 867–880, May 2016, doi: 10.1016/j.cmet.2016.03.016.
[163] A. K. Groen, H. J. Sips, R. C. Vervoorn, and J. M. Tager, 'Intracellular compartmentation and control of alanine metabolism in rat liver parenchymal cells', *Eur J Biochem*, vol. 122, no. 1, pp. 87–93, Feb. 1982, doi: 10.1111/j.1432-1033.1982.tb05851.x.
[164] C. M. Sousa *et al.*, 'Pancreatic stellate cells support tumour metabolism through autophagic alanine secretion', *Nature*, vol. 536, no. 7617, pp. 479–483, Aug. 2016, doi: 10.1038/nature19084.
[165] I. Elia *et al.*, 'Breast cancer cells rely on environmental pyruvate to shape the metastatic niche', *Nature*, vol. 568, no. 7750, pp. 117–121, Apr. 2019, doi: 10.1038/s41586-019-0977-x.
[166] J. S. Lee *et al.*, 'Urea Cycle Dysregulation Generates Clinically Relevant Genomic and Biochemical Signatures', *Cell*, vol. 174, no. 6, pp. 1559-1570.e22, Sep. 2018, doi: 10.1016/j.cell.2018.07.019.
[167] W. Barmore, F. Azad, and W. L. Stone, 'Physiology, Urea Cycle', in *StatPearls*, Treasure Island (FL): StatPearls Publishing, 2021. Accessed:

Oct. 05, 2021. [Online]. Available: http://www.ncbi.nlm.nih.gov/books/NBK513323/
[168] S. Matsumoto, J. Häberle, J. Kido, H. Mitsubuchi, F. Endo, and K. Nakamura, 'Urea cycle disorders—update', *J Hum Genet*, vol. 64, no. 9, pp. 833–847, Sep. 2019, doi: 10.1038/s10038-019-0614-4.
[169] R. Keshet, P. Szlosarek, A. Carracedo, and A. Erez, 'Rewiring urea cycle metabolism in cancer to support anabolism', *Nat Rev Cancer*, vol. 18, no. 10, pp. 634–645, Oct. 2018, doi: 10.1038/s41568-018-0054-z.
[170] S. Rabinovich *et al.*, 'Diversion of aspartate in ASS1-deficient tumours fosters de novo pyrimidine synthesis', *Nature*, vol. 527, no. 7578, pp. 379–383, Nov. 2015, doi: 10.1038/nature15529.
[171] M. Lu, L. Zhou, W. C. Stanley, M. E. Cabrera, G. M. Saidel, and X. Yu, 'Role of the Malate-Aspartate Shuttle on the Metabolic Response to Myocardial Ischemia', *J Theor Biol*, vol. 254, no. 2, pp. 466–475, Sep. 2008, doi: 10.1016/j.jtbi.2008.05.033.
[172] Z. Kovacević, 'Possibility for the transfer of reducing equivalents from the cytosol to the mitochondrial compartment in Ehrlich ascites tumor cells by the malate-aspartate shuttle', *Eur J Biochem*, vol. 25, no. 2, pp. 372–378, Feb. 1972, doi: 10.1111/j.1432-1033.1972.tb01706.x.
[173] H. Safer and J. R. Williamson, 'Functional significance of the malate-aspartate shuttle for the oxidation of cytoplasmic reducing equivalents in rat heart', *Recent Adv Stud Cardiac Struct Metab*, vol. 1, pp. 34–43, 1972.
[174] D. A. Kane, 'Lactate oxidation at the mitochondria: a lactate-malate-aspartate shuttle at work', *Frontiers in Neuroscience*, vol. 8, p. 366, 2014, doi: 10.3389/fnins.2014.00366.
[175] P. Borst, 'The malate-aspartate shuttle (Borst cycle): How it started and developed into a major metabolic pathway', *IUBMB Life*, vol. 72, no. 11, pp. 2241–2259, Nov. 2020, doi: 10.1002/iub.2367.
[176] H. Gu *et al.*, 'MDH1-mediated malate-aspartate NADH shuttle maintains the activity levels of fetal liver hematopoietic stem cells', *Blood*, vol. 136, no. 5, pp. 553–571, Jul. 2020, doi: 10.1182/blood.2019003940.
[177] A. S. Krall, S. Xu, T. G. Graeber, D. Braas, and H. R. Christofk, 'Asparagine promotes cancer cell proliferation through use as an amino acid exchange factor', *Nature Communications*, vol. 7, no. 1, Art. no. 1, Apr. 2016, doi: 10.1038/ncomms11457.
[178] K. Birsoy, T. Wang, W. W. Chen, E. Freinkman, M. Abu-Remaileh, and D. M. Sabatini, 'An Essential Role of the Mitochondrial Electron Transport Chain in Cell Proliferation Is to Enable Aspartate Synthesis', *Cell*, vol. 162, no. 3, pp. 540–551, Jul. 2015, doi: 10.1016/j.cell.2015.07.016.
[179] J. Garcia-Bermudez *et al.*, 'Aspartate is a limiting metabolite for cancer cell proliferation under hypoxia and in tumours', *Nature Cell Biology*, vol. 20, no. 7, Art. no. 7, Jul. 2018, doi: 10.1038/s41556-018-0118-z.
[180] S. M. Krane, 'The importance of proline residues in the structure, stability and susceptibility to proteolytic degradation of collagens', *Amino Acids*, vol. 35, no. 4, pp. 703–710, Nov. 2008, doi: 10.1007/s00726-008-0073-2.
[181] I. Elia *et al.*, 'Proline metabolism supports metastasis formation and could be inhibited to selectively target metastasizing cancer cells', *Nat Commun*, vol. 8, p. 15267, May 2017, doi: 10.1038/ncomms15267.
[182] W. Liu, K. Glunde, Z. M. Bhujwalla, V. Raman, A. Sharma, and J. M. Phang, 'Proline oxidase promotes tumor cell survival in hypoxic tumor

microenvironments', *Cancer Res*, vol. 72, no. 14, pp. 3677–3686, Jul. 2012, doi: 10.1158/0008-5472.CAN-12-0080.
[183] F. Loayza-Puch *et al.*, 'Tumour-specific proline vulnerability uncovered by differential ribosome codon reading', *Nature*, vol. 530, no. 7591, pp. 490–494, Feb. 2016, doi: 10.1038/nature16982.
[184] J. W. Locasale *et al.*, 'Phosphoglycerate dehydrogenase diverts glycolytic flux and contributes to oncogenesis', *Nat Genet*, vol. 43, no. 9, pp. 869–874, Jul. 2011, doi: 10.1038/ng.890.
[185] R. Possemato *et al.*, 'Functional genomics reveal that the serine synthesis pathway is essential in breast cancer', *Nature*, vol. 476, no. 7360, pp. 346–350, Aug. 2011, doi: 10.1038/nature10350.
[186] O. D. K. Maddocks *et al.*, 'Serine starvation induces stress and p53-dependent metabolic remodelling in cancer cells', *Nature*, vol. 493, no. 7433, pp. 542–546, Jan. 2013, doi: 10.1038/nature11743.
[187] J. Ding *et al.*, 'The histone H3 methyltransferase G9A epigenetically activates the serine-glycine synthesis pathway to sustain cancer cell survival and proliferation', *Cell Metab*, vol. 18, no. 6, pp. 896–907, Dec. 2013, doi: 10.1016/j.cmet.2013.11.004.
[188] J. Zhu *et al.*, 'High Expression of PHGDH Predicts Poor Prognosis in Non–Small Cell Lung Cancer', *Translational Oncology*, vol. 9, no. 6, pp. 592–599, Dec. 2016, doi: 10.1016/j.tranon.2016.08.003.
[189] Q. Wang *et al.*, 'Rational Design of Selective Allosteric Inhibitors of PHGDH and Serine Synthesis with Anti-tumor Activity', *Cell Chem Biol*, vol. 24, no. 1, pp. 55–65, Jan. 2017, doi: 10.1016/j.chembiol.2016.11.013.
[190] M. Tajan *et al.*, 'Serine synthesis pathway inhibition cooperates with dietary serine and glycine limitation for cancer therapy', *Nature Communications*, vol. 12, no. 1, Art. no. 1, Jan. 2021, doi: 10.1038/s41467-020-20223-y.
[191] B. Chaneton *et al.*, 'Serine is a natural ligand and allosteric activator of pyruvate kinase M2', *Nature*, vol. 491, no. 7424, pp. 458–462, Nov. 2012, doi: 10.1038/nature11540.
[192] M. A. Reid *et al.*, 'Serine synthesis through PHGDH coordinates nucleotide levels by maintaining central carbon metabolism', *Nature Communications*, vol. 9, no. 1, Art. no. 1, Dec. 2018, doi: 10.1038/s41467-018-07868-6.
[193] T. W. M. Fan *et al.*, 'De novo synthesis of serine and glycine fuels purine nucleotide biosynthesis in human lung cancer tissues', *J Biol Chem*, vol. 294, no. 36, pp. 13464–13477, Sep. 2019, doi: 10.1074/jbc.RA119.008743.
[194] X. Gao *et al.*, 'Serine Availability Influences Mitochondrial Dynamics and Function through Lipid Metabolism', *Cell Rep*, vol. 22, no. 13, pp. 3507–3520, Mar. 2018, doi: 10.1016/j.celrep.2018.03.017.
[195] A. A. for C. Research, 'Serine Restriction Alters Sphingolipid Synthesis to Lower Tumor Growth', *Cancer Discov*, vol. 10, no. 10, pp. 1440–1440, Oct. 2020, doi: 10.1158/2159-8290.CD-RW2020-121.
[196] L. E. S. Netto *et al.*, 'Reactive cysteine in proteins: Protein folding, antioxidant defense, redox signaling and more', *Comparative Biochemistry and Physiology Part C: Toxicology & Pharmacology*, vol. 146, no. 1, pp. 180–193, Jul. 2007, doi: 10.1016/j.cbpc.2006.07.014.
[197] N. Marino *et al.*, 'Upregulation of lipid metabolism genes in the breast prior to cancer diagnosis', *npj Breast Cancer*, vol. 6, no. 1, Art. no. 1, Oct. 2020, doi: 10.1038/s41523-020-00191-8.

[198] A. Meister and M. E. Anderson, ‘Glutathione’, *Annual Review of Biochemistry*, vol. 52, no. 1, pp. 711–760, 1983, doi: 10.1146/annurev.bi.52.070183.003431.
[199] A. Bansal and M. C. Simon, ‘Glutathione metabolism in cancer progression and treatment resistance’, *J Cell Biol*, vol. 217, no. 7, pp. 2291–2298, Jul. 2018, doi: 10.1083/jcb.201804161.
[200] H. Lv, C. Zhen, J. Liu, P. Yang, L. Hu, and P. Shang, ‘Unraveling the Potential Role of Glutathione in Multiple Forms of Cell Death in Cancer Therapy’, *Oxidative Medicine and Cellular Longevity*, vol. 2019, p. e3150145, Jun. 2019, doi: 10.1155/2019/3150145.
[201] S. L. Cramer *et al.*, ‘Systemic depletion of L-cyst(e)ine with cyst(e)inase increases reactive oxygen species and suppresses tumor growth’, *Nat Med*, vol. 23, no. 1, pp. 120–127, Jan. 2017, doi: 10.1038/nm.4232.
[202] L. A. Timmerman *et al.*, ‘Glutamine sensitivity analysis identifies the xCT antiporter as a common triple-negative breast tumor therapeutic target’, *Cancer Cell*, vol. 24, no. 4, pp. 450–465, Oct. 2013, doi: 10.1016/j.ccr.2013.08.020.
[203] P. Blume-Jensen and T. Hunter, ‘Oncogenic kinase signalling’, *Nature*, vol. 411, no. 6835, pp. 355–365, May 2001, doi: 10.1038/35077225.
[204] M. K. Paul and A. K. Mukhopadhyay, ‘Tyrosine kinase – Role and significance in Cancer’, *Int J Med Sci*, vol. 1, no. 2, pp. 101–115, Jun. 2004.
[205] Z. Wang *et al.*, ‘Mechanistic insights into the activation of oncogenic forms of EGF receptor’, *Nat Struct Mol Biol*, vol. 18, no. 12, pp. 1388–1393, Nov. 2011, doi: 10.1038/nsmb.2168.
[206] J. B. Casaletto and A. I. McClatchey, ‘Spatial regulation of receptor tyrosine kinases in development and cancer’, *Nat Rev Cancer*, vol. 12, no. 6, pp. 387–400, May 2012, doi: 10.1038/nrc3277.
[207] S. Medves and J.-B. Demoulin, ‘Tyrosine kinase gene fusions in cancer: translating mechanisms into targeted therapies’, *J Cell Mol Med*, vol. 16, no. 2, pp. 237–248, Feb. 2012, doi: 10.1111/j.1582-4934.2011.01415.x.
[208] H. Shigematsu *et al.*, ‘Clinical and biological features associated with epidermal growth factor receptor gene mutations in lung cancers’, *J Natl Cancer Inst*, vol. 97, no. 5, pp. 339–346, Mar. 2005, doi: 10.1093/jnci/dji055.
[209] C. A. Elstad and G. G. Meadows, ‘Modulation of B16-BL6 murine melanoma metastatic phenotype by tyrosine and phenylalanine restriction in the absence of host selection pressures’, *Anticancer Res*, vol. 13, no. 2, pp. 523–528, Apr. 1993.
[210] Y. M. Fu, Z. X. Yu, B. A. Pelayo, V. J. Ferrans, and G. G. Meadows, ‘Focal adhesion kinase-dependent apoptosis of melanoma induced by tyrosine and phenylalanine deficiency’, *Cancer Res*, vol. 59, no. 3, pp. 758–765, Feb. 1999.
[211] Y.-M. Fu *et al.*, ‘Specific amino acid dependency regulates invasiveness and viability of androgen-independent prostate cancer cells’, *Nutr Cancer*, vol. 45, no. 1, pp. 60–73, 2003, doi: 10.1207/S15327914NC4501_8.
[212] Y. Kanai, H. Segawa, K. i Miyamoto, H. Uchino, E. Takeda, and H. Endou, ‘Expression cloning and characterization of a transporter for large neutral amino acids activated by the heavy chain of 4F2 antigen (CD98)’, *J Biol Chem*, vol. 273, no. 37, pp. 23629–23632, Sep. 1998, doi: 10.1074/jbc.273.37.23629.

[213] C. Meier, Z. Ristic, S. Klauser, and F. Verrey, ‘Activation of system L heterodimeric amino acid exchangers by intracellular substrates’, *The EMBO Journal*, vol. 21, no. 4, pp. 580–589, Feb. 2002, doi: 10.1093/emboj/21.4.580.
[214] M. Scalise, M. Galluccio, L. Console, L. Pochini, and C. Indiveri, ‘The Human SLC7A5 (LAT1): The Intriguing Histidine/Large Neutral Amino Acid Transporter and Its Relevance to Human Health’, *Front. Chem.*, vol. 6, 2018, doi: 10.3389/fchem.2018.00243.
[215] B. C. Fuchs and B. P. Bode, ‘Amino acid transporters ASCT2 and LAT1 in cancer: Partners in crime?’, *Seminars in Cancer Biology*, vol. 15, no. 4, pp. 254–266, Aug. 2005, doi: 10.1016/j.semcancer.2005.04.005.
[216] K. Hayashi, P. Jutabha, H. Endou, and N. Anzai, ‘c-Myc is crucial for the expression of LAT1 in MIA Paca-2 human pancreatic cancer cells’, *Oncol Rep*, vol. 28, no. 3, pp. 862–866, Sep. 2012, doi: 10.3892/or.2012.1878.
[217] A. Elorza *et al.*, ‘HIF2α acts as an mTORC1 activator through the amino acid carrier SLC7A5’, *Mol Cell*, vol. 48, no. 5, pp. 681–691, Dec. 2012, doi: 10.1016/j.molcel.2012.09.017.
[218] Y. Onishi *et al.*, ‘Hypoxia affects Slc7a5 expression through HIF-2α in differentiated neuronal cells’, *FEBS Open Bio*, vol. 9, no. 2, pp. 241–247, Jan. 2019, doi: 10.1002/2211-5463.12559.
[219] K. M. Grzes, M. Swamy, J. L. Hukelmann, E. Emslie, L. V. Sinclair, and D. A. Cantrell, ‘Control of amino acid transport coordinates metabolic reprogramming in T-cell malignancy’, *Leukemia*, vol. 31, no. 12, pp. 2771–2779, Dec. 2017, doi: 10.1038/leu.2017.160.
[220] C. R. Green *et al.*, ‘Branched chain amino acid catabolism fuels adipocyte differentiation and lipogenesis’, *Nat Chem Biol*, vol. 12, no. 1, pp. 15–21, Jan. 2016, doi: 10.1038/nchembio.1961.
[221] M. D. Neinast *et al.*, ‘Quantitative Analysis of the Whole-Body Metabolic Fate of Branched-Chain Amino Acids’, *Cell Metab*, vol. 29, no. 2, pp. 417-429.e4, Feb. 2019, doi: 10.1016/j.cmet.2018.10.013.
[222] S. Sivanand and M. G. Vander Heiden, ‘Emerging Roles for Branched-Chain Amino Acid Metabolism in Cancer’, *Cancer Cell*, vol. 37, no. 2, pp. 147–156, Feb. 2020, doi: 10.1016/j.ccell.2019.12.011.
[223] W. Zhou *et al.*, ‘Over-expression of BCAT1, a c-Myc target gene, induces cell proliferation, migration and invasion in nasopharyngeal carcinoma’, *Mol Cancer*, vol. 12, p. 53, Jun. 2013, doi: 10.1186/1476-4598-12-53.
[224] M. Xu *et al.*, ‘BCAT1 promotes tumor cell migration and invasion in hepatocellular carcinoma’, *Oncology Letters*, vol. 12, no. 4, pp. 2648–2656, Oct. 2016, doi: 10.3892/ol.2016.4969.
[225] L. Zhang and J. Han, ‘Branched-chain amino acid transaminase 1 (BCAT1) promotes the growth of breast cancer cells through improving mTOR-mediated mitochondrial biogenesis and function’, *Biochem Biophys Res Commun*, vol. 486, no. 2, pp. 224–231, Apr. 2017, doi: 10.1016/j.bbrc.2017.02.101.
[226] Y. Xu *et al.*, ‘Overexpression of BCAT1 is a prognostic marker in gastric cancer’, *Hum Pathol*, vol. 75, pp. 41–46, May 2018, doi: 10.1016/j.humpath.2018.02.003.

[227] P. Häfliger and R.-P. Charles, 'The L-Type Amino Acid Transporter LAT1-An Emerging Target in Cancer', *Int J Mol Sci*, vol. 20, no. 10, May 2019, doi: 10.3390/ijms20102428.
[228] N. Singh and G. F. Ecker, 'Insights into the Structure, Function, and Ligand Discovery of the Large Neutral Amino Acid Transporter 1, LAT1', *Int J Mol Sci*, vol. 19, no. 5, Apr. 2018, doi: 10.3390/ijms19051278.
[229] M. Feng *et al.*, 'LAT2 regulates glutamine-dependent mTOR activation to promote glycolysis and chemoresistance in pancreatic cancer', *J Exp Clin Cancer Res*, vol. 37, no. 1, p. 274, Nov. 2018, doi: 10.1186/s13046-018-0947-4.
[230] J. M. Han *et al.*, 'Leucyl-tRNA synthetase is an intracellular leucine sensor for the mTORC1-signaling pathway', *Cell*, vol. 149, no. 2, pp. 410–424, Apr. 2012, doi: 10.1016/j.cell.2012.02.044.
[231] R. L. Wolfson *et al.*, 'Sestrin2 is a leucine sensor for the mTORC1 pathway', *Science*, vol. 351, no. 6268, pp. 43–48, Jan. 2016, doi: 10.1126/science.aab2674.
[232] S. M. Son *et al.*, 'Leucine Signals to mTORC1 via Its Metabolite Acetyl-Coenzyme A', *Cell Metab*, vol. 29, no. 1, pp. 192-201.e7, Jan. 2019, doi: 10.1016/j.cmet.2018.08.013.
[233] S.-C. Chuang *et al.*, 'Circulating Biomarkers of Tryptophan and the Kynurenine Pathway and Lung Cancer Risk', *Cancer Epidemiology*, p. 9.
[234] V. Audrito *et al.*, 'NAD-Biosynthetic and Consuming Enzymes as Central Players of Metabolic Regulation of Innate and Adaptive Immune Responses in Cancer', *Frontiers in Immunology*, vol. 10, Jul. 2019, doi: 10.3389/fimmu.2019.01720.
[235] B. Heng, C. K. Lim, D. B. Lovejoy, A. Bessede, L. Gluch, and G. J. Guillemin, 'Understanding the role of the kynurenine pathway in human breast cancer immunobiology', *Oncotarget*, vol. 7, no. 6, pp. 6506–6520, Dec. 2015, doi: 10.18632/oncotarget.6467.
[236] L. I. Greene *et al.*, 'A Role for Tryptophan-2,3-dioxygenase in CD8 T-cell Suppression and Evidence of Tryptophan Catabolism in Breast Cancer Patient Plasma', *Mol Cancer Res*, vol. 17, no. 1, pp. 131–139, Jan. 2019, doi: 10.1158/1541-7786.MCR-18-0362.
[237] B. Heng *et al.*, 'Differential kynurenine pathway metabolism in highly metastatic aggressive breast cancer subtypes: beyond IDO1-induced immunosuppression', *Breast Cancer Research*, vol. 22, no. 1, p. 113, Oct. 2020, doi: 10.1186/s13058-020-01351-1.
[238] N. Venkateswaran and M. Conacci-Sorrell, 'Kynurenine: an oncometabolite in colon cancer', *Cell Stress*, vol. 4, no. 1, p. 24, Jan. 2020, doi: 10.15698/cst2020.01.210.
[239] F. Sahm *et al.*, 'The endogenous tryptophan metabolite and NAD+ precursor quinolinic acid confers resistance of gliomas to oxidative stress', *Cancer Res*, vol. 73, no. 11, pp. 3225–3234, Jun. 2013, doi: 10.1158/0008-5472.CAN-12-3831.
[240] T. Sharif *et al.*, 'Regulation of Cancer and Cancer-Related Genes via NAD+', *Antioxidants & Redox Signaling*, vol. 30, no. 6, pp. 906–923, Jan. 2018, doi: 10.1089/ars.2017.7478.
[241] R. N. Freiman and R. Tjian, 'Regulating the Regulators: Lysine Modifications Make Their Mark', *Cell*, vol. 112, no. 1, pp. 11–17, Jan. 2003, doi: 10.1016/S0092-8674(02)01278-3.

[242] K. Hyun, J. Jeon, K. Park, and J. Kim, ‘Writing, erasing and reading histone lysine methylations’, *Exp Mol Med*, vol. 49, no. 4, p. e324, Apr. 2017, doi: 10.1038/emm.2017.11.
[243] J. McGrath and P. Trojer, ‘Targeting histone lysine methylation in cancer’, *Pharmacology & Therapeutics*, vol. 150, pp. 1–22, Jun. 2015, doi: 10.1016/j.pharmthera.2015.01.002.
[244] D. Han *et al.*, ‘Lysine methylation of transcription factors in cancer’, *Cell Death & Disease*, vol. 10, no. 4, Art. no. 4, Mar. 2019, doi: 10.1038/s41419-019-1524-2.
[245] Z. Wu *et al.*, ‘TPO-Induced Metabolic Reprogramming Drives Liver Metastasis of Colorectal Cancer CD110+ Tumor-Initiating Cells’, *Cell Stem Cell*, vol. 17, no. 1, pp. 47–59, Jul. 2015, doi: 10.1016/j.stem.2015.05.016.
[246] L. Chen *et al.*, ‘Pan-Cancer Analysis Reveals the Functional Importance of Protein Lysine Modification in Cancer Development’, *Front Genet*, vol. 9, Jul. 2018, doi: 10.3389/fgene.2018.00254.
[247] F. Papes, M. J. Surpili, F. Langone, J. R. Trigo, and P. Arruda, ‘The essential amino acid lysine acts as precursor of glutamate in the mammalian central nervous system’, *FEBS Letters*, vol. 488, no. 1, pp. 34–38, Jan. 2001, doi: 10.1016/S0014-5793(00)02401-7.
[248] P. Arruda and P. Barreto, ‘Lysine Catabolism Through the Saccharopine Pathway: Enzymes and Intermediates Involved in Plant Responses to Abiotic and Biotic Stress’, *Front Plant Sci*, vol. 11, May 2020, doi: 10.3389/fpls.2020.00587.
[249] J.-S. Kang, ‘Dietary restriction of amino acids for Cancer therapy’, *Nutr Metab (Lond)*, vol. 17, Mar. 2020, doi: 10.1186/s12986-020-00439-x.
[250] G. Vazquez Rodriguez, A. Abrahamsson, M. V. Turkina, and C. Dabrosin, ‘Lysine in Combination With Estradiol Promote Dissemination of Estrogen Receptor Positive Breast Cancer via Upregulation of U2AF1 and RPN2 Proteins’, *Front. Oncol.*, vol. 10, 2020, doi: 10.3389/fonc.2020.598684.
[251] N. Kanarek *et al.*, ‘Histidine catabolism is a major determinant of methotrexate sensitivity’, *Nature*, vol. 559, no. 7715, Art. no. 7715, Jul. 2018, doi: 10.1038/s41586-018-0316-7.
[252] F. Froldi *et al.*, ‘Histidine is selectively required for the growth of Myc-dependent dedifferentiation tumours in the Drosophila CNS’, *The EMBO Journal*, vol. 38, no. 7, p. e99895, Apr. 2019, doi: 10.15252/embj.201899895.
[253] W.-C. Lin, ‘Histidine-Dependent Protein Methylation Is Required for Compartmentalization of CTP Synthase’, p. 21.
[254] N. Shyh-Chang *et al.*, ‘Influence of threonine metabolism on S-adenosylmethionine and histone methylation’, *Science*, vol. 339, no. 6116, pp. 222–226, Jan. 2013, doi: 10.1126/science.1226603.
[255] J. Wang, P. Alexander, L. Wu, R. Hammer, O. Cleaver, and S. L. McKnight, ‘Dependence of mouse embryonic stem cells on threonine catabolism’, *Science*, vol. 325, no. 5939, pp. 435–439, Jul. 2009, doi: 10.1126/science.1173288.
[256] J. W. Locasale, ‘Serine, glycine and the one-carbon cycle: cancer metabolism in full circle’, *Nat Rev Cancer*, vol. 13, no. 8, pp. 572–583, Aug. 2013, doi: 10.1038/nrc3557.
[257] S. Farber and L. K. Diamond, ‘Temporary remissions in acute leukemia in children produced by folic acid antagonist, 4-aminopteroyl-glutamic acid’, *N*

Engl J Med, vol. 238, no. 23, pp. 787–793, Jun. 1948, doi: 10.1056/NEJM194806032382301.
[258] S. R. Davis *et al.*, 'Tracer-derived total and folate-dependent homocysteine remethylation and synthesis rates in humans indicate that serine is the main one-carbon donor', *Am J Physiol Endocrinol Metab*, vol. 286, no. 2, pp. E272-279, Feb. 2004, doi: 10.1152/ajpendo.00351.2003.
[259] W. C. Zhang *et al.*, 'Glycine decarboxylase activity drives non-small cell lung cancer tumor-initiating cells and tumorigenesis', *Cell*, vol. 148, no. 1–2, pp. 259–272, Jan. 2012, doi: 10.1016/j.cell.2011.11.050.
[260] G. Giardina *et al.*, 'The catalytic activity of serine hydroxymethyltransferase is essential for de novo nuclear dTMP synthesis in lung cancer cells', *The FEBS Journal*, vol. 285, no. 17, pp. 3238–3253, 2018, doi: https://doi.org/10.1111/febs.14610.
[261] A. S. Dekhne, Z. Hou, A. Gangjee, and L. H. Matherly, 'Therapeutic Targeting of Mitochondrial One-Carbon Metabolism in Cancer', *Mol Cancer Ther*, vol. 19, no. 11, pp. 2245–2255, Nov. 2020, doi: 10.1158/1535-7163.MCT-20-0423.
[262] K. Mahmood and A. Emadi, '1-C Metabolism—Serine, Glycine, Folates—In Acute Myeloid Leukemia', *Pharmaceuticals*, vol. 14, no. 3, Art. no. 3, Mar. 2021, doi: 10.3390/ph14030190.
[263] A. Vazquez, E. K. Markert, and Z. N. Oltvai, 'Serine biosynthesis with one carbon catabolism and the glycine cleavage system represents a novel pathway for ATP generation', *PLoS One*, vol. 6, no. 11, p. e25881, 2011, doi: 10.1371/journal.pone.0025881.
[264] P. M. Tedeschi *et al.*, 'Contribution of serine, folate and glycine metabolism to the ATP, NADPH and purine requirements of cancer cells', *Cell Death Dis*, vol. 4, p. e877, Oct. 2013, doi: 10.1038/cddis.2013.393.
[265] M. Yang and K. H. Vousden, 'Serine and one-carbon metabolism in cancer', *Nature Reviews Cancer*, vol. 16, no. 10, Art. no. 10, Oct. 2016, doi: 10.1038/nrc.2016.81.
[266] A.-W. Struck, M. L. Thompson, L. S. Wong, and J. Micklefield, 'S-Adenosyl-Methionine-Dependent Methyltransferases: Highly Versatile Enzymes in Biocatalysis, Biosynthesis and Other Biotechnological Applications', *ChemBioChem*, vol. 13, no. 18, pp. 2642–2655, 2012, doi: https://doi.org/10.1002/cbic.201200556.
[267] Q. Sun, M. Huang, and Y. Wei, 'Diversity of the reaction mechanisms of SAM-dependent enzymes', *Acta Pharmaceutica Sinica B*, vol. 11, no. 3, pp. 632–650, Mar. 2021, doi: 10.1016/j.apsb.2020.08.011.
[268] Y.-R. Lee, T.-S. Lin, S.-J. Lai, M.-S. Liu, M.-C. Lai, and N.-L. Chan, 'Structural Analysis of Glycine Sarcosine N-methyltransferase from Methanohalophilus portucalensis Reveals Mechanistic Insights into the Regulation of Methyltransferase Activity', *Scientific Reports*, vol. 6, no. 1, Art. no. 1, Dec. 2016, doi: 10.1038/srep38071.
[269] K. Soda, 'Polyamine Metabolism and Gene Methylation in Conjunction with One-Carbon Metabolism', *Int J Mol Sci*, vol. 19, no. 10, Oct. 2018, doi: 10.3390/ijms19103106.
[270] M. Sauter, B. Moffatt, M. C. Saechao, R. Hell, and M. Wirtz, 'Methionine salvage and S-adenosylmethionine: essential links between sulfur, ethylene and polyamine biosynthesis', *Biochem J*, vol. 451, no. 2, pp. 145–154, Apr. 2013, doi: 10.1042/BJ20121744.

[271] H. C. Affronti *et al.*, ‘Pharmacological polyamine catabolism upregulation with methionine salvage pathway inhibition as an effective prostate cancer therapy’, *Nature Communications*, vol. 11, no. 1, Art. no. 1, Jan. 2020, doi: 10.1038/s41467-019-13950-4.
[272] L. Frostesjö, I. Holm, B. Grahn, A. W. Page, T. H. Bestor, and O. Heby, ‘Interference with DNA methyltransferase activity and genome methylation during F9 teratocarcinoma stem cell differentiation induced by polyamine depletion’, *J Biol Chem*, vol. 272, no. 7, pp. 4359–4366, Feb. 1997, doi: 10.1074/jbc.272.7.4359.
[273] P. Ozfiliz *et al.*, ‘Bag-1 promotes cell survival through c-Myc-mediated ODC upregulation that is not preferred under apoptotic stimuli in MCF-7 cells’, *Cell Biochem Funct*, vol. 33, no. 5, pp. 293–307, Jul. 2015, doi: 10.1002/cbf.3114.
[274] D.-L. T. Koomoa *et al.*, ‘DFMO/eflornithine inhibits migration and invasion downstream of MYCN and involves p27Kip1 activity in neuroblastoma’, *Int J Oncol*, vol. 42, no. 4, pp. 1219–1228, Apr. 2013, doi: 10.3892/ijo.2013.1835.
[275] Y. Guo *et al.*, ‘Spermine synthase and MYC cooperate to maintain colorectal cancer cell survival by repressing Bim expression’, *Nature Communications*, vol. 11, no. 1, Art. no. 1, Jun. 2020, doi: 10.1038/s41467-020-17067-x.
[276] C. A. Elmets and M. Athar, ‘Targeting Ornithine Decarboxylase for the Prevention of Nonmelanoma Skin Cancer in Humans’, *Cancer Prev Res*, vol. 3, no. 1, pp. 8–11, Jan. 2010, doi: 10.1158/1940-6207.CAPR-09-0248.
[277] A. Manni, R. Grove, S. Kunselman, and M. Aldaz, ‘Involvement of the polyamine pathway in breast cancer progression’, *Cancer Letters*, vol. 92, no. 1, pp. 49–57, May 1995, doi: 10.1016/0304-3835(95)03763-M.
[278] J. R. J. Upp, R. Saydjari, C. M. J. Townsend, P. Singh, S. C. Barranco, and J. C. Thompson, ‘Polyamine Levels and Gastrin Receptors in Colon Cancers’, *Annals of Surgery*, vol. 207, no. 6, pp. 662–669, Jun. 1988.
[279] J. Li, Y. Meng, X. Wu, and Y. Sun, ‘Polyamines and related signaling pathways in cancer’, *Cancer Cell International*, vol. 20, no. 1, p. 539, Nov. 2020, doi: 10.1186/s12935-020-01545-9.
[280] S. Rimpi and J. A. Nilsson, ‘Metabolic enzymes regulated by the Myc oncogene are possible targets for chemotherapy or chemoprevention’, *Biochem Soc Trans*, vol. 35, no. Pt 2, pp. 305–310, Apr. 2007, doi: 10.1042/BST0350305.
[281] R. A. Casero, T. M. Stewart, and A. E. Pegg, ‘Polyamine metabolism and cancer: treatments, challenges and opportunities’, *Nat Rev Cancer*, vol. 18, no. 11, pp. 681–695, Nov. 2018, doi: 10.1038/s41568-018-0050-3.
[282] X. Gu *et al.*, ‘SAMTOR is an S-adenosylmethionine sensor for the mTORC1 pathway’, *Science*, vol. 358, no. 6364, pp. 813–818, Nov. 2017, doi: 10.1126/science.aao3265.
[283] R. J. Shaw, ‘GATORs Take a Bite Out of mTOR’, *Science*, vol. 340, no. 6136, pp. 1056–1057, May 2013, doi: 10.1126/science.1240315.
[284] R. A. Saxton and D. M. Sabatini, ‘mTOR Signaling in Growth, Metabolism, and Disease’, *Cell*, vol. 168, no. 6, pp. 960–976, Mar. 2017, doi: 10.1016/j.cell.2017.02.004.
[285] M. R. Sullivan *et al.*, ‘Quantification of microenvironmental metabolites in murine cancers reveals determinants of tumor nutrient availability’, *eLife*, vol. 8, p. e44235, Apr. 2019, doi: 10.7554/eLife.44235.
[286] J. Zhu, M. Berisa, S. Schwörer, W. Qin, J. R. Cross, and C. B. Thompson, ‘Transsulfuration activity can support cell growth upon extracellular cysteine

limitation', *Cell Metab*, vol. 30, no. 5, pp. 865-876.e5, Nov. 2019, doi: 10.1016/j.cmet.2019.09.009.
[287] N. Kaplowitz, T. Y. Aw, and M. Ookhtens, 'The regulation of hepatic glutathione', *Annu Rev Pharmacol Toxicol*, vol. 25, pp. 715–744, 1985, doi: 10.1146/annurev.pa.25.040185.003435.
[288] Y. C. Chai, S. S. Ashraf, K. Rokutan, R. B. Johnston, and J. A. Thomas, 'S-thiolation of individual human neutrophil proteins including actin by stimulation of the respiratory burst: evidence against a role for glutathione disulfide', *Arch Biochem Biophys*, vol. 310, no. 1, pp. 273–281, Apr. 1994, doi: 10.1006/abbi.1994.1167.
[289] O. ZITKA *et al.*, 'Redox status expressed as GSH:GSSG ratio as a marker for oxidative stress in paediatric tumour patients', *Oncol Lett*, vol. 4, no. 6, pp. 1247–1253, Dec. 2012, doi: 10.3892/ol.2012.931.
[290] M. P. Gamcsik, M. S. Kasibhatla, S. D. Teeter, and O. M. Colvin, 'Glutathione levels in human tumors', *Biomarkers*, vol. 17, no. 8, pp. 671–691, Dec. 2012, doi: 10.3109/1354750X.2012.715672.
[291] A. A. Hakimi *et al.*, 'An Integrated Metabolic Atlas of Clear Cell Renal Cell Carcinoma', *Cancer Cell*, vol. 29, no. 1, pp. 104–116, Jan. 2016, doi: 10.1016/j.ccell.2015.12.004.
[292] Z. Z. Huang *et al.*, 'Mechanism and significance of increased glutathione level in human hepatocellular carcinoma and liver regeneration', *FASEB J*, vol. 15, no. 1, pp. 19–21, Jan. 2001, doi: 10.1096/fj.00-0445fje.
[293] J. Carretero, E. Obrador, M. J. Anasagasti, J. J. Martin, F. Vidal-Vanaclocha, and J. M. Estrela, 'Growth-associated changes in glutathione content correlate with liver metastatic activity of B16 melanoma cells', *Clin Exp Metastasis*, vol. 17, no. 7, pp. 567–574, 1999, doi: 10.1023/a:1006725226078.
[294] E. H. Cheteh *et al.*, 'Human cancer-associated fibroblasts enhance glutathione levels and antagonize drug-induced prostate cancer cell death', *Cell Death & Disease*, vol. 8, no. 6, Art. no. 6, Jun. 2017, doi: 10.1038/cddis.2017.225.
[295] D. Khynriam and S. B. Prasad, 'Changes in endogenous tissue glutathione level in relation to murine ascites tumor growth and the anticancer activity of cisplatin', *Brazilian Journal of Medical and Biological Research*, vol. 36, no. 1, pp. 53–63, Jan. 2003, doi: 10.1590/S0100-879X2003000100008.
[296] D. B. Oien, J. Chien, and N. Cheng, 'Regulation of chemo-sensitivity in ovarian cancer via a stroma dependent glutathione pathway', *Translational Cancer Research*, vol. 3, no. 5, Sep. 2016, doi: 10.21037/9473.
[297] T. Bernig, S. Ritz, G. Brodt, I. Volkmer, and M. S. Staege, 'Glutathione-S-transferases and Chemotherapy Resistance of Hodgkin's Lymphoma Cell Lines', *Anticancer Research*, vol. 36, no. 8, pp. 3905–3915, Aug. 2016.
[298] A. D. Luca *et al.*, 'A structure-based mechanism of cisplatin resistance mediated by glutathione transferase P1-1', *PNAS*, vol. 116, no. 28, pp. 13943–13951, Jul. 2019, doi: 10.1073/pnas.1903297116.
[299] S. Arisawa *et al.*, 'Ursodeoxycholic acid induces glutathione synthesis through activation of PI3K/Akt pathway in HepG2 cells', *Biochem Pharmacol*, vol. 77, no. 5, pp. 858–866, Mar. 2009, doi: 10.1016/j.bcp.2008.11.012.
[300] B. Chen *et al.*, 'Glutathione Peroxidase 1 Promotes NSCLC Resistance to Cisplatin via ROS-Induced Activation of PI3K/AKT Pathway', *BioMed*

Research International, vol. 2019, p. e7640547, Mar. 2019, doi: 10.1155/2019/7640547.
[301] E. C. Lien *et al.*, 'Glutathione biosynthesis is a metabolic vulnerability in PI3K/Akt-driven breast cancer', *Nat Cell Biol*, vol. 18, no. 5, pp. 572–578, May 2016, doi: 10.1038/ncb3341.
[302] N. Koundouros and G. Poulogiannis, 'Phosphoinositide 3-Kinase/Akt Signaling and Redox Metabolism in Cancer', *Front. Oncol.*, vol. 8, 2018, doi: 10.3389/fonc.2018.00160.
[303] L. Wang *et al.*, 'A small molecule targeting glutathione activates Nrf2 and inhibits cancer cell growth through promoting Keap-1 S-glutathionylation and inducing apoptosis', *RSC Adv.*, vol. 8, no. 2, pp. 792–804, Jan. 2018, doi: 10.1039/C7RA11935F.
[304] M. M. Silva, C. R. R. Rocha, G. S. Kinker, A. L. Pelegrini, and C. F. M. Menck, 'The balance between NRF2/GSH antioxidant mediated pathway and DNA repair modulates cisplatin resistance in lung cancer cells', *Scientific Reports*, vol. 9, no. 1, Art. no. 1, Nov. 2019, doi: 10.1038/s41598-019-54065-6.
[305] K. Okazaki, T. Papagiannakopoulos, and H. Motohashi, 'Metabolic features of cancer cells in NRF2 addiction status', *Biophys Rev*, vol. 12, no. 2, pp. 435–441, Apr. 2020, doi: 10.1007/s12551-020-00659-8.
[306] M. Jaganjac, L. Milkovic, S. B. Sunjic, and N. Zarkovic, 'The NRF2, Thioredoxin, and Glutathione System in Tumorigenesis and Anticancer Therapies', *Antioxidants (Basel)*, vol. 9, no. 11, Nov. 2020, doi: 10.3390/antiox9111151.
[307] B. Anderton *et al.*, 'MYC-driven inhibition of the glutamate-cysteine ligase promotes glutathione depletion in liver cancer', *EMBO Rep*, vol. 18, no. 4, pp. 569–585, Apr. 2017, doi: 10.15252/embr.201643068.
[308] M. P. Murphy, 'How mitochondria produce reactive oxygen species', *Biochem J*, vol. 417, no. Pt 1, pp. 1–13, Jan. 2009, doi: 10.1042/BJ20081386.
[309] B. Chance, H. Sies, and A. Boveris, 'Hydroperoxide metabolism in mammalian organs', *Physiol Rev*, vol. 59, no. 3, pp. 527–605, Jul. 1979, doi: 10.1152/physrev.1979.59.3.527.
[310] M. Itsumi *et al.*, 'Idh1 protects murine hepatocytes from endotoxin-induced oxidative stress by regulating the intracellular NADP(+)/NADPH ratio', *Cell Death Differ*, vol. 22, no. 11, pp. 1837–1845, Nov. 2015, doi: 10.1038/cdd.2015.38.
[311] G. M. DeNicola *et al.*, 'Oncogene-induced Nrf2 transcription promotes ROS detoxification and tumorigenesis', *Nature*, vol. 475, no. 7354, pp. 106–109, Jul. 2011, doi: 10.1038/nature10189.
[312] I. S. Harris *et al.*, 'Glutathione and thioredoxin antioxidant pathways synergize to drive cancer initiation and progression', *Cancer Cell*, vol. 27, no. 2, pp. 211–222, Feb. 2015, doi: 10.1016/j.ccell.2014.11.019.
[313] E. C. Cheung *et al.*, 'Dynamic ROS Control by TIGAR Regulates the Initiation and Progression of Pancreatic Cancer', *Cancer Cell*, vol. 37, no. 2, pp. 168-182.e4, Feb. 2020, doi: 10.1016/j.ccell.2019.12.012.
[314] V. Aggarwal *et al.*, 'Role of Reactive Oxygen Species in Cancer Progression: Molecular Mechanisms and Recent Advancements', *Biomolecules*, vol. 9, no. 11, Nov. 2019, doi: 10.3390/biom9110735.
[315] K. K. Andringa *et al.*, 'Inhibition of glutamate cysteine ligase activity sensitizes human breast cancer cells to the toxicity of 2-deoxy-D-glucose',

Cancer Res, vol. 66, no. 3, pp. 1605–1610, Feb. 2006, doi: 10.1158/0008-5472.CAN-05-3462.
[316] B. Li *et al.*, 'Fructose-1,6-bisphosphatase opposes renal carcinoma progression', *Nature*, vol. 513, no. 7517, pp. 251–255, Sep. 2014, doi: 10.1038/nature13557.
[317] H.-L. Ke *et al.*, 'Genetic Variations in Glutathione Pathway Genes Predict Cancer Recurrence in Patients Treated with Transurethral Resection and Bacillus Calmette–Guerin Instillation for Non-muscle Invasive Bladder Cancer', *Ann Surg Oncol*, vol. 22, no. 12, pp. 4104–4110, Nov. 2015, doi: 10.1245/s10434-015-4431-5.
[318] S. Fujimori *et al.*, 'The subunits of glutamate cysteine ligase enhance cisplatin resistance in human non-small cell lung cancer xenografts in vivo', *Int J Oncol*, vol. 25, no. 2, pp. 413–418, Aug. 2004.
[319] M. Febbraio, D. P. Hajjar, and R. L. Silverstein, 'CD36: a class B scavenger receptor involved in angiogenesis, atherosclerosis, inflammation, and lipid metabolism', *J Clin Invest*, vol. 108, no. 6, pp. 785–791, Sep. 2001, doi: 10.1172/JCI14006.
[320] G. Carta, E. Murru, S. Banni, and C. Manca, 'Palmitic Acid: Physiological Role, Metabolism and Nutritional Implications', *Front. Physiol.*, vol. 8, 2017, doi: 10.3389/fphys.2017.00902.
[321] A. Carracedo *et al.*, 'A metabolic prosurvival role for PML in breast cancer', *J Clin Invest*, vol. 122, no. 9, pp. 3088–3100, Sep. 2012, doi: 10.1172/JCI62129.
[322] K. Zaugg *et al.*, 'Carnitine palmitoyltransferase 1C promotes cell survival and tumor growth under conditions of metabolic stress', *Genes Dev*, vol. 25, no. 10, pp. 1041–1051, May 2011, doi: 10.1101/gad.1987211.
[323] A. M. Johnson, E. K. Kleczko, and R. A. Nemenoff, 'Eicosanoids in Cancer: New Roles in Immunoregulation', *Front. Pharmacol.*, vol. 11, 2020, doi: 10.3389/fphar.2020.595498.
[324] D. Hwang, D. Scollard, J. Byrne, and E. Levine, 'Expression of cyclooxygenase-1 and cyclooxygenase-2 in human breast cancer', *J Natl Cancer Inst*, vol. 90, no. 6, pp. 455–460, Mar. 1998, doi: 10.1093/jnci/90.6.455.
[325] C. E. Eberhart, R. J. Coffey, A. Radhika, F. M. Giardiello, S. Ferrenbach, and R. N. DuBois, 'Up-regulation of cyclooxygenase 2 gene expression in human colorectal adenomas and adenocarcinomas', *Gastroenterology*, vol. 107, no. 4, pp. 1183–1188, Oct. 1994, doi: 10.1016/0016-5085(94)90246-1.
[326] H. Koga *et al.*, 'Expression of cyclooxygenase-2 in human hepatocellular carcinoma: relevance to tumor dedifferentiation', *Hepatology*, vol. 29, no. 3, pp. 688–696, Mar. 1999, doi: 10.1002/hep.510290355.
[327] O. N. Tucker *et al.*, 'Cyclooxygenase-2 expression is up-regulated in human pancreatic cancer', *Cancer Res*, vol. 59, no. 5, pp. 987–990, Mar. 1999.
[328] B. Liu, L. Qu, and S. Yan, 'Cyclooxygenase-2 promotes tumor growth and suppresses tumor immunity', *Cancer Cell International*, vol. 15, no. 1, p. 106, Nov. 2015, doi: 10.1186/s12935-015-0260-7.
[329] B. Xiong, T.-J. Sun, H.-Y. Yuan, M.-B. Hu, W.-D. Hu, and F.-L. Cheng, 'Cyclooxygenase-2 expression and angiogenesis in colorectal cancer', *World J Gastroenterol*, vol. 9, no. 6, pp. 1237–1240, Jun. 2003, doi: 10.3748/wjg.v9.i6.1237.

[330] F. P. Kuhajda *et al.*, ‘Fatty acid synthesis: a potential selective target for antineoplastic therapy’, *Proc Natl Acad Sci U S A*, vol. 91, no. 14, pp. 6379–6383, Jul. 1994, doi: 10.1073/pnas.91.14.6379.
[331] J. A. Menendez and R. Lupu, ‘Fatty acid synthase and the lipogenic phenotype in cancer pathogenesis’, *Nature Reviews Cancer*, vol. 7, no. 10, Art. no. 10, Oct. 2007, doi: 10.1038/nrc2222.
[332] R. Camarda *et al.*, ‘Inhibition of fatty acid oxidation as a therapy for MYC-overexpressing triple-negative breast cancer’, *Nat Med*, vol. 22, no. 4, pp. 427–432, Apr. 2016, doi: 10.1038/nm.4055.
[333] J. Jia *et al.*, ‘Pivotal Role of Fatty Acid Synthase in c-MYC Driven Hepatocarcinogenesis’, *Int J Mol Sci*, vol. 21, no. 22, Nov. 2020, doi: 10.3390/ijms21228467.
[334] J. C. Casciano *et al.*, ‘MYC regulates fatty acid metabolism through a multigenic program in claudin-low triple negative breast cancer’, *Br J Cancer*, vol. 122, no. 6, pp. 868–884, Mar. 2020, doi: 10.1038/s41416-019-0711-3.
[335] X. Zhong, Z. Liu, Q. Luo, J. Li, W. Zhang, and Y. Shuang, ‘Upregulation of fatty acid synthase in MYC and BCL-2 double-expressor lymphoma’, *Oncol Lett*, vol. 21, no. 4, Apr. 2021, doi: 10.3892/ol.2021.12506.
[336] A. M. Gouw *et al.*, ‘Oncogene KRAS activates fatty acid synthase, resulting in specific ERK and lipid signatures associated with lung adenocarcinoma’, *PNAS*, vol. 114, no. 17, pp. 4300–4305, Apr. 2017, doi: 10.1073/pnas.1617709114.
[337] A. Singh *et al.*, ‘De novo lipogenesis represents a therapeutic target in mutant Kras non-small cell lung cancer’, *FASEB J*, p. fj201800204, Jun. 2018, doi: 10.1096/fj.201800204.
[338] J. A. Menendez *et al.*, ‘Inhibition of fatty acid synthase (FAS) suppresses HER2/neu (erbB-2) oncogene overexpression in cancer cells’, *Proc Natl Acad Sci U S A*, vol. 101, no. 29, pp. 10715–10720, Jul. 2004, doi: 10.1073/pnas.0403390101.
[339] N. Li, X. Bu, P. Wu, P. Wu, and P. Huang, ‘The “HER2-PI3K/Akt-FASN Axis” regulated malignant phenotype of colorectal cancer cells’, *Lipids*, vol. 47, no. 4, pp. 403–411, Apr. 2012, doi: 10.1007/s11745-011-3649-7.
[340] R. Wagner *et al.*, ‘Multi-level suppression of receptor-PI3K-mTORC1 by fatty acid synthase inhibitors is crucial for their efficacy against ovarian cancer cells’, *Oncotarget*, vol. 8, no. 7, pp. 11600–11613, Feb. 2017, doi: 10.18632/oncotarget.14591.
[341] T. Porstmann *et al.*, ‘SREBP activity is regulated by mTORC1 and contributes to Akt-dependent cell growth’, *Cell Metab*, vol. 8, no. 3, pp. 224–236, Sep. 2008, doi: 10.1016/j.cmet.2008.07.007.
[342] Y. Y. Zaytseva *et al.*, ‘Increased expression of fatty acid synthase provides a survival advantage to colorectal cancer cells via upregulation of cellular respiration’, *Oncotarget*, vol. 6, no. 22, pp. 18891–18904, Aug. 2015, doi: 10.18632/oncotarget.3783.
[343] M. Chen and J. Huang, ‘The expanded role of fatty acid metabolism in cancer: new aspects and targets’, *Precis Clin Med*, vol. 2, no. 3, pp. 183–191, Sep. 2019, doi: 10.1093/pcmedi/pbz017.
[344] J. Duan, L. Sun, H. Huang, Z. Wu, L. Wang, and W. Liao, ‘Overexpression of fatty acid synthase predicts a poor prognosis for human gastric cancer’, *Mol Med Rep*, vol. 13, no. 4, pp. 3027–3035, Apr. 2016, doi: 10.3892/mmr.2016.4902.

[345] Z. Cao *et al.*, 'FASN Protein Overexpression Indicates Poor Biochemical Recurrence-Free Survival in Prostate Cancer', *Disease Markers*, vol. 2020, p. e3904947, Jun. 2020, doi: 10.1155/2020/3904947.
[346] S. Xu *et al.*, 'Fatty acid synthase promotes breast cancer metastasis by mediating changes in fatty acid metabolism', *Oncol Lett*, vol. 21, no. 1, Jan. 2021, doi: 10.3892/ol.2020.12288.
[347] L. Yao, X. Guo, and Y. Gui, 'Acetyl-CoA Synthetase 2 Promotes Cell Migration and Invasion of Renal Cell Carcinoma by Upregulating Lysosomal-Associated Membrane Protein 1 Expression', *CPB*, vol. 45, no. 3, pp. 984–992, 2018, doi: 10.1159/000487293.
[348] X. Yang *et al.*, 'Prognostic Impact of Metabolism Reprogramming Markers Acetyl-CoA Synthetase 2 Phosphorylation and Ketohexokinase-A Expression in Non-Small-Cell Lung Carcinoma', *Front. Oncol.*, vol. 9, 2019, doi: 10.3389/fonc.2019.01123.
[349] V. Bulusu *et al.*, 'Acetate Recapturing by Nuclear Acetyl-CoA Synthetase 2 Prevents Loss of Histone Acetylation during Oxygen and Serum Limitation', *Cell Rep*, vol. 18, no. 3, pp. 647–658, Jan. 2017, doi: 10.1016/j.celrep.2016.12.055.
[350] D. C. Berwick, I. Hers, K. J. Heesom, S. K. Moule, and J. M. Tavare, 'The identification of ATP-citrate lyase as a protein kinase B (Akt) substrate in primary adipocytes', *J Biol Chem*, vol. 277, no. 37, pp. 33895–33900, Sep. 2002, doi: 10.1074/jbc.M204681200.
[351] D. E. Bauer, G. Hatzivassiliou, F. Zhao, C. Andreadis, and C. B. Thompson, 'ATP citrate lyase is an important component of cell growth and transformation', *Oncogene*, vol. 24, no. 41, Art. no. 41, Sep. 2005, doi: 10.1038/sj.onc.1208773.
[352] G. Hatzivassiliou *et al.*, 'ATP citrate lyase inhibition can suppress tumor cell growth', *Cancer Cell*, vol. 8, no. 4, pp. 311–321, Oct. 2005, doi: 10.1016/j.ccr.2005.09.008.
[353] J. Wen *et al.*, 'ACLY facilitates colon cancer cell metastasis by CTNNB1', *Journal of Experimental & Clinical Cancer Research*, vol. 38, no. 1, p. 401, Sep. 2019, doi: 10.1186/s13046-019-1391-9.
[354] C. Granchi, 'ATP citrate lyase (ACLY) inhibitors: An anti-cancer strategy at the crossroads of glucose and lipid metabolism', *Eur J Med Chem*, vol. 157, pp. 1276–1291, Sep. 2018, doi: 10.1016/j.ejmech.2018.09.001.
[355] K. D. Miller *et al.*, 'Targeting ACSS2 with a Transition-State Mimetic Inhibits Triple-Negative Breast Cancer Growth', *Cancer Res*, vol. 81, no. 5, pp. 1252–1264, Mar. 2021, doi: 10.1158/0008-5472.CAN-20-1847.
[356] A. Nath, I. Li, L. R. Roberts, and C. Chan, 'Elevated free fatty acid uptake via CD36 promotes epithelial-mesenchymal transition in hepatocellular carcinoma', *Sci Rep*, vol. 5, p. 14752, Oct. 2015, doi: 10.1038/srep14752.
[357] J. Zhao *et al.*, 'Exogenous lipids promote the growth of breast cancer cells via CD36', *Oncol Rep*, vol. 38, no. 4, pp. 2105–2115, Oct. 2017, doi: 10.3892/or.2017.5864.
[358] G. Pascual *et al.*, 'Targeting metastasis-initiating cells through the fatty acid receptor CD36', *Nature*, vol. 541, no. 7635, pp. 41–45, Jan. 2017, doi: 10.1038/nature20791.
[359] A. Ladanyi *et al.*, 'Adipocyte-induced CD36 expression drives ovarian cancer progression and metastasis', *Oncogene*, vol. 37, no. 17, pp. 2285–2301, Apr. 2018, doi: 10.1038/s41388-017-0093-z.

[360] M. J. Watt *et al.*, ‘Suppressing fatty acid uptake has therapeutic effects in preclinical models of prostate cancer’, *Sci Transl Med*, vol. 11, no. 478, Feb. 2019, doi: 10.1126/scitranslmed.aau5758.
[361] C.-H. Yao *et al.*, ‘Exogenous Fatty Acids are the Preferred Source of Membrane Lipids in Proliferating Fibroblasts’, *Cell Chem Biol*, vol. 23, no. 4, pp. 483–493, Apr. 2016, doi: 10.1016/j.chembiol.2016.03.007.
[362] H. Wang *et al.*, ‘CD36-mediated metabolic adaptation supports regulatory T cell survival and function in tumors’, *Nature Immunology*, vol. 21, no. 3, Art. no. 3, Mar. 2020, doi: 10.1038/s41590-019-0589-5.
[363] K. Rabold *et al.*, ‘Enhanced lipid biosynthesis in human tumor-induced macrophages contributes to their protumoral characteristics’, *J Immunother Cancer*, vol. 8, no. 2, p. e000638, Sep. 2020, doi: 10.1136/jitc-2020-000638.
[364] J. Drury *et al.*, ‘Inhibition of Fatty Acid Synthase Upregulates Expression of CD36 to Sustain Proliferation of Colorectal Cancer Cells’, *Front Oncol*, vol. 10, Jul. 2020, doi: 10.3389/fonc.2020.01185.
[365] A. Nath and C. Chan, ‘Genetic alterations in fatty acid transport and metabolism genes are associated with metastatic progression and poor prognosis of human cancers’, *Sci Rep*, vol. 6, p. 18669, Jan. 2016, doi: 10.1038/srep18669.
[366] J. A. Olzmann and P. Carvalho, ‘Dynamics and functions of lipid droplets’, *Nat Rev Mol Cell Biol*, vol. 20, no. 3, pp. 137–155, Mar. 2019, doi: 10.1038/s41580-018-0085-z.
[367] A. Aiderus, M. A. Black, and A. K. Dunbier, ‘Fatty acid oxidation is associated with proliferation and prognosis in breast and other cancers’, *BMC Cancer*, vol. 18, no. 1, p. 805, Aug. 2018, doi: 10.1186/s12885-018-4626-9.
[368] D. Samovski *et al.*, ‘Regulation of AMPK activation by CD36 links fatty acid uptake to β-oxidation’, *Diabetes*, vol. 64, no. 2, pp. 353–359, Feb. 2015, doi: 10.2337/db14-0582.
[369] G. B. Mills and W. H. Moolenaar, ‘The emerging role of lysophosphatidic acid in cancer’, *Nat Rev Cancer*, vol. 3, no. 8, pp. 582–591, Aug. 2003, doi: 10.1038/nrc1143.
[370] S. Willier, E. Butt, and T. G. P. Grunewald, ‘Lysophosphatidic acid (LPA) signalling in cell migration and cancer invasion: a focussed review and analysis of LPA receptor gene expression on the basis of more than 1700 cancer microarrays’, *Biol Cell*, vol. 105, no. 8, pp. 317–333, Aug. 2013, doi: 10.1111/boc.201300011.
[371] V. Zuckerman *et al.*, ‘Expression and function of lysophosphatidic acid receptors (LPARs) 1 and 3 in human hepatic cancer progenitor cells’, *Oncotarget*, vol. 7, no. 3, pp. 2951–2967, Jan. 2016, doi: 10.18632/oncotarget.6696.
[372] Y. Xu, X. J. Fang, G. Casey, and G. B. Mills, ‘Lysophospholipids activate ovarian and breast cancer cells’, *Biochem J*, vol. 309 (Pt 3), pp. 933–940, Aug. 1995, doi: 10.1042/bj3090933.
[373] K. J. Jeong *et al.*, ‘The Rho/ROCK pathway for lysophosphatidic acid-induced proteolytic enzyme expression and ovarian cancer cell invasion’, *Oncogene*, vol. 31, no. 39, Art. no. 39, Sep. 2012, doi: 10.1038/onc.2011.595.
[374] E. K. Kim *et al.*, ‘Lysophosphatidic acid induces cell migration through the selective activation of Akt1’, *Exp Mol Med*, vol. 40, no. 4, pp. 445–452, Aug. 2008, doi: 10.3858/emm.2008.40.4.445.

[375] A. Toschi, E. Lee, L. Xu, A. Garcia, N. Gadir, and D. A. Foster, 'Regulation of mTORC1 and mTORC2 complex assembly by phosphatidic acid: competition with rapamycin', *Mol Cell Biol*, vol. 29, no. 6, pp. 1411–1420, Mar. 2009, doi: 10.1128/MCB.00782-08.
[376] M.-S. Yoon, Y. Sun, E. Arauz, Y. Jiang, and J. Chen, 'Phosphatidic acid activates mammalian target of rapamycin complex 1 (mTORC1) kinase by displacing FK506 binding protein 38 (FKBP38) and exerting an allosteric effect', *J Biol Chem*, vol. 286, no. 34, pp. 29568–29574, Aug. 2011, doi: 10.1074/jbc.M111.262816.
[377] M. A. Zhukovsky, A. Filograna, A. Luini, D. Corda, and C. Valente, 'Phosphatidic acid in membrane rearrangements', *FEBS Lett*, vol. 593, no. 17, pp. 2428–2451, Sep. 2019, doi: 10.1002/1873-3468.13563.
[378] R. Thakur, A. Naik, A. Panda, and P. Raghu, 'Regulation of Membrane Turnover by Phosphatidic Acid: Cellular Functions and Disease Implications', *Front. Cell Dev. Biol.*, vol. 7, 2019, doi: 10.3389/fcell.2019.00083.
[379] A. M. Gouw *et al.*, 'The MYC Oncogene Cooperates with Sterol-Regulated Element-Binding Protein to Regulate Lipogenesis Essential for Neoplastic Growth', *Cell Metab*, vol. 30, no. 3, pp. 556-572.e5, Sep. 2019, doi: 10.1016/j.cmet.2019.07.012.
[380] H.-M. Feng *et al.*, 'Expression and potential mechanism of metabolism-related genes and CRLS1 in non-small cell lung cancer', *Oncol Lett*, vol. 15, no. 2, pp. 2661–2668, Feb. 2018, doi: 10.3892/ol.2017.7591.
[381] M. Terao *et al.*, 'Role of mitochondria and cardiolipins in growth inhibition of breast cancer cells by retinoic acid', *J Exp Clin Cancer Res*, vol. 38, no. 1, p. 436, Oct. 2019, doi: 10.1186/s13046-019-1438-y.
[382] A. Sapandowski *et al.*, 'Cardiolipin composition correlates with prostate cancer cell proliferation', *Mol Cell Biochem*, vol. 410, no. 1–2, pp. 175–185, Dec. 2015, doi: 10.1007/s11010-015-2549-1.
[383] A. J. Chicco and G. C. Sparagna, 'Role of cardiolipin alterations in mitochondrial dysfunction and disease', *American Journal of Physiology-Cell Physiology*, vol. 292, no. 1, pp. C33–C44, Jan. 2007, doi: 10.1152/ajpcell.00243.2006.
[384] B. H. Falkenburger, J. B. Jensen, E. J. Dickson, B.-C. Suh, and B. Hille, 'Phosphoinositides: lipid regulators of membrane proteins', *J Physiol*, vol. 588, no. Pt 17, pp. 3179–3185, Sep. 2010, doi: 10.1113/jphysiol.2010.192153.
[385] Y. Arai, T. Shibata, S. Matsuoka, M. J. Sato, T. Yanagida, and M. Ueda, 'Self-organization of the phosphatidylinositol lipids signaling system for random cell migration', *PNAS*, vol. 107, no. 27, pp. 12399–12404, Jul. 2010, doi: 10.1073/pnas.0908278107.
[386] E. Yamamoto *et al.*, 'Multiple lipid binding sites determine the affinity of PH domains for phosphoinositide-containing membranes', *Science Advances*, vol. 6, no. 8, p. eaay5736, Feb. 2020, doi: 10.1126/sciadv.aay5736.
[387] C. Fumarola, M. A. Bonelli, P. G. Petronini, and R. R. Alfieri, 'Targeting PI3K/AKT/mTOR pathway in non small cell lung cancer', *Biochem Pharmacol*, vol. 90, no. 3, pp. 197–207, Aug. 2014, doi: 10.1016/j.bcp.2014.05.011.
[388] E. G. Sarris, M. W. Saif, and K. N. Syrigos, 'The Biological Role of PI3K Pathway in Lung Cancer', *Pharmaceuticals (Basel)*, vol. 5, no. 11, pp. 1236–1264, Nov. 2012, doi: 10.3390/ph5111236.

[389] P. Liu, H. Cheng, T. M. Roberts, and J. J. Zhao, 'Targeting the phosphoinositide 3-kinase pathway in cancer', *Nat Rev Drug Discov*, vol. 8, no. 8, pp. 627–644, Aug. 2009, doi: 10.1038/nrd2926.
[390] C.-M. Hung, L. Garcia-Haro, C. A. Sparks, and D. A. Guertin, 'mTOR-dependent cell survival mechanisms', *Cold Spring Harb Perspect Biol*, vol. 4, no. 12, Dec. 2012, doi: 10.1101/cshperspect.a008771.
[391] M. Kawashima *et al.*, 'High-resolution imaging mass spectrometry reveals detailed spatial distribution of phosphatidylinositols in human breast cancer', *Cancer Sci*, vol. 104, no. 10, pp. 1372–1379, Oct. 2013, doi: 10.1111/cas.12229.
[392] S. Guenther *et al.*, 'Spatially Resolved Metabolic Phenotyping of Breast Cancer by Desorption Electrospray Ionization Mass Spectrometry', *Cancer Res*, vol. 75, no. 9, pp. 1828–1837, May 2015, doi: 10.1158/0008-5472.CAN-14-2258.
[393] R. B. Birge *et al.*, 'Phosphatidylserine is a global immunosuppressive signal in efferocytosis, infectious disease, and cancer', *Cell Death & Differentiation*, vol. 23, no. 6, Art. no. 6, Jun. 2016, doi: 10.1038/cdd.2016.11.
[394] I. Shlomovitz, M. Speir, and M. Gerlic, 'Flipping the dogma – phosphatidylserine in non-apoptotic cell death', *Cell Communication and Signaling*, vol. 17, no. 1, p. 139, Oct. 2019, doi: 10.1186/s12964-019-0437-0.
[395] O. Belzile *et al.*, 'Antibody targeting of phosphatidylserine for the detection and immunotherapy of cancer', *Immunotargets Ther*, vol. 7, pp. 1–14, 2018, doi: 10.2147/ITT.S134834.
[396] P. Patel and X. Qi, 'Phosphatidylserine Externalization in Pancreatic Cancer Cells is Associated with Increased Oxidative Stress, Actin Rearrangement and p38 Activation', *Undergradshowcase*, vol. 2, no. 1, Art. no. 1, Oct. 2020, Accessed: Apr. 18, 2021. [Online]. Available: https://journals.uc.edu/index.php/Undergradshowcase/article/view/4085
[397] K. F. N'Guessan, P. H. Patel, and X. Qi, 'SapC-DOPS – a Phosphatidylserine-targeted Nanovesicle for selective Cancer therapy', *Cell Communication and Signaling*, vol. 18, no. 1, p. 6, Jan. 2020, doi: 10.1186/s12964-019-0476-6.
[398] W. Chang, H. Fa, D. Xiao, and J. Wang, 'Targeting phosphatidylserine for Cancer therapy: prospects and challenges', *Theranostics*, vol. 10, no. 20, p. 9214, 2020, doi: 10.7150/thno.45125.
[399] D. Patel and S. N. Witt, 'Ethanolamine and Phosphatidylethanolamine: Partners in Health and Disease', *Oxid Med Cell Longev*, vol. 2017, 2017, doi: 10.1155/2017/4829180.
[400] E. van den Brink-van der Laan, J. Antoinette Killian, and B. de Kruijff, 'Nonbilayer lipids affect peripheral and integral membrane proteins via changes in the lateral pressure profile', *Biochimica et Biophysica Acta (BBA) - Biomembranes*, vol. 1666, no. 1, pp. 275–288, Nov. 2004, doi: 10.1016/j.bbamem.2004.06.010.
[401] V. E. Kagan *et al.*, 'Oxidized Arachidonic/Adrenic Phosphatidylethanolamines Navigate Cells to Ferroptosis', *Nat Chem Biol*, vol. 13, no. 1, pp. 81–90, Jan. 2017, doi: 10.1038/nchembio.2238.
[402] C. M. Bebber, F. Müller, L. Prieto Clemente, J. Weber, and S. von Karstedt, 'Ferroptosis in Cancer Cell Biology', *Cancers (Basel)*, vol. 12, no. 1, Jan. 2020, doi: 10.3390/cancers12010164.

[403] S. Zuo, J. Yu, H. Pan, and L. Lu, ‘Novel insights on targeting ferroptosis in cancer therapy’, *Biomarker Research*, vol. 8, no. 1, p. 50, Oct. 2020, doi: 10.1186/s40364-020-00229-w.
[404] J. N. van der Veen, J. P. Kennelly, S. Wan, J. E. Vance, D. E. Vance, and R. L. Jacobs, ‘The critical role of phosphatidylcholine and phosphatidylethanolamine metabolism in health and disease’, *Biochimica et Biophysica Acta (BBA) - Biomembranes*, vol. 1859, no. 9, Part B, pp. 1558–1572, Sep. 2017, doi: 10.1016/j.bbamem.2017.04.006.
[405] N. D. Ridgway, ‘The role of phosphatidylcholine and choline metabolites to cell proliferation and survival’, *Crit Rev Biochem Mol Biol*, vol. 48, no. 1, pp. 20–38, Feb. 2013, doi: 10.3109/10409238.2012.735643.
[406] Y. Qiu *et al.*, ‘Mass spectrometry-based quantitative metabolomics revealed a distinct lipid profile in breast cancer patients’, *Int J Mol Sci*, vol. 14, no. 4, pp. 8047–8061, Apr. 2013, doi: 10.3390/ijms14048047.
[407] Y. Ide *et al.*, ‘Human breast cancer tissues contain abundant phosphatidylcholine(36:1) with high stearoyl-CoA desaturase-1 expression’, *PLoS One*, vol. 8, no. 4, p. e61204, 2013, doi: 10.1371/journal.pone.0061204.
[408] O. A. Zeleznik, C. B. Clish, P. Kraft, J. Avila-Pacheco, A. H. Eliassen, and S. S. Tworoger, ‘Circulating Lysophosphatidylcholines, Phosphatidylcholines, Ceramides, and Sphingomyelins and Ovarian Cancer Risk: A 23-Year Prospective Study’, *J Natl Cancer Inst*, vol. 112, no. 6, pp. 628–636, Jun. 2020, doi: 10.1093/jnci/djz195.
[409] L. Yang *et al.*, ‘Comprehensive lipid profiling of plasma in patients with benign breast tumor and breast cancer reveals novel biomarkers’, *Anal Bioanal Chem*, vol. 407, no. 17, pp. 5065–5077, Jul. 2015, doi: 10.1007/s00216-015-8484-x.
[410] C. Ye, B. M. Sutter, Y. Wang, Z. Kuang, and B. P. Tu, ‘A Metabolic Function for Phospholipid and Histone Methylation’, *Molecular Cell*, vol. 66, no. 2, pp. 180-193.e8, Apr. 2017, doi: 10.1016/j.molcel.2017.02.026.
[411] F. Visioli, C. Colombo, S. Monti, P. Giulidori, and C. Galli, ‘S-adenosyl-L-methionine: role in phosphatidylcholine synthesis and in vitro effects on the ethanol-induced alterations of lipid metabolism’, *Pharmacol Res*, vol. 37, no. 3, pp. 203–206, Mar. 1998, doi: 10.1006/phrs.1997.0282.
[412] M. Martínez-Uña *et al.*, ‘Excess S-adenosylmethionine reroutes phosphatidylethanolamine towards phosphatidylcholine and triglyceride synthesis’, *Hepatology*, vol. 58, no. 4, pp. 1296–1305, Oct. 2013, doi: 10.1002/hep.26399.
[413] R. A. Coleman and D. G. Mashek, ‘Mammalian Triacylglycerol Metabolism: Synthesis, Lipolysis and Signaling’, *Chem Rev*, vol. 111, no. 10, pp. 6359–6386, Oct. 2011, doi: 10.1021/cr100404w.
[414] P. Fagone and S. Jackowski, ‘Membrane phospholipid synthesis and endoplasmic reticulum function’, *J Lipid Res*, vol. 50 Suppl, pp. S311-316, Apr. 2009, doi: 10.1194/jlr.R800049-JLR200.
[415] H. Ulmer *et al.*, ‘Serum triglyceride concentrations and cancer risk in a large cohort study in Austria’, *Br J Cancer*, vol. 101, no. 7, pp. 1202–1206, Oct. 2009, doi: 10.1038/sj.bjc.6605264.
[416] I. R. Schlaepfer *et al.*, ‘Hypoxia induces triglycerides accumulation in prostate cancer cells and extracellular vesicles supporting growth and invasiveness

following reoxygenation', *Oncotarget*, vol. 6, no. 26, pp. 22836–22856, Sep. 2015, doi: 10.18632/oncotarget.4479.
[417] S. Morel *et al.*, 'Lipid and lipoprotein abnormalities in acute lymphoblastic leukemia survivors', *J Lipid Res*, vol. 58, no. 5, pp. 982–993, May 2017, doi: 10.1194/jlr.M072207.
[418] J. Long *et al.*, 'Lipid metabolism and carcinogenesis, cancer development', *Am J Cancer Res*, vol. 8, no. 5, pp. 778–791, May 2018.
[419] C. Corbet *et al.*, 'TGFβ2-induced formation of lipid droplets supports acidosis-driven EMT and the metastatic spreading of cancer cells', *Nature Communications*, vol. 11, no. 1, Art. no. 1, Jan. 2020, doi: 10.1038/s41467-019-14262-3.
[420] Y. Y. Wang *et al.*, 'Mammary adipocytes stimulate breast cancer invasion through metabolic remodeling of tumor cells', *JCI Insight*, vol. 2, no. 4, Feb. 2017, doi: 10.1172/jci.insight.87489.
[421] X. Liu *et al.*, 'Long non-coding RNA NEAT1-modulated abnormal lipolysis via ATGL drives hepatocellular carcinoma proliferation', *Mol Cancer*, vol. 17, no. 1, p. 90, May 2018, doi: 10.1186/s12943-018-0838-5.
[422] H. Xie *et al.*, 'Adipose triglyceride lipase activity regulates cancer cell proliferation via AMP-kinase and mTOR signaling', *Biochimica et Biophysica Acta (BBA) - Molecular and Cell Biology of Lipids*, vol. 1865, no. 9, p. 158737, Sep. 2020, doi: 10.1016/j.bbalip.2020.158737.
[423] S. K. Das and G. Hoefler, 'The role of triglyceride lipases in cancer associated cachexia', *Trends Mol Med*, vol. 19, no. 5, pp. 292–301, May 2013, doi: 10.1016/j.molmed.2013.02.006.
[424] L. R. Engelking, 'Chapter 59 - Sphingolipids', in *Textbook of Veterinary Physiological Chemistry (Third Edition)*, L. R. Engelking, Ed. Boston: Academic Press, 2015, pp. 378–383. doi: 10.1016/B978-0-12-391909-0.50059-1.
[425] Y. A. Hannun and L. M. Obeid, 'Sphingolipids and their metabolism in physiology and disease', *Nat Rev Mol Cell Biol*, vol. 19, no. 3, pp. 175–191, Mar. 2018, doi: 10.1038/nrm.2017.107.
[426] A. C. Carreira *et al.*, 'Mammalian sphingoid bases: Biophysical, physiological and pathological properties', *Progress in Lipid Research*, vol. 75, p. 100988, Jul. 2019, doi: 10.1016/j.plipres.2019.100988.
[427] T. D. Mullen and L. M. Obeid, 'Ceramide and apoptosis: exploring the enigmatic connections between sphingolipid metabolism and programmed cell death', *Anticancer Agents Med Chem*, vol. 12, no. 4, pp. 340–363, May 2012, doi: 10.2174/187152012800228661.
[428] S. Schüll *et al.*, 'Cytochrome c oxidase deficiency accelerates mitochondrial apoptosis by activating ceramide synthase 6', *Cell Death & Disease*, vol. 6, no. 3, Art. no. 3, Mar. 2015, doi: 10.1038/cddis.2015.62.
[429] L. M. Obeid, C. M. Linardic, L. A. Karolak, and Y. A. Hannun, 'Programmed cell death induced by ceramide', *Science*, vol. 259, no. 5102, pp. 1769–1771, Mar. 1993, doi: 10.1126/science.8456305.
[430] J. E. Chipuk *et al.*, 'Sphingolipid Metabolism Cooperates with BAK and BAX to Promote the Mitochondrial Pathway of Apoptosis', *Cell*, vol. 148, no. 5, pp. 988–1000, Mar. 2012, doi: 10.1016/j.cell.2012.01.038.
[431] K.-T. Chang, A. Anishkin, G. A. Patwardhan, L. J. Beverly, L. J. Siskind, and M. Colombini, 'Ceramide channels: destabilization by Bcl-xL and role in

apoptosis', *Biochim Biophys Acta*, vol. 1848, no. 10 Pt A, pp. 2374–2384, Oct. 2015, doi: 10.1016/j.bbamem.2015.07.013.
[432] H. Wang, A. E. Giuliano, and M. C. Cabot, 'Enhanced de novo ceramide generation through activation of serine palmitoyltransferase by the P-glycoprotein antagonist SDZ PSC 833 in breast cancer cells', *Mol Cancer Ther*, vol. 1, no. 9, pp. 719–726, Jul. 2002.
[433] J. M. Kraveka *et al.*, 'Involvement of Dihydroceramide Desaturase in Cell Cycle Progression in Human Neuroblastoma Cells*', *Journal of Biological Chemistry*, vol. 282, no. 23, pp. 16718–16728, Jun. 2007, doi: 10.1074/jbc.M700647200.
[434] S. White-Gilbertson *et al.*, 'Ceramide synthase 6 modulates TRAIL sensitivity and nuclear translocation of active caspase-3 in colon cancer cells', *Oncogene*, vol. 28, no. 8, Art. no. 8, Feb. 2009, doi: 10.1038/onc.2008.468.
[435] B. Ogretmen, 'Sphingolipid metabolism in cancer signalling and therapy', *Nature Reviews Cancer*, vol. 18, no. 1, Art. no. 1, Jan. 2018, doi: 10.1038/nrc.2017.96.
[436] K. Moro, M. Nagahashi, E. Gabriel, K. Takabe, and T. Wakai, 'Clinical application of ceramide in cancer treatment', *Breast Cancer*, vol. 26, no. 4, pp. 407–415, Jul. 2019, doi: 10.1007/s12282-019-00953-8.
[437] S. Calise, S. Blescia, F. Cencetti, C. Bernacchioni, C. Donati, and P. Bruni, 'Sphingosine 1-phosphate stimulates proliferation and migration of satellite cells: role of S1P receptors', *Biochim Biophys Acta*, vol. 1823, no. 2, pp. 439–450, Feb. 2012, doi: 10.1016/j.bbamcr.2011.11.016.
[438] A. W. Payne, D. K. Pant, T.-C. Pan, and L. A. Chodosh, 'Ceramide Kinase Promotes Tumor Cell Survival and Mammary Tumor Recurrence', *Cancer Res*, vol. 74, no. 21, pp. 6352–6363, Nov. 2014, doi: 10.1158/0008-5472.CAN-14-1292.
[439] A. Yamada *et al.*, 'ABCC1-Exported Sphingosine-1-phosphate, Produced by Sphingosine Kinase 1, Shortens Survival of Mice and Patients with Breast Cancer', *Mol Cancer Res*, vol. 16, no. 6, pp. 1059–1070, Jun. 2018, doi: 10.1158/1541-7786.MCR-17-0353.
[440] Y.-X. Guo, Y.-J. Ma, L. Han, Y.-J. Wang, J.-A. Han, and Y. Zhu, 'Role of sphingosine 1-phosphate in human pancreatic cancer cells proliferation and migration', *Int J Clin Exp Med*, vol. 8, no. 11, pp. 20349–20354, 2015.
[441] S. Modok, C. Heyward, and R. Callaghan, 'P-glycoprotein retains function when reconstituted into a sphingolipid- and cholesterol-rich environment', *Journal of Lipid Research*, vol. 45, no. 10, pp. 1910–1918, Oct. 2004, doi: 10.1194/jlr.M400220-JLR200.
[442] E. Corcelle-Termeau *et al.*, 'Excess sphingomyelin disturbs ATG9A trafficking and autophagosome closure', *Autophagy*, vol. 12, no. 5, pp. 833–849, May 2016, doi: 10.1080/15548627.2016.1159378.
[443] K. Zheng *et al.*, 'Sphingomyelin synthase 2 promotes an aggressive breast cancer phenotype by disrupting the homoeostasis of ceramide and sphingomyelin', *Cell Death & Disease*, vol. 10, no. 3, Art. no. 3, Feb. 2019, doi: 10.1038/s41419-019-1303-0.
[444] J. D. Greenlee, T. Subramanian, K. Liu, and M. R. King, 'Rafting Down the Metastatic Cascade: The Role of Lipid Rafts in Cancer Metastasis, Cell Death, and Clinical Outcomes', *Cancer Res*, vol. 81, no. 1, pp. 5–17, Jan. 2021, doi: 10.1158/0008-5472.CAN-20-2199.

[445] I. Buhaescu and H. Izzedine, ‘Mevalonate pathway: a review of clinical and therapeutical implications’, *Clin Biochem*, vol. 40, no. 9–10, pp. 575–584, Jun. 2007, doi: 10.1016/j.clinbiochem.2007.03.016.
[446] M. S. Brown and J. L. Goldstein, ‘A receptor-mediated pathway for cholesterol homeostasis’, *Science*, vol. 232, no. 4746, pp. 34–47, Apr. 1986, doi: 10.1126/science.3513311.
[447] M. A. Ayee and I. Levitan, ‘Paradoxical impact of cholesterol on lipid packing and cell stiffness’, *Front Biosci (Landmark Ed)*, vol. 21, pp. 1245–1259, Jun. 2016, doi: 10.2741/4454.
[448] R. S. Gracià, N. Bezlyepkina, R. L. Knorr, R. Lipowsky, and R. Dimova, ‘Effect of cholesterol on the rigidity of saturated and unsaturated membranes: fluctuation and electrodeformation analysis of giant vesicles’, *Soft Matter*, vol. 6, no. 7, pp. 1472–1482, Mar. 2010, doi: 10.1039/B920629A.
[449] K. L. Hoejholt *et al.*, ‘Calcium electroporation and electrochemotherapy for cancer treatment: Importance of cell membrane composition investigated by lipidomics, calorimetry and in vitro efficacy’, *Scientific Reports*, vol. 9, no. 1, Art. no. 1, Mar. 2019, doi: 10.1038/s41598-019-41188-z.
[450] Z. Zhao *et al.*, ‘CtBP promotes metastasis of breast cancer through repressing cholesterol and activating TGF-β signaling’, *Oncogene*, vol. 38, no. 12, Art. no. 12, Mar. 2019, doi: 10.1038/s41388-018-0570-z.
[451] Nagao Tomokazu, Qin Chunbo, Grosheva Inna, Maxfield Frederick R., and Pierini Lynda M., ‘Elevated Cholesterol Levels in the Plasma Membranes of Macrophages Inhibit Migration by Disrupting RhoA Regulation’, *Arteriosclerosis, Thrombosis, and Vascular Biology*, vol. 27, no. 7, pp. 1596–1602, Jul. 2007, doi: 10.1161/ATVBAHA.107.145086.
[452] T. Murai, Y. Maruyama, K. Mio, H. Nishiyama, M. Suga, and C. Sato, ‘Low cholesterol triggers membrane microdomain-dependent CD44 shedding and suppresses tumor cell migration’, *J Biol Chem*, vol. 286, no. 3, pp. 1999–2007, Jan. 2011, doi: 10.1074/jbc.M110.184010.
[453] T. Murai, ‘The Role of Lipid Rafts in Cancer Cell Adhesion and Migration’, *Int J Cell Biol*, vol. 2012, 2012, doi: 10.1155/2012/763283.
[454] S. Ehmsen *et al.*, ‘Increased Cholesterol Biosynthesis Is a Key Characteristic of Breast Cancer Stem Cells Influencing Patient Outcome’, *Cell Reports*, vol. 27, no. 13, pp. 3927-3938.e6, Jun. 2019, doi: 10.1016/j.celrep.2019.05.104.
[455] S. Borgquist *et al.*, ‘Cholesterol, Cholesterol-Lowering Medication Use, and Breast Cancer Outcome in the BIG 1-98 Study’, *J Clin Oncol*, vol. 35, no. 11, pp. 1179–1188, Apr. 2017, doi: 10.1200/JCO.2016.70.3116.
[456] J. Vaquero, T. H. Nguyen Ho-Bouldoires, A. Clapéron, and L. Fouassier, ‘Role of the PDZ-scaffold protein NHERF1/EBP50 in cancer biology: from signaling regulation to clinical relevance’, *Oncogene*, vol. 36, no. 22, pp. 3067–3079, Jun. 2017, doi: 10.1038/onc.2016.462.
[457] R. Sheng *et al.*, ‘Cholesterol modulates cell signaling and protein networking by specifically interacting with PDZ domain-containing scaffold proteins’, *Nat Commun*, vol. 3, p. 1249, 2012, doi: 10.1038/ncomms2221.
[458] G. Luchetti *et al.*, ‘Cholesterol activates the G-protein coupled receptor Smoothened to promote Hedgehog signaling’, *Elife*, vol. 5, Oct. 2016, doi: 10.7554/eLife.20304.
[459] C. V. Dang, K. A. O’Donnell, K. I. Zeller, T. Nguyen, R. C. Osthus, and F. Li, ‘The c-Myc target gene network’, *Semin Cancer Biol*, vol. 16, no. 4, pp. 253–264, Aug. 2006, doi: 10.1016/j.semcancer.2006.07.014.

[460] C. V. Dang, ‘c-Myc Target Genes Involved in Cell Growth, Apoptosis, and Metabolism’, *Molecular and Cellular Biology*, vol. 19, no. 1, pp. 1–11, Jan. 1999, doi: 10.1128/MCB.19.1.1.
[461] C. V. Dang, ‘MYC on the Path to Cancer’, *Cell*, vol. 149, no. 1, pp. 22–35, Mar. 2012, doi: 10.1016/j.cell.2012.03.003.
[462] J. Blancato, B. Singh, A. Liu, D. J. Liao, and R. B. Dickson, ‘Correlation of amplification and overexpression of the c-myc oncogene in high-grade breast cancer: FISH, in situ hybridisation and immunohistochemical analyses’, *Br J Cancer*, vol. 90, no. 8, pp. 1612–1619, Apr. 2004, doi: 10.1038/sj.bjc.6601703.
[463] C. Dani, J. M. Blanchard, M. Piechaczyk, S. El Sabouty, L. Marty, and P. Jeanteur, ‘Extreme instability of myc mRNA in normal and transformed human cells.’, *Proc Natl Acad Sci U S A*, vol. 81, no. 22, pp. 7046–7050, Nov. 1984.
[464] S. H. Choi, J. B. Wright, S. A. Gerber, and M. D. Cole, ‘Myc protein is stabilized by suppression of a novel E3 ligase complex in cancer cells’, *Genes Dev*, vol. 24, no. 12, pp. 1236–1241, Jun. 2010, doi: 10.1101/gad.1920310.
[465] S. Li *et al.*, ‘Regulation of c-Myc protein stability by proteasome activator REGγ’, *Cell Death Differ*, vol. 22, no. 6, pp. 1000–1011, Jun. 2015, doi: 10.1038/cdd.2014.188.
[466] T. R. Kress, A. Sabò, and B. Amati, ‘MYC: connecting selective transcriptional control to global RNA production’, *Nat Rev Cancer*, vol. 15, no. 10, pp. 593–607, Oct. 2015, doi: 10.1038/nrc3984.
[467] Y. Su *et al.*, ‘Post-translational modification localizes MYC to the nuclear pore basket to regulate a subset of target genes involved in cellular responses to environmental signals’, *Genes Dev*, vol. 32, no. 21–22, pp. 1398–1419, Nov. 2018, doi: 10.1101/gad.314377.118.
[468] A. Cascón and M. Robledo, ‘MAX and MYC: a heritable breakup’, *Cancer Res*, vol. 72, no. 13, pp. 3119–3124, Jul. 2012, doi: 10.1158/0008-5472.CAN-11-3891.
[469] C. Grandori, S. M. Cowley, L. P. James, and R. N. Eisenman, ‘The Myc/Max/Mad network and the transcriptional control of cell behavior’, *Annu Rev Cell Dev Biol*, vol. 16, pp. 653–699, 2000, doi: 10.1146/annurev.cellbio.16.1.653.
[470] M. Okada and Y.-B. Shi, ‘The balance of two opposing factors Mad and Myc regulates cell fate during tissue remodeling’, *Cell Biosci*, vol. 8, p. 51, 2018, doi: 10.1186/s13578-018-0249-8.
[471] S. B. McMahon, ‘Emerging Concepts in the Analysis of Transcriptional Targets of the MYC Oncoprotein’, *Genes Cancer*, vol. 1, no. 6, pp. 560–567, Jun. 2010, doi: 10.1177/1947601910379011.
[472] A. Menssen and H. Hermeking, ‘Characterization of the c-MYC-regulated transcriptome by SAGE: Identification and analysis of c-MYC target genes’, *Proc Natl Acad Sci U S A*, vol. 99, no. 9, pp. 6274–6279, Apr. 2002, doi: 10.1073/pnas.082005599.
[473] H. A. Coller *et al.*, ‘Expression analysis with oligonucleotide microarrays reveals that MYC regulates genes involved in growth, cell cycle, signaling, and adhesion’, *Proc Natl Acad Sci U S A*, vol. 97, no. 7, pp. 3260–3265, Mar. 2000.

[474] R. Wang *et al.*, 'The Transcription Factor Myc Controls Metabolic Reprogramming upon T Lymphocyte Activation', *Immunity*, vol. 35, no. 6, pp. 871–882, Dec. 2011, doi: 10.1016/j.immuni.2011.09.021.
[475] N. Sharma, A. Bhushan, J. He, G. Kaushal, and V. Bhardwaj, 'Metabolic plasticity imparts erlotinib-resistance in pancreatic cancer by upregulating glucose-6-phosphate dehydrogenase', *Cancer & Metabolism*, vol. 8, no. 1, p. 19, Sep. 2020, doi: 10.1186/s40170-020-00226-5.
[476] R. C. Osthus *et al.*, 'Deregulation of glucose transporter 1 and glycolytic gene expression by c-Myc', *J Biol Chem*, vol. 275, no. 29, pp. 21797–21800, Jul. 2000, doi: 10.1074/jbc.C000023200.
[477] R. El Ansari *et al.*, 'The amino acid transporter SLC7A5 confers a poor prognosis in the highly proliferative breast cancer subtypes and is a key therapeutic target in luminal B tumours', *Breast Cancer Research*, vol. 20, no. 1, p. 21, Mar. 2018, doi: 10.1186/s13058-018-0946-6.
[478] P. Gao *et al.*, 'c-Myc suppression of miR-23a/b enhances mitochondrial glutaminase expression and glutamine metabolism', *Nature*, vol. 458, no. 7239, Art. no. 7239, Apr. 2009, doi: 10.1038/nature07823.
[479] T. Wang *et al.*, 'MYCN drives glutaminolysis in neuroblastoma and confers sensitivity to an ROS augmenting agent', *Cell Death & Disease*, vol. 9, no. 2, Art. no. 2, Feb. 2018, doi: 10.1038/s41419-018-0295-5.
[480] L. Sun *et al.*, 'cMyc-mediated activation of serine biosynthesis pathway is critical for cancer progression under nutrient deprivation conditions', *Cell Research*, vol. 25, no. 4, Art. no. 4, Apr. 2015, doi: 10.1038/cr.2015.33.
[481] M. A. Nikiforov *et al.*, 'A Functional Screen for Myc-Responsive Genes Reveals Serine Hydroxymethyltransferase, a Major Source of the One-Carbon Unit for Cell Metabolism', *Mol Cell Biol*, vol. 22, no. 16, pp. 5793–5800, Aug. 2002, doi: 10.1128/MCB.22.16.5793-5800.2002.
[482] M. Pourdehnad, M. L. Truitt, I. N. Siddiqi, G. S. Ducker, K. M. Shokat, and D. Ruggero, 'Myc and mTOR converge on a common node in protein synthesis control that confers synthetic lethality in Myc-driven cancers', *PNAS*, vol. 110, no. 29, pp. 11988–11993, Jul. 2013, doi: 10.1073/pnas.1310230110.
[483] D. Horiuchi *et al.*, 'MYC pathway activation in triple-negative breast cancer is synthetic lethal with CDK inhibition', *J Exp Med*, vol. 209, no. 4, pp. 679–696, Apr. 2012, doi: 10.1084/jem.20111512.
[484] A. Terunuma *et al.*, 'MYC-driven accumulation of 2-hydroxyglutarate is associated with breast cancer prognosis', *J Clin Invest*, vol. 124, no. 1, pp. 398–412, Jan. 2014, doi: 10.1172/JCI71180.
[485] X. Guan, 'Cancer metastases: challenges and opportunities', *Acta Pharmaceutica Sinica B*, vol. 5, no. 5, pp. 402–418, Sep. 2015, doi: 10.1016/j.apsb.2015.07.005.
[486] T. Schild, V. Low, J. Blenis, and A. P. Gomes, 'Unique Metabolic Adaptations Dictate Distal Organ-Specific Metastatic Colonization', *Cancer Cell*, vol. 33, no. 3, pp. 347–354, Mar. 2018, doi: 10.1016/j.ccell.2018.02.001.
[487] P. Kreuzaler, Y. Panina, J. Segal, and M. Yuneva, 'Adapt and conquer: Metabolic flexibility in cancer growth, invasion and evasion', *Molecular Metabolism*, vol. 33, pp. 83–101, Mar. 2020, doi: 10.1016/j.molmet.2019.08.021.
[488] G. Bergers and S.-M. Fendt, 'The metabolism of cancer cells during metastasis', *Nat Rev Cancer*, vol. 21, no. 3, pp. 162–180, Mar. 2021, doi: 10.1038/s41568-020-00320-2.

[489] X. Ye and R. A. Weinberg, ‘Epithelial-Mesenchymal Plasticity: A central regulator of cancer progression’, *Trends Cell Biol*, vol. 25, no. 11, pp. 675–686, Nov. 2015, doi: 10.1016/j.tcb.2015.07.012.
[490] M. Anderson, R. Marayati, R. Moffitt, and J. J. Yeh, ‘Hexokinase 2 promotes tumor growth and metastasis by regulating lactate production in pancreatic cancer’, *Oncotarget*, vol. 8, no. 34, pp. 56081–56094, Aug. 2017, doi: 10.18632/oncotarget.9760.
[491] H. Sun, A. Zhu, L. Zhang, J. Zhang, Z. Zhong, and F. Wang, ‘Knockdown of PKM2 Suppresses Tumor Growth and Invasion in Lung Adenocarcinoma’, *Int J Mol Sci*, vol. 16, no. 10, pp. 24574–24587, Oct. 2015, doi: 10.3390/ijms161024574.
[492] A. Ahmad *et al.*, ‘Phosphoglucose Isomerase/Autocrine Motility Factor mediates epithelial-mesenchymal transition regulated by miR-200 in breast cancer cells’, *Cancer research*, vol. 71, no. 9, p. 3400, May 2011, doi: 10.1158/0008-5472.CAN-10-0965.
[493] A. R. Grassian *et al.*, ‘Isocitrate dehydrogenase (IDH) mutations promote a reversible ZEB1/microRNA (miR)-200-dependent epithelial-mesenchymal transition (EMT)’, *J Biol Chem*, vol. 287, no. 50, pp. 42180–42194, Dec. 2012, doi: 10.1074/jbc.M112.417832.
[494] M. Sciacovelli *et al.*, ‘Fumarate is an epigenetic modifier that elicits epithelial-to-mesenchymal transition’, *Nature*, vol. 537, no. 7621, Art. no. 7621, Sep. 2016, doi: 10.1038/nature19353.
[495] S. R. V. Knott *et al.*, ‘Asparagine bioavailability governs metastasis in a model of breast cancer’, *Nature*, vol. 554, no. 7692, pp. 378–381, Feb. 2018, doi: 10.1038/nature25465.
[496] E. Gaude and C. Frezza, ‘Tissue-specific and convergent metabolic transformation of cancer correlates with metastatic potential and patient survival’, *Nature Communications*, vol. 7, no. 1, Art. no. 1, Oct. 2016, doi: 10.1038/ncomms13041.
[497] M. Masin *et al.*, ‘GLUT3 is induced during epithelial-mesenchymal transition and promotes tumor cell proliferation in non-small cell lung cancer’, *Cancer Metab*, vol. 2, p. 11, 2014, doi: 10.1186/2049-3002-2-11.
[498] H.-A. Park, S. R. Brown, and Y. Kim, ‘Cellular Mechanisms of Circulating Tumor Cells During Breast Cancer Metastasis’, *Int J Mol Sci*, vol. 21, no. 14, Jul. 2020, doi: 10.3390/ijms21145040.
[499] S. Baldelli, K. Aquilano, and M. R. Ciriolo, ‘PGC-1α buffers ROS-mediated removal of mitochondria during myogenesis’, *Cell Death Dis*, vol. 5, p. e1515, Nov. 2014, doi: 10.1038/cddis.2014.458.
[500] V. S. LeBleu *et al.*, ‘PGC-1α mediates mitochondrial biogenesis and oxidative phosphorylation to promote metastasis’, *Nat Cell Biol*, vol. 16, no. 10, pp. 992–15, Oct. 2014, doi: 10.1038/ncb3039.
[501] E. Ivanova, A. Ward, A. P. Wiegmans, and D. J. Richard, ‘Circulating Tumor Cells in Metastatic Breast Cancer: From Genome Instability to Metastasis’, *Frontiers in Molecular Biosciences*, vol. 7, p. 134, 2020, doi: 10.3389/fmolb.2020.00134.
[502] I. Krol *et al.*, ‘Detection of clustered circulating tumour cells in early breast cancer’, *Br J Cancer*, vol. 125, no. 1, pp. 23–27, Jul. 2021, doi: 10.1038/s41416-021-01327-8.

[503] M. A. Hawk and Z. T. Schafer, ‘Mechanisms of redox metabolism and cancer cell survival during extracellular matrix detachment’, *J Biol Chem*, vol. 293, no. 20, pp. 7531–7537, May 2018, doi: 10.1074/jbc.TM117.000260.
[504] E. Piskounova *et al.*, ‘Oxidative stress inhibits distant metastasis by human melanoma cells’, *Nature*, vol. 527, no. 7577, pp. 186–191, Nov. 2015, doi: 10.1038/nature15726.
[505] K. Le Gal *et al.*, ‘Antioxidants can increase melanoma metastasis in mice’, *Sci Transl Med*, vol. 7, no. 308, p. 308re8, Oct. 2015, doi: 10.1126/scitranslmed.aad3740.
[506] M. Riihimäki, H. Thomsen, K. Sundquist, J. Sundquist, and K. Hemminki, ‘Clinical landscape of cancer metastases’, *Cancer Med*, vol. 7, no. 11, pp. 5534–5542, Oct. 2018, doi: 10.1002/cam4.1697.
[507] V. Stresing *et al.*, ‘Peroxiredoxin 2 specifically regulates the oxidative and metabolic stress response of human metastatic breast cancer cells in lungs’, *Oncogene*, vol. 32, no. 6, Art. no. 6, Feb. 2013, doi: 10.1038/onc.2012.93.
[508] P. Bu *et al.*, ‘Aldolase B-Mediated Fructose Metabolism Drives Metabolic Reprogramming of Colon Cancer Liver Metastasis’, *Cell Metabolism*, vol. 27, no. 6, pp. 1249-1262.e4, Jun. 2018, doi: 10.1016/j.cmet.2018.04.003.
[509] J. Neman *et al.*, ‘Human breast cancer metastases to the brain display GABAergic properties in the neural niche’, *PNAS*, vol. 111, no. 3, pp. 984–989, Jan. 2014, doi: 10.1073/pnas.1322098111.
[510] B. Ngo *et al.*, ‘Limited Environmental Serine and Glycine Confer Brain Metastasis Sensitivity to PHGDH Inhibition’, *Cancer Discov*, vol. 10, no. 9, pp. 1352–1373, Sep. 2020, doi: 10.1158/2159-8290.CD-19-1228.
[511] S. Pollari *et al.*, ‘Enhanced serine production by bone metastatic breast cancer cells stimulates osteoclastogenesis’, *Breast Cancer Res Treat*, vol. 125, no. 2, pp. 421–430, Jan. 2011, doi: 10.1007/s10549-010-0848-5.
[512] A. Kogure *et al.*, ‘Cancer cells with high-metastatic potential promote a glycolytic shift in activated fibroblasts’, *PLOS ONE*, vol. 15, no. 6, p. e0234613, Jun. 2020, doi: 10.1371/journal.pone.0234613.
[513] J. Gong *et al.*, ‘Reprogramming of lipid metabolism in cancer-associated fibroblasts potentiates migration of colorectal cancer cells’, *Cell Death & Disease*, vol. 11, no. 4, Art. no. 4, Apr. 2020, doi: 10.1038/s41419-020-2434-z.
[514] Y. Chen, Y. Song, W. Du, L. Gong, H. Chang, and Z. Zou, ‘Tumor-associated macrophages: an accomplice in solid tumor progression’, *Journal of Biomedical Science*, vol. 26, no. 1, p. 78, Oct. 2019, doi: 10.1186/s12929-019-0568-z.
[515] B. Ruffell, N. I. Affara, and L. M. Coussens, ‘Differential macrophage programming in the tumor microenvironment’, *Trends Immunol*, vol. 33, no. 3, pp. 119–126, Mar. 2012, doi: 10.1016/j.it.2011.12.001.
[516] S. Singh, N. Mehta, J. Lilan, M. B. Budhthoki, F. Chao, and L. Yong, ‘Initiative action of tumor-associated macrophage during tumor metastasis’, *Biochim Open*, vol. 4, pp. 8–18, Jun. 2017, doi: 10.1016/j.biopen.2016.11.002.
[517] D. F. Quail and J. A. Joyce, ‘Microenvironmental regulation of tumor progression and metastasis’, *Nat Med*, vol. 19, no. 11, pp. 1423–1437, Nov. 2013, doi: 10.1038/nm.3394.
[518] S. S. McAllister and R. A. Weinberg, ‘The tumour-induced systemic environment as a critical regulator of cancer progression and metastasis’, *Nat Cell Biol*, vol. 16, no. 8, pp. 717–727, Aug. 2014, doi: 10.1038/ncb3015.

[519] H. L. Penny *et al.*, ‘Warburg metabolism in tumor-conditioned macrophages promotes metastasis in human pancreatic ductal adenocarcinoma’, *Oncoimmunology*, vol. 5, no. 8, p. e1191731, Aug. 2016, doi: 10.1080/2162402X.2016.1191731.
[520] F. J. Rios, M. M. Koga, M. Pecenin, M. Ferracini, M. Gidlund, and S. Jancar, ‘Oxidized LDL induces alternative macrophage phenotype through activation of CD36 and PAFR’, *Mediators Inflamm*, vol. 2013, p. 198193, 2013, doi: 10.1155/2013/198193.
[521] M. Qin *et al.*, ‘Oxidized LDL activated eosinophil polarize macrophage phenotype from M2 to M1 through activation of CD36 scavenger receptor’, *Atherosclerosis*, vol. 263, pp. 82–91, Aug. 2017, doi: 10.1016/j.atherosclerosis.2017.05.011.
[522] Q. Zhang *et al.*, ‘Fatty acid oxidation contributes to IL-1β secretion in M2 macrophages and promotes macrophage-mediated tumor cell migration’, *Mol Immunol*, vol. 94, pp. 27–35, Feb. 2018, doi: 10.1016/j.molimm.2017.12.011.
[523] S. O. Rahaman, D. J. Lennon, M. Febbraio, E. A. Podrez, S. L. Hazen, and R. L. Silverstein, ‘A CD36-dependent signaling cascade is necessary for macrophage foam cell formation’, *Cell Metab*, vol. 4, no. 3, pp. 211–221, Sep. 2006, doi: 10.1016/j.cmet.2006.06.007.
[524] J. J. Pitt, ‘Principles and Applications of Liquid Chromatography-Mass Spectrometry in Clinical Biochemistry’, *Clin Biochem Rev*, vol. 30, no. 1, pp. 19–34, Feb. 2009.
[525] N. Krone, B. A. Hughes, G. G. Lavery, P. M. Stewart, W. Arlt, and C. H. L. Shackleton, ‘Gas chromatography/mass spectrometry (GC/MS) remains a pre-eminent discovery tool in clinical steroid investigations even in the era of fast liquid chromatography tandem mass spectrometry (LC/MS/MS)’, *J Steroid Biochem Mol Biol*, vol. 121, no. 3–5, pp. 496–504, Aug. 2010, doi: 10.1016/j.jsbmb.2010.04.010.
[526] O. Coskun, ‘Separation techniques: Chromatography’, *North Clin Istanb*, vol. 3, no. 2, pp. 156–160, Nov. 2016, doi: 10.14744/nci.2016.32757.
[527] R. A. Zubarev and A. Makarov, ‘Orbitrap Mass Spectrometry’, *Anal. Chem.*, vol. 85, no. 11, pp. 5288–5296, Jun. 2013, doi: 10.1021/ac4001223.
[528] G. A. N. Gowda and D. Djukovic, ‘Overview of Mass Spectrometry-Based Metabolomics: Opportunities and Challenges’, *Methods Mol Biol*, vol. 1198, pp. 3–12, 2014, doi: 10.1007/978-1-4939-1258-2_1.
[529] J. S. Kirkwood, C. Maier, and J. F. Stevens, ‘Simultaneous, untargeted metabolic profiling of polar and non-polar metabolites by LC-Q-TOF mass spectrometry’, *Curr Protoc Toxicol*, vol. 0 4, p. Unit4.39, May 2013, doi: 10.1002/0471140856.tx0439s56.
[530] B. Zhou, J. F. Xiao, L. Tuli, and H. W. Ressom, ‘LC-MS-based metabolomics’, *Mol Biosyst*, vol. 8, no. 2, pp. 470–481, Feb. 2012, doi: 10.1039/c1mb05350g.
[531] A. C. Schrimpe-Rutledge, S. G. Codreanu, S. D. Sherrod, and J. A. McLean, ‘Untargeted metabolomics strategies – Challenges and Emerging Directions’, *J Am Soc Mass Spectrom*, vol. 27, no. 12, pp. 1897–1905, Dec. 2016, doi: 10.1007/s13361-016-1469-y.
[532] C. A. Andersen, H. J. Roden, and C. F. Robinson, ‘Negative Ion Bombardment of Insulators to Alleviate Surface Charge-Up’, *Journal of Applied Physics*, vol. 40, no. 8, pp. 3419–3420, Jul. 1969, doi: 10.1063/1.1658212.

[533] M. Sans, C. L. Feider, and L. S. Eberlin, ‘Advances in Mass Spectrometry Imaging coupled to Ion Mobility Spectrometry for Enhanced Imaging of Biological Tissues’, *Curr Opin Chem Biol*, vol. 42, pp. 138–146, Feb. 2018, doi: 10.1016/j.cbpa.2017.12.005.
[534] M. K. Passarelli *et al.*, ‘The 3D OrbiSIMS—label-free metabolic imaging with subcellular lateral resolution and high mass-resolving power’, *Nature Methods*, vol. 14, no. 12, Art. no. 12, Dec. 2017, doi: 10.1038/nmeth.4504.
[535] R. V. Bennet, C. M. Gamage, and F. M. Fernández, ‘Imaging of Biological Tissues by Desorption Electrospray Ionization Mass Spectrometry’, *J Vis Exp*, no. 77, Jul. 2013, doi: 10.3791/50575.
[536] E. K. Neumann, K. V. Djambazova, R. M. Caprioli, and J. M. Spraggins, ‘Multimodal Imaging Mass Spectrometry: Next Generation Molecular Mapping in Biology and Medicine’, *J. Am. Soc. Mass Spectrom.*, vol. 31, no. 12, pp. 2401–2415, Dec. 2020, doi: 10.1021/jasms.0c00232.
[537] T. Porta Siegel, G. Hamm, J. Bunch, J. Cappell, J. S. Fletcher, and K. Schwamborn, ‘Mass Spectrometry Imaging and Integration with Other Imaging Modalities for Greater Molecular Understanding of Biological Tissues’, *Mol Imaging Biol*, vol. 20, no. 6, pp. 888–901, Dec. 2018, doi: 10.1007/s11307-018-1267-y.
[538] D. R. N. Vos, S. R. Ellis, B. Balluff, and R. M. A. Heeren, ‘Experimental and Data Analysis Considerations for Three-Dimensional Mass Spectrometry Imaging in Biomedical Research’, *Mol Imaging Biol*, vol. 23, no. 2, pp. 149–159, Apr. 2021, doi: 10.1007/s11307-020-01541-5.
[539] J. Clerc, C. Fourré, and P. Fragu, ‘SIMS microscopy: methodology, problems and perspectives in mapping drugs and nuclear medicine compounds’, *Cell Biol Int*, vol. 21, no. 10, pp. 619–633, Oct. 1997, doi: 10.1006/cbir.1998.0205.
[540] F. Kollmer, W. Paul, M. Krehl, and E. Niehuis, ‘Ultra high spatial resolution SIMS with cluster ions — approaching the physical limits’, *Surface and Interface Analysis*, vol. 45, no. 1, pp. 312–314, 2013, doi: https://doi.org/10.1002/sia.5093.
[541] A. M. Belu, D. J. Graham, and D. G. Castner, ‘Time-of-flight secondary ion mass spectrometry: techniques and applications for the characterization of biomaterial surfaces’, *Biomaterials*, vol. 24, no. 21, pp. 3635–3653, Sep. 2003, doi: 10.1016/s0142-9612(03)00159-5.
[542] J. Zhang *et al.*, ‘Cryo-OrbiSIMS for 3D Molecular Imaging of a Bacterial Biofilm in Its Native State’, *Anal Chem*, vol. 92, no. 13, pp. 9008–9015, Jul. 2020, doi: 10.1021/acs.analchem.0c01125.
[543] P. A. van Veelen *et al.*, ‘Direct peptide profiling of single neurons by matrix-assisted laser desorption–ionization mass spectrometry’, *Organic Mass Spectrometry*, vol. 28, no. 12, pp. 1542–1546, 1993, doi: https://doi.org/10.1002/oms.1210281229.
[544] L. Crossman, N. A. McHugh, Y. Hsieh, W. A. Korfmacher, and J. Chen, ‘Investigation of the profiling depth in matrix-assisted laser desorption/ionization imaging mass spectrometry’, *Rapid Commun Mass Spectrom*, vol. 20, no. 2, pp. 284–290, 2006, doi: 10.1002/rcm.2259.
[545] S. Francese, F. R. Dani, P. Traldi, G. Mastrobuoni, G. Pieraccini, and G. Moneti, ‘MALDI mass spectrometry imaging, from its origins up to today: the state of the art’, *Comb Chem High Throughput Screen*, vol. 12, no. 2, pp. 156–174, Feb. 2009, doi: 10.2174/138620709787315454.

[546] V. Mainini, M. Lalowski, A. Gotsopoulos, V. Bitsika, M. Baumann, and F. Magni, 'MALDI-imaging mass spectrometry on tissues', *Methods Mol Biol*, vol. 1243, pp. 139–164, 2015, doi: 10.1007/978-1-4939-1872-0_8.
[547] E. Gemperline, S. Rawson, and L. Li, 'Optimization and Comparison of Multiple MALDI Matrix Application Methods for Small Molecule Mass Spectrometric Imaging', *Anal. Chem.*, vol. 86, no. 20, pp. 10030–10035, Oct. 2014, doi: 10.1021/ac5028534.
[548] C. Meisenbichler, C. Doppler, D. Bernhard, and T. Müller, 'Improved matrix coating for positive- and negative-ion-mode MALDI-TOF imaging of lipids in blood vessel tissues', *Anal Bioanal Chem*, vol. 411, no. 15, pp. 3221–3227, Jun. 2019, doi: 10.1007/s00216-019-01826-x.
[549] Q. Zhou, A. Fülöp, and C. Hopf, 'Recent developments of novel matrices and on-tissue chemical derivatization reagents for MALDI-MSI', *Anal Bioanal Chem*, vol. 413, no. 10, pp. 2599–2617, Apr. 2021, doi: 10.1007/s00216-020-03023-7.
[550] P. Kobylis, P. Stepnowski, and M. Caban, 'Review of the applicability of ionic liquid matrices for the quantification of small molecules by MALDI MS', *Microchemical Journal*, vol. 164, p. 105983, May 2021, doi: 10.1016/j.microc.2021.105983.
[551] Z. Takáts, J. M. Wiseman, B. Gologan, and R. G. Cooks, 'Mass Spectrometry Sampling Under Ambient Conditions with Desorption Electrospray Ionization', *Science*, vol. 306, no. 5695, pp. 471–473, Oct. 2004, doi: 10.1126/science.1104404.
[552] E. Claude, 'Ion Mobility Separation Coupled With Desorption Electrospray Ionization Mass Spectrometry for High Specificity MS Imaging', p. 3, 2017.
[553] F. M. Green, T. L. Salter, I. S. Gilmore, P. Stokes, and G. O'Connor, 'The effect of electrospray solvent composition on desorption electrospray ionisation (DESI) efficiency and spatial resolution', *Analyst*, vol. 135, no. 4, pp. 731–737, Apr. 2010, doi: 10.1039/b924208b.
[554] L. Konermann, E. Ahadi, A. D. Rodriguez, and S. Vahidi, 'Unraveling the mechanism of electrospray ionization', *Anal Chem*, vol. 85, no. 1, pp. 2–9, Jan. 2013, doi: 10.1021/ac302789c.
[555] A. Venter, P. E. Sojka, and R. G. Cooks, 'Droplet dynamics and ionization mechanisms in desorption electrospray ionization mass spectrometry', *Anal Chem*, vol. 78, no. 24, pp. 8549–8555, Dec. 2006, doi: 10.1021/ac0615807.
[556] A. B. Costa and R. Graham Cooks, 'Simulated splashes: Elucidating the mechanism of desorption electrospray ionization mass spectrometry', *Chemical Physics Letters*, vol. 464, pp. 1–8, Oct. 2008, doi: 10.1016/j.cplett.2008.08.020.
[557] E. L. Gill, R. A. Yost, V. Vedam-Mai, and T. J. Garrett, 'Precast Gelatin-Based Molds for Tissue Embedding Compatible with Mass Spectrometry Imaging', *Anal Chem*, vol. 89, no. 1, pp. 576–580, Jan. 2017, doi: 10.1021/acs.analchem.6b04185.
[558] A. Dannhorn *et al.*, 'Universal Sample Preparation Unlocking Multimodal Molecular Tissue Imaging', *Anal. Chem.*, vol. 92, no. 16, pp. 11080–11088, Aug. 2020, doi: 10.1021/acs.analchem.0c00826.
[559] M. B. O'Rourke, B. B. A. Raymond, S. P. Djordjevic, and M. P. Padula, 'A versatile cost-effective method for the analysis of fresh frozen tissue sections via matrix-assisted laser desorption/ionisation imaging mass spectrometry',

Rapid Commun Mass Spectrom, vol. 29, no. 7, pp. 637–644, Apr. 2015, doi: 10.1002/rcm.7138.
[560] Q. Wu, T. J. Comi, B. Li, S. S. Rubakhin, and J. V. Sweedler, 'On-Tissue Derivatization via Electrospray Deposition for Matrix-Assisted Laser Desorption/Ionization Mass Spectrometry Imaging of Endogenous Fatty Acids in Rat Brain Tissues', *Anal Chem*, vol. 88, no. 11, pp. 5988–5995, Jun. 2016, doi: 10.1021/acs.analchem.6b01021.
[561] M. Shariatgorji *et al.*, 'Direct targeted quantitative molecular imaging of neurotransmitters in brain tissue sections', *Neuron*, vol. 84, no. 4, pp. 697–707, Nov. 2014, doi: 10.1016/j.neuron.2014.10.011.
[562] S. Holst *et al.*, 'Linkage-Specific in Situ Sialic Acid Derivatization for N-Glycan Mass Spectrometry Imaging of Formalin-Fixed Paraffin-Embedded Tissues', *Anal Chem*, vol. 88, no. 11, pp. 5904–5913, Jun. 2016, doi: 10.1021/acs.analchem.6b00819.
[563] H. Wang, J. P. DeGnore, B. D. Kelly, J. True, K. Garsha, and C. Bieniarz, 'A technique for relative quantitation of cancer biomarkers in formalin-fixed, paraffin-embedded (FFPE) tissue using stable-isotope-label based mass spectrometry imaging (SILMSI)', *J Mass Spectrom*, vol. 50, no. 9, pp. 1088–1095, Sep. 2015, doi: 10.1002/jms.3623.
[564] O. J. R. Gustafsson, J. S. Eddes, S. Meding, S. R. McColl, M. K. Oehler, and P. Hoffmann, 'Matrix-assisted laser desorption/ionization imaging protocol for in situ characterization of tryptic peptide identity and distribution in formalin-fixed tissue', *Rapid Communications in Mass Spectrometry*, vol. 27, no. 6, pp. 655–670, 2013, doi: https://doi.org/10.1002/rcm.6488.
[565] R. Casadonte and R. M. Caprioli, 'Proteomic analysis of formalin-fixed paraffin-embedded tissue by MALDI imaging mass spectrometry', *Nat Protoc*, vol. 6, no. 11, pp. 1695–1709, Nov. 2011, doi: 10.1038/nprot.2011.388.
[566] M. Gessel, J. M. Spraggins, P. Voziyan, B. G. Hudson, and R. M. Caprioli, 'Decellularization of intact tissue enables MALDI imaging mass spectrometry analysis of the extracellular matrix', *J Mass Spectrom*, vol. 50, no. 11, pp. 1288–1293, Nov. 2015, doi: 10.1002/jms.3696.
[567] F. Donnarumma, F. Cao, and K. K. Murray, 'Laser Ablation with Vacuum Capture for MALDI Mass Spectrometry of Tissue', *J Am Soc Mass Spectrom*, vol. 27, no. 1, pp. 108–116, Jan. 2016, doi: 10.1007/s13361-015-1249-0.
[568] M. Stoeckli, P. Chaurand, D. E. Hallahan, and R. M. Caprioli, 'Imaging mass spectrometry: a new technology for the analysis of protein expression in mammalian tissues', *Nat Med*, vol. 7, no. 4, pp. 493–496, Apr. 2001, doi: 10.1038/86573.
[569] C. Ds, R. Ml, C. P, and C. Rm, 'MALDI imaging mass spectrometry: molecular snapshots of biochemical systems', *Nature methods*, vol. 4, no. 10, Oct. 2007, doi: 10.1038/nmeth1094.
[570] P. Chaurand, S. A. Schwartz, and R. M. Caprioli, 'Assessing Protein Patterns in Disease Using Imaging Mass Spectrometry', *J. Proteome Res.*, vol. 3, no. 2, pp. 245–252, Apr. 2004, doi: 10.1021/pr0341282.
[571] S. Rauser *et al.*, 'Classification of HER2 receptor status in breast cancer tissues by MALDI imaging mass spectrometry', *J Proteome Res*, vol. 9, no. 4, pp. 1854–1863, Apr. 2010, doi: 10.1021/pr901008d.

[572] S. M. J. Rahman *et al.*, 'Lung cancer diagnosis from proteomic analysis of preinvasive lesions', *Cancer Res*, vol. 71, no. 8, pp. 3009–3017, Apr. 2011, doi: 10.1158/0008-5472.CAN-10-2510.
[573] H. K. Kim *et al.*, 'Gastric Cancer-Specific Protein Profile Identified Using Endoscopic Biopsy Samples via MALDI Mass Spectrometry', *J. Proteome Res.*, vol. 9, no. 8, pp. 4123–4130, Aug. 2010, doi: 10.1021/pr100302b.
[574] L. H. Cazares *et al.*, 'Imaging mass spectrometry of a specific fragment of mitogen-activated protein kinase/extracellular signal-regulated kinase kinase kinase 2 discriminates cancer from uninvolved prostate tissue', *Clin Cancer Res*, vol. 15, no. 17, pp. 5541–5551, Sep. 2009, doi: 10.1158/1078-0432.CCR-08-2892.
[575] R. Lemaire *et al.*, 'Specific MALDI imaging and profiling for biomarker hunting and validation: fragment of the 11S proteasome activator complex, Reg alpha fragment, is a new potential ovary cancer biomarker', *J Proteome Res*, vol. 6, no. 11, pp. 4127–4134, Nov. 2007, doi: 10.1021/pr0702722.
[576] F. Pagni *et al.*, 'Proteomics for the diagnosis of thyroid lesions: preliminary report', *Cytopathology*, vol. 26, no. 5, pp. 318–324, Oct. 2015, doi: 10.1111/cyt.12166.
[577] S. A. Patel *et al.*, 'Imaging mass spectrometry using chemical inkjet printing reveals differential protein expression in human oral squamous cell carcinoma', *Analyst*, vol. 134, no. 2, pp. 301–307, Feb. 2009, doi: 10.1039/B812533C.
[578] H. S. Kang *et al.*, 'Protein and lipid MALDI profiles classify breast cancers according to the intrinsic subtype', *BMC Cancer*, vol. 11, no. 1, p. 465, Oct. 2011, doi: 10.1186/1471-2407-11-465.
[579] A. L. Santoro *et al.*, 'In Situ DESI-MSI Lipidomic Profiles of Breast Cancer Molecular Subtypes and Precursor Lesions', *Cancer Res*, vol. 80, no. 6, pp. 1246–1257, Mar. 2020, doi: 10.1158/0008-5472.CAN-18-3574.
[580] G. K. Lee *et al.*, 'Lipid MALDI profile classifies non-small cell lung cancers according to the histologic type', *Lung Cancer*, vol. 76, no. 2, pp. 197–203, May 2012, doi: 10.1016/j.lungcan.2011.10.016.
[581] M. Waki *et al.*, 'Single-cell time-of-flight secondary ion mass spectrometry reveals that human breast cancer stem cells have significantly lower content of palmitoleic acid compared to their counterpart non-stem cancer cells', *Biochimie*, vol. 107 Pt A, pp. 73–77, Dec. 2014, doi: 10.1016/j.biochi.2014.10.003.
[582] M. A. Robinson, D. J. Graham, F. Morrish, D. Hockenbery, and L. J. Gamble, 'Lipid analysis of eight human breast cancer cell lines with ToF-SIMS', *Biointerphases*, vol. 11, no. 2, Aug. 2015, doi: 10.1116/1.4929633.
[583] K. Dimovska Nilsson, N. Neittaanmäki, O. Zaar, T. B. Angerer, J. Paoli, and J. S. Fletcher, 'TOF-SIMS imaging reveals tumor heterogeneity and inflammatory response markers in the microenvironment of basal cell carcinoma', *Biointerphases*, vol. 15, no. 4, p. 041012, Jul. 2020, doi: 10.1116/6.0000340.
[584] B. M. Bluestein *et al.*, 'An unsupervised MVA method to compare specific regions in human breast tumor tissue samples using ToF-SIMS', *Analyst*, vol. 141, no. 6, pp. 1947–1957, Mar. 2016, doi: 10.1039/C5AN02406D.
[585] T. B. Angerer, Y. Magnusson, G. Landberg, and J. S. Fletcher, 'Lipid Heterogeneity Resulting from Fatty Acid Processing in the Human Breast Cancer Microenvironment Identified by GCIB-ToF-SIMS Imaging', *Anal.*

Chem., vol. 88, no. 23, pp. 11946–11954, Dec. 2016, doi: 10.1021/acs.analchem.6b03884.
[586] S. K. Gularyan *et al.*, 'Investigation of Inter- and Intratumoral Heterogeneity of Glioblastoma Using TOF-SIMS*', *Molecular & Cellular Proteomics*, vol. 19, no. 6, pp. 960–970, Jun. 2020, doi: 10.1074/mcp.RA120.001986.
[587] N. Abbassi-Ghadi *et al.*, 'Imaging of Esophageal Lymph Node Metastases by Desorption Electrospray Ionization Mass Spectrometry', *Cancer Res*, vol. 76, no. 19, pp. 5647–5656, Oct. 2016, doi: 10.1158/0008-5472.CAN-16-0699.
[588] D. Calligaris *et al.*, 'Application of desorption electrospray ionization mass spectrometry imaging in breast cancer margin analysis', *PNAS*, vol. 111, no. 42, pp. 15184–15189, Oct. 2014, doi: 10.1073/pnas.1408129111.
[589] L. S. Eberlin *et al.*, 'Classifying human brain tumors by lipid imaging with mass spectrometry', *Cancer Res*, vol. 72, no. 3, pp. 645–654, Feb. 2012, doi: 10.1158/0008-5472.CAN-11-2465.
[590] A. L. Dill *et al.*, 'Multivariate statistical identification of human bladder carcinomas using ambient ionization imaging mass spectrometry', *Chemistry*, vol. 17, no. 10, pp. 2897–2902, Mar. 2011, doi: 10.1002/chem.201001692.
[591] J. Alexander *et al.*, 'A novel methodology for in vivo endoscopic phenotyping of colorectal cancer based on real-time analysis of the mucosal lipidome: a prospective observational study of the iKnife', *Surg Endosc*, vol. 31, no. 3, pp. 1361–1370, Mar. 2017, doi: 10.1007/s00464-016-5121-5.
[592] M. Fala *et al.*, 'Comparison of 13C MRI of hyperpolarized [1-13C]pyruvate and lactate with the corresponding mass spectrometry images in a murine lymphoma model', *Magnetic Resonance in Medicine*, vol. 85, no. 6, pp. 3027–3035, 2021, doi: https://doi.org/10.1002/mrm.28652.
[593] J. G. Swales *et al.*, 'Quantitation of Endogenous Metabolites in Mouse Tumors Using Mass-Spectrometry Imaging', *Anal. Chem.*, vol. 90, no. 10, pp. 6051–6058, May 2018, doi: 10.1021/acs.analchem.7b05239.
[594] A. Midey, H. Olivos, and B. Shrestha, 'Spatial Mapping of Cellular Metabolites Using DESI Ion Mobility Mass Spectrometry', in *Single Cell Metabolism: Methods and Protocols*, B. Shrestha, Ed. New York, NY: Springer, 2020, pp. 181–190. doi: 10.1007/978-1-4939-9831-9_14.
[595] K. Vijayalakshmi *et al.*, 'Identification of diagnostic metabolic signatures in clear cell renal cell carcinoma using mass spectrometry imaging', *International Journal of Cancer*, vol. 147, no. 1, pp. 256–265, 2020, doi: https://doi.org/10.1002/ijc.32843.
[596] H.M.S.O., 'Animals (Scientific Procedures) Act 1986'. London, 1990.
[597] E. Kerr, E. Gaude, F. Turrell, C. Frezza, and C. P. Martins, 'Mutant Kras copy number defines metabolic reprogramming and therapeutic susceptibilities', *Nature*, vol. 531, no. 7592, pp. 110–113, Mar. 2016, doi: 10.1038/nature16967.
[598] A. M. Race, A. D. Palmer, A. Dexter, R. T. Steven, I. B. Styles, and J. Bunch, 'SpectralAnalysis: Software for the Masses', *Anal Chem*, vol. 88, no. 19, pp. 9451–9458, Oct. 2016, doi: 10.1021/acs.analchem.6b01643.
[599] P. Inglese *et al.*, 'Network analysis of mass spectrometry imaging data from colorectal cancer identifies key metabolites common to metastatic development', *bioRxiv*, p. 230052, Jan. 2018, doi: 10.1101/230052.
[600] P. Inglese, G. Correia, Z. Takats, J. K. Nicholson, and R. C. Glen, 'SPUTNIK: an R package for filtering of spatially related peaks in mass spectrometry

imaging data', *Bioinformatics*, vol. 35, no. 1, pp. 178–180, Jan. 2019, doi: 10.1093/bioinformatics/bty622.
[601] 'Label-free Imaging of Biomolecules in Murine Brain Sections Using the 3D OrbiSIMS', Dec. 05, 2017. https://www.researchsquare.com (accessed Mar. 25, 2021).
[602] W. Luan *et al.*, 'PKM2 promotes glucose metabolism and cell growth in gliomas through a mechanism involving a let-7a/c-Myc/hnRNPA1 feedback loop', *Oncotarget*, vol. 6, no. 15, pp. 13006–13018, May 2015, doi: 10.18632/oncotarget.3514.
[603] Z. Hall *et al.*, 'Myc Expression Drives Aberrant Lipid Metabolism in Lung Cancer', *Cancer Res*, vol. 76, no. 16, pp. 4608–4618, Aug. 2016, doi: 10.1158/0008-5472.CAN-15-3403.
[604] J. Y. Leung, E. R. Andrechek, R. D. Cardiff, and J. R. Nevins, 'Heterogeneity in MYC-induced mammary tumors contributes to escape from oncogene dependence', *Oncogene*, vol. 31, no. 20, Art. no. 20, May 2012, doi: 10.1038/onc.2011.433.
[605] Z. P. Pavelic, K. Pavelic, C. P. Carter, and L. Pavelic, 'Heterogeneity of c-myc expression in histologically similar infiltrating ductal carcinomas of the breast', *J Cancer Res Clin Oncol*, vol. 118, no. 1, pp. 16–22, Jan. 1992, doi: 10.1007/BF01192306.
[606] P. Kreuzaler *et al.*, 'Heterogeneity of Myc expression in breast cancer exposes pharmacological vulnerabilities revealed through executable mechanistic modeling', *PNAS*, vol. 116, no. 44, pp. 22399–22408, Oct. 2019, doi: 10.1073/pnas.1903485116.
[607] A. R. Green *et al.*, 'MYC functions are specific in biological subtypes of breast cancer and confers resistance to endocrine therapy in luminal tumours', *British Journal of Cancer*, vol. 114, no. 8, Art. no. 8, Apr. 2016, doi: 10.1038/bjc.2016.46.
[608] S. Yin, V. T. Cheryan, L. Xu, A. K. Rishi, and K. B. Reddy, 'Myc mediates cancer stem-like cells and EMT changes in triple negative breast cancers cells', *PLOS ONE*, vol. 12, no. 8, p. e0183578, Aug. 2017, doi: 10.1371/journal.pone.0183578.
[609] E. Wagenblast *et al.*, 'A model of breast cancer heterogeneity reveals vascular mimicry as a driver of metastasis', *Nature*, vol. 520, no. 7547, Art. no. 7547, Apr. 2015, doi: 10.1038/nature14403.
[610] Y. Kang *et al.*, 'A multigenic program mediating breast cancer metastasis to bone', *Cancer Cell*, vol. 3, no. 6, pp. 537–549, Jun. 2003, doi: 10.1016/S1535-6108(03)00132-6.
[611] G. V. Echeverria *et al.*, 'High-resolution clonal mapping of multi-organ metastasis in triple negative breast cancer', *Nature Communications*, vol. 9, no. 1, Art. no. 1, Nov. 2018, doi: 10.1038/s41467-018-07406-4.
[612] A. R. Cantelmo *et al.*, 'Inhibition of the Glycolytic Activator PFKFB3 in Endothelium Induces Tumor Vessel Normalization, Impairs Metastasis, and Improves Chemotherapy', *Cancer Cell*, vol. 30, no. 6, pp. 968–985, Dec. 2016, doi: 10.1016/j.ccell.2016.10.006.
[613] K. M. Nieman *et al.*, 'Adipocytes promote ovarian cancer metastasis and provide energy for rapid tumor growth', *Nature Medicine*, vol. 17, no. 11, Art. no. 11, Nov. 2011, doi: 10.1038/nm.2492.

[614] M. Y. Fong *et al.*, 'Breast-cancer-secreted miR-122 reprograms glucose metabolism in premetastatic niche to promote metastasis', *Nat Cell Biol*, vol. 17, no. 2, pp. 183–194, Feb. 2015, doi: 10.1038/ncb3094.
[615] G. Bonuccelli *et al.*, 'Ketones and lactate "fuel" tumor growth and metastasis: Evidence that epithelial cancer cells use oxidative mitochondrial metabolism', *Cell Cycle*, vol. 9, no. 17, pp. 3506–3514, Sep. 2010, doi: 10.4161/cc.9.17.12731.
[616] M.-J. Nokin *et al.*, 'Methylglyoxal, a glycolysis side-product, induces Hsp90 glycation and YAP-mediated tumor growth and metastasis', *Elife*, vol. 5, Oct. 2016, doi: 10.7554/eLife.19375.
[617] J. Qu *et al.*, 'MYC overexpression with its prognostic and clinicopathological significance in breast cancer', *Oncotarget*, vol. 8, no. 55, pp. 93998–94008, Oct. 2017, doi: 10.18632/oncotarget.21501.
[618] T. A. Stewart, P. K. Pattengale, and P. Leder, 'Spontaneous mammary adenocarcinomas in transgenic mice that carry and express MTV/myc fusion genes', *Cell*, vol. 38, no. 3, pp. 627–637, Oct. 1984, doi: 10.1016/0092-8674(84)90257-5.
[619] C. A. Schoenenberger, A. C. Andres, B. Groner, M. van der Valk, M. LeMeur, and P. Gerlinger, 'Targeted c-myc gene expression in mammary glands of transgenic mice induces mammary tumours with constitutive milk protein gene transcription', *EMBO J*, vol. 7, no. 1, pp. 169–175, Jan. 1988.
[620] J. E. Hundley, S. K. Koester, D. A. Troyer, S. G. Hilsenbeck, R. E. Barrington, and J. J. Windle, 'Differential regulation of cell cycle characteristics and apoptosis in MMTV-myc and MMTV-ras mouse mammary tumors', *Cancer Res*, vol. 57, no. 4, pp. 600–603, Feb. 1997.
[621] E. P. Sandgren, J. A. Schroeder, T. H. Qui, R. D. Palmiter, R. L. Brinster, and D. C. Lee, 'Inhibition of mammary gland involution is associated with transforming growth factor alpha but not c-myc-induced tumorigenesis in transgenic mice', *Cancer Res*, vol. 55, no. 17, pp. 3915–3927, Sep. 1995.
[622] J. P. Thiery, 'Epithelial–mesenchymal transitions in tumour progression', *Nature Reviews Cancer*, vol. 2, no. 6, Art. no. 6, Jun. 2002, doi: 10.1038/nrc822.
[623] H. Wang and J. J. Unternaehrer, 'Epithelial-mesenchymal Transition and Cancer Stem Cells: At the Crossroads of Differentiation and Dedifferentiation', *Developmental Dynamics*, vol. 248, no. 1, pp. 10–20, 2019, doi: https://doi.org/10.1002/dvdy.24678.
[624] 'Frederick National Lab: LASP - Mouse Models Protocol Information'. https://frederick.cancer.gov/resources/repositories/nci-mouse-repository/mousemodels/Protocols.aspx?s=01XG2&g=MYC&p=1 (accessed Oct. 07, 2021).
[625] D. J. Bearss, R. J. Lee, D. A. Troyer, R. G. Pestell, and J. J. Windle, 'Differential Effects of p21WAF1/CIP1 Deficiency on MMTV-ras and MMTV-myc Mammary Tumor Properties', *Cancer Res*, vol. 62, no. 7, pp. 2077–2084, Apr. 2002.
[626] E. R. Andrechek *et al.*, 'Genetic heterogeneity of Myc-induced mammary tumors reflecting diverse phenotypes including metastatic potential', *PNAS*, vol. 106, no. 38, pp. 16387–16392, Sep. 2009, doi: 10.1073/pnas.0901250106.

[627] S. T. Eblen, ‘Extracellular Regulated Kinases: Signaling from Ras to ERK Substrates to Control Biological Outcomes’, *Adv Cancer Res*, vol. 138, pp. 99–142, 2018, doi: 10.1016/bs.acr.2018.02.004.
[628] H. Lavoie, J. Gagnon, and M. Therrien, ‘ERK signalling: a master regulator of cell behaviour, life and fate’, *Nat Rev Mol Cell Biol*, vol. 21, no. 10, pp. 607–632, Oct. 2020, doi: 10.1038/s41580-020-0255-7.
[629] L. C. Cantley, ‘The phosphoinositide 3-kinase pathway’, *Science*, vol. 296, no. 5573, pp. 1655–1657, May 2002, doi: 10.1126/science.296.5573.1655.
[630] B. A. Hemmings and D. F. Restuccia, ‘PI3K-PKB/Akt Pathway’, *Cold Spring Harbor Perspectives in Biology*, vol. 4, no. 9, Sep. 2012, doi: 10.1101/cshperspect.a011189.
[631] D. A. Fruman, H. Chiu, B. D. Hopkins, S. Bagrodia, L. C. Cantley, and R. T. Abraham, ‘The PI3K pathway in human disease’, *Cell*, vol. 170, no. 4, pp. 605–635, Aug. 2017, doi: 10.1016/j.cell.2017.07.029.
[632] J. T. Zilfou and S. W. Lowe, ‘Tumor Suppressive Functions of p53’, *Cold Spring Harb Perspect Biol*, vol. 1, no. 5, p. a001883, Nov. 2009, doi: 10.1101/cshperspect.a001883.
[633] F. Mantovani, L. Collavin, and G. Del Sal, ‘Mutant p53 as a guardian of the cancer cell’, *Cell Death Differ*, vol. 26, no. 2, pp. 199–212, Jan. 2019, doi: 10.1038/s41418-018-0246-9.
[634] A. Walvekar, Z. Rashida, H. Maddali, and S. Laxman, ‘A versatile LC-MS/MS approach for comprehensive, quantitative analysis of central metabolic pathways’, *Wellcome Open Res*, vol. 3, p. 122, Sep. 2018, doi: 10.12688/wellcomeopenres.14832.1.
[635] G. Boyce *et al.*, ‘Using liquid chromatography mass spectrometry (LC-MS) to assess the effect of age, high-fat diet, and rat strain on the liver metabolome’, *PLOS ONE*, vol. 15, no. 7, p. e0235338, Jul. 2020, doi: 10.1371/journal.pone.0235338.
[636] M. A. Kowalik *et al.*, ‘Metabolic reprogramming identifies the most aggressive lesions at early phases of hepatic carcinogenesis’, *Oncotarget*, vol. 7, no. 22, pp. 32375–32393, May 2016, doi: 10.18632/oncotarget.8632.
[637] S. Langbein *et al.*, ‘Metastasis is promoted by a bioenergetic switch: New targets for progressive renal cell cancer’, *International Journal of Cancer*, vol. 122, no. 11, pp. 2422–2428, 2008, doi: https://doi.org/10.1002/ijc.23403.
[638] S.-M. Jeon, N. S. Chandel, and N. Hay, ‘AMPK regulates NADPH homeostasis to promote tumour cell survival during energy stress’, *Nature*, vol. 485, no. 7400, Art. no. 7400, May 2012, doi: 10.1038/nature11066.
[639] O. Warburg, ‘The Metabolism of Carcinoma Cells’, *The Journal of Cancer Research*, vol. 9, no. 1, pp. 148–163, Mar. 1925, doi: 10.1158/jcr.1925.148.
[640] E. S. Ali *et al.*, ‘ERK2 Phosphorylates PFAS to Mediate Posttranslational Control of De Novo Purine Synthesis’, *Molecular Cell*, vol. 78, no. 6, pp. 1178-1191.e6, Jun. 2020, doi: 10.1016/j.molcel.2020.05.001.
[641] W. Wang, X. Yang, I. L. de Silanes, D. Carling, and M. Gorospe, ‘Increased AMP:ATP Ratio and AMP-activated Protein Kinase Activity during Cellular Senescence Linked to Reduced HuR Function *’, *Journal of Biological Chemistry*, vol. 278, no. 29, pp. 27016–27023, Jul. 2003, doi: 10.1074/jbc.M300318200.
[642] H. Sies, ‘Glutathione and its role in cellular functions’, *Free Radical Biology and Medicine*, vol. 27, no. 9, pp. 916–921, Nov. 1999, doi: 10.1016/S0891-5849(99)00177-X.

[643] P. Calvert, K.-S. Yao, T. C. Hamilton, and P. J. O'Dwyer, 'Clinical studies of reversal of drug resistance based on glutathione', *Chemico-Biological Interactions*, vol. 111–112, pp. 213–224, Apr. 1998, doi: 10.1016/S0009-2797(98)00008-8.
[644] Q. Chen *et al.*, 'Pharmacologic doses of ascorbate act as a prooxidant and decrease growth of aggressive tumor xenografts in mice', *Proc Natl Acad Sci U S A*, vol. 105, no. 32, pp. 11105–11109, Aug. 2008, doi: 10.1073/pnas.0804226105.
[645] E. Pawlowska, J. Szczepanska, and J. Blasiak, 'Pro- and Antioxidant Effects of Vitamin C in Cancer in correspondence to Its Dietary and Pharmacological Concentrations', *Oxid Med Cell Longev*, vol. 2019, Dec. 2019, doi: 10.1155/2019/7286737.
[646] M. F. Ullah, H. Y. Khan, H. Zubair, U. Shamim, and S. M. Hadi, 'The antioxidant ascorbic acid mobilizes nuclear copper leading to a prooxidant breakage of cellular DNA: implications for chemotherapeutic action against cancer', *Cancer Chemother Pharmacol*, vol. 67, no. 1, pp. 103–110, Jan. 2011, doi: 10.1007/s00280-010-1290-4.
[647] A. K. Chauhan, K.-J. Min, and T. K. Kwon, 'RIP1-dependent reactive oxygen species production executes artesunate-induced cell death in renal carcinoma Caki cells', *Mol Cell Biochem*, vol. 435, no. 1–2, pp. 15–24, Nov. 2017, doi: 10.1007/s11010-017-3052-7.
[648] H.-Q. Ju *et al.*, 'Disrupting G6PD-mediated Redox homeostasis enhances chemosensitivity in colorectal cancer', *Oncogene*, vol. 36, no. 45, Art. no. 45, Nov. 2017, doi: 10.1038/onc.2017.227.
[649] A. Kathagen-Buhmann *et al.*, 'Glycolysis and the pentose phosphate pathway are differentially associated with the dichotomous regulation of glioblastoma cell migration versus proliferation', *Neuro Oncol*, vol. 18, no. 9, pp. 1219–1229, Sep. 2016, doi: 10.1093/neuonc/now024.
[650] O. Vafa *et al.*, 'c-Myc can induce DNA damage, increase reactive oxygen species, and mitigate p53 function: a mechanism for oncogene-induced genetic instability', *Mol Cell*, vol. 9, no. 5, pp. 1031–1044, May 2002, doi: 10.1016/s1097-2765(02)00520-8.
[651] G. J. Burton and E. Jauniaux, 'Oxidative stress', *Best Pract Res Clin Obstet Gynaecol*, vol. 25, no. 3, pp. 287–299, Jun. 2011, doi: 10.1016/j.bpobgyn.2010.10.016.
[652] G. Pani, T. Galeotti, and P. Chiarugi, 'Metastasis: cancer cell's escape from oxidative stress', *Cancer Metastasis Rev*, vol. 29, no. 2, pp. 351–378, Jun. 2010, doi: 10.1007/s10555-010-9225-4.
[653] T. Fiaschi and P. Chiarugi, 'Oxidative Stress, Tumor Microenvironment, and Metabolic Reprogramming: A Diabolic Liaison', *Int J Cell Biol*, vol. 2012, 2012, doi: 10.1155/2012/762825.
[654] G. Mantovani *et al.*, 'Reactive oxygen species, antioxidant mechanisms and serum cytokine levels in cancer patients: impact of an antioxidant treatment', *Journal of Cellular and Molecular Medicine*, vol. 6, no. 4, pp. 570–582, 2002, doi: https://doi.org/10.1111/j.1582-4934.2002.tb00455.x.
[655] X. Liu and Z. Chen, 'The pathophysiological role of mitochondrial oxidative stress in lung diseases', *Journal of Translational Medicine*, vol. 15, no. 1, p. 207, Oct. 2017, doi: 10.1186/s12967-017-1306-5.
[656] E. Giannoni, T. Fiaschi, G. Ramponi, and P. Chiarugi, 'Redox regulation of anoikis resistance of metastatic prostate cancer cells: key role for Src and

EGFR-mediated pro-survival signals', *Oncogene*, vol. 28, no. 20, pp. 2074–2086, May 2009, doi: 10.1038/onc.2009.77.
[657] Y. Lv *et al.*, 'Nucleotide de novo synthesis increases breast cancer stemness and metastasis via cGMP-PKG-MAPK signaling pathway', *PLOS Biology*, vol. 18, no. 11, p. e3000872, Nov. 2020, doi: 10.1371/journal.pbio.3000872.
[658] M. A. Caudill *et al.*, 'Intracellular S-Adenosylhomocysteine Concentrations Predict Global DNA Hypomethylation in Tissues of Methyl-Deficient Cystathionine β-Synthase Heterozygous Mice', *The Journal of Nutrition*, vol. 131, no. 11, pp. 2811–2818, Nov. 2001, doi: 10.1093/jn/131.11.2811.
[659] P. G. Corn *et al.*, 'Transcriptional silencing of the p73 gene in acute lymphoblastic leukemia and Burkitt's lymphoma is associated with 5' CpG island methylation', *Cancer Res*, vol. 59, no. 14, pp. 3352–3356, Jul. 1999.
[660] J. M. Bhasin *et al.*, 'Methylome-wide Sequencing Detects DNA Hypermethylation Distinguishing Indolent from Aggressive Prostate Cancer', *Cell Rep*, vol. 13, no. 10, pp. 2135–2146, Dec. 2015, doi: 10.1016/j.celrep.2015.10.078.
[661] M. Reyngold *et al.*, 'Remodeling of the methylation landscape in breast cancer metastasis', *PLoS One*, vol. 9, no. 8, p. e103896, 2014, doi: 10.1371/journal.pone.0103896.
[662] G. Bretones, M. D. Delgado, and J. León, 'Myc and cell cycle control', *Biochim Biophys Acta*, vol. 1849, no. 5, pp. 506–516, May 2015, doi: 10.1016/j.bbagrm.2014.03.013.
[663] D. S. Askew, R. A. Ashmun, B. C. Simmons, and J. L. Cleveland, 'Constitutive c-myc expression in an IL-3-dependent myeloid cell line suppresses cell cycle arrest and accelerates apoptosis', *Oncogene*, vol. 6, no. 10, pp. 1915–1922, Oct. 1991.
[664] K. O. Mitchell *et al.*, 'Bax is a transcriptional target and mediator of c-myc-induced apoptosis', *Cancer Res*, vol. 60, no. 22, pp. 6318–6325, Nov. 2000.
[665] B. Teissedre, A. Pinderhughes, A. Incassati, S. J. Hatsell, M. Hiremath, and P. Cowin, 'MMTV-Wnt1 and -ΔN89β-Catenin Induce Canonical Signaling in Distinct Progenitors and Differentially Activate Hedgehog Signaling within Mammary Tumors', *PLOS ONE*, vol. 4, no. 2, p. e4537, Feb. 2009, doi: 10.1371/journal.pone.0004537.
[666] C. L. Chaffer *et al.*, 'Normal and neoplastic nonstem cells can spontaneously convert to a stem-like state', *PNAS*, vol. 108, no. 19, pp. 7950–7955, May 2011, doi: 10.1073/pnas.1102454108.
[667] S. Roy *et al.*, 'Rare somatic cells from human breast tissue exhibit extensive lineage plasticity', *Proc Natl Acad Sci U S A*, vol. 110, no. 12, pp. 4598–4603, Mar. 2013, doi: 10.1073/pnas.1218682110.
[668] J. Hu, G. Li, P. Zhang, X. Zhuang, and G. Hu, 'A CD44v+ subpopulation of breast cancer stem-like cells with enhanced lung metastasis capacity', *Cell Death Dis*, vol. 8, no. 3, p. e2679, Mar. 2017, doi: 10.1038/cddis.2017.72.
[669] E. Dornier *et al.*, 'Glutaminolysis drives membrane trafficking to promote invasiveness of breast cancer cells', *Nature Communications*, vol. 8, no. 1, Art. no. 1, Dec. 2017, doi: 10.1038/s41467-017-02101-2.
[670] S. Kim, D. H. Kim, W.-H. Jung, and J. S. Koo, 'Expression of glutamine metabolism-related proteins according to molecular subtype of breast cancer', *Endocr Relat Cancer*, vol. 20, no. 3, pp. 339–348, Jun. 2013, doi: 10.1530/ERC-12-0398.

[671] K. Jy *et al.*, 'Glutaminase expression is a poor prognostic factor in node-positive triple-negative breast cancer patients with a high level of tumor-infiltrating lymphocytes.', *Virchows Arch*, vol. 470, no. 4, pp. 381–389, Feb. 2017, doi: 10.1007/s00428-017-2083-5.
[672] S. Melnyk, M. Pogribna, I. P. Pogribny, P. Yi, and S. J. James, 'Measurement of Plasma and Intracellular S-Adenosylmethionine and S-Adenosylhomocysteine Utilizing Coulometric Electrochemical Detection: Alterations with Plasma Homocysteine and Pyridoxal 5′-Phosphate Concentrations', *Clinical Chemistry*, vol. 46, no. 2, pp. 265–272, Feb. 2000, doi: 10.1093/clinchem/46.2.265.
[673] C. Desjobert *et al.*, 'Combined analysis of DNA methylation and cell cycle in cancer cells', *Epigenetics*, vol. 10, no. 1, pp. 82–91, 2015, doi: 10.1080/15592294.2014.995542.
[674] G. P. Pfeifer, 'Defining Driver DNA Methylation Changes in Human Cancer', *Int J Mol Sci*, vol. 19, no. 4, Apr. 2018, doi: 10.3390/ijms19041166.
[675] T. Funasaka, T. Yanagawa, V. Hogan, and A. Raz, 'Regulation of phosphoglucose isomerase/autocrine motility factor expression by hypoxia', *FASEB J*, vol. 19, no. 11, pp. 1422–1430, Sep. 2005, doi: 10.1096/fj.05-3699com.
[676] S. Du *et al.*, 'Fructose-bisphosphate aldolase a is a potential metastasis-associated marker of lung squamous cell carcinoma and promotes lung cell tumorigenesis and migration', *PLoS One*, vol. 9, no. 1, p. e85804, 2014, doi: 10.1371/journal.pone.0085804.
[677] S. Kamarajugadda *et al.*, 'Glucose oxidation modulates anoikis and tumor metastasis', *Mol Cell Biol*, vol. 32, no. 10, pp. 1893–1907, May 2012, doi: 10.1128/MCB.06248-11.
[678] N. Wu, C. He, B. Zhu, J. Jiang, Y. Chen, and T. Ma, '3-Phosphoinositide Dependent Protein Kinase-1 (PDK-1) Promotes Migration and Invasion in Gastric Cancer Cells Through Activating the NF-κB Pathway', *Oncol Res*, vol. 25, no. 7, pp. 1153–1159, Aug. 2017, doi: 10.3727/096504017X14845839228545.
[679] L. Yang *et al.*, 'Twist promotes reprogramming of glucose metabolism in breast cancer cells through PI3K/AKT and p53 signaling pathways', *Oncotarget*, vol. 6, no. 28, pp. 25755–25769, Sep. 2015, doi: 10.18632/oncotarget.4697.
[680] C. Dong *et al.*, 'Loss of FBP1 by Snail-mediated repression provides metabolic advantages in basal-like breast cancer', *Cancer Cell*, vol. 23, no. 3, pp. 316–331, Mar. 2013, doi: 10.1016/j.ccr.2013.01.022.
[681] Y. Kondaveeti, I. K. Guttilla Reed, and B. A. White, 'Epithelial-mesenchymal transition induces similar metabolic alterations in two independent breast cancer cell lines', *Cancer Lett*, vol. 364, no. 1, pp. 44–58, Aug. 2015, doi: 10.1016/j.canlet.2015.04.025.
[682] H. Ito, M. Duxbury, M. J. Zinner, S. W. Ashley, and E. E. Whang, 'Glucose transporter-1 gene expression is associated with pancreatic cancer invasiveness and MMP-2 activity', *Surgery*, vol. 136, no. 3, pp. 548–556, Sep. 2004, doi: 10.1016/j.surg.2004.05.032.
[683] J. Jiang, K. Wang, Y. Chen, H. Chen, E. C. Nice, and C. Huang, 'Redox regulation in tumor cell epithelial–mesenchymal transition: molecular basis and therapeutic strategy', *Signal Transduct Target Ther*, vol. 2, p. 17036, Aug. 2017, doi: 10.1038/sigtrans.2017.36.

[684] R. Moreno-Sánchez, Á. Marín-Hernández, J. C. Gallardo-Pérez, C. Vázquez, S. Rodríguez-Enríquez, and E. Saavedra, 'Control of the NADPH supply and GSH recycling for oxidative stress management in hepatoma and liver mitochondria', *Biochimica et Biophysica Acta (BBA) - Bioenergetics*, vol. 1859, no. 10, pp. 1138–1150, Oct. 2018, doi: 10.1016/j.bbabio.2018.07.008.
[685] R. Moreno-Sánchez, J. C. Gallardo-Pérez, S. Rodríguez-Enríquez, E. Saavedra, and Á. Marín-Hernández, 'Control of the NADPH supply for oxidative stress handling in cancer cells', *Free Radical Biology and Medicine*, vol. 112, pp. 149–161, Nov. 2017, doi: 10.1016/j.freeradbiomed.2017.07.018.
[686] W. Lu, L. Wang, L. Chen, S. Hui, and J. D. Rabinowitz, 'Extraction and Quantitation of Nicotinamide Adenine Dinucleotide Redox Cofactors', *Antioxid Redox Signal*, vol. 28, no. 3, pp. 167–179, Jan. 2018, doi: 10.1089/ars.2017.7014.
[687] M. Ogrunc *et al.*, 'Oncogene-induced reactive oxygen species fuel hyperproliferation and DNA damage response activation', *Cell Death & Differentiation*, vol. 21, no. 6, Art. no. 6, Jun. 2014, doi: 10.1038/cdd.2014.16.
[688] J. El-Benna, M. Hurtado-Nedelec, V. Marzaioli, J.-C. Marie, M.-A. Gougerot-Pocidalo, and P. M.-C. Dang, 'Priming of the neutrophil respiratory burst: role in host defense and inflammation', *Immunol Rev*, vol. 273, no. 1, pp. 180–193, Sep. 2016, doi: 10.1111/imr.12447.
[689] Y. Zhang, S. Choksi, K. Chen, Y. Pobezinskaya, I. Linnoila, and Z.-G. Liu, 'ROS play a critical role in the differentiation of alternatively activated macrophages and the occurrence of tumor-associated macrophages', *Cell Research*, vol. 23, no. 7, Art. no. 7, Jul. 2013, doi: 10.1038/cr.2013.75.
[690] J. Zeng, W. K. K. Wu, H. Wang, and X. Li, 'Serine and one-carbon metabolism, a bridge that links mTOR signaling and DNA methylation in cancer', *Pharmacological Research*, vol. 149, p. 104352, Nov. 2019, doi: 10.1016/j.phrs.2019.104352.
[691] Y. Gu *et al.*, 'mTORC2 Regulates Amino Acid Metabolism in Cancer by Phosphorylation of the Cystine-Glutamate Antiporter xCT', *Mol Cell*, vol. 67, no. 1, pp. 128-138.e7, Jul. 2017, doi: 10.1016/j.molcel.2017.05.030.
[692] P. Giulidori, M. Galli-Kienle, E. Catto, and G. Stramentinoli, 'Transmethylation, transsulfuration, and aminopropylation reactions of S-adenosyl-L-methionine in vivo', *J Biol Chem*, vol. 259, no. 7, pp. 4205–4211, Apr. 1984.
[693] A. M. Devlin, E. Arning, T. Bottiglieri, F. M. Faraci, R. Rozen, and S. R. Lentz, 'Effect of Mthfr genotype on diet-induced hyperhomocysteinemia and vascular function in mice', *Blood*, vol. 103, no. 7, pp. 2624–2629, Apr. 2004, doi: 10.1182/blood-2003-09-3078.
[694] M. J. Aryee *et al.*, 'DNA methylation alterations exhibit intra-individual stability and inter-individual heterogeneity in prostate cancer metastases', *Sci Transl Med*, vol. 5, no. 169, p. 169ra10, Jan. 2013, doi: 10.1126/scitranslmed.3005211.
[695] K. Konishi *et al.*, 'DNA Methylation Profiles of Primary Colorectal Carcinoma and Matched Liver Metastasis', *PLoS One*, vol. 6, no. 11, Nov. 2011, doi: 10.1371/journal.pone.0027889.
[696] S. J. Nass *et al.*, 'Aberrant methylation of the estrogen receptor and E-cadherin 5' CpG islands increases with malignant progression in human breast cancer', *Cancer Res*, vol. 60, no. 16, pp. 4346–4348, Aug. 2000.

[697] F. Kottakis *et al.*, 'LKB1 loss links serine metabolism to DNA methylation and tumorigenesis', *Nature*, vol. 539, no. 7629, Art. no. 7629, Nov. 2016, doi: 10.1038/nature20132.
[698] N. Mahmood *et al.*, 'Methyl donor S-adenosylmethionine (SAM) supplementation attenuates breast cancer growth, invasion, and metastasis in vivo; therapeutic and chemopreventive applications', *Oncotarget*, vol. 9, no. 4, pp. 5169–5183, Dec. 2017, doi: 10.18632/oncotarget.23704.
[699] G. M. Son, M.-S. Kwon, D.-H. Shin, N. Shin, D. Ryu, and C.-D. Kang, 'Comparisons of cancer-associated fibroblasts in the intratumoral stroma and invasive front in colorectal cancer', *Medicine (Baltimore)*, vol. 98, no. 18, May 2019, doi: 10.1097/MD.0000000000015164.
[700] L. Du *et al.*, 'High Vimentin Expression Predicts a Poor Prognosis and Progression in Colorectal Cancer: A Study with Meta-Analysis and TCGA Database', *BioMed Research International*, vol. 2018, p. e6387810, May 2018, doi: 10.1155/2018/6387810.
[701] A. L. Berr *et al.*, 'Vimentin is Required for Tumor Progression and Metastasis in a Mouse Model of Non-Small Cell Lung Cancer', *bioRxiv*, p. 2020.06.04.130963, Jun. 2020, doi: 10.1101/2020.06.04.130963.
[702] Y. Fuyuhiro *et al.*, 'Clinical significance of vimentin-positive gastric cancer cells', *Anticancer Res*, vol. 30, no. 12, pp. 5239–5243, Dec. 2010.
[703] S. Ramaswamy, K. N. Ross, E. S. Lander, and T. R. Golub, 'A molecular signature of metastasis in primary solid tumors', *Nat Genet*, vol. 33, no. 1, pp. 49–54, Jan. 2003, doi: 10.1038/ng1060.
[704] J. E. Talmadge, 'Clonal Selection of Metastasis within the Life History of a Tumor', *Cancer Res*, vol. 67, no. 24, pp. 11471–11475, Dec. 2007, doi: 10.1158/0008-5472.CAN-07-2496.
[705] A. Walens *et al.*, 'Adaptation and selection shape clonal evolution of tumors during residual disease and recurrence', *Nature Communications*, vol. 11, no. 1, Art. no. 1, Oct. 2020, doi: 10.1038/s41467-020-18730-z.
[706] L. A. Baldwin *et al.*, 'DNA barcoding reveals ongoing immunoediting of clonal cancer populations during metastatic progression and in response to immunotherapy', *bioRxiv*, p. 2021.01.11.426174, Jan. 2021, doi: 10.1101/2021.01.11.426174.
[707] E.-J. Tan, A.-K. Olsson, and A. Moustakas, 'Reprogramming during epithelial to mesenchymal transition under the control of TGFβ', *Cell Adh Migr*, vol. 9, no. 3, pp. 233–246, Nov. 2014, doi: 10.4161/19336918.2014.983794.
[708] O. G. McDonald *et al.*, 'Epigenomic reprogramming during pancreatic cancer progression links anabolic glucose metabolism to distant metastasis', *Nat Genet*, vol. 49, no. 3, pp. 367–376, Mar. 2017, doi: 10.1038/ng.3753.
[709] P. Lindner *et al.*, 'EMT transcription factor ZEB1 alters the epigenetic landscape of colorectal cancer cells', *Cell Death Dis*, vol. 11, no. 2, Feb. 2020, doi: 10.1038/s41419-020-2340-4.
[710] V. L. Payen, P. E. Porporato, B. Baselet, and P. Sonveaux, 'Metabolic changes associated with tumor metastasis, part 1: tumor pH, glycolysis and the pentose phosphate pathway', *Cell Mol Life Sci*, vol. 73, no. 7, pp. 1333–1348, Apr. 2016, doi: 10.1007/s00018-015-2098-5.
[711] P. E. Porporato, V. L. Payen, B. Baselet, and P. Sonveaux, 'Metabolic changes associated with tumor metastasis, part 2: Mitochondria, lipid and amino acid metabolism', *Cell Mol Life Sci*, vol. 73, no. 7, pp. 1349–1363, Apr. 2016, doi: 10.1007/s00018-015-2100-2.

[712] M. Sciacovelli and C. Frezza, ‘Metabolic reprogramming and epithelial-to-mesenchymal transition in cancer’, *FEBS J*, vol. 284, no. 19, pp. 3132–3144, Oct. 2017, doi: 10.1111/febs.14090.
[713] M. R. Zanotelli, J. Zhang, and C. A. Reinhart-King, ‘Mechanoresponsive metabolism in cancer cell migration and metastasis’, *Cell Metabolism*, Apr. 2021, doi: 10.1016/j.cmet.2021.04.002.
[714] E. D. Montal *et al.*, ‘PEPCK Coordinates the Regulation of Central Carbon Metabolism to Promote Cancer Cell Growth’, *Molecular Cell*, vol. 60, no. 4, pp. 571–583, Nov. 2015, doi: 10.1016/j.molcel.2015.09.025.
[715] E. Smolle *et al.*, ‘Distribution and prognostic significance of gluconeogenesis and glycolysis in lung cancer’, *Molecular Oncology*, vol. 14, no. 11, pp. 2853–2867, 2020, doi: https://doi.org/10.1002/1878-0261.12780.
[716] G. Grasmann *et al.*, ‘PCK2 opposes mitochondrial respiration and maintains the redox balance in starved lung cancer cells’, *bioRxiv*, p. 2020.11.23.393686, Nov. 2020, doi: 10.1101/2020.11.23.393686.
[717] E. G. Beale, B. J. Harvey, and C. Forest, ‘PCK1 and PCK2 as candidate diabetes and obesity genes’, *Cell Biochem Biophys*, vol. 48, no. 2–3, pp. 89–95, 2007, doi: 10.1007/s12013-007-0025-6.
[718] D. M. Demas *et al.*, ‘Glutamine Metabolism Drives Growth in Advanced Hormone Receptor Positive Breast Cancer’, *Front. Oncol.*, vol. 9, 2019, doi: 10.3389/fonc.2019.00686.
[719] L. Xiang *et al.*, ‘Glutaminase 1 expression in colorectal cancer cells is induced by hypoxia and required for tumor growth, invasion, and metastatic colonization’, *Cell Death & Disease*, vol. 10, no. 2, Art. no. 2, Jan. 2019, doi: 10.1038/s41419-018-1291-5.
[720] L. Ren *et al.*, ‘Glutaminase-1 (GLS1) inhibition limits metastatic progression in osteosarcoma’, *Cancer & Metabolism*, vol. 8, no. 1, p. 4, Mar. 2020, doi: 10.1186/s40170-020-0209-8.
[721] J. Moreno-Felici *et al.*, ‘Phosphoenolpyruvate from Glycolysis and PEPCK Regulate Cancer Cell Fate by Altering Cytosolic Ca2+’, *Cells*, vol. 9, no. 1, Dec. 2019, doi: 10.3390/cells9010018.
[722] M. A. Hawk, C. McCallister, and Z. T. Schafer, ‘Antioxidant Activity during Tumor Progression: A Necessity for the Survival of Cancer Cells?’, *Cancers (Basel)*, vol. 8, no. 10, Oct. 2016, doi: 10.3390/cancers8100092.
[723] Y. Zhang, S. Lin, Y. Chen, F. Yang, and S. Liu, ‘LDH-Apromotes epithelial–mesenchymal transition by upregulating ZEB2 in intestinal-type gastric cancer’, *Onco Targets Ther*, vol. 11, pp. 2363–2373, Apr. 2018, doi: 10.2147/OTT.S163570.
[724] A. Forkasiewicz, M. Dorociak, K. Stach, P. Szelachowski, R. Tabola, and K. Augoff, ‘The usefulness of lactate dehydrogenase measurements in current oncological practice’, *Cellular & Molecular Biology Letters*, vol. 25, no. 1, p. 35, Jun. 2020, doi: 10.1186/s11658-020-00228-7.
[725] M. Arra *et al.*, ‘LDHA-mediated ROS generation in chondrocytes is a potential therapeutic target for osteoarthritis’, *Nature Communications*, vol. 11, no. 1, Art. no. 1, Jul. 2020, doi: 10.1038/s41467-020-17242-0.
[726] Y. Kolev, H. Uetake, Y. Takagi, and K. Sugihara, ‘Lactate dehydrogenase-5 (LDH-5) expression in human gastric cancer: association with hypoxia-inducible factor (HIF-1alpha) pathway, angiogenic factors production and poor prognosis’, *Ann Surg Oncol*, vol. 15, no. 8, pp. 2336–2344, Aug. 2008, doi: 10.1245/s10434-008-9955-5.

[727] I. Serganova *et al.*, 'LDH-A regulates the tumor microenvironment via HIF-signaling and modulates the immune response', *PLoS One*, vol. 13, no. 9, Sep. 2018, doi: 10.1371/journal.pone.0203965.
[728] L.-S. Hao *et al.*, 'Correlation and expression analysis of hypoxia-inducible factor 1α, glucose transporter 1 and lactate dehydrogenase 5 in human gastric cancer', *Oncology Letters*, vol. 18, no. 2, pp. 1431–1441, Aug. 2019, doi: 10.3892/ol.2019.10457.
[729] I. Georgakopoulos-Soares, D. V. Chartoumpekis, V. Kyriazopoulou, and A. Zaravinos, 'EMT Factors and Metabolic Pathways in Cancer', *Front. Oncol.*, vol. 10, 2020, doi: 10.3389/fonc.2020.00499.
[730] N. H. Kim *et al.*, 'Snail reprograms glucose metabolism by repressing phosphofructokinase PFKP allowing cancer cell survival under metabolic stress', *Nature Communications*, vol. 8, no. 1, Art. no. 1, Feb. 2017, doi: 10.1038/ncomms14374.
[731] L. Jin and Y. Zhou, 'Crucial role of the pentose phosphate pathway in malignant tumors', *Oncol Lett*, vol. 17, no. 5, pp. 4213–4221, May 2019, doi: 10.3892/ol.2019.10112.
[732] K. Y. Sletta *et al.*, 'Oxygen-dependent regulation of tumor growth and metastasis in human breast cancer xenografts', *PLOS ONE*, vol. 12, no. 8, p. e0183254, Aug. 2017, doi: 10.1371/journal.pone.0183254.
[733] Y. Audet-Delage and J. St-Pierre, 'Food for Growth: Distinct Nutrient Preferences between Primary Tumors and Metastases', *Mol Cell*, vol. 81, no. 2, pp. 220–222, Jan. 2021, doi: 10.1016/j.molcel.2020.12.044.
[734] T. Celià-Terrassa and Y. Kang, 'Metastatic niche functions and therapeutic opportunities', *Nature Cell Biology*, vol. 20, no. 8, Art. no. 8, Aug. 2018, doi: 10.1038/s41556-018-0145-9.
[735] G. Szczesny, A. Veihelmann, S. Massberg, D. Nolte, and K. Messmer, 'Long-term anaesthesia using inhalatory isoflurane in different strains of mice-the haemodynamic effects', *Lab Anim*, vol. 38, no. 1, pp. 64–69, Jan. 2004, doi: 10.1258/00236770460734416.
[736] K. K. Noguchi *et al.*, 'Isoflurane exposure for three hours triggers apoptotic cell death in neonatal macaque brain', *Br J Anaesth*, vol. 119, no. 3, pp. 524–531, Sep. 2017, doi: 10.1093/bja/aex123.
[737] M. R. Antoniewicz, 'A guide to 13C metabolic flux analysis for the cancer biologist', *Exp Mol Med*, vol. 50, no. 4, pp. 1–13, Apr. 2018, doi: 10.1038/s12276-018-0060-y.
[738] C. Jang, L. Chen, and J. D. Rabinowitz, 'Metabolomics and isotope tracing', *Cell*, vol. 173, no. 4, pp. 822–837, May 2018, doi: 10.1016/j.cell.2018.03.055.
[739] V. L. Kinnula and J. D. Crapo, 'Superoxide dismutases in the lung and human lung diseases', *Am J Respir Crit Care Med*, vol. 167, no. 12, pp. 1600–1619, Jun. 2003, doi: 10.1164/rccm.200212-1479SO.
[740] P. Cheresh, S.-J. Kim, S. Tulasiram, and D. W. Kamp, 'Oxidative Stress and Pulmonary Fibrosis', *Biochim Biophys Acta*, vol. 1832, no. 7, pp. 1028–1040, Jul. 2013, doi: 10.1016/j.bbadis.2012.11.021.
[741] A. Kuehne *et al.*, 'Acute Activation of Oxidative Pentose Phosphate Pathway as First-Line Response to Oxidative Stress in Human Skin Cells', *Mol Cell*, vol. 59, no. 3, pp. 359–371, Aug. 2015, doi: 10.1016/j.molcel.2015.06.017.
[742] H. C. Hope, R. J. Brownlie, L. Steele, and R. J. Salmond, 'Coordination of asparagine uptake and asparagine synthetase expression is required for T

cell activation', *bioRxiv*, p. 2020.02.28.969774, Mar. 2020, doi: 10.1101/2020.02.28.969774.
[743] A. Solans, X. Estivill, and S. de la Luna, 'Cloning and characterization of human FTCD on 21q22.3, a candidate gene for glutamate formiminotransferase deficiency', *Cytogenet Cell Genet*, vol. 88, no. 1–2, pp. 43–49, 2000, doi: 10.1159/000015483.
[744] S. Hui *et al.*, 'Quantitative fluxomics of circulating metabolites', *Cell Metab*, vol. 32, no. 4, pp. 676-688.e4, Oct. 2020, doi: 10.1016/j.cmet.2020.07.013.
[745] M. Yuan *et al.*, 'Ex vivo and in vivo stable isotope labelling of central carbon metabolism and related pathways with analysis by LC–MS/MS', *Nat Protoc*, vol. 14, no. 2, pp. 313–330, Feb. 2019, doi: 10.1038/s41596-018-0102-x.
[746] J. M. Buescher *et al.*, 'A roadmap for interpreting 13C metabolite labeling patterns from cells', *Curr Opin Biotechnol*, vol. 34, pp. 189–201, Aug. 2015, doi: 10.1016/j.copbio.2015.02.003.
[747] I.-Y. Kim, S.-H. Suh, I.-K. Lee, and R. R. Wolfe, 'Applications of stable, nonradioactive isotope tracers in in vivo human metabolic research', *Exp Mol Med*, vol. 48, no. 1, pp. e203–e203, Jan. 2016, doi: 10.1038/emm.2015.97.
[748] C. Lopes, C. Pereira, and R. Medeiros, 'ASCT2 and LAT1 Contribution to the Hallmarks of Cancer: From a Molecular Perspective to Clinical Translation', *Cancers*, vol. 13, no. 2, Art. no. 2, Jan. 2021, doi: 10.3390/cancers13020203.
[749] Y. Mitsuishi *et al.*, 'Nrf2 redirects glucose and glutamine into anabolic pathways in metabolic reprogramming', *Cancer Cell*, vol. 22, no. 1, pp. 66–79, Jul. 2012, doi: 10.1016/j.ccr.2012.05.016.
[750] M. C. Jaramillo and D. D. Zhang, 'The emerging role of the Nrf2-Keap1 signaling pathway in cancer', *Genes Dev*, vol. 27, no. 20, pp. 2179–2191, Oct. 2013, doi: 10.1101/gad.225680.113.
[751] H.-C. Yang *et al.*, 'The Redox Role of G6PD in Cell Growth, Cell Death, and Cancer', *Cells*, vol. 8, no. 9, Sep. 2019, doi: 10.3390/cells8091055.
[752] S. H. Mousavi-fard, 'Downregulation of the G6PDH Pathway Can Promote Oxidative Stress-Mediated Reversal of Drug Resistance in B-Cell Lymphoma cell Lines', *The FASEB Journal*, vol. 30, no. S1, p. 606.7-606.7, 2016, doi: https://doi.org/10.1096/fasebj.30.1_supplement.606.7.
[753] W. Xiao, R.-S. Wang, D. E. Handy, and J. Loscalzo, 'NAD(H) and NADP(H) Redox Couples and Cellular Energy Metabolism', *Antioxid Redox Signal*, vol. 28, no. 3, pp. 251–272, Jan. 2018, doi: 10.1089/ars.2017.7216.
[754] A. R. Mullen *et al.*, 'Reductive carboxylation supports growth in tumour cells with defective mitochondria', *Nature*, vol. 481, no. 7381, Art. no. 7381, Jan. 2012, doi: 10.1038/nature10642.
[755] L. Jiang *et al.*, 'Reductive carboxylation supports redox homeostasis during anchorage-independent growth', *Nature*, vol. 532, no. 7598, pp. 255–258, Apr. 2016, doi: 10.1038/nature17393.
[756] E. Gaude *et al.*, 'NADH Shuttling Couples Cytosolic Reductive Carboxylation of Glutamine with Glycolysis in Cells with Mitochondrial Dysfunction', *Molecular Cell*, vol. 69, no. 4, pp. 581-593.e7, Feb. 2018, doi: 10.1016/j.molcel.2018.01.034.
[757] N. N. Pavlova *et al.*, 'As Extracellular Glutamine Levels Decline, Asparagine Becomes an Essential Amino Acid', *Cell Metab*, vol. 27, no. 2, pp. 428-438.e5, Feb. 2018, doi: 10.1016/j.cmet.2017.12.006.

[758] M. Chiu, G. Taurino, M. G. Bianchi, M. S. Kilberg, and O. Bussolati, ‘Asparagine Synthetase in Cancer: Beyond Acute Lymphoblastic Leukemia’, *Front Oncol*, vol. 9, Jan. 2020, doi: 10.3389/fonc.2019.01480.
[759] J. H. Lee *et al.*, ‘Branched-chain amino acids sustain pancreatic cancer growth by regulating lipid metabolism’, *Experimental & Molecular Medicine*, vol. 51, no. 11, Art. no. 11, Nov. 2019, doi: 10.1038/s12276-019-0350-z.
[760] F. Xiao *et al.*, ‘Leucine deprivation inhibits proliferation and induces apoptosis of human breast cancer cells via fatty acid synthase’, *Oncotarget*, vol. 7, no. 39, pp. 63679–63689, Aug. 2016, doi: 10.18632/oncotarget.11626.
[761] A. K. Najumudeen *et al.*, ‘The amino acid transporter SLC7A5 is required for efficient growth of KRAS-mutant colorectal cancer’, *Nature Genetics*, vol. 53, no. 1, Art. no. 1, Jan. 2021, doi: 10.1038/s41588-020-00753-3.
[762] H. S. Park, S. R. Kim, and Y. C. Lee, ‘Impact of oxidative stress on lung diseases’, *Respirology*, vol. 14, no. 1, pp. 27–38, 2009, doi: https://doi.org/10.1111/j.1440-1843.2008.01447.x.
[763] N. Zhang, ‘Role of methionine on epigenetic modification of DNA methylation and gene expression in animals’, *Animal Nutrition*, vol. 4, no. 1, pp. 11–16, Mar. 2018, doi: 10.1016/j.aninu.2017.08.009.
[764] G. Rinaldi *et al.*, ‘In Vivo Evidence for Serine Biosynthesis-Defined Sensitivity of Lung Metastasis, but Not of Primary Breast Tumors, to mTORC1 Inhibition’, *Molecular Cell*, vol. 81, no. 2, pp. 386-397.e7, Jan. 2021, doi: 10.1016/j.molcel.2020.11.027.
[765] A. M. Li *et al.*, ‘Metabolic Profiling Reveals a Dependency of Human Metastatic Breast Cancer on Mitochondrial Serine and One-Carbon Unit Metabolism’, *Mol Cancer Res*, vol. 18, no. 4, pp. 599–611, Apr. 2020, doi: 10.1158/1541-7786.MCR-19-0606.
[766] D. P. Hollern, M. R. Swiatnicki, and E. R. Andrechek, ‘Histological subtypes of mouse mammary tumors reveal conserved relationships to human cancers’, *PLOS Genetics*, vol. 14, no. 1, p. e1007135, Jan. 2018, doi: 10.1371/journal.pgen.1007135.
[767] S. K. Wculek and I. Malanchi, ‘Neutrophils support lung colonization of metastasis-initiating breast cancer cells’, *Nature*, vol. 528, no. 7582, pp. 413–417, Dec. 2015, doi: 10.1038/nature16140.
[768] O. Shani *et al.*, ‘Evolution of metastases-associated fibroblasts in the lung microenvironment is driven by stage-specific transcriptional plasticity’, *bioRxiv*, p. 778936, Sep. 2019, doi: 10.1101/778936.
[769] M. Pein *et al.*, ‘Metastasis-initiating cells induce and exploit a fibroblast niche to fuel malignant colonization of the lungs’, *Nat Commun*, vol. 11, no. 1, p. 1494, Mar. 2020, doi: 10.1038/s41467-020-15188-x.
[770] M. Wenes *et al.*, ‘Macrophage Metabolism Controls Tumor Blood Vessel Morphogenesis and Metastasis’, *Cell Metab*, vol. 24, no. 5, pp. 701–715, Nov. 2016, doi: 10.1016/j.cmet.2016.09.008.
[771] J. B. Fenn, M. Mann, C. K. Meng, S. F. Wong, and C. M. Whitehouse, ‘Electrospray ionization for mass spectrometry of large biomolecules’, *Science*, vol. 246, no. 4926, pp. 64–71, Oct. 1989, doi: 10.1126/science.2675315.
[772] X. Han and R. W. Gross, ‘Global analyses of cellular lipidomes directly from crude extracts of biological samples by ESI mass spectrometry: a bridge to lipidomics’, *J Lipid Res*, vol. 44, no. 6, pp. 1071–1079, Jun. 2003, doi: 10.1194/jlr.R300004-JLR200.

[773] L. S. Eberlin, C. R. Ferreira, A. L. Dill, D. R. Ifa, and R. G. Cooks, ‘Desorption Electrospray Ionization Mass Spectrometry for Lipid Characterization and Biological Tissue Imaging’, *Biochim Biophys Acta*, vol. 1811, no. 11, pp. 946–960, Nov. 2011, doi: 10.1016/j.bbalip.2011.05.006.
[774] J. Leopold, Y. Popkova, K. M. Engel, and J. Schiller, ‘Recent Developments of Useful MALDI Matrices for the Mass Spectrometric Characterization of Lipids’, *Biomolecules*, vol. 8, no. 4, Dec. 2018, doi: 10.3390/biom8040173.
[775] S. Banerjee *et al.*, ‘Diagnosis of prostate cancer by desorption electrospray ionization mass spectrometric imaging of small metabolites and lipids’, *PNAS*, vol. 114, no. 13, pp. 3334–3339, Mar. 2017, doi: 10.1073/pnas.1700677114.
[776] J.-L. Ren, A.-H. Zhang, L. Kong, and X.-J. Wang, ‘Advances in mass spectrometry-based metabolomics for investigation of metabolites’, *RSC Advances*, vol. 8, no. 40, pp. 22335–22350, 2018, doi: 10.1039/C8RA01574K.
[777] A. Kleinridders *et al.*, ‘Regional differences in brain glucose metabolism determined by imaging mass spectrometry’, *Mol Metab*, vol. 12, pp. 113–121, Jun. 2018, doi: 10.1016/j.molmet.2018.03.013.
[778] Q. Wu, Y. Li, Y. Wang, and H. Lu, ‘Quantitative mass spectrometry imaging of amino acids with isomer differentiation in brain tissue via exhaustive liquid microjunction surface sampling–tandem mass tags labeling–ultra performance liquid chromatography–mass spectrometry’, *Journal of Chromatography A*, vol. 1621, p. 461086, Jun. 2020, doi: 10.1016/j.chroma.2020.461086.
[779] J. Upendra Rao *et al.*, ‘CBMT-13. UNRAVELLING METABOLISM OF GLIOBLASTOMA USING MASS SPECTROMETRY IMAGING’, *Neuro Oncol*, vol. 20, no. Suppl 6, p. vi35, Nov. 2018, doi: 10.1093/neuonc/noy148.132.
[780] A. Gil-de-la-Fuente *et al.*, ‘CEU Mass Mediator 3.0: A Metabolite Annotation Tool’, *J Proteome Res*, vol. 18, no. 2, pp. 797–802, Feb. 2019, doi: 10.1021/acs.jproteome.8b00720.
[781] A. Mestre-Farrera *et al.*, ‘Glutamine-Directed Migration of Cancer-Activated Fibroblasts Facilitates Epithelial Tumor Invasion’, *Cancer Res*, vol. 81, no. 2, pp. 438–451, Jan. 2021, doi: 10.1158/0008-5472.CAN-20-0622.
[782] L. Yang *et al.*, ‘Targeting Stromal Glutamine Synthetase in Tumors Disrupts Tumor Microenvironment-Regulated Cancer Cell Growth’, *Cell Metabolism*, vol. 24, no. 5, pp. 685–700, Nov. 2016, doi: 10.1016/j.cmet.2016.10.011.
[783] R. B. Hamanaka *et al.*, ‘Glutamine Metabolism Is Required for Collagen Protein Synthesis in Lung Fibroblasts’, *Am J Respir Cell Mol Biol*, vol. 61, no. 5, pp. 597–606, Apr. 2019, doi: 10.1165/rcmb.2019-0008OC.
[784] Y. Eguchi, S. Shimizu, and Y. Tsujimoto, ‘Intracellular ATP levels determine cell death fate by apoptosis or necrosis’, *Cancer Res*, vol. 57, no. 10, pp. 1835–1840, May 1997.
[785] Y. Shi, J. E. Evans, and K. L. Rock, ‘Molecular identification of a danger signal that alerts the immune system to dying cells’, *Nature*, vol. 425, no. 6957, Art. no. 6957, Oct. 2003, doi: 10.1038/nature01991.
[786] H. Kono, C.-J. Chen, F. Ontiveros, and K. L. Rock, ‘Uric acid promotes an acute inflammatory response to sterile cell death in mice’, *J Clin Invest*, vol. 120, no. 6, pp. 1939–1949, Jun. 2010, doi: 10.1172/JCI40124.

[787] L. Ombrato *et al.*, ‘Metastatic niche labelling reveals tissue parenchyma stem cell features’, *Nature*, vol. 572, no. 7771, pp. 603–608, Aug. 2019, doi: 10.1038/s41586-019-1487-6.
[788] D. Samanta, Y. Park, S. A. Andrabi, L. M. Shelton, D. M. Gilkes, and G. L. Semenza, ‘PHGDH Expression Is Required for Mitochondrial Redox Homeostasis, Breast Cancer Stem Cell Maintenance, and Lung Metastasis’, *Cancer Res*, vol. 76, no. 15, pp. 4430–4442, Aug. 2016, doi: 10.1158/0008-5472.CAN-16-0530.
[789] X. Li, J. Wu, X. Zhang, and W. Chen, ‘Glutathione reductase-mediated thiol oxidative stress suppresses metastasis of murine melanoma cells’, *Free Radical Biology and Medicine*, vol. 129, pp. 256–267, Dec. 2018, doi: 10.1016/j.freeradbiomed.2018.07.025.
[790] L. C. Burrage *et al.*, ‘Untargeted Metabolomic Profiling Reveals Multiple Pathway Perturbations and New Clinical Biomarkers in Urea Cycle Disorders’, *Genet Med*, vol. 21, no. 9, pp. 1977–1986, Sep. 2019, doi: 10.1038/s41436-019-0442-0.
[791] J. Huang, S. J. Weinstein, C. M. Kitahara, E. D. Karoly, J. N. Sampson, and D. Albanes, ‘A prospective study of serum metabolites and glioma risk’, *Oncotarget*, vol. 8, no. 41, pp. 70366–70377, Jul. 2017, doi: 10.18632/oncotarget.19705.
[792] S. Sarkari, C. D. Kaddi, R. V. Bennett, F. M. Fernandez, and M. D. Wang, ‘Comparison of clustering pipelines for the analysis of mass spectrometry imaging data’, *Annu Int Conf IEEE Eng Med Biol Soc*, vol. 2014, pp. 4771–4774, 2014, doi: 10.1109/EMBC.2014.6944691.
[793] P. W. Siy *et al.*, ‘Matrix Factorization Techniques for Analysis of Imaging Mass Spectrometry Data’, *Proc IEEE Int Symp Bioinformatics Bioeng*, vol. 2008, Oct. 2008, Accessed: May 05, 2021. [Online]. Available: https://www.ncbi.nlm.nih.gov/pmc/articles/PMC5382992/
[794] X.-C. Xiong, X. Fang, Z. Ouyang, Y. Jiang, Z.-J. Huang, and Y.-K. Zhang, ‘Feature Extraction Approach for Mass Spectrometry Imaging Data Using Non-negative Matrix Factorization’, *Chinese Journal of Analytical Chemistry*, vol. 40, no. 5, pp. 663–669, May 2012, doi: 10.1016/S1872-2040(11)60544-6.
[795] Y.-T. Cho, Y.-Y. Chiang, J. Shiea, and M.-F. Hou, ‘Combining MALDI-TOF and molecular imaging with principal component analysis for biomarker discovery and clinical diagnosis of cancer’, *Genomic Medicine, Biomarkers, and Health Sciences*, vol. 4, no. 1, pp. 3–6, Mar. 2012, doi: 10.1016/j.gmbhs.2012.04.022.
[796] A. Dexter *et al.*, ‘Training a neural network to learn other dimensionality reduction removes data size restrictions in bioinformatics and provides a new route to exploring data representations’, *bioRxiv*, p. 2020.09.03.269555, Sep. 2020, doi: 10.1101/2020.09.03.269555.
[797] Z. Takats, J. M. Wiseman, D. R. Ifa, and R. G. Cooks, ‘Desorption Electrospray Ionization (DESI) Analysis of Tryptic Digests/Peptides’, *CSH Protoc*, vol. 2008, p. pdb.prot4993, Apr. 2008, doi: 10.1101/pdb.prot4993.
[798] J. Tillner *et al.*, ‘Faster, More Reproducible DESI-MS for Biological Tissue Imaging’, *J Am Soc Mass Spectrom*, vol. 28, no. 10, pp. 2090–2098, Oct. 2017, doi: 10.1007/s13361-017-1714-z.
[799] T. B. Angerer *et al.*, ‘Exploiting the semi-destructive nature of GCIB-ToF-SIMS imaging for simultaneous localization and confident lipid annotations’,

Anal Chem, vol. 91, no. 23, pp. 15073–15080, Dec. 2019, doi: 10.1021/acs.analchem.9b03763.
[800] T. Armeni *et al.*, 'S-D-Lactoylglutathione can be an alternative supply of mitochondrial glutathione', *Free Radical Biology and Medicine*, vol. 67, pp. 451–459, Feb. 2014, doi: 10.1016/j.freeradbiomed.2013.12.005.
[801] T. Zech *et al.*, 'Accumulation of raft lipids in T-cell plasma membrane domains engaged in TCR signalling', *EMBO J*, vol. 28, no. 5, pp. 466–476, Mar. 2009, doi: 10.1038/emboj.2009.6.
[802] W. Szlasa, I. Zendran, A. Zalesińska, M. Tarek, and J. Kulbacka, 'Lipid composition of the cancer cell membrane', *J Bioenerg Biomembr*, vol. 52, no. 5, pp. 321–342, Oct. 2020, doi: 10.1007/s10863-020-09846-4.
[803] F. Mansilla *et al.*, 'Lysophosphatidylcholine acyltransferase 1 (LPCAT1) overexpression in human colorectal cancer', *J Mol Med (Berl)*, vol. 87, no. 1, pp. 85–97, Jan. 2009, doi: 10.1007/s00109-008-0409-0.
[804] D. Zinrajh, G. Hörl, G. Jürgens, J. Marc, M. Sok, and D. Cerne, 'Increased phosphatidylethanolamine N-methyltransferase gene expression in non-small-cell lung cancer tissue predicts shorter patient survival', *Oncology Letters*, vol. 7, no. 6, pp. 2175–2179, Jun. 2014, doi: 10.3892/ol.2014.2035.
[805] D. Ackerman *et al.*, 'Triglycerides Promote Lipid Homeostasis during Hypoxic Stress by Balancing Fatty Acid Saturation', *Cell Rep*, vol. 24, no. 10, pp. 2596-2605.e5, Sep. 2018, doi: 10.1016/j.celrep.2018.08.015.
[806] P. Su *et al.*, 'Enhanced Lipid Accumulation and Metabolism Are Required for the Differentiation and Activation of Tumor-Associated Macrophages', *Cancer Res*, vol. 80, no. 7, pp. 1438–1450, Apr. 2020, doi: 10.1158/0008-5472.CAN-19-2994.
[807] 'Neutrophils Provide Lipids to Metastatic Tumor Cells, Fueling Growth', *Cancer Discov*, vol. 10, no. 12, p. OF9, Dec. 2020, doi: 10.1158/2159-8290.CD-RW2020-143.
[808] S. García-Mulero *et al.*, 'Lung metastases share common immune features regardless of primary tumor origin', *J Immunother Cancer*, vol. 8, no. 1, p. e000491, Jun. 2020, doi: 10.1136/jitc-2019-000491.
[809] T. El Rayes *et al.*, 'Lung inflammation promotes metastasis through neutrophil protease-mediated degradation of Tsp-1', *Proc Natl Acad Sci U S A*, vol. 112, no. 52, pp. 16000–16005, Dec. 2015, doi: 10.1073/pnas.1507294112.
[810] J. Kong *et al.*, 'Extracellular vesicles of carcinoma-associated fibroblasts creates a pre-metastatic niche in the lung through activating fibroblasts', *Molecular Cancer*, vol. 18, no. 1, p. 175, Dec. 2019, doi: 10.1186/s12943-019-1101-4.
[811] T. Kitamura, B.-Z. Qian, and J. W. Pollard, 'Immune cell promotion of metastasis', *Nat Rev Immunol*, vol. 15, no. 2, pp. 73–86, Feb. 2015, doi: 10.1038/nri3789.
[812] O. S. Blomberg, L. Spagnuolo, and K. E. de Visser, 'Immune regulation of metastasis: mechanistic insights and therapeutic opportunities', *Dis Model Mech*, vol. 11, no. 10, Oct. 2018, doi: 10.1242/dmm.036236.
[813] S. Lee *et al.*, 'Surfactant Protein B Suppresses Lung Cancer Progression by Inhibiting Secretory Phospholipase A2 Activity and Arachidonic Acid Production', *CPB*, vol. 42, no. 4, pp. 1684–1700, 2017, doi: 10.1159/000479418.

[814] J. P. Koelmel *et al.*, 'LipidMatch: an automated workflow for rule-based lipid identification using untargeted high-resolution tandem mass spectrometry data', *BMC Bioinformatics*, vol. 18, no. 1, p. 331, Jul. 2017, doi: 10.1186/s12859-017-1744-3.
[815] M. Ahmadian, R. E. Duncan, K. Jaworski, E. Sarkadi-Nagy, and H. S. Sul, 'Triacylglycerol metabolism in adipose tissue', *Future Lipidol*, vol. 2, no. 2, pp. 229–237, Apr. 2007, doi: 10.2217/17460875.2.2.229.
[816] C. Nye, J. Kim, S. C. Kalhan, and R. W. Hanson, 'Reassessing triglyceride synthesis in adipose tissue', *Trends Endocrinol Metab*, vol. 19, no. 10, pp. 356–361, Dec. 2008, doi: 10.1016/j.tem.2008.08.003.
[817] M. Holzlechner, E. Eugenin, and B. Prideaux, 'Mass spectrometry imaging to detect lipid biomarkers and disease signatures in cancer', *Cancer Reports*, vol. 2, no. 6, p. e1229, 2019, doi: https://doi.org/10.1002/cnr2.1229.
[818] L. P. Fernández, M. Gómez de Cedrón, and A. Ramírez de Molina, 'Alterations of Lipid Metabolism in Cancer: Implications in Prognosis and Treatment', *Front. Oncol.*, vol. 10, 2020, doi: 10.3389/fonc.2020.577420.
[819] M. T. Snaebjornsson, S. Janaki-Raman, and A. Schulze, 'Greasing the Wheels of the Cancer Machine: The Role of Lipid Metabolism in Cancer', *Cell Metabolism*, vol. 31, no. 1, pp. 62–76, Jan. 2020, doi: 10.1016/j.cmet.2019.11.010.
[820] T. J. Rogers, 'The Role of Arachidonic Acid Metabolites in the Function of Murine Suppressor Cells', in *Prostaglandins and Immunity*, J. S. Goodwin, Ed. Boston, MA: Springer US, 1985, pp. 79–97. doi: 10.1007/978-1-4613-2603-8_4.
[821] H. Tallima and R. El Ridi, 'Arachidonic acid: Physiological roles and potential health benefits – A review', *J Adv Res*, vol. 11, pp. 33–41, Nov. 2017, doi: 10.1016/j.jare.2017.11.004.
[822] Y. Alvarez *et al.*, 'Eicosanoids in the Innate Immune Response: TLR and Non-TLR Routes', *Mediators of Inflammation*, vol. 2010, p. e201929, Jun. 2010, doi: 10.1155/2010/201929.
[823] E. Przybytkowski *et al.*, 'Upregulation of cellular triacylglycerol - free fatty acid cycling by oleate is associated with long-term serum-free survival of human breast cancer cells', *Biochem Cell Biol*, vol. 85, no. 3, pp. 301–310, Jun. 2007, doi: 10.1139/o07-001.
[824] S. Balaban *et al.*, 'Heterogeneity of fatty acid metabolism in breast cancer cells underlies differential sensitivity to palmitate-induced apoptosis', *Mol Oncol*, vol. 12, no. 9, pp. 1623–1638, Sep. 2018, doi: 10.1002/1878-0261.12368.
[825] A. Wolfer *et al.*, 'MYC regulation of a "poor-prognosis" metastatic cancer cell state', *Proc Natl Acad Sci U S A*, vol. 107, no. 8, pp. 3698–3703, Feb. 2010, doi: 10.1073/pnas.0914203107.
[826] R. Nair *et al.*, 'c-Myc and Her2 cooperate to drive a stem-like phenotype with poor prognosis in breast cancer', *Oncogene*, vol. 33, no. 30, Art. no. 30, Jul. 2014, doi: 10.1038/onc.2013.368.
[827] R. Camarda, J. Williams, and A. Goga, 'In vivo Reprogramming of Cancer Metabolism by MYC', *Front Cell Dev Biol*, vol. 5, Apr. 2017, doi: 10.3389/fcell.2017.00035.
[828] A. Ayala, I. Fabregat, and A. Machado, 'The role of NADPH in the regulation of glucose-6-phosphate and 6-phosphogluconate dehydrogenases in rat

adipose tissue', *Molecular and Cellular Biochemistry*, vol. 105, no. 1, pp. 1–5, 1991, doi: 10.1007/BF00230368.
[829] P. Jiang, W. Du, and M. Wu, 'Regulation of the pentose phosphate pathway in cancer', *Protein Cell*, vol. 5, no. 8, pp. 592–602, Aug. 2014, doi: 10.1007/s13238-014-0082-8.
[830] B. Aguilar-Bravo and P. Sancho-Bru, 'Laser capture microdissection: techniques and applications in liver diseases', *Hepatol Int*, vol. 13, no. 2, pp. 138–147, Mar. 2019, doi: 10.1007/s12072-018-9917-3.
[831] N. R. Bertos and M. Park, 'Laser Capture Microdissection as a Tool to Study Tumor Stroma', *Methods Mol Biol*, vol. 1458, pp. 13–25, 2016, doi: 10.1007/978-1-4939-3801-8_2.
[832] M. F. Dias, R. Blumenstein, and J. Russo, 'Use of laser capture microdissection allows detection of loss of heterozygosity in chromosome 9p in breast cancer', *Oncology Letters*, vol. 13, no. 5, pp. 3831–3836, May 2017, doi: 10.3892/ol.2017.5892.
[833] J. H. Cho-Vega *et al.*, 'Combined laser capture microdissection and serial analysis of gene expression from human tissue samples', *Modern Pathology*, vol. 18, no. 4, Art. no. 4, Apr. 2005, doi: 10.1038/modpathol.3800327.
[834] P. Inglese, G. Correia, P. Pruski, R. C. Glen, and Z. Takats, 'Colocalization Features for Classification of Tumors Using Desorption Electrospray Ionization Mass Spectrometry Imaging', *Anal Chem*, vol. 91, no. 10, pp. 6530–6540, May 2019, doi: 10.1021/acs.analchem.8b05598.
[835] C. L. Newell, J.-L. Vorng, J. I. MacRae, I. S. Gilmore, and A. P. Gould, 'Cryogenic OrbiSIMS Localizes Semi-Volatile Molecules in Biological Tissues', *Angewandte Chemie International Edition*, vol. 59, no. 41, pp. 18194–18200, 2020, doi: https://doi.org/10.1002/anie.202006881.
[836] G. P. Gupta *et al.*, 'Mediators of vascular remodelling co-opted for sequential steps in lung metastasis', *Nature*, vol. 446, no. 7137, pp. 765–770, Apr. 2007, doi: 10.1038/nature05760.
[837] H. M. Tunset, A. J. Feuerherm, L.-K. M. Selvik, B. Johansen, and S. A. Moestue, 'Cytosolic Phospholipase A2 Alpha Regulates TLR Signaling and Migration in Metastatic 4T1 Cells', *Int J Mol Sci*, vol. 20, no. 19, Sep. 2019, doi: 10.3390/ijms20194800.
[838] D. L. Herber *et al.*, 'Lipid accumulation and dendritic cell dysfunction in cancer', *Nat Med*, vol. 16, no. 8, pp. 880–886, Aug. 2010, doi: 10.1038/nm.2172.
[839] Y. Jin, Y. Tan, L. Chen, Y. Liu, and Z. Ren, 'Reactive Oxygen Species Induces Lipid Droplet Accumulation in HepG2 Cells by Increasing Perilipin 2 Expression', *Int J Mol Sci*, vol. 19, no. 11, Nov. 2018, doi: 10.3390/ijms19113445.
[840] L. Tirinato *et al.*, 'ROS and Lipid Droplet accumulation induced by high glucose exposure in healthy colon and Colorectal Cancer Stem Cells', *Genes & Diseases*, vol. 7, no. 4, pp. 620–635, Dec. 2020, doi: 10.1016/j.gendis.2019.09.010.
[841] C. Jin and P. Yuan, 'Implications of lipid droplets in lung cancer: Associations with drug resistance (Review)', *Oncology Letters*, vol. 20, no. 3, pp. 2091–2104, Sep. 2020, doi: 10.3892/ol.2020.11769.
[842] A. Islam *et al.*, 'FABP7 Protects Astrocytes Against ROS Toxicity via Lipid Droplet Formation', *Mol Neurobiol*, vol. 56, no. 8, pp. 5763–5779, Aug. 2019, doi: 10.1007/s12035-019-1489-2.

[843] A. P. Bailey *et al.*, 'Antioxidant Role for Lipid Droplets in a Stem Cell Niche of Drosophila', *Cell*, vol. 163, no. 2, pp. 340–353, Oct. 2015, doi: 10.1016/j.cell.2015.09.020.
[844] P. Shyu Jr, X. F. A. Wong, K. Crasta, and G. Thibault, 'Dropping in on lipid droplets: insights into cellular stress and cancer', *Bioscience Reports*, vol. 38, no. BSR20180764, Sep. 2018, doi: 10.1042/BSR20180764.
[845] R. H. Lambertucci, S. M. Hirabara, L. D. R. Silveira, A. C. Levada-Pires, R. Curi, and T. C. Pithon-Curi, 'Palmitate increases superoxide production through mitochondrial electron transport chain and NADPH oxidase activity in skeletal muscle cells', *J Cell Physiol*, vol. 216, no. 3, pp. 796–804, Sep. 2008, doi: 10.1002/jcp.21463.
[846] E. L. Seifert, C. Estey, J. Y. Xuan, and M.-E. Harper, 'Electron Transport Chain-dependent and -independent Mechanisms of Mitochondrial H2O2 Emission during Long-chain Fatty Acid Oxidation*', *Journal of Biological Chemistry*, vol. 285, no. 8, pp. 5748–5758, Feb. 2010, doi: 10.1074/jbc.M109.026203.
[847] L. D. Ly *et al.*, 'Oxidative stress and calcium dysregulation by palmitate in type 2 diabetes', *Experimental & Molecular Medicine*, vol. 49, no. 2, Art. no. 2, Feb. 2017, doi: 10.1038/emm.2016.157.
[848] C. Garrel, J.-M. Alessandri, P. Guesnet, and K. H. Al-Gubory, 'Omega-3 fatty acids enhance mitochondrial superoxide dismutase activity in rat organs during post-natal development', *Int J Biochem Cell Biol*, vol. 44, no. 1, pp. 123–131, Jan. 2012, doi: 10.1016/j.biocel.2011.10.007.
[849] J. F. Ferguson, K. Roberts-Lee, C. Borcea, H. M. Smith, Y. Midgette, and R. Shah, 'Omega-3 polyunsaturated fatty acids attenuate inflammatory activation and alter differentiation in human adipocytes', *J Nutr Biochem*, vol. 64, pp. 45–49, Feb. 2019, doi: 10.1016/j.jnutbio.2018.09.027.
[850] M. C. Mocellin, R. Fernandes, T. R. Chagas, and E. B. S. M. Trindade, 'A meta-analysis of n-3 polyunsaturated fatty acids effects on circulating acute-phase protein and cytokines in gastric cancer', *Clin Nutr*, vol. 37, no. 3, pp. 840–850, Jun. 2018, doi: 10.1016/j.clnu.2017.05.008.
[851] D. Richard, K. Kefi, U. Barbe, P. Bausero, and F. Visioli, 'Polyunsaturated fatty acids as antioxidants', *Pharmacological Research*, vol. 57, no. 6, pp. 451–455, Jun. 2008, doi: 10.1016/j.phrs.2008.05.002.
[852] Z. Gu, J. Suburu, H. Chen, and Y. Q. Chen, 'Mechanisms of Omega-3 Polyunsaturated Fatty Acids in Prostate Cancer Prevention', *BioMed Research International*, vol. 2013, p. e824563, May 2013, doi: 10.1155/2013/824563.
[853] L. T. Meital *et al.*, 'Omega-3 fatty acids decrease oxidative stress and inflammation in macrophages from patients with small abdominal aortic aneurysm', *Sci Rep*, vol. 9, Sep. 2019, doi: 10.1038/s41598-019-49362-z.
[854] H. J. Wright *et al.*, 'CDCP1 drives triple-negative breast cancer metastasis through reduction of lipid-droplet abundance and stimulation of fatty acid oxidation', *Proc Natl Acad Sci U S A*, vol. 114, no. 32, pp. E6556–E6565, Aug. 2017, doi: 10.1073/pnas.1703791114.
[855] H. Orita *et al.*, 'Selective inhibition of fatty acid synthase for lung cancer treatment', *Clin Cancer Res*, vol. 13, no. 23, pp. 7139–7145, Dec. 2007, doi: 10.1158/1078-0432.CCR-07-1186.
[856] J. N. Thupari, M. L. Pinn, and F. P. Kuhajda, 'Fatty acid synthase inhibition in human breast cancer cells leads to malonyl-CoA-induced inhibition of fatty

acid oxidation and cytotoxicity', *Biochem Biophys Res Commun*, vol. 285, no. 2, pp. 217–223, Jul. 2001, doi: 10.1006/bbrc.2001.5146.
[857] W. Zhou *et al.*, 'Fatty acid synthase inhibition activates AMP-activated protein kinase in SKOV3 human ovarian cancer cells', *Cancer Res*, vol. 67, no. 7, pp. 2964–2971, Apr. 2007, doi: 10.1158/0008-5472.CAN-06-3439.
[858] M. J. Bueno *et al.*, 'Essentiality of fatty acid synthase in the 2D to anchorage-independent growth transition in transforming cells', *Nature Communications*, vol. 10, no. 1, Art. no. 1, Nov. 2019, doi: 10.1038/s41467-019-13028-1.
[859] J. M. Berg, J. L. Tymoczko, and L. Stryer, 'Fatty Acids Are Synthesized and Degraded by Different Pathways', *Biochemistry. 5th edition*, 2002, Accessed: May 09, 2021. [Online]. Available: https://www.ncbi.nlm.nih.gov/books/NBK22554/
[860] K.-P. Chung *et al.*, 'Mitofusins regulate lipid metabolism to mediate the development of lung fibrosis', *Nature Communications*, vol. 10, no. 1, Art. no. 1, Jul. 2019, doi: 10.1038/s41467-019-11327-1.
[861] M.-Y. Jung *et al.*, 'Fatty acid synthase is required for profibrotic TGF-β signaling', *The FASEB Journal*, vol. 32, no. 7, pp. 3803–3815, 2018, doi: https://doi.org/10.1096/fj.201701187R.
[862] Z. Takáts, J. M. Wiseman, and R. G. Cooks, 'Ambient mass spectrometry using desorption electrospray ionization (DESI): instrumentation, mechanisms and applications in forensics, chemistry, and biology', *Journal of Mass Spectrometry*, vol. 40, no. 10, pp. 1261–1275, 2005, doi: https://doi.org/10.1002/jms.922.
[863] A. Dexter *et al.*, 'Imaging drugs, metabolites and biomarkers in rodent lung: a DESI MS strategy for the evaluation of drug-induced lipidosis', *Anal Bioanal Chem*, vol. 411, no. 30, pp. 8023–8032, Dec. 2019, doi: 10.1007/s00216-019-02151-z.
[864] C. S. Clendinen, M. E. Monge, and F. M. Fernández, 'Ambient Mass Spectrometry in Metabolomics', *Analyst*, vol. 142, no. 17, pp. 3101–3117, Aug. 2017, doi: 10.1039/c7an00700k.
[865] D. Parrot, S. Papazian, D. Foil, and D. Tasdemir, 'Imaging the Unimaginable: Desorption Electrospray Ionization – Imaging Mass Spectrometry (DESI-IMS) in Natural Product Research', *Planta Med*, vol. 84, no. 09–10, pp. 584–593, Jul. 2018, doi: 10.1055/s-0044-100188.
[866] M. E. Dueñas, E. A. Larson, and Y. J. Lee, 'Toward Mass Spectrometry Imaging in the Metabolomics Scale: Increasing Metabolic Coverage Through Multiple On-Tissue Chemical Modifications', *Front. Plant Sci.*, vol. 10, 2019, doi: 10.3389/fpls.2019.00860.
[867] C. Wu, A. L. Dill, L. S. Eberlin, R. G. Cooks, and D. R. Ifa, 'Mass Spectrometry Imaging under Ambient Conditions', *Mass Spectrom Rev*, vol. 32, no. 3, pp. 218–243, May 2013, doi: 10.1002/mas.21360.
[868] A. J. Taylor, A. Dexter, and J. Bunch, 'Exploring Ion Suppression in Mass Spectrometry Imaging of a Heterogeneous Tissue', *Anal Chem*, vol. 90, no. 9, pp. 5637–5645, May 2018, doi: 10.1021/acs.analchem.7b05005.
[869] C. J. Perez and D. R. Ifa, 'Internal standard application strategies in mass spectrometry imaging by desorption electrospray ionization mass spectrometry', *Rapid Commun Mass Spectrom*, vol. 35, no. 8, p. e9053, Apr. 2021, doi: 10.1002/rcm.9053.

[870] D. Unsihuay, D. Mesa Sanchez, and J. Laskin, ‘Quantitative Mass Spectrometry Imaging of Biological Systems’, *Annu Rev Phys Chem*, vol. 72, pp. 307–329, Apr. 2021, doi: 10.1146/annurev-physchem-061020-053416.
[871] A. Römpp *et al.*, ‘A public repository for mass spectrometry imaging data’, *Anal Bioanal Chem*, vol. 407, no. 8, pp. 2027–2033, 2015, doi: 10.1007/s00216-014-8357-8.
[872] K. Veselkov *et al.*, ‘BASIS: High-performance bioinformatics platform for processing of large-scale mass spectrometry imaging data in chemically augmented histology’, *Scientific Reports*, vol. 8, no. 1, Art. no. 1, Mar. 2018, doi: 10.1038/s41598-018-22499-z.
[873] M. C. Föll *et al.*, ‘Accessible and reproducible mass spectrometry imaging data analysis in Galaxy’, *GigaScience*, vol. 8, no. giz143, Dec. 2019, doi: 10.1093/gigascience/giz143.